Natural and synthetic metabolism of plant photorespiration

Inaugural-Dissertation

zur

Erlangung des Doktorgrades

der Mathematisch-Naturwissenschaftlichen Fakultät

der Heinrich-Heine-Universität Düsseldorf

vorgelegt von

Marc-Sven Röll

aus Wuppertal

Düsseldorf, Oktober 2020

aus dem
Institut für Biochemie der Pflanzen
der Heinrich-Heine-Universität Düsseldorf

Gedruckt mit der Genehmigung
der Mathematisch-Naturwissenschaftlichen Fakultät
der Heinrich-Heine-Universität Düsseldorf

Referent: Prof. Dr. Andreas P.M. Weber

Korreferent: Prof. Dr. Matias D. Zurbriggen

Tag der mündlichen Prüfung: 18. Dezember 2020

Eidesstattliche Erklärung

Ich versichere an Eides Statt, dass die Dissertation von mir selbständig und ohne unzulässige fremde Hilfe unter Beachtung der „Grundsätze zur Sicherung guter wissenschaftlicher Praxis an der Heinrich-Heine-Universität Düsseldorf“ erstellt worden ist.

Die Dissertation habe ich in der vorgelegten oder in ähnlicher Form noch bei keiner anderen Institution eingereicht.

Ich habe bisher keine erfolglosen Promotionsversuche unternommen.

Düsseldorf, den

Marc-Sven Röll

Statement of authorship

I hereby certify that this dissertation is the result of my own work. No other person’s work has been used without due acknowledgement. This dissertation has not been submitted in the same or similar form to other institutions. I have not previously failed a doctoral examination procedure.

“To Winfried Noack”

Summary

The basis to meet the global food demands of a growing world population is the photosynthetic conversion of carbon dioxide into biomass. The enzyme ribulose-1,5-bisphosphate carboxylase/oxygenase (Rubisco) accounts for the majority of all carbon fixing reactions on earth but remains error prone. On average, one of four Rubisco catalyzed reactions are oxygenations, that necessitate photorespiration to retain the photosynthetically fixed carbon. However, photorespiration recycles only 75% of carbon – a matter that diminishes plant yield by up to 30%. Synthetic biochemical bypasses hold the potential to facilitate efficient photorespiration by conserving carbon and nitrogen at reduced energetic costs. Deriving from this, elucidating the natural metabolic interactions profits the fundamental understanding and future engineering on photorespiration.

The aim of this work was to understand the consequences on plant growth and metabolism of two synthetic bypasses that avoid the carbon-, nitrogen- and energy losses of canonical photorespiration. We established the ß-hydroxyaspartate cycle in peroxisomes of the model plant *Arabidopsis thaliana* (Manuscript I). The pathway itself operates at lower energetic costs, without carbon or nitrogen losses and alters the carbon stoichiometry of photorespiration by producing a C4 acid instead of a C3 acid. We demonstrated peroxisomal targeting and enzyme functionality of all four enzymes. Further the functionality of the cycle as photorespiratory bypass was addressed. So far, the unconstraint conversion of the cycle's product limited a positive growth effects but can be overcome via synthetic C4 photosynthesis. In an alternative approach to frame efficient photorespiration, we implemented the reductive glycine pathway in *Arabidopsis thaliana* to bypass the enzyme of photorespiratory carbon dioxide release by engineering a cytosolic one carbon unit sink (Manuscript II). We identified the metabolic bottlenecks and addressed these by a developed photosynthetic tissue specific genome editing tool to optimize flux and eliminate the carbon dioxide releasing reactions of photorespiration. Within this work, we characterized the mitochondrial formate dehydrogenase and propose a role as regulator of the one carbon shunt that connects mitochondrial and cytosolic one carbon metabolism (Manuscript III). The distribution of one carbon units from the mitochondria depending on cytosolic needs is a previously unknown mechanism in plants and unravels part of the interaction between photorespiration and one carbon metabolism.

In summary, the used synthetic biochemical pathways and the characterization of formate dehydrogenase contribute to the understanding natural metabolic interactions and future engineering approaches of plant photorespiration.

Zusammenfassung

Photosynthese ist ein fundamentaler Prozess zur Sicherung des globalen Nahrungsbedarf einer wachsenden Weltbevölkerung. Das Enzym Ribulose-1,5-bisphosphat Carboxylase/Oxygenase (Rubisco) ist verantwortlich für den Großteil der Kohlenstoff-fixierenden Reaktionen der Erde, aber ist gleichzeitig fehleranfällig. Im Mittel ist jede vierte durch Rubisco katalysierte Reaktion eine Oxygenierung, die den Stoffwechselweg der Photorespiration erfordert um den bereits fixierten Kohlenstoff wieder verfügbar zu machen. Bei der Photorespiration – auch „Lichtatmung" genannt – können nur 75% des Kohlenstoffs wieder nutzbar gemacht werden. Dieser Aspekt führt zu einer Verringerung des pflanzlichen Wachstums um bis zu 30%. Synthetische biochemische Stoffwechselwege liefern Lösungsansätze für eine effizientere Photorespiration durch die Konservierung von Kohlen- und Stickstoff bei reduzierten Energiekosten. Dadurch gewonnene Kenntnisse können genutzt werden um zum einen die metabolischen Wechselwirkungen der Photorespiration zu verstehen und um zukünftige Verbesserungsansätze zu vereinfachen.

Ziel dieser Arbeit war es, den grundlegenden Metabolismus der Photorespiration zu verändern und die Folgen auf den pflanzlichen primären Stoffwechsel und das Pflanzenwachstum zu untersuchen. Im Zuge dessen wurden die Effekte von zwei synthetischen Stoffwechselwegen in der Modellpflanze *Arabidopsis thaliana* analysiert. Der Einbau des ß-Hydroxyaspartat Zyklus in pflanzliche Peroxisomen führt zu einer effizienteren Stickstoffnutzung und verändert die grundlegende Stöchiometrie der pflanzlichen Photorespiration durch die Bildung einer C4-Säure anstelle einer C3-Säure (Manuskript I). Als Teil dessen wurde die peroxisomale Lokalisierung der vier beteiligten Enzyme sowie deren Aktivität in der Pflanze validiert. Außerdem wurden die metabolischen Konsequenzen des Zyklus auf den pflanzlichen Primärstoffwechsel analysiert. Zum jetzigen Zeitpunkt, limitiert die Verwertung der produzierten C4-Säure in verschiedenen Stoffwechselwegen einen Wachstumszuwachs, jedoch kann dies über einen synthetischen C4-Photosynthese Zyklus adressiert werden. In einem alternativen Ansatz, wurde ein synthetischer Stoffwechselweg genutzt um eine zytosolische Alternative für die Bereitstellung von Einkohlenstoff Molekülen zu erzeugen, was eine Umgehung des Kohlenstoffdioxid freisetzenden Enzyms der Photorespiration ermöglicht (Manuskript II). Basierend auf der Analyse des primären Stoffwechsels konnten die limitierenden Schritte des synthetischen Stoffwechselweges identifiziert werden. Durch ein entwickeltes CRISPR/Cas9 System zur Erzeugung von Mutationen im photosynthetisch-aktiven Gewebe wurden die limitierenden Schritte addressiert und gleichzeitig die Kohlenstoffdioxid freisetzenden Reaktionen der pflanzlichen

Photorespiration eliminiert. Als Teil dieser Arbeit, wurde die mitochondriale Formiat-Dehydrogenase charakterisiert (Manuskript III). Nach momentanem Stand hypothetisieren wir die Rolle der Formiat-Dehydrogenase als regulierendes Enzym des metabolischen Flusses von Einkohlenstoffverbindungen zwischen dem Mitochondrium und dem Zytosol.

Zusammenfassend, tragen die hier verwendeten synthetischen biochemischen Stoffwechselwege und die Untersuchung der Formiat-Dehydrogenase zum grundlegenden Verständnis der Rolle der Photorespiration im pflanzlichen Metabolismus bei und ermöglichen weiterführende Verbesserungsansätze.

Acknowledgement

First, I would like to thank my thesis advisor **Prof. Dr. Andreas P.M. Weber**. I truly admire his scientific thinking and knowledge and gratefully acknowledge the support and guidance I received by him during the last years, including the attendance of several conferences. Critically scrutinizing my ideas and results but being at the same time supportive, open-minded and handing out advice helped me to grow as scientist and person.

Further, I would like to thank my thesis mentor **Prof. Dr. Matias D. Zurbriggen** for fruitful discussion and critical feedback including the opportunity to express my ideas in the joint review on plant synthetic biology. I also would like to thank my third committee member **Prof. Dr. Wolf B. Frommer** for valuable feedback during the committee meetings.

I am grateful to all collaborators that contributed to the work described in this thesis including **Dr. Lennart Schada von Borzykowski** and **Prof. Dr. Tobias J. Erb** (Max-Planck Institute for Terrestrial Microbiology), **Dr. Arren Bar-Even** (Max-Planck Institute of Molecular Plant Physiology), **Prof. Dr. Sanja Roje** and **Sompop Saehang** (Washington State University), **Dr. Simon Strobbe**, **Prof. Dr. Dominque von der Straeten**, **Jana Verstraete**, and **Prof. Dr. Christopher Strove** (Ghent University).

I thank **Dr. Petra Fackendahl,** coordinator of the iGRAD Plant program, and all **iGRAD Plant students** for discussion and inimitable retreats.

I also would like to thank the **German Federal Ministry of Education and Research** as funding agency of this work.

I am grateful to the whole **AG Weber** for creating an atmosphere of friendship and support as well as our former secretary **Anja Nöcker** for her patient help with bureaucratic problems.

I would like to thank **PD Dr. Marion Eisenhut** and **Dr. Miguel Minambres Martin** for productive and supportive collaborations and **Elisabeth Klemp**, **Maria Graf**, **Katrin Weber** and **Raja Stracke** for excellent technical assistance.

I am obliged to all internship, Bachelor and Master students, I had the pleasure to work with, including **Briaunna Murray**, **Birger Wolter**, **Maryam Forough**, **Balraj Singh**, **Leonie Wirth** and **Mirko Kraus**.

During the last years many colleagues have become friends. Therefore, I wish to thank **apl. Prof. Dr. Nicole Linka**, **Dr. Tabea Mettler-Altmann** and **Dr. Philipp Westhoff**, for their contribution to my scientific progress, as well as tremendous support and guidance. Further, I would like to thank **Anastasjia Plett**, **Dr. Lennart Charton**, **Dr. Franziska Kuhnert** and **Dr. Eva Maleckova** for daily scientific discussion during the coffee breaks and being collaborative and supportive in the daily lab work.

Explicitly, I thank **Dr. Dominik Brilhaus** for friendship, warmth, discussion, sporting activity and his taunts. Further, I am grateful to my long-standing friends **Maximilian Buchwald-Podder**, **Dr. Frederic Sahnen**, **Jan-Martin Boinski** and **Jannice Beckschebe** for their encouragement.

I express my deepest gratitude to my mom, dad, sister and grandma for their unconfined support and to my departed grandpa for early child education in the fascinating field of biology.

Finally, I also express my deep gratitude to **Milena Malisic** for her admirable scientific thinking and curiosity as well as the trust, emotional support and empathy I received from her.

TABLE OF CONTENTS

Preface

Motivation and research aim

Photosynthesis is an efficient – probably the most efficient – natural strategy to convert light energy into biomass by sequestering atmospheric carbon dioxide. Error prone photosynthesis by the primary carbon dioxide fixing enzyme ribulose-1,5-bisphoshate carboxylase/oxygenase (Rubisco) is caused by the acceptance of oxygen. Photorespiration detoxifies the produced molecule and recycles the containing carbon. However, high energetic costs and the release of carbon dioxide by photorespiration negatively affect plant biomass yield. Further, rising temperatures and severe drought caused by climate change favor Rubisco oxygenation/photorespiration and accelerate photorespiratory drawbacks. The aim of this work is to design, construct and test synthetic metabolic pathways that enable carbon-neutral, energy efficient photorespiration in plants. Analyzing the consequences of such a metabolic redesign will contribute to understand the integration of photorespiration in the cellular metabolic network.

Outline

This dissertation consists of three chapters and includes three manuscripts that cover the experimental work and results obtained during my doctorate. In the following section, I will give a brief introduction on oxygenic photosynthesis and a detailed description of photorespiration with an emphasize on the underlying metabolic nature. In this part, I will explicitly highlight the role of one carbon metabolism in plants and finally give a summary on engineering strategies to improve photosynthesis with the focus the photosynthetic carbon reactions.

The second chapter contains three scientific manuscripts envisaged to be published in international peer-review journals. My contribution to the respective manuscript is indicated on the front page of each manuscript. Manuscript I and II describe engineering strategies of two synthetic biochemical bypasses of photorespiratory metabolism in *Arabidopsis thaliana*. In Manuscript I, the metabolic effects of the peroxisomal ß-hydroxyaspartate cycle as photorespiratory bypass are analyzed and a perspective on this bypass as first engineering step of a synthetic C4 photosynthetic cycle is given. Part of this work is a pending EU patent application and a brief summary of the patent including the made claims is added. In Manuscript II, a one carbon based metabolic engineering strategy is employed to bypass the mitochondrial glycine decarboxylase complex, the carbon dioxide releasing enzyme of canonical photorespiration. In a follow-up story described in

Manuscript III, we propose that mitochondrial formate dehydrogenase regulates the one carbon shunt that connects mitochondrial and cytosolic one carbon metabolism. The final chapter of this dissertation comprises two review articles published in international peer-review journals. The review article, "Mechanistic understanding of photorespiration paves the way to a new green revolution" (in *New Phytologist*), summarizes the biochemical fundamentals of photorespiration and validated engineering approaches. In the review article, "The impact of synthetic biology for future agriculture and nutrition" (in *Current Opinion in Biotechnology*), the multifaceted contribution of synthetic biology to plant biology is pictured with a focus on agriculture and nutrition. Finally, three News and Views articles are included, that are published in the international peer-review journal *Plant Physiology*, and address the topics photorespiration, terpene biosynthesis in cannabis and nanoparticle mediated plant transformation.

Introduction

Oxygenic photosynthesis

Oxygenic photosynthesis provides the basis for urban life by converting light energy into chemical energy stored as reduced carbon (Sharkey, 2020). Historically, photosynthesis is divided into the light-dependent reactions and the light-independent carbon reactions (Cardona et al., 2018). The light-dependent reactions produce chemical energy as adenosine triphosphate (ATP) and reduced nicotinamide adenine dinucleotide phosphate (NADPH). Chlorophyll molecules in the photosystems I and II are excited by light energy and electrons are transferred to $NADP^+$ via several electron carriers (Kramer et al., 2004). The release of protons from the oxygen evolving complex, by splitting water to produce oxygen, and proton shuttling across the thylakoid membrane generates a proton motif force that drives ATP synthesis by chemiosmosis (Mitchell, 1961; Kramer et al., 2004). Both, the produced ATP and NADPH are required for the photosynthetic carbon assimilation to convert carbon dioxide (CO_2) into organic molecules via the Calvin-Benson-Bassham cycle (CBBC; Bassham et al., 1954; Benson, 2010; Sharkey, 2019). A crucial role in the CBBC states ribulose-1,5-bisphosphate carboxylase/oxygenase (Rubisco) - the most abundant enzyme on earth - that carries out the carboxylation of the primary CO_2 acceptor molecule ribulose 1,5-bisphosphate (RuBP; Stitt et al., 2010; Bar-On and Milo, 2019). A single carboxylation event yields two molecules of 3-phosphoglycerate (3-PGA), the stable C3 intermediate of CO_2 fixation, that defines the photosynthesis type as C3 photosynthesis. The following stepwise reduction of 3-PGA to triosephosphate (TP) consumes the majority of ATP and NADPH produced by the light reactions. Overall within the CBBC, three CO_2 molecules are fixed producing six TPs at the cost of nine ATP and six NADPH (Stitt et al., 2010; Sharkey, 2020). Whereas, one TP molecule can be used for cellular anabolism, five TPs are required to recycle the primary acceptor molecule RuBP via a series of isomerization-, aldol-, phosphorylation- and dephosphorylation reactions (Stitt et al., 2010).

The early evolution in an oxygen (O_2) depleted atmosphere favored Rubisco's carboxylation reaction but over time, oxygenic photosynthesis accelerated the atmospheric O_2/CO_2 ratio (Schlueter and Weber, 2020). Under current atmospheric conditions 25% of Rubisco's catalyzed reactions are oxygenations that cause the high metabolic flux in a process, called photorespiration (Walker et al., 2016).

Photorespiration

In 1920, Otto Warburg discovered that oxygen inhibits photosynthesis in the unicellular green alga *Chlorella sp.* (Warburg, 1920; Nickelsen, 2007). Historically known as the "green Warburg effect", photorespiration – often called C2 cycle or oxidative photosynthetic carbon cycle – describes the light-dependent CO_2-release of photosynthetic organisms (Busch, 2020; Kutschera et al., 2020). After Otto Warburg's observation, it took half a century to unravel the metabolic pathway and the biochemical reasons of photorespiration (Rabson et al., 1962). The ability of Rubisco to fix oxygen instead of CO_2 causes the oxygenation of the substrate RuBP and yields 2-phosphoglycolate (2-PG) and 3-PGA (Bowes et al., 1971). The produced 2-PG by RuBP oxygenation inhibits enzymes of the CBBC (triose phosphate isomerase and sedoheptulose-1,7-bisphosphatase) and starch biosynthesis (phosphofructokinase) and is therefore rapidly metabolized by photorespiration (Anderson, 1971; Kelly and Latzko, 1976; Flügel et al., 2017). In C3 plants, ~25% of Rubisco catalyzed reactions are oxygenations, quantitatively depending on the CO_2/O_2 ratio around the active site, the kinetic properties of the enzyme and temperature (Eisenhut et al., 2019). The net carbon equation of photorespiration defines the conversion of two 2-PG molecules into one 3-PGA and CO_2, thereby recycling 75% of previously fixed carbon (Weber and Bar-Even, 2019). In addition, nitrogen reassimilation and chemical energy consumption (3.5 ATP and two NADPH per 3-PGA molecule), reason the hypothesis of photorespiration as a 'wasteful' process that reduces plant yield by approximately 30% (Walker et al., 2016). Opposing the consequences of rising atmospheric CO_2 concentration and changing environmental conditions, e.g. drought and rising temperature, on Rubisco, likely favors RuBP oxygenation and following photorespiration (Ehlers et al., 2015; Walker et al., 2016). Given this, circumventing the accelerated drawbacks of increased photorespiration on plant yield justify the urgent need to engineer and improve the photorespiratory pathway in an efficient manner (Walker et al., 2016; Simkin et al., 2019; Weber and Bar-Even, 2019). However, the multifaceted role of photorespiration as electron sink under environmental stress conditions and the metabolic interactions with nitrogen-, sulfur-, one carbon (C_1) metabolism and the tricarboxylic acid cycle (TCA cycle) are often overlooked, marginally understood and their consequences on plant growth in changing environmental conditions are not predictable (Huang et al., 2015; Eisenhut et al., 2019; Busch, 2020).

The biochemistry of photorespiration

Photorespiration is a highly compartmentalized metabolic processes and includes enzymatic steps carried out in the chloroplast, peroxisome, mitochondria and the cytosol (Fig. 1). In total, the core cycle includes nine enzymatic steps and requires multiple solute carriers to shuttle intermediates and cofactors across organellar membranes. So far, the two plastidial carriers of the core cycle are biochemically and physiologically characterized (Pick et al., 2013; South et al., 2017). However, the definition of a 'photorespiratory' phenotype, that is rescued under non-photorespiratory conditions in CO_2 enriched air, led to the identification of genes and enzymes involved in photorespiration (Somerville and Ogren, 1981; Somerville, 2001; a list of photorespiration associated genes is given in Eisenhut et al., 2019).

In the chloroplast RuBP oxygenation produces 2-phosphoglycolate that is dephosphorylated by phosphoglycolate phosphatase (PGLP) and yields glycolate (Schwarte and Bauwe, 2007). Glycolate is exported from the chloroplast by the plastid glycolate/glycerate transporter1 (PLGG1) and the bile acid sodium symporter 6 (BASS6, Pick et al., 2013; South et al., 2017). Although the mechanism of glycolate import into the peroxisome remains unknown, in the peroxisome glycolate is oxidized to glyoxylate by glycolate oxidase that produces hydrogen peroxide as byproduct (Dellero et al., 2016). Catalase directly detoxifies hydrogen peroxide into water (Queval et al., 2007). Multiple nitrogen donors serve for glyoxylate transamination to produce glycine (Fig. 1). Glutamate by glutamate:glyoxylate transaminase (GGAT) and serine by serine:glyoxylate aminotransferase (SGAT) are considered the major nitrogen donors, supported by the photorespiratory and lethal phenotypes of loss-of-function mutants respectively (Liepman and Olsen, 2001; Dellero et al., 2015; Modde et al., 2017). Further, alanine is hypothesized to play a minor role in maintaining peroxisomal transamination of glyoxylate (Liepman and Olsen, 2001). The involved transporters to export glycine from the peroxisome and into mitochondria are unknown. In mitochondria glycine is converted into serine by the joint action of the multienzyme complex glycine decarboxylase (GDC) and serine hydroxymethyltransferase 1 (SHM1; Douce et al., 2001; Bauwe, 2003; Voll et al., 2006; Engel et al., 2007; Timm et al., 2012; Timm et al., 2015; Timm et al., 2017). As source of photorespiratory CO_2 and NH_3 release the GDC has been the subject of intensive studies to understand the biochemical, structural and physiological details. In particular the physiological role of the GDC remains to be fully understood but is limited by seedling lethality of *Arabidopsis thaliana* (Arabidopsis) loss-of-function mutants (Engel et al., 2007; Timm et al., 2017). In order to prevent the unhampered loss of photorespired CO_2,

plants position their chloroplasts at the mesophyll periphery to reassimilate ~30 % of the mitochondrial released CO_2 by the CBBC (Busch et al., 2013).

Structurally, the GDC consists of four protein subunits, the P- (GLDP), T- (GLDT), H- (GLDH) and L-protein (GLDL), that are arranged in a stoichiometry of $1L_2$-$4P_2$-8T and 20 or 26 GLDH proteins in Arabidopsis and pea respectively (Douce et al., 2001; Wittmiß et al., 2020). The pyridoxal-dependent GLDP catalyzes the reductive methylamination of glycine, releasing the CO_2 and transferring the reduced methylamine to the GLDH protein that acts as mobile element between the subunits of the complex (Douce et al., 2001). The methylamine is deaminated by the T-protein in a tetrahydrofolate (THF)-dependent process to produce the C_1-intermediate, 5,10-methylene-THF. The electron transfer from GLDT via the GLDH finally produces NADH by the GLDL and recycles the H-protein (Douce et al., 2001). A second glycine molecule is then condensed with 5,10-methylene-THF to produce serine by SHM1 (Voll et al., 2006). The following deamination of serine by SGAT produces hydroxypyruvate (Fig. 1). The peroxisomal reduction of hydroxypyruvate by NAD-dependent hydroxypyruvate reductase 1 (HPR1) is the preferred route of glycerate production (Timm et al., 2011). However, the cytosolic (HPR2) and chloroplastic isoform (HPR3) serve as peroxisomal bypasses of the redox-dependent step of photorespiration (Timm et al., 2008; Timm et al., 2011). Glycerate is imported into the chloroplast by PLGG1 and phosphorylated by glycerate kinase under ATP-consumption to produce 3-PGA that enters the CBBC (Boldt et al., 2005; Pick et al., 2013).

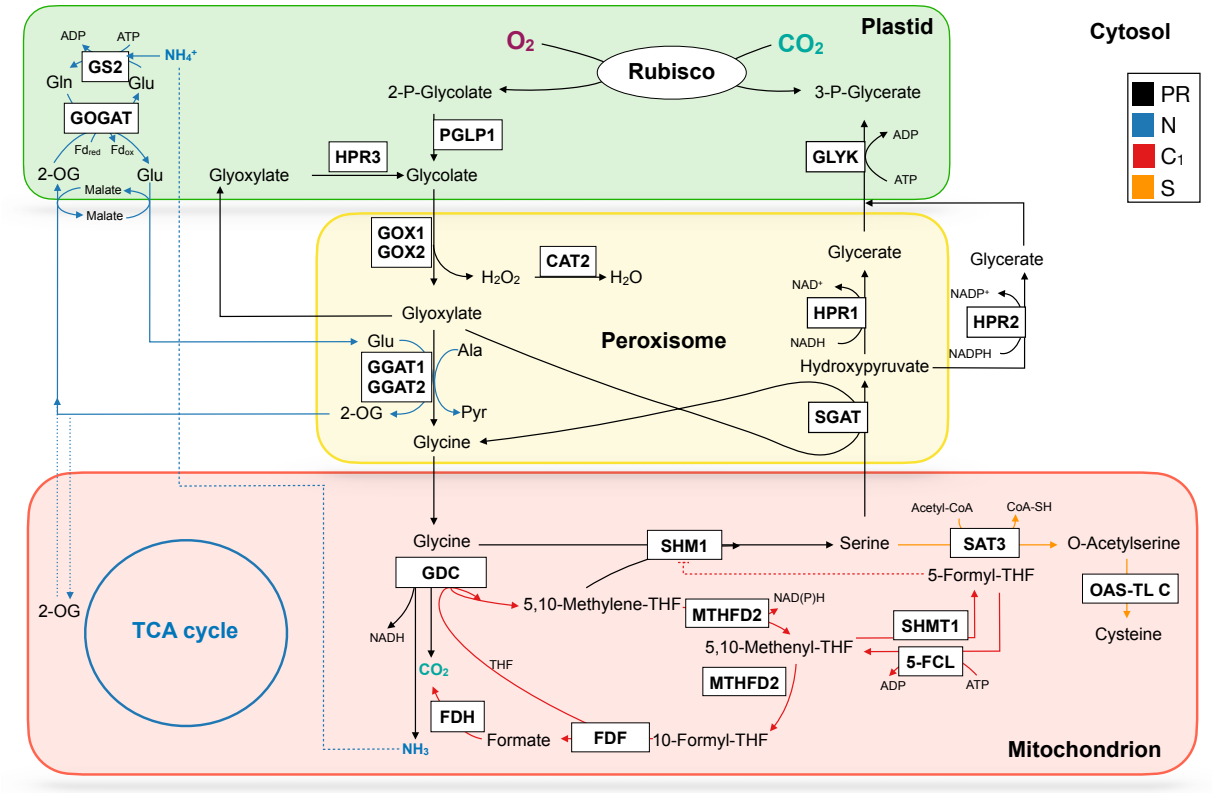

Fig. 1: Photorespiratory metabolism and the interaction with cellular metabolism. Photorespiratory metabolism in *Arabidopsis thaliana*. Interdependency of photorespiration (PR) with nitrogen (N), one carbon (C_1), and sulfur (S) metabolism. Abbreviations: PGLP1, phosphoglycolate phosphatase 1; GOX1, glycolate oxidase 1; GOX2, glycolate oxidase 2; CAT2, catalase 2; GGAT1, glutamate:glyoxylate aminotransferase 1; GGAT2, glutamate:glyoxylate aminotransferase 2; GDC, glycine decarboxylase complex; SHM1, serine hydroxymethyltransferase 1; SGAT, serine:glyoxylate aminotransferase; HPR1, hydroxypyruvate reductase 1; HPR2, hydroxypyruvate reductase 2; HPR3, hydroxypyruvate reductase 3, GLYK, glycerate kinase, GS2, glutamine synthetase 2; GOGAT, glutamine:oxoglutarate aminotransferase; THF, tetrahydrofolate; MTHFD2, Bifunctional 5,10-methylene-THF dehydrogenase/5,10-methenyl-THF cyclohydrolase; 5-FCL, 5-formyl-THF cycloligase; FDF, 10-formyl deformylase; FDH, formate dehydrogenase; SAT3, serine o-acetyltransferase; OAS-TL C, *O*-acetylserine lyase isoform C. Figure adapted from Eisenhut et al., 2019.

The integration of photorespiration in cellular metabolism

In C3 plants photorespiration is an integral part of cellular metabolism and interacts with several auxiliary metabolic pathways (Fig. 1). Whereas the uptake of nitrogen depends on overall photorespiratory flux, the mitochondrial NH_3 release connects photorespiration and nitrogen reassimilation (Bloom, 2015). The chloroplastic ATP- and reducing power consuming glutamine synthetase/ferredoxin-dependent glutamine:oxoglutarate aminotransferase system (GS2/Fd-GOGAT) reassimilates nitrogen, released by glycine oxidation (Coschigano et al., 1998). Initially, glutamate and ammonia are converted into glutamine by GS2 and the Fd-GOGAT mediated transamination produces two glutamate molecules (Fig. 1). One glutamate is reused by GS2 and the second glutamate is exported

from the chloroplast (Fig. 1). In sum, the reassimilation of photorespiratory released nitrogen to produce glutamate consumes one ATP and two reduced ferredoxins per two 2-PG molecules (Weber and Bar-Even, 2019). Two chloroplastic transport proteins are essential for nitrogen reassimilation. The 2-oxoglutarate/glutamate transporter DiT1 imports 2-oxoglutarate required for glutamate production by Fd-GOGAT (Kinoshita et al., 2011). Glutamate is exported from the chloroplast by the glutamate/malate transporter DiT2 and serves as amino group donor for the peroxisomal transamination of glyoxylate into glycine by GGAT1, that produces 2-oxoglutrate (Fig. 1; Renné et al., 2003; Dellero et al., 2015).

The metabolism of 2-oxoglutarate connects photorespiration with the TCA cycle and the gamma-aminobutyric acid (GABA) shunt (see Obata et al., 2016 and references therein). The positive correlation between photorespiration- and day respiration rates indicates that mitochondrial metabolism recycles carbon backbones for photorespiratory nitrogen reassimilation and maintains the redox homeostasis in the mitochondrial matrix (Tcherkez et al., 2012). In order to avoid overreduction of the mitochondrial matrix by high rates of glycine oxidation, the produced NADH is oxidized by the respiratory chain. Thereby, the cytosolic ATP/ADP ratio is increased and the mitochondrial redox homeostasis is maintained (Gardeström and Wigge, 1988; Wigge et al., 1993). Further, the export of reducing power from the mitochondria by the uncoupling protein 1 and 2, biochemically characterized as solute carriers for aspartate, glutamate and dicarboxylates, supplies the mitochondrial/cytosolic redox shuttles and glutamate:oxaloacetate transaminase reactions with their respective substrates (Sweetlove et al., 2006; Monné et al., 2018; Eisenhut et al., 2019). Malate valves play a pivotal role in maintaining organellar NAD(P)/NAD(P)H ratios (Selinski and Scheibe, 2019). The peroxisomal reduction of hydroxypyruvate by HPR1 produces NAD^+ that needs to be reduced to maintain the high photorespiratory flux (Fig. 1). The peroxisomal malate dehydrogenase is only marginally involved in this process, reasoned by the lack of the photorespiratory phenotype in the *Arabidopsis* double mutant (Cousins et al., 2008). Instead, the regeneration of NADH involves the mitochondrial malate dehydrogenase to return reducing power generated by glycine oxidation to the peroxisome (Tomaz et al., 2010; Lindén et al., 2016; Shameer et al., 2019).

Finally, photorespiratory derived serine constitutes the largest part of the soluble pool in an illuminated leaf (Li et al., 2003) and the conversion of mitochondrial serine for cysteine and glutathione biosynthesis connects photorespiration and sulfur metabolism (Samuilov et al., 2018).

The role of one carbon metabolism in photorespiration

The dependency of the GDC/SHM1 reactions on THF and 5,10-methylene-THF respectively, connect photorespiration and one carbon (C_1) metabolism (Fig. 1; Eisenhut et al., 2019). Within mitochondria, 5,10-methylene-THF produced by glycine oxidation enters the THF cycle, as alternate flux to serine biosynthesis by SHM (Fig. 1). The stepwise oxidation of 5,10-methylene-THF finally releases THF and produces formate, oxidized to CO_2 by NAD-dependent formate dehydrogenase (Fig. 1). THF regeneration by the THF-cycle is an integral to sustain mitochondrial photorespiratory flux, shown by the photorespiratory phenotype of the 10-formyl-deformylase double knockout mutant (Fig. 1; Collakova et al., 2008). The second catalytical reaction of SHM with 5,10-methenyl-THF produces 5-formyl-THF, a stable storage form of C_1 THF-intermediates (Goyer et al., 2005). The recycling of 5-formyl-THF by 5-formyl-THF cycloligase is an essential metabolic repair mechanism to prevent the 5-formyl-THF dependent inhibition of SHM (Goyer et al., 2005).

The biochemistry of one carbon metabolism

C_1 metabolism is essential to all living organisms (Hanson and Roje, 2001). In eukaryotes the transfer of C_1 units relies on derivatives of folic acid (folates) and C_1 THF-intermediates (C_1 folates). Further, *S*-adenosyl-*L*-methionine (SAM) serves as universal donor for cellular methylation reactions (Hanson et al., 2000). The enzymatic transfer of C_1 units contributes to glycine/serine metabolism, methionine-, pantothenate-, purine- and thymidylate biosynthesis and organellar protein biosynthesis (Hanson et al., 2000; Hanson and Roje, 2001; Hanson and Gregory, 2011). Further methylated molecules, like lignin, alkaloids and betaines depend on C_1 metabolism as well as chlorophyll biosynthesis (Hanson and Roje, 2001; Van Wilder et al., 2009). The fundamental function in cellular metabolism prevents to study form and function of C_1 metabolism by classical biochemistry and genetic approaches (Hanson and Roje, 2001). Lethal loss-of-function mutants, intermediate instability and a high degree of genetic redundancy still limit the understanding of C_1 metabolism in plants (Hanson and Roje, 2001).

The central dogma of C_1 metabolism states the reversible conversion of formate into 5,10-methylene-THF and in Arabidopsis the necessary enzymes are predicted to exists in the cytosol, mitochondria and plastid (Fig. 2; Hanson et al., 2000). Formate is converted into 10-formyl-THF by 10-formyl-THF synthetase (FTHFS). The produced 10-formyl-THF is used for *de novo* purine biosynthesis by glycinamide ribonucleotide transformylase and 5-aminoimidazole-4-carboxamide ribonucleotide transformylase/inosine monophosphate

cyclohydrolase to catalyze the attachment of the formyl group (Zrenner et al., 2006). Alternatively, 10-formyl-THF is cyclized to 5,10-methenyl-THF and subsequently reduced to 5,10-methylene-THF by the bifunctional enzyme 5,10-methenyl cycloligase/5,10-methylen-THF reductase (MTHFD; Hanson and Roje, 2001). Whereas in plants joint FTHFS and bifunctional MTHFD activity mediates formate to 5,10-methylene-THF conversion, heterotrophic eukaryotes rely on a trifunctional C_1-THF synthase (Song and Rabinowitz, 1993).

The metabolization in several pathways defines the fate of 5,10-methylene-THF (Fig. 2). In addition to the discussed role in glycine/serine metabolism, methionine biosynthesis is one fate of 5,10-methylene-THF by reduction to 5-methyl-THF and C_1 unit transfer to homocysteine (Fig. 2; Ravanel et al., 1998; Ravanel et al., 2004). Methionine is either incorporated into proteins or used in the cytosolic methyl-cycle to produce SAM for cellular methylation reactions (Sauter et al., 2013). Whereas DNA methylation strongly depends on cytosolic C_1 metabolism, plastids import SAM as methyl-group donor by the SAMT1 transporter (Bouvier et al., 2006; Groth et al., 2016).

Finally, 5,10-methylene-THF is used for pantothenate- and thymidylate biosynthesis (Hanson and Roje, 2001). The bifunctional dihydrofolate reductase-thymidylate synthase converts 5,10-methylene-THF into THF and produces deoxythymidine monophosphate (Gorelova et al., 2017). The NADP-dependency of this process contributes to the cellular redox state and maintains folate integrity (Gorelova et al., 2017).

THF is the essential co-factor of eukaryotic C_1 metabolism (Hanson and Gregory, 2011). Whereas mammals depend on the dietary supply of THF (vitamin B_{12}), plants synthesize THF *de novo* in mitochondria (Hanson and Gregory, 2011). In order to stabilize the THF-pool and increase the affinity of folate-depending enzymes, cellular folates are mono- or polyglutamylated (Mehrshahi et al., 2010). In Arabidopsis three folylpolyglutamate synthetases (FPGS) with redundant compartmentalization across mitochondria, plastids and cytosol, maintain the polyglutamylated folate pools (Mehrshahi et al., 2010). The dominant mitochondrial isoform FPGS2 is essential for plant viability, in line with mitochondrial THF *de novo* biosynthesis (Mehrshahi et al., 2010).

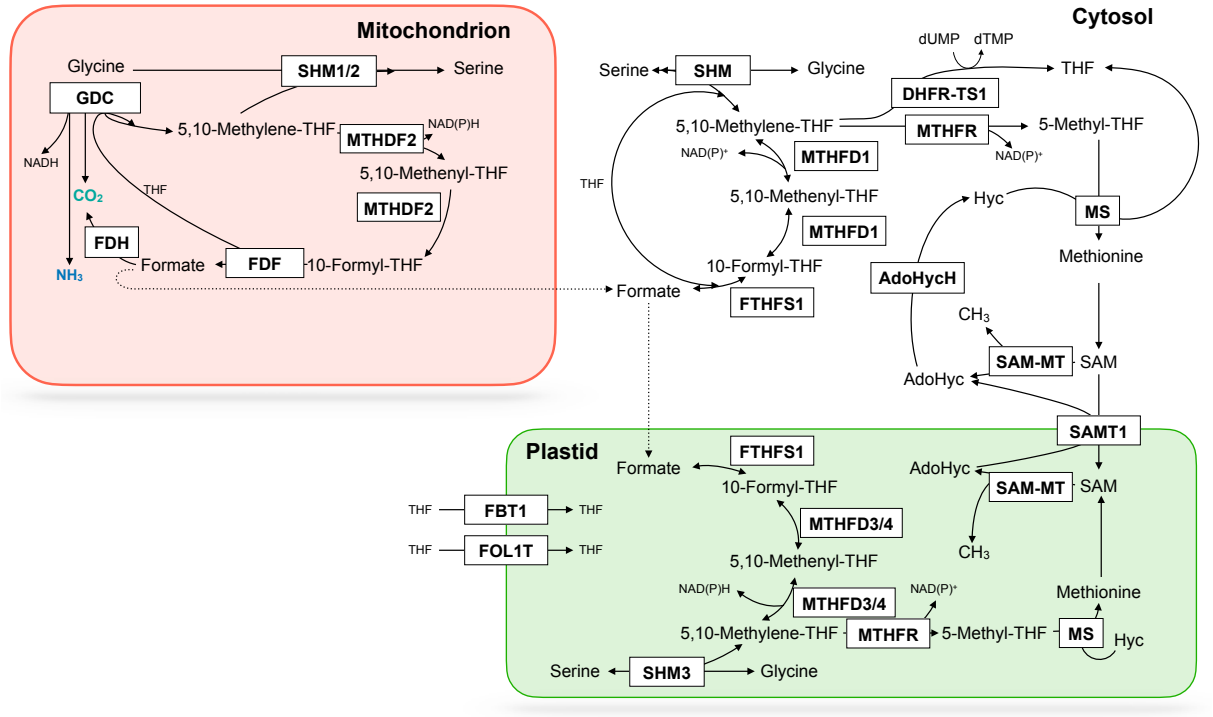

Fig. 2: One carbon metabolism in plants. Schematic representation of one carbon metabolism in *Arabidopsis thaliana*. Abbreviations: THF, tetrahydrofolate; Hyc, homocysteine; SAM, *S*-adenosyl-*L*-methionine; AdoHyc, *S*-adenosyl-*L*-homocysteine; GDC, glycine decarboxylase complex; SHM, serine hydroxymethyltransferase; MTHFD, Bifunctional 5,10-methylene-THF dehydrogenase/5,10-methenyl-THF cyclohydrolase; FDF, 10-formyl deformylase; FDH, formate dehydrogenase; DHFR-TS1, bifunctional dihydrofolate reductase-thymidylate synthase; MTHFR, methylene-THF reductase; MS, methionine synthase; AdoHycH, *S*-adenosyl-*L*-homocysteine hydrolase; SAM-MT, *S*-adenosyl-*L*-methionine dependent methyltransferase; SAMT1, *S*-adenosyl-*L*-methionine transporter 1; FBT1, folate-biopterin transporter 1; FOL1T, folate transporter 1.

Open questions on one carbon metabolism in plants

Since the transport of C_1 folates across biological membranes is unlikely, the distribution of folates and THF within the plant cell is a pressing question (Cybulski and Fisher, 1981). So far, the transporter for plastidial THF import was identified, but the mitochondrial counterpart remains be discovered (Bedhomme et al., 2005; Hanson and Gregory, 2011). If the mitochondrial carrier A BOUT DE SOUFFLE is directly involved in C_1 metabolism to sustain mitochondrial glutamate levels and the polyglutamylated THF pool to drive the photorespiratory GDC/SHM1 reactions remains to be proven (Eisenhut et al., 2013; Porcelli et al., 2018). Further, the role of vacuolar THF transport and polyglutamyl-tail cleavage by ɣ-glutamyl hydrolase in maintaining cellular folate homeostasis remains to be fully understood (Raichaudhuri et al., 2009; Akhtar et al., 2010).

In addition, the origin, cellular/organellar pool sizes and the role of formate in C_1 metabolism need to be understood (Igamberdiev et al., 1999). Although, formate is used

as a C_1 source for 5,10-methylene-THF production, the existence of SHM isoforms in the cytosol, mitochondria, plastid and nucleus, remain the possibility of 5,10-methylene-THF production by serine catabolism (Zhang et al., 2010). In mammalian cells, the serine/formate shuttle between cellular compartments adjusts C_1 metabolic fluxes according to the redox state (Ducker et al., 2016; Ducker and Rabinowitz, 2017; Morscher et al., 2018; Zheng et al., 2018). In comparison in plant cells, mitochondria are also considered the hub of cellular C_1 metabolism, an hypothesis reasoned by lethality of *gldp1gldp2*, *gldt* and *shm1shm2* loss-of-function mutants (Engel et al., 2007; Engel et al., 2011; Timm et al., 2017). However, the underlying C_1 fluxes in plants likely differ between photosynthesizing and heterotrophic tissue and one could only assume a serine/formate shuttle like in mammalian cells (Zhang et al., 2010; Engel et al., 2011; Nunes-Nesi et al., 2014, see for details Manuscript III in this thesis).

Plant synthetic biology

The rising field of plant synthetic biology (SynBio) will contribute to fundamental and applied plant science (Wurtzel et al., 2019; Patron, 2020; Roell and Zurbriggen, 2020). Various definitions of SynBio share the common syntax of applying engineering principles to a biological system at the DNA level (Arkin et al., 2009). Based on established modular genetic parts and tools, synthetic systems were developed to modulate gene expression, using synthetic promoters, optogenetic systems and genetic switches (Sarrion-Perdigones et al., 2011; Engler et al., 2014; Müller et al., 2014; Patron et al., 2015; Chatelle et al., 2018; Andres et al., 2019; Belcher et al., 2020; Cai et al., 2020; Ochoa-Fernandez et al., 2020). Combining established SynBio tools with the expanding repertoire of genome editing is essential to engineer multigenic traits in plants (Schindele et al., 2019; Anzalone et al., 2020; Gaillochet et al., 2020).

Improving the photosynthetic carbon use efficiency

Applied plant science aims to close the yield gap but yield remains a complex trait (Weber and Bar-Even, 2019). The interception efficiency (ability to harvest the light), the partitioning index (the biomass portion in the harvestable part of the plant) and the conversion efficiency - the conversion of light into biomass are deterministic factors of agricultural yield (Long et al., 2015; Weber and Bar-Even, 2019). In modern cultivars the conversion efficiency only reaches 20% of its theoretical potential - 0.02 vs 0.1 in C3 plants and 0.13 in C4 plants- and is considered an approachable engineering target to improve yield and meet the global food demands (Zhu et al., 2008; Zhu et al., 2010; Tilman et al., 2011; Tilman and Clark, 2014; Ort et al., 2015; Clark and Tilman, 2017). Optimizing the

capacity of linear photosynthetic electron flux by an accelerated recovery from photoprotection and faster D1 protein synthesis improved plant growth under field conditions (Kromdijk et al., 2016; Chen et al., 2020). However, constraints on photosynthetic carbon metabolism limit the use of ATP and NADPH produced by the light reactions (Long et al., 2015). Based on computational modeling a higher investment in the CBBC enzyme seduheptulose-1,7-bisphosphatase was hypothesized to accelerate RuBP regeneration and photosynthetic carbon assimilation (Zhu et al., 2007). Overexpression of the cyanobacterial bifunctional enzyme fructose-1,6-bisphosphatase/sedoheptulose-1,7-bisphosphatase increased biomass yield under field conditions (Lopez-Calcagno et al., 2020). Further, combining accelerated photosynthetic electron transport by expression of the red algae cytochrome c_6 and increased capacity of RuBP regeneration by sedoheptulose-1,7-bisphosphatase overexpression caused an additive positive effect on biomass yield (Lopez-Calcagno et al., 2020).

The before mentioned issue of photorespiratory CO_2 loss lowers the photosynthetic carbon use efficiency. Therefore, photorespiration has gained much attention for crop improvement and overcoming rate-limiting steps of canonical photorespiration by overexpression of the GDLH or GLDL subunit seems a valuable approach to increase biomass (Timm et al., 2012; Timm et al., 2015; Lopez-Calcagno et al., 2019). In general, bacterial 2-phosphoglycolate salvage pathways are well-suited as metabolic bypasses of plant photorespiration (Eisenhut et al., 2008; Claassens et al., 2020). In a pioneering study, the implementation of the bacterial glycerate pathway in Arabidopsis was the first bypass of plant photorespiration, followed by engineering a plastidial malate cycle (Kebeish et al., 2007; Maier et al., 2012). Both pathways share the oxidation of glycolate and release either one (glycerate pathway) or two CO_2 molecules (malate cycle) per glycolate in the chloroplast to enrich CO_2 around Rubisco (Kebeish et al., 2007; Maier et al., 2012). The use of *the Chlamydomonas reinhardtii* glycolate dehydrogenase in the malate cycle in combination with flux optimization by transcriptional repression of *PLGG1*, resulted in a 24% biomass yield increase in field grown tobacco (South et al., 2019). Finally, the third bacterial route of glycolate metabolization via oxalate decarboxylation improved biomass yield in field grown rice plants (Shen et al., 2019). Although, all photorespiratory bypasses positively influenced plant growth and biomass, the underlying metabolic reasons remain to be clarified and are controversially discussed (Weber and Bar-Even, 2019; Sharkey, 2020).

A rational approach to circumvent photorespiration is to increase the carboxylation- or reduce the oxygenation reaction of Rubisco (Ort et al., 2015). The renaissance of Rubisco research in the last years holds the promise of creating a version with improved

carboxylation efficiency, although the phylogenetic and catalytic constrains of earth's most abundant enzyme are still under debate (Flamholz et al., 2019). A key in Rubisco engineering is to combine the aspects of the historical evolution of the enzyme, a cross-kingdom analysis of its kinetic parameters as well as bacterial and plant screening systems to assemble and test different Rubisco variants (Lin et al., 2014; Flamholz et al., 2019; Banda et al., 2020; Davidi et al., 2020; Flamholz and Shih, 2020; Gunn et al., 2020; Martin-Avila et al., 2020).

As an alternative, carbon concentrating mechanisms (CCM) are a natural strategy to enrich CO_2 at the site of Rubisco, reduce the oxygenation reaction and improve the water use efficiency of plants (Weber and Bar-Even, 2019). C4 photosynthesis – the spatial separation of CO_2 prefixation by PEPC in mesophyll- and the decarboxylation of the C4 acid malate in bundle sheath cells at the site of Rubisco has gained much attention for implementation in C3 crops (Ermakova et al., 2020). A major achievement includes the cell-specific reconstruction of a minimal biochemical C4 cycle in rice and CO_2 fixation via this path (Lin et al., 2020). A single cell CCM alternative are cyanobacterial carboxysomes and algal pyrenoids, that encapsulate Rubisco and enrich CO_2 by carbonic anhydrases and bicarbonate/CO_2 transporter (Kerfeld et al., 2018; Hennacy and Jonikas, 2020). Plant yield is predicted to improve up to 60% by a cyanobacterial CCM (McGrath and Long, 2014) and the implementation of a Rubisco containing α-carboxysome in tobacco was the first step to achieve this goal (Long et al., 2018). The algal pyrenoid is a eukaryotic alternative to the cyanobacterial CCM (Hennacy and Jonikas, 2020). Several breakthroughs contribute to the understanding of form and function of the pyrenoid and highlight the role of the Rubisco linking protein Essential Pyrenoid Component 1, as critical component for formation of the highly dynamic pyrenoid structure (Mackinder et al., 2016; Freeman Rosenzweig et al., 2017; Mackinder et al., 2017; Li et al., 2019).

Synthetic CO_2 fixation

The accelerating pace in the SynBio field enables the design of new-to-nature solutions for CO_2 fixation exemplified by engineering the canonical CBBC in *E. coli* to produce all carbon biomass from CO_2 (Bar-Even et al., 2012; Antonovsky et al., 2016; Gleizer et al., 2019). Further, C_1 compounds like methanol and formate are efficient electron carriers to combine the CO_2 reduction by renewable energy sources with microbial biological utilization for industriell relevant product generation (Yishai et al., 2017; Claassens et al., 2019; Kim et al., 2020; Satanowski and Bar-Even, 2020). Additionally, the advances in protein engineering enable to design novel biochemical reactions including new-to-nature chemistry (Erb and Zarzycki, 2016; Erb et al., 2017; Erb, 2019). Mix-and-match of novel

reactions with existing biochemistry sets the basis for synthetic CO_2 fixation by the crotonyl-coenzyme A (CoA)/ethylmalonyl-CoA/hydroxybutyryl-CoA (CETCH) cycle (Schwander et al., 2016). Construction of a chloroplast mimic with light-empowered CO_2 fixation via the CETCH cycle now paves the way for CBBC-independent CO_2 fixation (Schwander et al., 2016; Miller et al., 2020).

Outlook

Optimizing photorespiration promises increased plant growth and yield (Ort et al., 2015; Hagemann and Bauwe, 2016; Bar-Even, 2018; Weber and Bar-Even, 2019). The aim of this thesis is to test and analyze the consequences of carbon-neutral and energy efficient photorespiratory bypasses on plant metabolism and growth. We aim to use the recently discovered ß-hydroxyaspartate cycle (Schada von Borzyskowski et al., 2019) as driving force of a photorespiration dependent synthetic C4 photosynthesis cycle in plants (Manuscript I). Further, based on the current understanding of C_1 metabolism in plants, we establish a C_1 based bypass that should facilitate carbon neutral photorespiration (Manuscript II). In addition, we characterized the mitochondrial formate dehydrogenase at the interface of mitochondrial and cytosolic C_1 metabolism (Manuscript III).

Literature cited

Akhtar TA, Orsomando G, Mehrshahi P, Lara-Núñez A, Bennett MJ, Gregory JF, Hanson AD (2010) A central role for gamma-glutamyl hydrolases in plant folate homeostasis. Plant J **64**: 256–266

Anderson LE (1971) Chloroplast and cytoplasmic enzymes II. Pea leaf triose phosphate isomerases. Biochimica et Biophysica Acta (BBA) - Bioenergetics **235**: 237–244

Andres J, Blomeier T, Zurbriggen MD (2019) Synthetic switches and regulatory circuits in plants. Plant Physiol **179**: 862–884

Antonovsky N, Gleizer S, Noor E, Zohar Y, Herz E, Barenholz U, Zelcbuch L, Amram S, Wides A, Tepper N, et al (2016) Sugar synthesis from CO_2 in *Escherichia coli*. Cell **166**: 115–125

Anzalone AV, Koblan LW, Liu DR (2020) Genome editing with CRISPR–Cas nucleases, base editors, transposases and prime editors. Nat Biotechnol **7**: 824-844

Arkin A, Berry D, Church G, Arnold F, Boldt J, Müller O, Ellington AD, Endy D, Fussenegger M, Gold ER, et al (2009) What's in a name? Nat Biotechnol **27**: 1071–1073

Banda DM, Pereira JH, Liu AK, Orr DJ, Hammel M, He C, Parry MAJ, Carmo-Silva E, Adams PD, Banfield JF, et al (2020) Novel bacterial clade reveals origin of form I Rubisco. Nat Plants **6**: 1158–1166

Bar-Even A (2018) Daring metabolic designs for enhanced plant carbon fixation. Plant Science **273**: 71–83

Bar-Even A, Noor E, Milo R (2012) A survey of carbon fixation pathways through a quantitative lens. J Exp Bot **63**: 2325–2342

Bar-On YM, Milo R (2019) The global mass and average rate of rubisco. Proc Natl Acad Sci USA **116**: 4738–4743

Bassham JA, Benson AA, Kay LD, Harris AZ, Wilson AT, Calvin M (1954) The path of carbon in photosynthesis. XXI. The cyclic regeneration of carbon dioxide acceptor. J Am Chem Soc **76**: 1760–1770

Bauwe H (2003) Genetic manipulation of glycine decarboxylation. J Exp Bot **54**: 1523–1535

Bedhomme M, Hoffmann M, McCarthy EA, Gambonnet B, Moran RG, Rébeillé F, Ravanel S (2005) Folate metabolism in plants: An Arabidopsis homolog of the mammalian mitochondrial folate transporter mediates folate import into chloroplasts. J Biol Chem **280**: 34823–34831

Belcher MS, Vuu KM, Zhou A, Mansoori N, Agosto Ramos A, Thompson MG, Scheller HV, Loque D, Shih PM (2020) Design of orthogonal regulatory systems for modulating gene expression in plants. Nat Chem Biol **8**: 857-865

Benson AA (2010) Last days in the old radiation laboratory, Berkeley, California, 1954. Photosyn Res **105**: 209–212

Bloom AJ (2015) Photorespiration and nitrate assimilation: A major intersection between plant carbon and nitrogen. Photosyn Res **123**: 117–128

Boldt R, Edner C, Kolukisaoglu Ü, Hagemann M, Weckwerth W, Wienkoop S, Morgenthal K, Bauwe H (2005) D-GLYCERATE 3-KINASE, the last unknown enzyme in the photorespiratory cycle in Arabidopsis, belongs to a novel kinase family. Plant Cell **17**: 2413–2420

Bouvier F, Linka N, Isner J-C, Mutterer J, Weber APM, Camara B (2006) Arabidopsis SAMT1 defines a plastid transporter regulating plastid biogenesis and plant development. Plant Cell **18**: 3088–3105

Bowes G, Ogren WL, Hageman RH (1971) Phosphoglycolate production catalyzed by ribulose diphosphate carboxylase. Biochem Biophys Res Commun **45**: 716–722

Busch FA (2020) Photorespiration in the context of Rubisco biochemistry, CO_2 diffusion and metabolism. Plant J **101**: 919–939

Busch FA, Sage TL, Cousins AB, Sage RF (2013) C3 plants enhance rates of photosynthesis by reassimilating photorespired and respired CO_2. Plant Cell Environ **36**: 200–212

Cai Y-M, Kallam K, Tidd H, Gendarini G, Salzman A, Patron NJ (2020) Rational design of minimal synthetic promoters for plants. Nucleic Acids Res. doi: 10.1093/nar/gkaa682

Cardona T, Shao S, Nixon PJ (2018) Enhancing photosynthesis in plants: the light reactions. Essays Biochem **62**: 85–94

Chatelle C, Ochoa-Fernandez R, Engesser R, Schneider N, Beyer HM, Jones AR, Timmer J, Zurbriggen MD, Weber W (2018) A green-light-responsive system for the control of transgene expression in mammalian and plant cells. ACS Synth Biol **7**: 1349–1358

Chen J-H, Chen S-T, He N-Y, Wang Q-L, Zhao Y, Gao W, Guo F-Q (2020) Nuclear-encoded synthesis of the D1 subunit of photosystem II increases photosynthetic efficiency and crop yield. Nat Plants **98**: 541–11

Claassens NJ, Cotton CAR, Kopljar D, Bar-Even A (2019) Making quantitative sense of electromicrobial production. Nat Catal **2**: 437–447

Claassens NJ, Scarinci G, Fischer A, Flamholz AI, Newell W, Frielingsdorf S, Lenz O, Bar-Even A (2020) Phosphoglycolate salvage in a chemolithoautotroph using the Calvin cycle. Proc Natl Acad Sci USA **50**: 202012288

Clark M, Tilman D (2017) Comparative analysis of environmental impacts of agricultural production systems, agricultural input efficiency, and food choice. Environmental Research Letters **12**: 064016

Collakova E, Goyer A, Naponelli V, Krassovskaya I, Gregory JF, Hanson AD, Shachar-Hilla Y (2008) Arabidopsis 10-formyl tetrahydrofolate deformylases are essential for photorespiration. Plant Cell **20**: 1818–1832

Coschigano KT, Melo-Oliveira R, Lim J, Coruzzi GM (1998) Arabidopsis *gls* mutants and distinct Fd-GOGAT genes: Implications for photorespiration and primary nitrogen assimilation. Plant Cell **10**: 741–752

Cousins AB, Pracharoenwattana I, Zhou W, Smith SM, Badger MR (2008) Peroxisomal malate dehydrogenase is not essential for photorespiration in Arabidopsis but its absence causes an increase in the stoichiometry of photorespiratory CO_2 release. Plant Physiol **148**: 786–795

Cybulski RL, Fisher RR (1981) Uptake of oxidized folates by rat liver mitochondria. Biochim Biophys Acta **646**: 329–333

Davidi D, Shamshoum M, Guo Z, Bar-On YM, Prywes N, Oz A, Jablonska J, Flamholz A, Wernick DG, Antonovsky N, et al (2020) Highly active rubiscos discovered by systematic interrogation of natural sequence diversity. EMBO J **39**: e104081

Dellero Y, Jossier M, Glab N, Oury C, Tcherkez G, Hodges M (2016) Decreased glycolate oxidase activity leads to altered carbon allocation and leaf senescence after a transfer from high CO_2 to ambient air in *Arabidopsis thaliana*. J Exp Bot **67**: 3149–3163

Dellero Y, Lamothe-Sibold M, Jossier M, Hodges M (2015) *Arabidopsis thaliana ggt1* photorespiratory mutants maintain leaf carbon/nitrogen balance by reducing RuBisCO content and plant growth. Plant J **83**: 1005–1018

Douce R, Bourguignon J, Neuburger M, Rébeillé F (2001) The glycine decarboxylase system: a fascinating complex. Trends Plant Sci **6**: 167–176

Ducker GS, Chen L, Morscher RJ, Ghergurovich JM, Esposito M, Teng X, Kang Y, Rabinowitz JD (2016) Reversal of cytosolic one-carbon flux compensates for loss of the mitochondrial folate pathway. Cell Metab **23**: 1140–1153

Ducker GS, Rabinowitz JD (2017) One-carbon metabolism in health and disease. Cell Metab **25**: 27–42

Ehlers I, Augusti A, Betson TR, Nilsson MB, Marshall JD, Schleucher J (2015) Detecting long-term metabolic shifts using isotopomers: CO_2-driven suppression of photorespiration in C3 plants over the 20th century. Proc Natl Acad Sci USA **112**: 15585–15590

Eisenhut M, Planchais S, Cabassa C, Guivarc'h A, Justin A-M, Taconnat L, Renou J-P, Linka M, Gagneul D, Timm S, et al (2013) Arabidopsis A BOUT de SOUFFLE is a putative mitochondrial transporter involved in photorespiratory metabolism and is required for meristem growth at ambient CO_2 levels. Plant J **73**: 836–849

Eisenhut M, Roell M-S, Weber APM (2019) Mechanistic understanding of photorespiration paves the way to a new green revolution. New Phytol **223**: 1762–1769

Eisenhut M, Ruth W, Haimovich M, Bauwe H, Kaplan A, Hagemann M (2008) The photorespiratory glycolate metabolism is essential for cyanobacteria and might have been conveyed endosymbiontically to plants. Proc Natl Acad Sci USA **105**: 17199–17204

Engel N, Ewald R, Gupta KJ, Zrenner R, Hagemann M, Bauwe H (2011) The presequence of Arabidopsis serine hydroxymethyltransferase SHM2 selectively prevents import into mesophyll mitochondria. Plant Physiol **157**: 1711–1720

Engel N, Van Den Daele K, Kolukisaoglu Ü, Morgenthal K, Weckwerth W, Pärnik T, Keerberg O, Bauwe H (2007) Deletion of glycine decarboxylase in Arabidopsis is lethal under nonphotorespiratory conditions. Plant Physiol **144**: 1328–1335

Engler C, Youles M, Gruetzner R, Ehnert T-M, Werner S, Jones JDG, Patron NJ, Marillonnet S (2014) A golden gate modular cloning toolbox for plants. ACS Synth Biol **3**: 839–843

Erb TJ (2019) Back to the future: Why we need enzymology to build a synthetic metabolism of the future. Beilstein J Org Chem **15**: 551–557

Erb TJ, Jones PR, Bar-Even A (2017) Synthetic metabolism: metabolic engineering meets enzyme design. Current Opinion in Chemical Biology **37**: 56–62

Erb TJ, Zarzycki J (2016) Biochemical and synthetic biology approaches to improve photosynthetic CO_2-fixation. Current Opinion in Chemical Biology **34**: 72–79

Ermakova M, Danila FR, Furbank RT, Caemmerer von S (2020) On the road to C4 rice: advances and perspectives. Plant J **101**: 940–950

Flamholz A, Shih PM (2020) Cell biology of photosynthesis over geologic time. Curr Biol **30**: R490–R494

Flamholz AI, Prywes N, Moran U, Davidi D, Bar-On YM, Oltrogge LM, Alves R, Savage D, Milo R (2019) Revisiting trade-offs between Rubisco kinetic parameters. Biochemistry **58**: 3365–3376

Flügel F, Timm S, Arrivault S, Florian A, Stitt M, Fernie AR, Bauwe H (2017) The photorespiratory metabolite 2-phosphoglycolate regulates photosynthesis and starch accumulation in Arabidopsis. Plant Cell **29**: 2537–2551

Freeman Rosenzweig ES, Xu B, Kuhn Cuellar L, Martinez-Sanchez A, Schaffer M, Strauss M, Cartwright HN, Ronceray P, Plitzko JM, Förster F, et al (2017) The eukaryotic CO_2-concentrating organelle is liquid-like and exhibits dynamic reorganization. Cell **171**: 148–162.e19

Gaillochet C, Develtere W, Jacobs TB (2020) CRISPR screens in plants: Approaches, guidelines, and future prospects. Plant Cell. doi: 10.1105/tpc.20.00463

Gardeström P, Wigge B (1988) Influence of photorespiration on ATP/ADP ratios in the chloroplasts, mitochondria, and cytosol, studied by rapid fractionation of barley (*Hordeum vulgare*) protoplasts. Plant Physiol **88**: 69–76

Gleizer S, Ben-Nissan R, Bar-On YM, Antonovsky N, Noor E, Zohar Y, Jona G, Krieger E, Shamshoum M, Bar-Even A, et al (2019) Conversion of *Escherichia coli* to generate all biomass carbon from CO_2. Cell **179**: 1255–1263.e12

Gorelova V, De Lepeleire J, Van Daele J, Pluim D, Meï C, Cuypers A, Leroux O, Rébeillé F, Schellens JHM, Blancquaert D, et al (2017) Dihydrofolate reductase/thymidylate synthase fine-tunes the folate status and controls redox homeostasis in plants. Plant Cell **29**: 2831–2853

Goyer A, Collakova E, Díaz de la Garza R, Quinlivan EP, Williamson J, Gregory JF, Shachar-Hill Y, Hanson AD (2005) 5-Formyltetrahydrofolate is an inhibitory but well tolerated metabolite in Arabidopsis leaves. J Biol Chem **280**: 26137–26142

Groth M, Moissiard G, Wirtz M, Wang H, Garcia-Salinas C, Ramos-Parra PA, Bischof S, Feng S, Cokus SJ, John A, et al (2016) MTHFD1 controls DNA methylation in Arabidopsis. Nat Commun **7**: 11640

Gunn LH, Martin-Avila E, Birch R, Whitney SM (2020) The dependency of red Rubisco on its cognate activase for enhancing plant photosynthesis and growth. Proc Natl Acad Sci USA. doi: 10.1073/pnas.2011641117

Hagemann M, Bauwe H (2016) Photorespiration and the potential to improve photosynthesis. Current Opinion in Chemical Biology **35**: 109–116

Hanson AD, Gage DA, Shachar-Hill Y (2000) Plant one-carbon metabolism and its engineering. Trends Plant Sci **5**: 206–213

Hanson AD, Gregory JF (2011) Folate biosynthesis, turnover, and transport in plants. Annu Rev Plant Biol **62**: 105–125

Hanson AD, Roje S (2001) One-carbon metabolism in higher plants. Annu Rev Plant Physiol **52**: 119–137

Hennacy JH, Jonikas MC (2020) Prospects for engineering biophysical CO_2 concentrating mechanisms into land plants to enhance yields. Annu Rev Plant Biol **71**: 461–485

Huang W, Hu H, Zhang S-B (2015) Photorespiration plays an important role in the regulation of photosynthetic electron flow under fluctuating light in tobacco plants grown under full sunlight. Front Plant Sci **6**: 621

Igamberdiev AU, Bykova NV, Kleczkowski LA (1999) Origins and metabolism of formate in higher plants. Plant Physiol Biochem **37**: 503–513

Kebeish R, Niessen M, Thiruveedhi K, Bari R, Hirsch H-J, Rosenkranz R, Stäbler N, Schönfeld B, Kreuzaler F, Peterhänsel C (2007) Chloroplastic photorespiratory bypass increases photosynthesis and biomass production in *Arabidopsis thaliana*. Nat Biotechnol **25**: 593–599

Kelly GJ, Latzko E (1976) Inhibition of spinach-leaf phosphofructokinase by 2-phosphoglycollate. FEBS Lett **68**: 55–58

Kerfeld CA, Aussignargues C, Zarzycki J, Cai F, Sutter M (2018) Bacterial microcompartments. Nat Rev Microbiol **16**: 277–290

Kim S, Lindner SN, Aslan S, Yishai O, Wenk S, Schann K, Bar-Even A (2020) Growth of *E. coli* on formate and methanol via the reductive glycine pathway. Nat Chem Biol **332**: 805–8

Kinoshita H, Nagasaki J, Yoshikawa N, Yamamoto A, Takito S, Kawasaki M, Sugiyama T, Miyake H, Weber APM, Taniguchi M (2011) The chloroplastic 2-oxoglutarate/malate transporter has dual function as the malate valve and in carbon/nitrogen metabolism. Plant J **65**: 15–26

Kramer DM, Avenson TJ, Edwards GE (2004) Dynamic flexibility in the light reactions of photosynthesis governed by both electron and proton transfer reactions. Trends Plant Sci **9**: 349–357

Kromdijk J, Głowacka K, Leonelli L, Gabilly ST, Iwai M, Niyogi KK, Long SP (2016) Improving photosynthesis and crop productivity by accelerating recovery from photoprotection. Science **354**: 857–861

Kutschera U, Pieruschka R, Farmer S, Berry JA (2020) The Warburg-effects: basic metabolic processes with reference to cancer development and global photosynthesis. Plant Signal Behav **15**: 1776477

Li R, Moore M, King J (2003) Investigating the regulation of one-carbon metabolism in *Arabidopsis thaliana*. Plant Cell Physiol **44**: 233–241

Li X, Patena W, Fauser F, Jinkerson RE, Saroussi S, Meyer MT, Ivanova N, Robertson JM, Yue R, Zhang R, et al (2019) A genome-wide algal mutant library and functional screen identifies genes required for eukaryotic photosynthesis. Nat Genet **51**: 627–635

Liepman AH, Olsen LJ (2001) Peroxisomal alanine: Glyoxylate aminotransferase (AGT1) is a photorespiratory enzyme with multiple substrates in *Arabidopsis thaliana*. Plant J **25**: 487–498

Lin H-C, Arrivault S, Coe RA, Karki S, Covshoff S, Bagunu E, Lunn JE, Stitt M, Furbank RT, Hibberd JM, et al (2020) A partial C4 photosynthetic biochemical pathway in rice. bioRxiv **12**: 128

Lin MT, Occhialini A, Andralojc PJ, Parry MAJ, Hanson MR (2014) A faster Rubisco with potential to increase photosynthesis in crops. Nature **513**: 547–550

Lindén P, Keech O, Stenlund H, Gardeström P, Moritz T (2016) Reduced mitochondrial malate dehydrogenase activity has a strong effect on photorespiratory metabolism as revealed by ^{13}C labelling. J Exp Bot **67**: 3123–3135

Long BM, Hee WY, Sharwood RE, Rae BD, Kaines S, Lim Y-L, Nguyen ND, Massey B, Bala S, Caemmerer von S, et al (2018) Carboxysome encapsulation of the CO_2-fixing enzyme Rubisco in tobacco chloroplasts. Nat Commun **9**: 3570

Long SP, Marshall-Colon A, Zhu X-G (2015) Meeting the global food demand of the future by engineering crop photosynthesis and yield potential. Cell **161**: 56–66

Lopez-Calcagno PE, Brown KL, Simkin AJ, Fisk SJ, Vialet-Chabrand S, Lawson T, Raines CA (2020) Stimulating photosynthetic processes increases productivity and water-use efficiency in the field. Nat Plants **6**: 1054–1063

Lopez-Calcagno PE, Fisk S, Brown KL, Bull SE, South PF, Raines CA (2019) Overexpressing the H-protein of the glycine cleavage system increases biomass yield in glasshouse and field-grown transgenic tobacco plants. Plant Biotechnol J **17**: 141–151

Mackinder LCM, Chen C, Leib RD, Patena W, Blum SR, Rodman M, Ramundo S, Adams CM, Jonikas MC (2017) A spatial interactome reveals the protein organization of the algal CO_2-concentrating mechanism. Cell **171**: 133–147.e14

Mackinder LCM, Meyer MT, Mettler-Altmann T, Chen VK, Mitchell MC, Caspari O, Rosenzweig ESF, Pallesen L, Reeves G, Itakura A, et al (2016) A repeat protein links Rubisco to form the eukaryotic carbon-concentrating organelle. Proc Natl Acad Sci USA **113**: 5958–5963

Maier A, Fahnenstich H, Caemmerer von S, Engqvist MKM, Weber APM, Flügge U-I, Maurino VG (2012) Transgenic introduction of a glycolate oxidative cycle into *A. thaliana* chloroplasts leads to growth improvement. Front Plant Sci **3**: 38

Martin-Avila E, Lim Y-L, Birch R, Dirk LMA, Buck S, Rhodes T, Sharwood RE, Kapralov MV, Whitney SM (2020) Modifying plant photosynthesis and growth via simultaneous chloroplast transformation of Rubisco large and small subunits. Plant Cell **32**: 2898–2916

McGrath JM, Long SP (2014) Can the cyanobacterial carbon-concentrating mechanism increase photosynthesis in crop species? A theoretical analysis. Plant Physiol **164**: 2247–2261

Mehrshahi P, Gonzalez-Jorge S, Akhtar TA, Ward JL, Santoyo-Castelazo A, Marcus SE, Lara-Núñez A, Ravanel S, Hawkins ND, Beale MH, et al (2010) Functional analysis of folate polyglutamylation and its essential role in plant metabolism and development. Plant J **64**: 267–279

Miller TE, Beneyton T, Schwander T, Diehl C, Girault M, McLean R, Chotel T, Claus P, Cortina NS, Baret J-C, et al (2020) Light-powered CO_2 fixation in a chloroplast mimic with natural and synthetic parts. Science **368**: 649–654

Mitchell P (1961) Coupling of phosphorylation to electron and hydrogen transfer by a chemi-osmotic type of mechanism. Nature **191**: 144–148

Modde K, Timm S, Florian A, Michl K, Fernie AR, Bauwe H (2017) High serine:glyoxylate aminotransferase activity lowers leaf daytime serine levels, inducing the phosphoserine pathway in Arabidopsis. J Exp Bot **68**: 643–656

Monné M, Daddabbo L, Gagneul D, Obata T, Hielscher B, Palmieri L, Miniero DV, Fernie AR, Weber APM, Palmieri F (2018) Uncoupling proteins 1 and 2 (UCP1 and UCP2) from *Arabidopsis thaliana* are mitochondrial transporters of aspartate, glutamate, and dicarboxylates. J Biol Chem **293**: 4213–4227

Morscher RJ, Ducker GS, Li SH-J, Mayer JA, Gitai Z, Sperl W, Rabinowitz JD (2018) Mitochondrial translation requires folate-dependent tRNA methylation. Nature **554**: 128–132

Müller K, Siegel D, Rodriguez Jahnke F, Gerrer K, Wend S, Decker EL, Reski R, Weber W, Zurbriggen MD (2014) A red light-controlled synthetic gene expression switch for plant systems. Mol Biosyst **10**: 1679–1688

Nickelsen K (2007) Otto Warburg's first approach to photosynthesis. Photosyn Res **92**: 109–120

Nunes-Nesi A, Florian A, Howden A, Jahnke K, Timm S, Bauwe H, Sweetlove L, Fernie AR (2014) Is there a metabolic requirement for photorespiratory enzyme activities in heterotrophic tissues? Molecular Plant **7**: 248–251

Obata T, Florian A, Timm S, Bauwe H, Fernie AR (2016) On the metabolic interactions of (photo)respiration. J Exp Bot **67**: 3003–3014

Ochoa-Fernandez R, Abel NB, Wieland F-G, Schlegel J, Koch L-A, Miller JB, Engesser R, Giuriani G, Brandl SM, Timmer J, et al (2020) Optogenetic control of gene expression in plants in the presence of ambient white light. Nat Methods **17**: 717–725

Ort DR, Merchant SS, Alric J, Barkan A, Blankenship RE, Bock R, Croce R, Hanson MR, Hibberd JM, Long SP, et al (2015) Redesigning photosynthesis to sustainably meet global food and bioenergy demand. Proc Natl Acad Sci USA **112**: 8529–8536

Patron N, Orzaez D, Marillonnet S, Warzecha H, Matthewman C, Youles M, Raitskin O, Leveau A, Farre G, Rogers C, et al (2015) Standards for plant synthetic biology: a common syntax for exchange of DNA parts. New Phytol **208**: 13–19

Patron NJ (2020) Beyond natural: synthetic expansions of botanical form and function. New Phytol **227**: 295–310

Pick TR, Bräutigam A, Schulz MA, Obata T, Fernie AR, Weber APM (2013) PLGG1, a plastidic glycolate glycerate transporter, is required for photorespiration and defines a unique class of metabolite transporters. Proc Natl Acad Sci USA **110**: 3185–3190

Porcelli V, Vozza A, Calcagnile V, Gorgoglione R, Arrigoni R, Fontanesi F, Marobbio CMT, Castegna A, Palmieri F, Palmieri L (2018) Molecular identification and functional characterization of a novel glutamate transporter in yeast and plant mitochondria. Biochim Biophys Acta Bioenerg **1859**: 1249–1258

Queval G, Issakidis-Bourguet E, Hoeberichts FA, Vandorpe M, Gakière B, Vanacker H, Miginiac-Maslow M, Van Breusegem F, Noctor G (2007) Conditional oxidative stress responses in the Arabidopsis photorespiratory mutant *cat2* demonstrate that redox state is a key modulator of daylength-dependent gene expression, and define photoperiod as a crucial factor in the regulation of H_2O_2-induced cell death. Plant J **52**: 640–657

Rabson R, Tolbert NE, Kearney PC (1962) Formotion of serine and glyceric acid by the glycolate pathway. Archives of Biochemistry and Biophysics **98**: 154–163

Raichaudhuri A, Peng M, Naponelli V, Chen S, Sánchez-Fernández R, Gu H, Gregory JF, Hanson AD, Rea PA (2009) Plant vacuolar ATP-binding cassette transporters that translocate folates and antifolates *in vitro* and contribute to antifolate tolerance *in vivo*. J Biol Chem **284**: 8449–8460

Ravanel S, Block MA, Rippert P, Jabrin S, Curien G, Rébeillé F, Douce R (2004) Methionine metabolism in plants: Chloroplasts are autonomous for *de novo* methionine synthesis and can import S-adenosylmethionine from the cytosol. J Biol Chem **279**: 22548–22557

Ravanel S, Gakiere B, Job D, Douce R (1998) The specific features of methionine biosynthesis and metabolism in plants. Proc Natl Acad Sci USA **95**: 7805–7812

Renné P, Dreßen U, Hebbeker U, Hille D, Flügge U-I, Westhoff P, Weber APM (2003) The Arabidopsis mutant *dct* is deficient in the plastidic glutamate/malate translocator DiT2. Plant J **35**: 316–331

Roell M-S, Zurbriggen MD (2020) The impact of synthetic biology for future agriculture and nutrition. Curr Opin Biotechnol **61**: 102–109

Samuilov S, Brilhaus D, Rademacher N, Flachbart S, Arab L, Alfarraj S, Kuhnert F, Kopriva S, Weber APM, Mettler-Altmann T, et al (2018) The photorespiratory *BOU* gene mutation alters sulfur assimilation and its crosstalk with carbon and nitrogen metabolism in *Arabidopsis thaliana*. Front Plant Sci **871**: 1709

Sarrion-Perdigones A, Falconi EE, Zandalinas SI, Juárez P, Fernández-del-Carmen A, Granell A, Orzaez D (2011) GoldenBraid: an iterative cloning system for standardized assembly of reusable genetic modules. PLoS ONE **6**: e21622

Satanowski A, Bar-Even A (2020) A one-carbon path for fixing CO_2: C_1 compounds, produced by chemical catalysis and upgraded via microbial fermentation, could become key intermediates in the valorization of CO_2 into commodity chemicals. EMBO Reports **21**: e50273

Sauter M, Moffatt B, Saechao MC, Hell R, Wirtz M (2013) Methionine salvage and S-adenosylmethionine: Essential links between sulfur, ethylene and polyamine biosynthesis. Biochemical Journal **451**: 145–154

Schada von Borzyskowski L, Severi F, Krüger K, Hermann L, Gilardet A, Sippel F, Pommerenke B, Claus P, Cortina NS, Glatter T, et al (2019) Marine proteobacteria metabolize glycolate via the ß-hydroxyaspartate cycle. Nature **575**: 500–504

Schindele A, Dorn A, Puchta H (2019) CRISPR/Cas brings plant biology and breeding into the fast lane. Curr Opin Biotechnol **61**: 7–14

Schlueter U, Weber APM (2020) Regulation and Evolution of C4 Photosynthesis. Annu Rev Plant Biol **71**: 183–215

Schwander T, Schada von Borzyskowski L, Burgener S, Cortina NS, Erb TJ (2016) A synthetic pathway for the fixation of carbon dioxide *in vitro*. Science **354**: 900–904

Schwarte S, Bauwe H (2007) Identification of the Photorespiratory 2-Phosphoglycolate Phosphatase, PGLP1, in Arabidopsis. Plant Physiol **144**: 1580–1586

Selinski J, Scheibe R (2019) Malate valves: old shuttles with new perspectives. Plant Biol (Stuttg) **21**: 21–30

Shameer S, Ratcliffe RG, Sweetlove LJ (2019) Leaf energy balance requires mitochondrial respiration and export of chloroplast NADPH in the light. Plant Physiol **180**: 1947–1961

Sharkey TD (2020) Emerging research in plant photosynthesis. Emerg Top Life Sci **4**: 137–150

Sharkey TD (2019) Discovery of the canonical Calvin–Benson cycle. Photosyn Res **140**: 235–252

Shen B-R, Wang L-M, Lin X-L, Yao Z, Xu H-W, Zhu C-H, Teng H-Y, Cui L-L, Liu EE, Zhang J-J, et al (2019) Engineering a new chloroplastic photorespiratory bypass to increase photosynthetic efficiency and productivity in rice. Molecular Plant **12**: 199–214

Simkin AJ, Lopez-Calcagno PE, Raines CA (2019) Feeding the world: improving photosynthetic efficiency for sustainable crop production. J Exp Bot **70**: 1119–1140

Somerville CR (2001) An early Arabidopsis demonstration. Resolving a few issues concerning photorespiration. Plant Physiol **125**: 20–24

Somerville CR, Ogren WL (1981) Photorespiration-deficient mutants of *Arabidopsis thaliana* lacking mitochondrial serine transhydroxymethylase activity. Plant Physiol **67**: 666–671

Song JM, Rabinowitz JC (1993) Function of yeast cytoplasmic C_1-tetrahydrofolate synthase. Proc Natl Acad Sci USA **90**: 2636–2640

South PF, Cavanagh AP, Liu HW, Ort DR (2019) Synthetic glycolate metabolism pathways stimulate crop growth and productivity in the field. Science **363**: eaat9077

South PF, Walker BJ, Cavanagh AP, Rolland V, Badger M, Ort DR (2017) Bile acid sodium symporter BASS6 can transport glycolate and is involved in photorespiratory metabolism in *Arabidopsis thaliana*. Plant Cell **29**: 808–823

Stitt M, Lunn J, Usadel B (2010) Arabidopsis and primary photosynthetic metabolism - More than the icing on the cake. Plant J **61**: 1067–1091

Sweetlove LJ, Lytovchenko A, Morgan M, Nunes-Nesi A, Taylor NL, Baxter CJ, Eickmeier I, Fernie AR (2006) Mitochondrial uncoupling protein is required for efficient photosynthesis. Proc Natl Acad Sci USA **103**: 19587–19592

Tcherkez G, Boex-Fontvieille E, Mahé A, Hodges M (2012) Respiratory carbon fluxes in leaves. Curr Opin Plant Biol **15**: 308–314

Tilman D, Balzer C, Hill J, Befort BL (2011) Global food demand and the sustainable intensification of agriculture. Proc Natl Acad Sci USA **108**: 20260–20264

Tilman D, Clark M (2014) Global diets link environmental sustainability and human health. Nature **515**: 518–522

Timm S, Florian A, Arrivault S, Stitt M, Fernie AR, Bauwe H (2012) Glycine decarboxylase controls photosynthesis and plant growth. FEBS Lett **586**: 3692–3697

Timm S, Florian A, Jahnke K, Nunes-Nesi A, Fernie AR, Bauwe H (2011) The hydroxypyruvate-reducing system in Arabidopsis: Multiple enzymes for the same end. Plant Physiol **155**: 694–705

Timm S, Giese J, Engel N, Wittmiß M, Florian A, Fernie AR, Bauwe H (2017) T-protein is present in large excess over the other proteins of the glycine cleavage system in leaves of Arabidopsis. Planta **301**: 1–11

Timm S, Nunes-Nesi A, Pärnik T, Morgenthal K, Wienkoop S, Keerberg O, Weckwerth W, Kleczkowski LA, Fernie AR, Bauwe H (2008) A cytosolic pathway for the conversion of hydroxypyruvate to glycerate during photorespiration in Arabidopsis. Plant Cell **20**: 2848–2859

Timm S, Wittmiß M, Gamlien S, Ewald R, Florian A, Frank M, Wirtz M, Hell R, Fernie AR, Bauwe H (2015) Mitochondrial dihydrolipoyl dehydrogenase activity shapes photosynthesis and photorespiration of *Arabidopsis thaliana*. Plant Cell **27**: 1968–1984

Tomaz T, Bagard M, Pracharoenwattana I, Lindén P, Lee CP, Carroll AJ, Ströher E, Smith SM, Gardeström P, Millar AH (2010) Mitochondrial malate dehydrogenase lowers leaf respiration and alters photorespiration and plant growth in Arabidopsis. Plant Physiol **154**: 1143–1157

Van Wilder V, De Brouwer V, Loizeau K, Gambonnet B, Albrieux C, Van Der Straeten D, Lambert WE, Douce R, Block MA, Rébeillé F, et al (2009) C_1 metabolism and chlorophyll synthesis: The Mg-protoporphyrin IX methyltransferase activity is dependent on the folate status. New Phytol **182**: 137–145

Voll LM, Jamai A, Renné P, Voll H, McClung CR, Weber APM (2006) The photorespiratory Arabidopsis *shm1* mutant is deficient in SHM1. Plant Physiol **140**: 59–66

Walker BJ, VanLoocke A, Bernacchi CJ, Ort DR (2016) The costs of photorespiration to food production now and in the future. Annu Rev Plant Biol **67**: 107–129

Warburg O (1920) Über die Geschwindigkeit der photochemischen Kohlensäurezersetzung in lebenden Zellen II. Biochemische Zeitschrift **103**: 188–217

Weber APM, Bar-Even A (2019) Update: Improving the efficiency of photosynthetic carbon reactions. Plant Physiol **179**: 803–812

Wigge B, Krömer S, Gardeström P (1993) The redox levels and subcellular distribution of pyridine nucleotides in illuminated barley leaf protoplasts studied by rapid fractionation. Physiol Plant **88**: 10–18

Wittmiß M, Mikkat S, Hagemann M, Bauwe H (2020) Stoichiometry of two plant glycine decarboxylase complexes and comparison with a cyanobacterial glycine cleavage system. Plant J **103**: 801–813

Wurtzel ET, Vickers CE, Hanson AD, Millar AH, Cooper M, Voss-Fels KP, Nikel PI, Erb TJ (2019) Revolutionizing agriculture with synthetic biology. Nat Plants **5**: 1207–1210

Yishai O, Goldbach L, Tenenboim H, Lindner SN, Bar-Even A (2017) Engineered assimilation of exogenous and endogenous formate in *Escherichia coli*. ACS Synth Biol **6**: 1722–1731

Zhang Y, Sun K, Sandoval FJ, Santiago K, Roje S (2010) One-carbon metabolism in plants: characterization of a plastid serine hydroxymethyltransferase. Biochemical Journal **430**: 97–105

Zheng Y, Lin T-Y, Lee G, Paddock MN, Momb J, Cheng Z, Li Q, Fei DL, Stein BD, Ramsamooj S, et al (2018) Mitochondrial one-carbon pathway supports cytosolic folate integrity in cancer cells. Cell **175**: 1546–1560.e17

Zhu X-G, de Sturler E, Long SP (2007) Optimizing the distribution of resources between enzymes of carbon metabolism can dramatically increase photosynthetic rate: A numerical simulation using an evolutionary algorithm. Plant Physiol **145**: 513–526

Zhu X-G, Long SP, Ort DR (2008) What is the maximum efficiency with which photosynthesis can convert solar energy into biomass? Curr Opin Biotechnol **19**: 153–159

Zhu X-G, Long SP, Ort DR (2010) Improving photosynthetic efficiency for greater yield. Annu Rev Plant Biol **61**: 235–261

Zrenner R, Stitt M, Sonnewald U, Boldt R (2006) Pyrimidine and purine biosynthesis and degradation in plants. Annu Rev Plant Biol **57**: 805–836

Manuscripts

Manuscript I

A synthetic C4 shuttle via the ß-hydroxyaspartate cycle in C3 plants

Marc-Sven Roell,[a] Lennart Schada von Borzykowski,[c] Philipp Westhoff,[a,b] Nicole Paczia,[c] Peter Claus,[c] Tobias J. Erb,[c,d] Andreas P.M. Weber [a,b,1]

[a] Institute of Plant Biochemistry, Heinrich Heine University, Düsseldorf, 40225 Germany

[b] Cluster of Excellence on Plant Science (CEPLAS), Heinrich Heine University, Düsseldorf, 40225 Germany

[c] Department of Biochemistry & Synthetic Metabolism, Max Planck Institute for Terrestrial Microbiology, Marburg, 35043 Germany

[d] LOEWE-Center for Synthetic Microbiology, Philipps-University Marburg, Marburg, 35043 Germany

Status: in preparation

Own contribution:

I developed the underlying engineering strategy to implement the ß-hydroxyaspartate cycle in Arabidopsis peroxisomes, including the construct design for localization studies and cycle integration. All generated transgenic lines were established by myself. Further, the localization studies were performed by myself and I jointly with Dr. Lennart Schada von Borzykowski performed the biochemical assays of the ß-hydroxyaspartate cycle enzymes. Further, the metabolomics experiments, including data analysis, and the physiological characterization of all transgenic plant lines was performed by me.

A synthetic C4 shuttle via the ß-hydroxyaspartate cycle in C3 plants

Marc-Sven Roell,[a] Lennart Schada von Borzykowski,[c] Philipp Westhoff,[a,b] Nicole Paczia,[c] Peter Claus,[c] Tobias J. Erb,[c,d] Andreas P.M. Weber [a,b,1]

[a] Institute of Plant Biochemistry, Heinrich Heine University, Düsseldorf, 40225 Germany

[b] Cluster of Excellence on Plant Science (CEPLAS), Heinrich Heine University, Düsseldorf, 40225 Germany

[c] Department of Biochemistry & Synthetic Metabolism, Max Planck Institute for Terrestrial Microbiology, Marburg, 35043 Germany

[d] LOEWE-Center for Synthetic Microbiology, Philipps-University Marburg, Marburg, 35043 Germany

[1] For correspondence (E-mail: andreas.weber@hhu.de)

ORCID-IDs: 0000-0003-2714-8729 (MSR); 0000-0003-2952-4572 (LSvB); 0000-0003-3685-0894 (TJE); 0000-0003-0970-4672 (APMW)

Classification

Biological Science | Plant Biology

Keywords

Plant Synthetic Biology | Photorespiration | Metabolic engineering

Author contributions

M-S.R., L.S.v.B., P.W., T.J.E., A.P.M.W designed research. M-S.R., L.S.v.B., P.W., N.C. N.P. and P.C. performed research. M-S.R., L.S.v.B., P.W., T.J.E., A.P.M.W analyzed data. M-S.R., L.S.v.B., P.W., T.J.E., A.P.M.W wrote the manuscript.

This Manuscript includes:

Main text, 6 figures, supplemental information

Abstract

Plants depend on the enzyme ribulose-1,5-bisphosphate carboxylase/oxygenase (Rubisco) for CO_2 fixation. However, especially in C3 plants, photosynthetic yield is reduced by formation of 2-phosphogyloclate, a toxic oxygenation product of Rubisco, which needs to be recycled in a high flux-demanding metabolic process, called photorespiration. Canonical photorespiration dissipates energy and causes carbon and nitrogen losses. Reducing photorespiration by carbon concentrating mechanisms, such as C4 photosynthesis, or bypassing photorespiration by metabolic engineering is expected to improve plant growth and yield. The ß-hydroxyaspartate cycle (BHAC) is a recently described microbial pathway that converts glyoxylate, a metabolite of plant photorespiration, into oxaloacetate in a highly efficient, carbon-, nitrogen- and energy conserving manner. Here, we engineered a functional BHAC in plant peroxisomes, to create the first photorespiratory bypass that is independent of 3-phosphoglycerate regeneration or decarboxylation of photorespiratory precursors. While efficient oxaloacetate conversion in *Arabidopsis thaliana* still masks the full potential of the BHAC, nitrogen conservation and accumulation of signature C4 metabolites demonstrate the proof-of-principle, opening the way for engineering a photorespiration-dependent synthetic C4 carbon concentrating mechanism in C3 plants.

Introduction

Future agriculture must reconcile sustainability with increased productivity to supply global food demands that will have doubled by 2050 (Tilman et al., 2011; Jones and Sands, 2013). To fulfill this goal, agricultural yields will have to increase annually by 2.4%. However, yields currently plateau at 1% annual increase in all major food crops, including maize, rice and wheat (Ray et al., 2013; Pradhan et al., 2015). In high-yielding crop varieties, both plant architecture and the harvest index - the fraction of total energy in plant biomass contained in the harvestable organs - approach their theoretical limits (Long et al., 2015).

Synthetic biology based approaches are focusing on improving the carbon conversion efficiency of plants that currently only reaches 20% of its theoretical potential (Long et al., 2015; Wurtzel et al., 2019). Synthetic biology applies engineering principles to biological systems and multiple synthetic-biological solutions to improve the carbon conversion efficiency of plants were recently proposed (Weber and Bar-Even, 2019; Wurtzel et al., 2019). These include pathways for improved CO_2 fixation (Rubisco-based and Rubisco-independent), such as the crotonyl-coenzyme A (CoA)/ethylmalonyl-CoA/hydroxybutyryl-

CoA (CETCH) cycle, photorespiratory bypasses, including the Tartonyl-CoA (TaCo) pathway and a modified 3-hydroxypropionate bi-cycle, as well as synthetic carbon concentrating mechanisms (Schwander et al., 2016; Miller et al., 2020; Scheffen et al., 2020). Altogether, these proposed solutions showcase the potential of plant synthetic biology to increase productivity and sustainability of future agriculture beyond the realms of natural evolution (Bar-Even et al., 2010; Weber and Bar-Even, 2019; Roell and Zurbriggen, 2020).

Natural carbon concentrating mechanisms boost carbon fixation by concentrating CO_2 at the site of Rubisco and have independently evolved in cyanobacteria (carboxysomes), green algae (pyrenoids) and plants (C4 photosynthesis and crassulacean acid metabolism; Kerfeld et al., 2018; Weber and Bar-Even, 2019; Hennacy and Jonikas, 2020). In C4 photosynthesis, primary CO_2 fixation is spatially separated from Rubisco. First, CO_2 is captured into a C4 acid via phosphoenolpyruvate carboxylase (PEPC) in mesophyll cells and this C4 acid is then decarboxylated in bundle sheath cells, where Rubisco is located. The increase in the local CO_2 concentration reduces the oxygenation reaction of Rubisco, as well as the subsequent process of photorespiration (Schlueter and Weber, 2020). Consequently, implementation of C4 photosynthesis into C3 plants has received much attention to increase yield in crop plants that suffer from photorespiration (Schuler et al., 2016; Ermakova et al., 2020).

Another target to improve plant growth is photorespiration itself. During natural photorespiration, the Rubisco oxygenation product 2-phosphoglycolate is recycled back into 3-phosphoglycerate. However, natural photorespiration comes with the loss of up to 30% of previously fixed carbon, release of nitrogen and the dissipation of energy, which has led to the engineering of photorespiratory bypasses to mitigate the deleterious effects of photorespiration (Walker et al., 2016; Eisenhut et al., 2019) . In particular glycolate, formed by dephosphorylation of 2-phosphoglycolate, has been considered an ideal starting metabolite for several photorespiratory bypasses (Trudeau et al., 2018; Weber and Bar-Even, 2019). Photorespiratory bypasses that recycle glycolate into 3-phosphoglycerate by the cyanobacterial 'glycerate pathway' or oxidize glycolate in the chloroplast have already shown growth benefits in green-house grown *Arabidopsis thaliana* and tobacco and rice in field experiments (Kebeish et al., 2007; Maier et al., 2012; South et al., 2019; Shen et al., 2019). However, all these bypasses still release CO_2, which limits their efficiency compared to natural photorespiration.

Recently, the ß-hydroxyaspartate cycle (BHAC) was described as primary pathway of glycolate assimilation in marine proteobacteria (Schada von Borzyskowski et al., 2019). In this pathway, glycolate is first oxidized into glyoxylate, which is further converted into oxaloacetate (OAA) in four enzymatic steps (Fig. 1). Notably, the BHAC enables the direct formation of a C4 compound from glycolate, without the loss of carbon and nitrogen, which render the BHAC more efficient than natural photorespiration and all other photorespiration bypasses engineered so far.

Here we demonstrate the implementation of the BHAC in *Arabidopsis thaliana* (Arabidopsis) peroxisomes. We validate activity of the BHAC *in planta* by demonstrating ß-hydroxyaspartate (BHA) formation under photorespiratory conditions. Further, we show improved nitrogen conversation through the BHAC, which results in reduced free ammonia levels compared to natural photorespiration. We also determine the metabolic fate of BHAC-derived OAA and outline a strategy to use BHAC-derived OAA to establish a synthetic C4 cycle in C3 plants. Altogether, our proof-of-principle study demonstrates a novel approach to turn a photorespiratory bypass into a carbon concentrating mechanism. Synergistically coupling photorespiration and C4 metabolism, two of the main targets in primary plant metabolism, thus creates novel opportunities for improved agricultural productivity in the future.

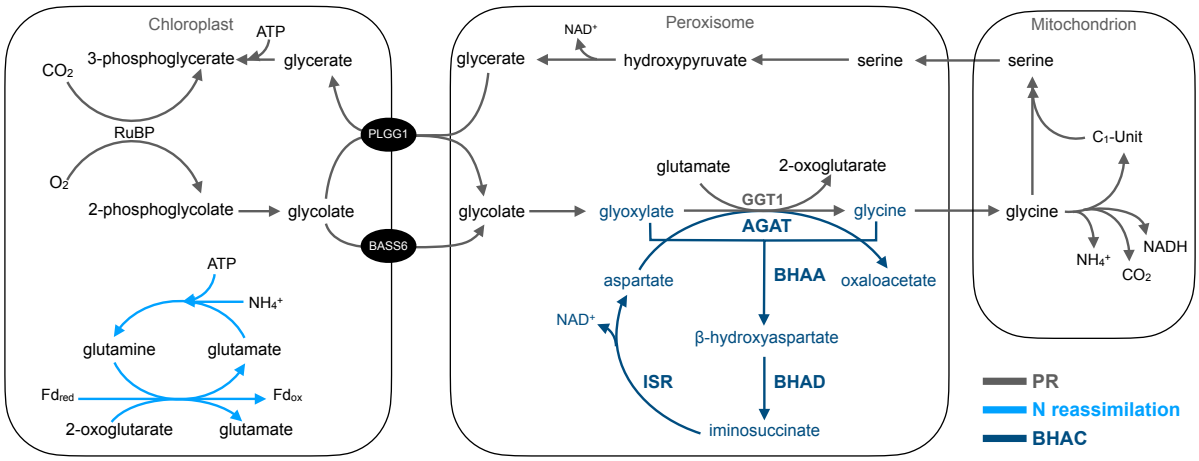

Fig. 1: The BHAC as photorespiratory bypass in plant peroxisomes. Schematic representation of plant photorespiration (PR) and photorespiratory nitrogen (N) reassimilation (light blue) and the BHAC (dark blue). Aspartate:glyolxyate aminotransferase (AGAT), ß-hydroxyaspartate aldolase (BHAA), ß-hydroxyaspartate dehydratase (BHAD), iminosuccinate reductase (ISR), glutamate:glyoxylate aminotransferase (GGT1), ribulose-1,5-bisphosphate (RuBP), plastidial glycolate/glycerate transporter 1 (PLGG1), bile-acid sodium symporter 6 (BASS6).

Results

BHAC implementation in plant peroxisomes

Photorespiratory glycolate is converted to glyoxylate in peroxisomes. Since glyoxylate is the starting substrate of the BHAC, we implemented the BHAC in the peroxisomal matrix. The four BHAC enzymes, aspartate:glyoxylate aminotransferase (AGAT, EC: 2.6.1.35), ß-hydroxyaspartate aldolase (BHAA, EC: 4.1.3.41), ß-hydroxyaspartate dehydratase (BHAD, EC: 4.3.1.20), and iminosuccinate reductase (ISR), were targeted to plant peroxisomes, by fusion of a peroxisomal target signal (PTS). AGAT, BHAD and ISR were C-terminally fused with PTS1 (Lingner et al., 2011). BHAA was fused N-terminally with the peroxisomal target signal 2 from Arabidopsis citrate synthase 3 (At2g42790; Lingner et al., 2011). Peroxisomal localization of the four BHAC enzymes was confirmed by fluorescence co-localization with a peroxisomal marker in *Nicotiana benthamiana* protoplasts (Fig. 2A).

We selected four Arabidopsis photosynthetic promoters (Rubisco small subunit 1B, 2B, 3B and chlorophyll A/B binding protein 1; Dedonder et al., 1993; Mitra et al., 2009) to restrict BHAC enzyme expression to photosynthetic tissue (Supplemental Fig. S1). Further, we hypothesized that reduced conversion of glyoxylate to glycine would enhance metabolic flux through the BHAC. Besides Arabidopsis wild type *Col-0* (WT), we therefore selected the photorespiratory *ggt1-1* mutant as background for BHAC implementation. The *ggt1-1* mutant is deficient in the peroxisomal glutamate glyoxylate aminotransferase 1 (Dellero et al., 2015) and shows a strong photorespiratory phenotype, which allowed us to screen for the function of the BHAC via a convenient visual readout.

Two independent lines each were established in the WT (*Col::BHAC#1* and *#2*) and *ggt1-1* background, respectively (*ggt1-1::BHAC#1* and *#2*, Supplemental Fig. S1), and expression of all four BHAC enzymes in the transgenic lines was verified by immunoblot analysis (Supplemental Fig. S1). We quantified activity of each BHAC enzyme in mature rosette leave extracts of four-weeks-old air grown plants by enzyme activity assays (Fig. 2B and C). AGAT was highest in both WT and *ggt1-1* background compared to BHAA and BHAD activity (Fig. 2B). Iminosuccinate is a labile product formed by BHAD (Schada von Borzyskowski et al., 2019). To demonstrate functional expression of ISR, we therefore quantified the rate of ^{15}N-incorporation into L-aspartate, which confirmed ISR activity in BHAC plants (Fig. 2B). In summary, these experiments confirmed the successful expression of all enzymes *in planta*

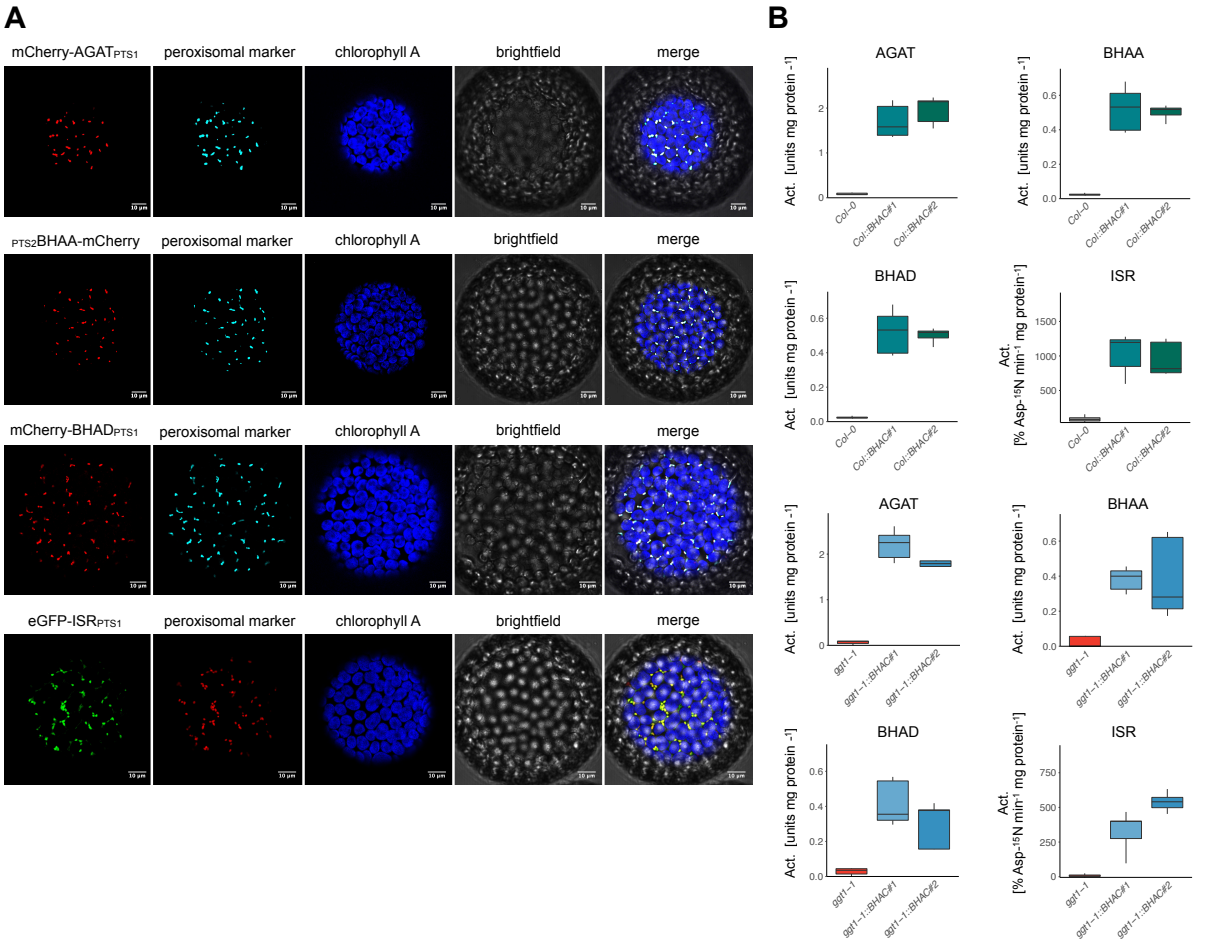

Fig. 2: Peroxisomal targeting and enzyme activity of the BHAC. A) Fluorescent fusion constructs for each BHAC enzyme were co-infiltrated with a peroxisomal marker in *N. benthamiana* leaves and protoplasts were analyzed by confocal microscopy two days post infection. Both, the peroxisomal targeting sequence (subscripted) and the fluorescent fusion protein are indicated based on the protein N- or C-terminal position. Aspartate:glyolxyate aminotransferase (AGAT), ß-hydroxyaspartate aldolase (BHAA), ß-hydroxyaspartate dehydratase (BHAD), iminosuccinate reductase (ISR). Images were analyzed using Fiji. Chlorophyll A autofluorescence: blue, peroxisomal marker: cyan fluorescent protein or mCherry (only for ISR) with C-terminal PTS1. B) BHAC enzyme activity in Arabidopsis mature rosette leave extracts of four-weeks-old air grown plants. n = 3.

Peroxisomal BHAC functions as photorespiratory bypass

Next, we verified that the peroxisomal BHAC functions as photorespiratory bypass by steady-state metabolomics on green tissue of 14 days old seedlings either grown in CO_2 enriched air (3000 ppm CO_2, HC), ambient air (400 ppm CO_2, AC), or shifted from CO_2 enriched to ambient air three days before sampling (Shift, Fig. 3). Our metabolomics analysis included the BHAC intermediates BHA and glycine; malate, produced by reduction of BHAC-derived OAA by peroxisomal NAD-dependent MDH (Cousins et al., 2008), as well as aspartate, which can regarded both as BHAC intermediate and product of OAA transamination (Fig. 3).

BHA is a unique metabolite of the BHAC and not naturally present in Arabidopsis (Fig. 3A-D). We analyzed analytical standards of BHA diastereomers via gas-chromatography time of flight mass spectrometry to annotate BHA according to the electron impact mass spectral fragmentation pattern (Supplemental Fig. S2). As expected, BHA specific fragments were neither detected in WT nor in *ggt1-1* controls under all conditions tested (Fig. 3A and B). In contrast, BHA could be detected in plants carrying the BHAC (Fig. 3A-D). However, relative quantification revealed that BHA was only detectable when plants were grown in ambient air or shifted from CO_2 enriched to ambient air, but not in CO_2 enriched air (Fig. 3C and D). This confirmed function of the BHAC *in planta* and suggested that BHA formation is exclusively linked to photorespiratory conditions.

Glycine levels decreased 2-fold in both *Col::BHAC* lines, which is consistent with glycine conversion into BHA by BHAA under photorespiratory conditions in ambient air (Fig. 3E). In the *ggt1-1* mutant total glycine levels were 10-fold lower compared to WT (Dellero et al., 2015), remained unaltered in *ggt1-1::BHAC#1* and increased 1.2-fold in *ggt1-1::BHAC#2* (Fig. 3E). In line with BHAC activity, aspartate and malate levels were elevated 6- and 2-fold, respectively, in BHAC plants grown in ambient air (Fig. 3E). Together, the formation and accumulation of BHAC-specific metabolites exclusively in photorespiratory conditions demonstrated that the peroxisomal BHAC indeed functions as photorespiratory bypass.

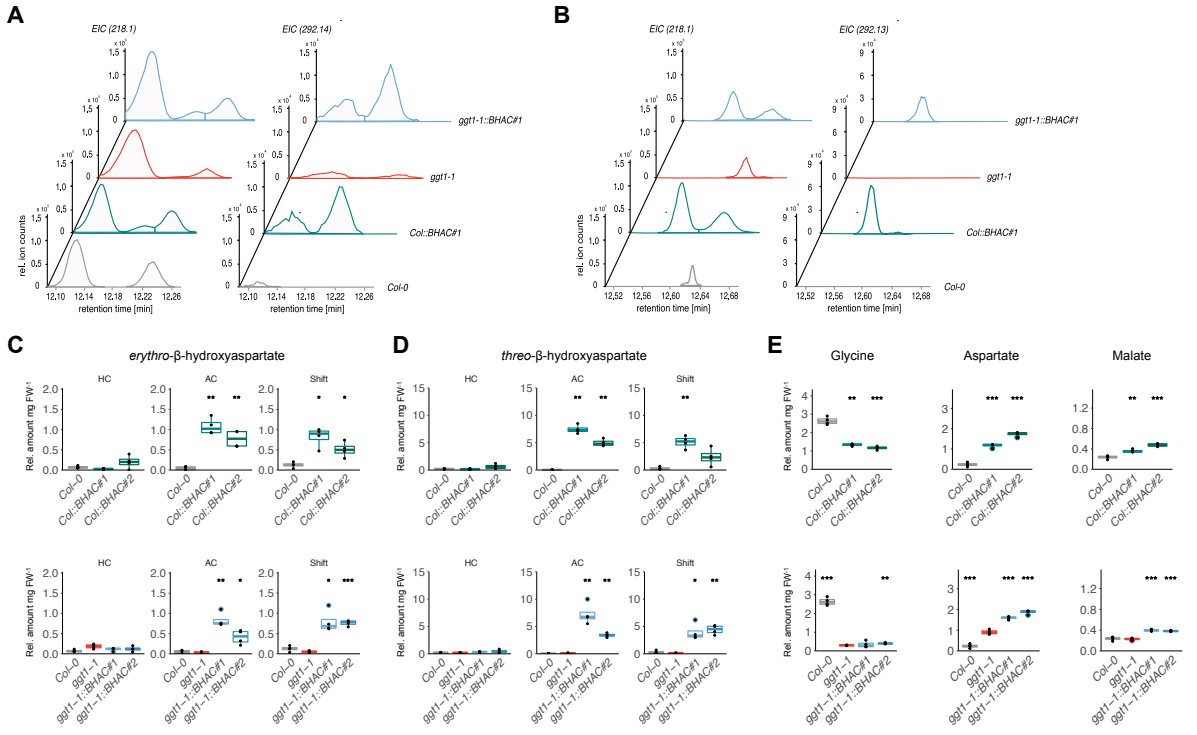

Fig. 3: The BHAC functions as photorespiratory bypass. A and B) Representative extracted ion chromatogram of the ß-hydroxyaspartate specific masses. *In vivo* formation of both diastereomers, *erythro*-ß-hydroxyaspartate (A) and *threo*-ß-hydroxyaspartate (B) is shown in one T-DNA line per background genotype. C and D) Relative metabolite levels per mg fresh weight (FW) of *in vivo erythro*-ß-hydroxyaspartate (C) and *threo*-ß-hydroxyaspartate (D) formation in wild type *Col-0* (top) and *ggt1-1* background (bottom). Green tissue of 14 days old seedlings was harvested in the middle of the light phase. Plants were grown either in CO_2 enriched air (3000 ppm CO_2, HC), ambient air (400 ppm CO_2, AC) or shifted from HC to AC three days prior to harvest (Shift). E) Relative metabolite levels per mg fresh weight (FW) of glycine, aspartate and malate in BHAC plants in wild type *Col-0* (top) and *ggt1-1* background (bottom) grown in AC. Student's *t*-test against background genotype. Shown *Col-0* in bottom panel is same as in top and added for comparative reasons. Asterisks indicate significance after multiple testing correction using Benjamini-Hochberg. $p < 0.05$ = *, < 0.01 = **, < 0.001 = ***. n = 4.

The BHAC reshapes carbon and nitrogen metabolism

To better understand the metabolic implications of the BHAC, we generated metabolite profiles for all four BHAC lines (BHAC plants) and their background genotypes at different CO_2 concentrations (HC, AC, Shift, Supplemental Fig. S3 for WT background and Supplemental Fig. S4 for *ggt1-1* background). Growth condition dependent principle component analysis revealed that the metabolic profiles of BHAC plants are clearly distinct from their background genotypes (Fig. 4A), and that all BHAC plants cluster together, independent of their genetic background under photorespiratory conditions (AC or Shift, Fig. 4A). Notably, we did not observe such clustering of genotypes under HC

(Fig. 4A), which is consistent with the observation that the BHAC is only active under photorespiration.

We further focused on the metabolite profile of BHAC plants in comparison to the WT and *ggt1-1* mutant backgrounds grown under photorespiratory conditions in ambient air (Fig. 4B). In plant photorespiration mitochondrial glycine decarboxylase is the major hub of carbon and nitrogen losses (Eisenhut et al., 2019; Fernie and Bauwe, 2020). Nitrogen conservation by the BHAC is assumed to prevent mitochondrial ammonia release and avoid chloroplastic nitrogen re-assimilation by glutamine synthase. Consequently, cellular free ammonia levels were reduced on average by 20% compared to WT under photorespiratory conditions (Fig. 4C). Further, ambient air-grown BHAC plants accumulated soluble amino acids that are either involved in the urea cycle (glutamate and ornithine) or depend on OAA-derived carbon skeletons (lysine, methionine, Fig. 4B).

Besides peroxisomal reduction to malate, three further routes of OAA assimilation are theoretically possible that are all coupled to the direct export of OAA from the peroxisome (Charton et al., 2019). Cytosolic phosphoenolpyruvate carboxykinase 1 (PCK1) could decarboxylate OAA to phosphoenolpyruvate (PEP; Eastmond et al., 2015). PEP is then used either for gluconeogenesis or converted into pyruvate by pyruvate kinase (PK; Wulfert et al., 2020). The accumulation of pyruvate strongly indicated that the cytosolic PK route is active in BHAC plants and that PEP is not channeled into gluconeogenesis, which was supported by reduced glucose and fructose levels in the same plants (Fig. 4B). In addition to cytosolic decarboxylation, OAA could also be transported into mitochondria, where it could fuel the mitochondrial TCA cycle. Accumulation of citrate in ambient air-grown BHAC plants suggested that this route was also active, eventually in combination with an increased flux of pyruvate into the TCA cycle (Fig. 4B).

To further validate that reshaping of the metabolome in BHAC plants is caused by an active BHAC and not AGAT alone, we complemented the *ggt1-1* mutant with AGAT under control of the chlorophyll A/B binding protein 1 promoter, also used for AGAT expression in *ggt1-1::BHAC* plants (Supplemental Fig. S5). Steady-state metabolomics on plants grown under photorespiratory conditions in ambient air, revealed that AGAT expression was not sufficient to cause the metabolome signature of BHAC plants. Instead AGAT expression restored canonical photorespiration, probably by using aspartate as amino donor for the peroxisomal transamination reaction (Supplemental Fig. S5).

In summary, these experiments showed that the BHAC is active under photorespiratory conditions and reshapes the metabolome in plants by altering nitrogen metabolism (amino

acid accumulation and free ammonia reduction) and OAA utilization in the cytosol and/or mitochondrial TCA cycle.

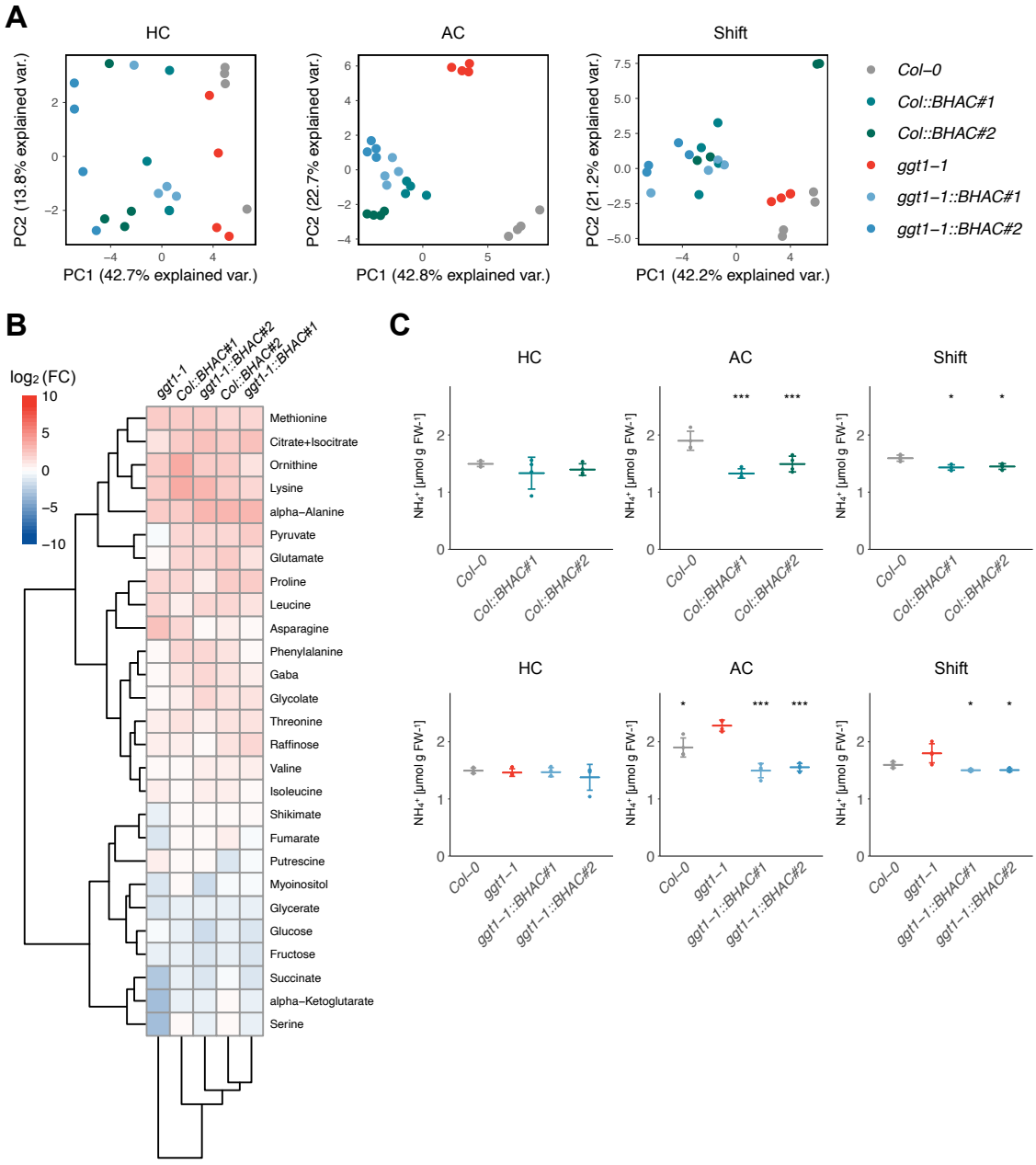

Fig. 4: The BHAC reshapes the plant metabolome. Metabolite profiles were generated using green tissue of 14-days-old seedlings grown either at 3000 ppm CO_2 (HC), 400 ppm CO_2 (AC) or shifted from 3000 ppm CO_2 to 400 ppm CO_2 three days prior to harvest at the middle of the light phase (Shift). A) Principle component analysis. B) Metabolome profiles of AC grown plants. Log2 fold change (FC) was calculated compared to wild type *Col-0* and clustered based on Pearson correlation. C) Quantification of free ammonium in BHAC plants. Shown *Col-0* in bottom panel is same as in top and added for comparative reasons. Student's *t*-test against background genotype. $p < 0.05$ = *, < 0.01 = **, < 0.001 = ***. n = 4, biological replicates measured in technical triplicates.

The BHAC reduces plant growth by impaired photosynthesis in the WT background

Despite carbon and nitrogen conservation by the BHAC, *Col::BHAC* plants are reduced in growth as compared to WT controls in ambient air (Fig. 5A, Supplemental Fig. S6). Rosettes of four-weeks-old air-grown *Col::BHAC* plants are decreased by 70% in area and 50% in diameter (Fig. 5B). However, BHAC implementation in the *ggt1-1* mutant partially suppressed the photorespiratory phenotype of the mutant (Fig. 5C) and growth was comparable to *Col::BHAC* plants (Fig. 5B and D). In CO_2 enriched air, growth of BHAC plants was not altered compared to the background genotype (Fig. 5).

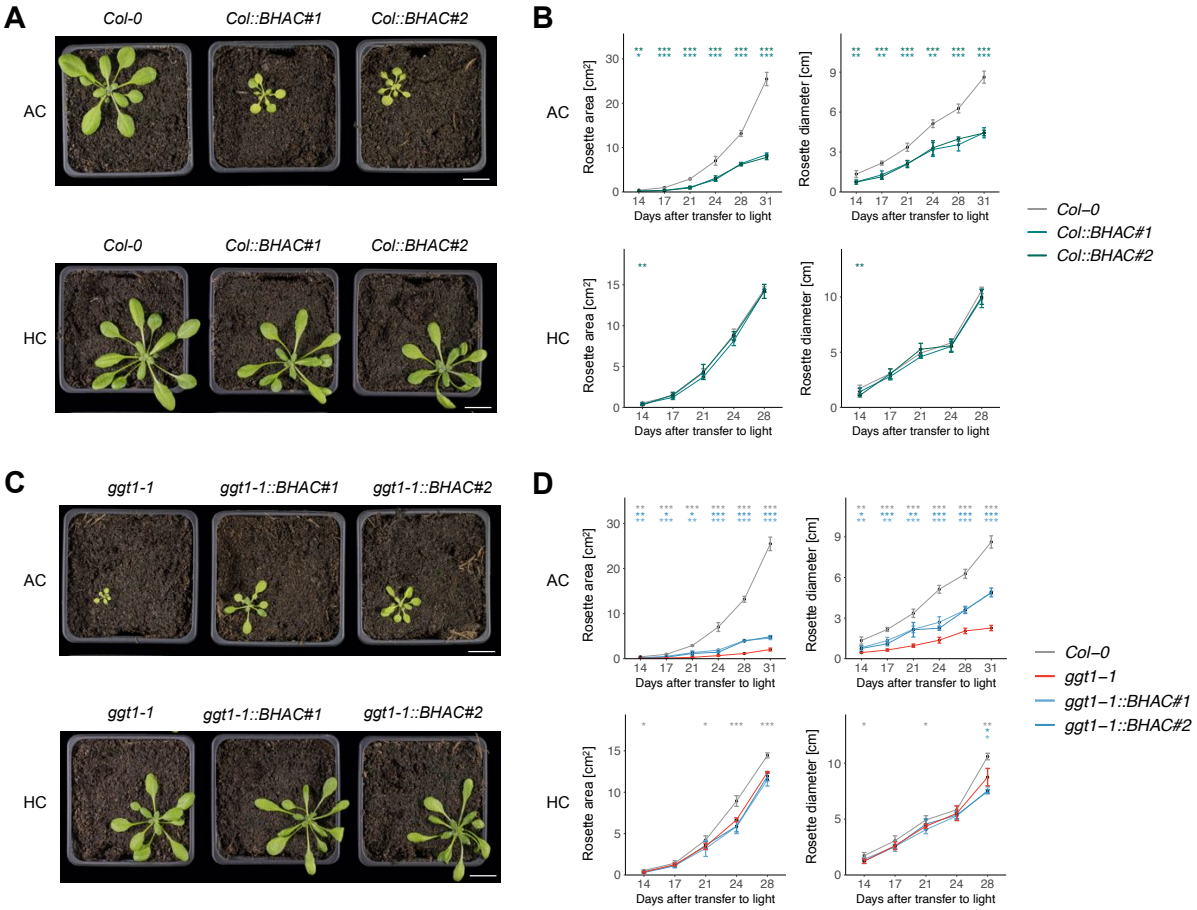

Fig. 5: The BHAC reduces plant growth in air. A and C) Representative images of BHAC plants in wild type *Col-0* (A) or *ggt1-1* mutant (C) background grown in ambient air (400 ppm CO_2, AC) or CO_2 enriched air (3000 ppm CO_2 HC). Images were taken 28 days after transfer to light. scalebar = 2 cm. B & D) Growth of BHAC containing plants in wild type *Col-0* (B) or *ggt1-1* mutant (D) background. Rosette area and rosette diameter were measured over time for plants grown under AC (top) or HC (bottom). Student's *t*-test against background genotype. Colored asterisks represent the significance for the respective genotype. p< 0.05 = *, p < 0.01 =**, < 0.001 = ***. n = 5. Shown *Col-0* in C) and D) is same as in top and added for comparative reasons.

To test if the reduced growth in BHAC plants resulted from affected photosynthesis, we generated A/C_i curves, the rate of CO_2 assimilation (A) in relation to intercellular CO_2 concentration (C_i) under saturating light (1000 µmol s^{-1} m_2^{-2}), by leaf-gas exchange measurements of six-week old ambient air-grown plants (Fig. 6A). Based on the A/C_i curve, we determined the CO_2 compensation point (CCP), a net quotient of zero for photosynthetic CO_2 assimilation and respiratory CO_2 release (Schlueter et al., 2017). *Col::BHAC* plants displayed an increased CCP compared to WT (Fig. 6B). The *ggt1-1* mutant itself had a higher CCP and the BHAC did not significantly alter the CCP in this photorespiratory mutant (Fig. 6B).

Finally, we modelled the A/C_i curves based on the Farquhar, von Cammerer, Berry model of C3 photosynthesis to estimate the maximum rate of Rubisco carboxylation efficiency (V_{cmax}) and maximum electron transport rate (J_{max}; Farquhar et al., 1980). Both V_{cmax} and J_{max} were reduced in *Col::BHAC* plants by 15% and 25% respectively (Fig. 6C). Comparison of Rubisco large subunit abundance by immunoblot analysis revealed no changes in Rubisco content in BHAC plant leaves that could explain the reduced V_{cmax} (Supplemental Fig. S1). Implementation of the BHAC in the *ggt1-1* mutant did not alter V_{cmax} and J_{max} was only reduced in *ggt1-1::BHAC#2* compared to the mutant background, but remained lower compared to WT (Fig. 6C).

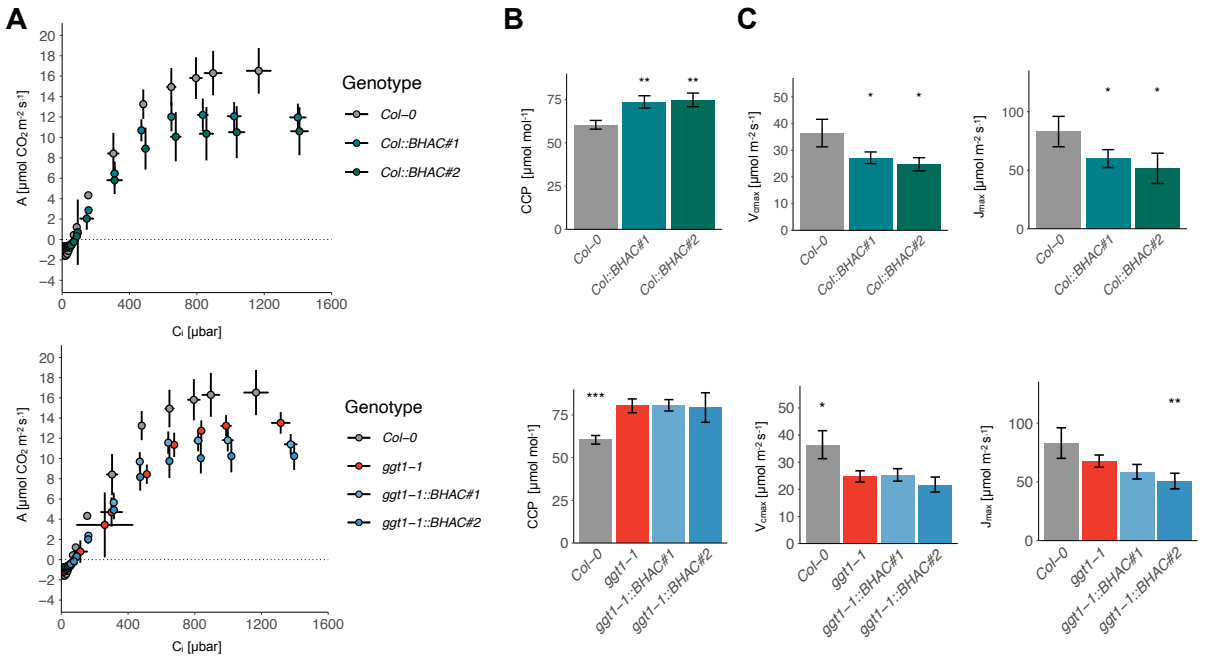

Fig. 6: Photosynthesis is impaired in BHAC plants. A) CO_2 assimilation based on intracellular CO_2 concentration (C_i) for BHAC plants in wild type *Col-0* (left) and *ggt1-1* background (right). Shown mean ± SD. n = 4 per genotype. B) Calculated CO_2 compensation point (CCP) from the A-Ci curves (A) for BHAC plants in wild type *Col-0* (top) and *ggt1-1* background (bottom). C) Maximum rate of Rubisco carboxylation (V_{cmax}) and maximum rate of electron transport (J_{max}) for BHAC plants in wild type *Col-0* (top) and *ggt1-1* background (background) modeled using the Farquhar, von Caemmerer, Berry model of C3 photosynthesis (Farquhar et al., 1980). Student's *t*-test against background genotype. p < 0.05 = *, < 0.01 = **, < 0.001 = ***. Shown mean ± SD. n = 4 per genotype. Shown *Col-0* in bottom panel is same as in top and added for comparative reasons.

Discussion

An estimated loss of 30% photosynthetically fixed carbon define photorespiration as a limiting factor of plant growth. However, photorespiratory bypasses can address this issue and improve plant yield (Wurtzel et al., 2019; Roell and Zurbriggen, 2020). The recently described ß-hydroxyaspartate cycle (BHAC), naturally found in marine proteobacteria, allows the direct conversion of glyoxylate into oxaloacetate, providing new options to assimilate photorespiratory glyoxylate without the loss of carbon and nitrogen (Schada von Borzyskowski et al., 2019). Here, we report on engineering a functional BHAC in Arabidopsis peroxisomes, the first photorespiratory bypass independent of 3-phosphoglycerate regeneration or decarboxylation of a photorespiratory precursor.

Redirecting the metabolic flux towards a synthetic pathway was demonstrated by combining transcriptional suppression of the plastidial glycolate/glycerate transporter 1 with chloroplastic glycolate decarboxylation in field-grown tobacco plants (South et al., 2019). Similarly, implementing the BHAC in the *ggt1-1* mutant to push pathway flux improved plant growth compared to the mutant background (Fig. 5C). In plant

peroxisomes the BHAC bypasses the mitochondrial glycine decarboxylase complex that would otherwise releases ammonia during photorespiration (Fig. 1). Ammonia re-assimilation by passive transport to the chloroplast and re-fixation by the glutamine synthetase 2/ ferredoxin-dependent glutamine:oxoglutarate aminotransferase complex (GS2/Fd-GOGAT) is an integral part of photorespiration (Bloom, 2015; Eisenhut et al., 2019). Based on the metabolite profiles, we hypothesize three metabolic adaptations that compensate the impaired nitrogen shuttle in BHAC plants. A general response upon impaired GS2/Fd-GOGAT-dependent nitrogen assimilation is the use of cytosolic glutamine synthetases and glutamate dehydrogenases (Pérez-Delgado et al., 2015). Further, excess nitrogen is stored in the urea cycle (Blume et al., 2019) and the ornithine–citrulline shuttle would ensure mitochondrial-chloroplastic nitrogen exchange (Linka and Weber, 2005). Finally, BHAC-derived OAA can be directly converted into aspartate by aspartate aminotransferase (Schultz and Coruzzi, 1995). Produced aspartate is used for chloroplastic *de-novo* biosynthesis of amino acids dependent on C4-carbon skeletons, in particular lysine, threonine and methionine that accumulate in BHAC plants (Fig. 4; Ravanel et al., 2004; Kirma et al., 2012). This implies that the BHAC functions as nitrogen conserving pathway and allows rerouting of photorespiratory glycolate into amino acids.

In contrast to previous photorespiratory bypasses, the BHAC also alters the carbon stoichiometry of photorespiration (Fig. 1; Kebeish et al., 2007; Maier et al., 2012; Shen et al., 2019; South et al., 2019). C3 plants depend on the regeneration of 3-PGA by photorespiration, which is exemplified by the strong phenotype of several photorespiratory mutants (Boldt et al., 2005; Voll et al., 2006; Eisenhut et al., 2013; Dellero et al., 2015). It is reasonable to believe that both reduced carboxylation (V_{cmax}) and ribulose-1,5-bisphosphate regeneration (J_{max}) are caused by lowered metabolic flux in the 3-phosphoglycerate regenerating branch of photorespiration (Fig. 1). Whereas previously described photorespiratory bypasses release four CO_2 molecules per two molecules of glycolate (Maier et al., 2012; South et al., 2019), the BHAC is carbon neutral and maximally releases one CO_2 molecule, in case OAA is decarboxylated into PEP (Schada von Borzyskowski et al., 2019). This suggests that either streamlining OAA assimilation or re-integration of the produced C3-intermediate PEP and/or CO_2 into the CBBC will be the key to achieve the full potential of the BHAC. At current stage, however, pleiotropic effects of diffuse OAA metabolism by several routes (amino acid biosynthesis, TCA cycle, PEP/pyruvate metabolism) likely mask the full potential of the BHAC (Fig. 4). Integrating the BHAC into kinetic- and genome-scale metabolic models will help to identify further engineering targets (Sweetlove and Ratcliffe, 2011; Trudeau et al., 2018; Küken and

Nikoloski, 2019; Matuszyńska et al., 2019). Finally, the construction of a synthetic C4 cycle based on BHAC-derived OAA, either as single-celled- or spatial-separated between mesophyll- and bundle sheath cells would allow to enhance carbon assimilation in plants (Jurić et al., 2019; Ermakova et al., 2020). Note that using photorespiration as source of the synthetic C4 cycle would circumvent the need to establish PEPC-dependent CO_2 fixation in C3 plants, make an ATP-dependent regeneration of PEP dispensable and ultimately conserve energy. Further, the dependency of the BHAC on C2 intermediates (glyoxylate and glycine) allows to decarboxylate BHAC-derived OAA twice and thereby boost CO_2 enrichment around Rubisco.

In summary, this work on engineering a functional BHAC into Arabidopsis is a first starting point to turn a photorespiratory bypass into a synthetic C4 cycle, constituting a promising novel approach towards creating higher crop yields in the future.

Materials and Methods

Chemicals

D-*Erythro*-BHA ([2R,3S]-ß-hydroxyaspartate) was custom-synthesized by NewChem (Newcastle upon Tyne, United Kingdom), and determined to be >95% pure by NMR analysis. DL-*threo*-BHA was purchased as racemic mixture (Sigma Aldrich).

Plasmid construction

BHAC genes were codon optimized for expression in *Arabidopsis thaliana* by gene synthesis (ThermoFisher Scientific) and matured for golden-gate cloning. All plasmids were generated with the MoClo tool kit, including vector backbones and genetic parts (Engler et al., 2014). Plasmids were sequenced by Sanger sequencing (Microsynth). Plasmids and primers used in this study are listed in Supplemental Tables S1 and S2, respectively.

BHAC enzyme activity assays

BHAC enzyme activity was measured in total leaf protein extracts from four-week old air grown *Arabidopsis* plants. Purified recombinant BHAC enzymes were produced as described in (Schada von Borzyskowski et al., 2019). The reaction mixture to assay AGAT activity contained 100 mM potassium phosphate buffer pH 7.5, 0.1 mM PLP, 0.2 mM NADH, 5 mM glyoxylate, 20 mM aspartate, 25 µl of leaf extract and 8.75 µg NAD-dependent malate dehydrogenase (Sigma Aldrich). The reaction mixture to assay BHAA activity contained 100 mM potassium phosphate buffer pH 7.5, 0.1 mM PLP, 0.2 mM

NADH, 0.5 mM $MgCl_2$, 5 mM glyoxylate, 10 mM glycine, 25 µl of leaf extract and 7 µg purified BHAD and 7 µg purified ISR enzyme. The reaction mixture to assay BHAD activity contained 100 mM potassium phosphate buffer pH 7.5, 0.1 mM PLP, 0.2 mM NADH, 2 mM *erythro*-BHA, 25 µl of leaf extract and 7 µg purified ISR enzyme. The reaction mixture to assay ISR activity contained 100 mM potassium phosphate buffer pH 7.5, 0.1 mM PLP, 0.2 mM NADH, 5 mM glyoxylate and 10 mM ^{15}N-glycine, 50 µl of leaf extract and 7 µg purified BHAA and BHAD enzyme. The formation of ^{15}N-aspartate by ISR activity was confirmed by LC-MS/MS. A detailed description of the LC-MS/MS method is provided in the Supplementary text.

Plant material and cultivation conditions

The *Arabidopsis thaliana* ecotype *Col-0* and the *ggt1-1* mutant (Dellero et al., 2015), deficient in the peroxisomal glutamate:glyoxylate aminotransferase 1 (GGT1) were used as reference backgrounds. Seeds were surface-sterilized using the vapor-phase sterilization method (Clough and Bent, 1998). Seeds were grown on half-strength Murashige and Skoog medium (pH 5.7) supplemented with 0.8% (w/v) agar. Seeds were cold stratified for two days at 4°C. After germination, seedlings were grown for 14 days at 100 µmol m^{-2} s^{-1} light intensity, at atmospheric CO_2 concentration (400 ppm) or in CO_2 enriched air (3000 ppm) in 12-h light/12-h dark photoperiod prior transfer to soil.

Metabolite profiling

For metabolite profiling green tissue of 14-days-old seedlings was harvested by liquid nitrogen dousing. immediate quenching with liquid nitrogen at the middle of the light phase. 50 mg of leaf material was used for metabolite profiling using one-phase extraction as previously described (Fiehn et al., 2000) and was analysed by gas-chromatography time of flight mass spectrometry (GC/MS Q-TOF, Agilent). For relative quantification metabolite peak areas are normalized to the internal extraction standard and the material fresh weight. A detailed description is provided in the Supplemental Information.

Gas exchange measurements

Mature rosette leaves of six weeks old, air grown plants were used for gas exchange measurements. Measurement were performed using a LICOR6800 (Licor Bioscience) with a flow set to 300 µmol s^{-1}, saturating light intensity of 1000 µmol m^{-2} s^{-1}, leaf temperature of 25 °C and a vapor pressure deficit below 1.5 kPa. A-C_i curves were measured via stepwise changes in external CO_2 supply ranging from 0 µbar to 1600 µbar. From the A-C_i curves the CO_2 compensation point was calculated as x-intercept (Sharkey et al., 2007).

The initial slope of the A-C_i curve was calculated in the linear range between 0 and 200 µbar external CO_2 and the maximal assimilation rate above 1000 µbar CO_2 was determined. Further, the A-C_i curves were fitted with the classic Farquhar, von Caemmerer and Berry model of photosynthesis (Farquhar et al., 1980) to estimate the maximum ribulose-1,5-bisphosphate saturated rate of carboxylation (V_{cmax}) and the maximum rate of electron transport (J_{max}).

Accession Numbers

The protein accession numbers used in this study are: GGT1 (Q9LR30), BHAA (A1B8Z1), BHAD (A1B8Z2), AGAT (A1B8Z3), ISR (A1B8Z0).

Acknowledgment

We would like to thank Raja Stracke, Elisabeth Klemp, Maria Graf and Katrin Weber for excellent technical assistance and Nina Cortina for her contribution on developing the ISR MS-method. Work in the laboratory of A.P.M.W was funded by the German Research Foundation (DFG) under Germany's Excellence Strategy (CEPLAS – Cluster of Excellence on Plant Science) and the iGRAD Plant Graduate School (IGK 2466) and the European Union H2020 project 862087-GAIN4CROPS. Work in the laboratory of T.J.E. was funded by the Max-Planck-Society and the German Research Foundation (SFB987 'Microbial diversity in environmental signal response').

Conflict of interest statement

The Heinrich-Heine University and the Max-Planck-Gesellschaft zur Förderung der Wissenschaften are the patent applicants for the European patent application no. EP 19190404.4 that includes a method for the production of plants with altered photorespiration and improved CO_2 fixation due to the BHAC.

Literature Cited

Bar-Even A, Noor E, Lewis NE, Milo R (2010) Design and analysis of synthetic carbon fixation pathways. Proc Natl Acad Sci USA **107**: 8889–8894

Bloom AJ (2015) Photorespiration and nitrate assimilation: A major intersection between plant carbon and nitrogen. Photosyn Res **123**: 117–128

Blume C, Ost J, Mühlenbruch M, Peterhänsel C, Laxa M (2019) Low CO_2 induces urea cycle intermediate accumulation in *Arabidopsis thaliana*. PLoS ONE **14**: e0210342

Boldt R, Edner C, Kolukisaoglu Ü, Hagemann M, Weckwerth W, Wienkoop S, Morgenthal K, Bauwe H (2005) D-GLYCERATE 3-KINASE, the last unknown enzyme in the photorespiratory cycle in Arabidopsis, belongs to a novel kinase family. Plant Cell **17**: 2413–2420

Bräutigam A, Gagneul D, Weber APM (2007) High-throughput colorimetric method for the parallel assay of glyoxylic acid and ammonium in a single extract. Anal Biochem **362**: 151–153

Charton L, Plett A, Linka N (2019) Plant peroxisomal solute transporter proteins. J Integr Plant Biol **61**: 817–835

Clough SJ, Bent AF (1998) Floral dip: a simplified method for Agrobacterium-mediated transformation of *Arabidopsis thaliana*. Plant J **16**: 735–743

Cousins AB, Pracharoenwattana I, Zhou W, Smith SM, Badger MR (2008) Peroxisomal malate dehydrogenase is not essential for photorespiration in Arabidopsis but its absence causes an increase in the stoichiometry of photorespiratory CO_2 release. Plant Physiol **148**: 786–795

Dedonder A, Rethy R, Fredericq H, Van Montagu M, Krebbers E (1993) Arabidopsis *rbcS* genes are differentially regulated by light. Plant Physiol **101**: 801–808

Dellero Y, Lamothe-Sibold M, Jossier M, Hodges M (2015) *Arabidopsis thaliana ggt1* photorespiratory mutants maintain leaf carbon/nitrogen balance by reducing RuBisCO content and plant growth. Plant J **83**: 1005–1018

Duursma RA (2015) Plantecophys - An R package for analysing and modelling leaf gas exchange data. PLoS ONE **10**: e0143346

Eastmond PJ, Astley HM, Parsley K, Aubry S, Williams BP, Menard GN, Craddock CP, Nunes-Nesi A, Fernie AR, Hibberd JM (2015) Arabidopsis uses two gluconeogenic gateways for organic acids to fuel seedling establishment. Nat Commun **6**: 6659–8

Eisenhut M, Planchais S, Cabassa C, Guivarc'h A, Justin A-M, Taconnat L, Renou J-P, Linka M, Gagneul D, Timm S, et al (2013) Arabidopsis A BOUT de SOUFFLE is a putative mitochondrial transporter involved in photorespiratory metabolism and is required for meristem growth at ambient CO_2 levels. Plant J **73**: 836–849

Eisenhut M, Roell M-S, Weber APM (2019) Mechanistic understanding of photorespiration paves the way to a new green revolution. New Phytol **223**: 1762–1769

Engler C, Youles M, Gruetzner R, Ehnert T-M, Werner S, Jones JDG, Patron NJ, Marillonnet S (2014) A golden gate modular cloning toolbox for plants. ACS Synth Biol **3**: 839–843

Ermakova M, Danila FR, Furbank RT, Caemmerer von S (2020) On the road to C4 rice: advances and perspectives. Plant J **101**: 940–950

Farquhar GD, Caemmerer von S, Berry JA (1980) A biochemical model of photosynthetic CO2 assimilation in leaves of C3 species. Planta **149**: 78–90

Fernie AR, Bauwe H (2020) Wasteful, essential, evolutionary stepping stone? The multiple personalities of the photorespiratory pathway. Plant J **102**: 666–677

Fiehn O, Kopka J, Dörmann P, Altmann T, Trethewey RN, Willmitzer L (2000) Metabolite profiling for plant functional genomics. Nat Biotechnol **18**: 1157–1161

Hennacy JH, Jonikas MC (2020) Prospects for engineering biophysical CO_2 concentrating mechanisms into land plants to enhance yields. Annu Rev Plant Biol **71**: 461–485

Jones CA, Sands RD (2013) Impact of agricultural productivity gains on greenhouse gas emissions: A global analysis. American Journal of Agricultural Economics **95**: 1309–1316

Jurić I, Hibberd JM, Blatt M, Burroughs NJ (2019) Computational modelling predicts substantial carbon assimilation gains for C3 plants with a single-celled C4 biochemical pump. PLoS Comput Biol **15**: e1007373

Kebeish R, Niessen M, Thiruveedhi K, Bari R, Hirsch H-J, Rosenkranz R, Stäbler N, Schönfeld B, Kreuzaler F, Peterhänsel C (2007) Chloroplastic photorespiratory bypass increases photosynthesis and biomass production in *Arabidopsis thaliana*. Nat Biotechnol **25**: 593–599

Kerfeld CA, Aussignargues C, Zarzycki J, Cai F, Sutter M (2018) Bacterial microcompartments. Nat Rev Microbiol **16**: 277–290

Kirma M, Araujo WL, Fernie AR, Galili G (2012) The multifaceted role of aspartate-family amino acids in plant metabolism. J Exp Bot **63**: 4995–5001

Koncz C, Schell J (1986) The promoter of TL-DNA gene 5 controls the tissue-specific expression of chimaeric genes carried by a novel type of Agrobacterium binary vector. Mol Gen Genet **204**: 383–396

Krause GH, Weis E (1991) Chlorophyll fluorescence and photosynthesis - the Basics. Annu Rev Plant Physiol **42**: 313–349

Kuhnert F, Stefanski A, Overbeck N, Drews L, Reichert AS, Stühler K, Weber APM (2020) Rapid single-step affinity purification of HA-tagged plant mitochondria. Plant Physiol **182**: 692–706

Küken A, Nikoloski Z (2019) Computational approaches to design and test plant synthetic metabolic pathways. Plant Physiol **179**: 894–906

Laemmli UK (1970) Cleavage of structural proteins during the assembly of the head of bacteriophage T4. Nature **227**: 680–685

Lingner T, Kataya AR, Antonicelli GE, Benichou A, Nilssen K, Chen X-Y, Siemsen T, Morgenstern B, Meinicke P, Reumann S (2011) Identification of novel plant peroxisomal targeting signals by a combination of machine learning methods and in vivo subcellular targeting analyses. Plant Cell **23**: 1556–1572

Linka M, Weber APM (2005) Shuffling ammonia between mitochondria and plastids during photorespiration. Trends Plant Sci **10**: 461–465

Long SP, Marshall-Colon A, Zhu X-G (2015) Meeting the global food demand of the future by engineering crop photosynthesis and yield potential. Cell **161**: 56–66

Maier A, Fahnenstich H, Caemmerer von S, Engqvist MKM, Weber APM, Flügge U-I, Maurino VG (2012) Transgenic introduction of a glycolate oxidative cycle into *A. thaliana* chloroplasts leads to growth improvement. Front Plant Sci **3**: 38

Matuszyńska A, Saadat NP, Ebenhöh O (2019) Balancing energy supply during photosynthesis – a theoretical perspective. Physiol Plant **166**: 392–402

Miller TE, Beneyton T, Schwander T, Diehl C, Girault M, McLean R, Chotel T, Claus P, Cortina NS, Baret J-C, et al (2020) Light-powered CO_2 fixation in a chloroplast mimic with natural and synthetic parts. Science **368**: 649–654

Mitra A, Han J, Zhang ZJ, Mitra A (2009) The intergenic region of *Arabidopsis thaliana cab1* and *cab2* divergent genes functions as a bidirectional promoter. Planta **229**: 1015–1022

Pérez-Delgado CM, García-Calderón M, Márquez AJ, Betti M (2015) Reassimilation of photorespiratory ammonium in *Lotus japonicus* plants deficient in plastidic glutamine synthetase. PLoS ONE **10**: e0130438

Pradhan P, Fischer G, van Velthuizen H, Reusser DE, Kropp JP (2015) Closing yield gaps: How sustainable can we be? PLoS ONE **10**: e0129487

Ravanel S, Block MA, Rippert P, Jabrin S, Curien G, Rébeillé F, Douce R (2004) Methionine metabolism in plants: chloroplasts are autonomous for de novo methionine synthesis and can import S-adenosylmethionine from the cytosol. J Biol Chem **279**: 22548–22557

Ray DK, Mueller ND, West PC, Foley JA (2013) Yield trends are insufficient to double global crop production by 2050. PLoS ONE **8**: e66428

Roell M-S, Zurbriggen MD (2020) The impact of synthetic biology for future agriculture and nutrition. Curr Opin Biotechnol **61**: 102–109

Schada von Borzyskowski L, Severi F, Krüger K, Hermann L, Gilardet A, Sippel F, Pommerenke B, Claus P, Cortina NS, Glatter T, et al (2019) Marine proteobacteria metabolize glycolate via the ß-hydroxyaspartate cycle. Nature **575**: 500–504

Scheffen M, Marchal DG, Beneyton T, Schuller SK, Klose M, Diehl C, Lehmann J, Pfister P, Carrillo M, He H, et al (2020) A new-to-nature carboxylation module to improve natural and synthetic CO_2 fixation. Nature Catalysis (in press)

Schindelin J, Arganda-Carreras I, Frise E, Kaynig V, Longair M, Pietzsch T, Preibisch S, Rueden C, Saalfeld S, Schmid B, et al (2012) Fiji: an open-source platform for biological-image analysis. Nat Methods **9**: 676–682

Schlueter U, Weber APM (2020) Regulation and evolution of C4 photosynthesis. Annu Rev Plant Biol **71**: 183–215

Schlueter U, Bräutigam A, Gowik U, Melzer M, Christin P-A, Kurz S, Mettler-Altmann T, Weber AP (2017) Photosynthesis in C3-C4 intermediate Moricandia species. J Exp Bot **68**: 191–206

Schuler ML, Mantegazza O, Weber APM (2016) Engineering C4 photosynthesis into C3 chassis in the synthetic biology age. Plant J **87**: 51–65

Schultz CJ, Coruzzi GM (1995) The aspartate-aminotransferase gene family of Arabidopsis encodes isoenzymes localized to 3 distinct subcellular compartments. Plant J **7**: 61–75

Schwander T, Schada von Borzyskowski L, Burgener S, Cortina NS, Erb TJ (2016) A synthetic pathway for the fixation of carbon dioxide *in vitro*. Science **354**: 900–904

Sharkey TD, Bernacchi CJ, Farquhar GD, Singsaas EL (2007) Fitting photosynthetic carbon dioxide response curves for C3 leaves. Plant Cell Environ **30**: 1035–1040

Shen B-R, Wang L-M, Lin X-L, Yao Z, Xu H-W, Zhu C-H, Teng H-Y, Cui L-L, Liu EE, Zhang J-J, et al (2019) Engineering a new chloroplastic photorespiratory bypass to increase photosynthetic efficiency and productivity in rice. Molecular Plant **12**: 199–214

South PF, Cavanagh AP, Liu HW, Ort DR (2019) Synthetic glycolate metabolism pathways stimulate crop growth and productivity in the field. Science **363**: eaat9077

Sweetlove LJ, Ratcliffe RG (2011) Flux-balance modeling of plant metabolism. Front Plant Sci **2**: 38

Tilman D, Balzer C, Hill J, Befort BL (2011) Global food demand and the sustainable intensification of agriculture. Proc Natl Acad Sci USA **108**: 20260–20264

Trudeau DL, Edlich-Muth C, Zarzycki J, Scheffen M, Goldsmith M, Khersonsky O, Avizemer Z, Fleishman SJ, Cotton CAR, Erb TJ, et al (2018) Design and *in vitro* realization of carbon-conserving photorespiration. Proc Natl Acad Sci USA **115**: E11455–E11464

Voll LM, Jamai A, Renné P, Voll H, McClung CR, Weber APM (2006) The photorespiratory Arabidopsis *shm1* mutant is deficient in SHM1. Plant Physiol **140**: 59–66

Walker BJ, VanLoocke A, Bernacchi CJ, Ort DR (2016) The costs of photorespiration to food production now and in the future. Annu Rev Plant Biol **67**: 107–129

Weber APM, Bar-Even A (2019) Update: Improving the efficiency of photosynthetic carbon reactions. Plant Physiol **179**: 803–812

Wulfert S, Schilasky S, Krueger S (2020) Transcriptional and biochemical characterization of cytosolic pyruvate kinases in Arabidopsis thaliana. Plants. doi: 10.3390/plants9030353

Wurtzel ET, Vickers CE, Hanson AD, Millar AH, Cooper M, Voss-Fels KP, Nikel PI, Erb TJ (2019) Revolutionizing agriculture with synthetic biology. Nat Plants **5**: 1207–1210

Supplemental Information

Supplementary Text

Genetic transformation of *Arabidopsis thaliana*

T-DNA constructs were introduced into *Agrobacterium tumefaciens* strain GV3101::pMP90 (Koncz and Schell, 1986) and *Arabidopsis thaliana* plants were transformed via agrobacterium-mediated transformation (Clough and Bent, 1998). Homozygous T3 plants were used for further analysis.

Transient expression in *Nicotiana benthamiana* and protoplast isolation

Overnight grown *Agrobacterium tumefaciens* GV3101::pMP90 cells, carrying the T-DNA construct were diluted in infiltration medium (10 mM $MgCl_2$, 10 mM MES [pH 5.7], 100 µM acetosyringone) to an OD_{600} of 0.4. Leaves of four-week old greenhouse-grown *Nicotiana benthamiana* plants were infiltrated using a syringe without a needle. For co-localization analysis T-DNA peroxisomal marker constructs were co-infiltrated, expressing either cyan fluorescent protein or mCherry, C-terminally fused with peroxisomal target signal 1 (PTS1). Protoplasts were isolated two days post infection. Leaves were sliced into small pieces, vacuum-infiltrated with protoplast digestion solution (1.5% [w/v] cellulase R-10, 0.4 % [w/v] macerozyme R-10, 0.4 M mannitol, 20 mM KCl, 20 mM MES [pH 5.7], 10 mM $CaCl_2$, 0.1% [w/v] bovine serum albumin) and incubated for 2 hours at 28°C. Sedimented protoplasts were resuspended in W5 solution (154 mM NaCl, 125 mM $CaCl_2$, 5 mM KCl, 2 mM MES [pH5.7]) and analyzed by confocal laser scanning microscopy.

Confocal laser scanning microscopy

Zeiss LSM780 confocal microscope and Zeiss ZEN software (Zeiss) was used for confocal laser scanning microscopy. Excitation/emission wavelengths were as followed: mCherry (561 nm/580 to 625), cyan fluorescent protein (450 nm/510 to 550) nm), green fluorescent protein (488 nm/490 to 550 nm), chlorophyll A (488 nm/640 to 710 nm). Images were processed with Fiji (Schindelin et al., 2012).

Enzyme activity assays

Total leaf protein was isolated from four-week old air grown *Arabidopsis* plants. Leaf material was frozen in liquid nitrogen and grinded, using glass beads and windmill, and resuspended in 700 µl extraction buffer (50 mM potassium phosphate pH 7.5, 5 mM $MgCl_2$, 1 mM EDTA, 0.1% [v/v] Triton-X 100). After centrifugation for 10 min at 12,000 rpm at

4°C, 25 µl of the supernatant was used for enzyme assays. All assays were carried out at 30°C in a total volume of 300 µl. The oxidation of NADH was followed at 340 nm on a Cary 60 UV-Vis photospectrometer (Agilent) in quartz cuvettes with a path length of 10 mm (Hellma Analytics).

Glutamate:glyoxylate activity measurements were performed based on AGAT assays as described. Aspartate was replaced by 50 mM glutamate.

To take samples for LC-MS/MS analysis, the reaction volume of the assay was increased to 600 µl. 90 µL aliquots were taken after 0, 1, 2 and 3 minutes and the reaction was immediately stopped by addition of formic acid (4% final concentration). The samples were centrifuged at 17,000 x g and 4°C for 15 min and the supernatant was subsequently used for LC-MS analysis. Quantitative determination of ^{15}N-aspartate (Asp-^{15}N) and Aspartate (Asp) was performed using a LC-MS/MS. The chromatographic separation was performed on an Agilent Infinity II 1290 HPLC system using a ZicHILIC SeQuant column (150 × 2.1 mm, 3.5 µm particle size, 100 Å pore size) connected to a ZicHILIC guard column (20 × 2.1 mm, 5 µm particle size) (Merck KgAA) at a constant flow rate of 0.3 ml/min with mobile phase A being 0.1% formic acid in 99:1 water:acetonitrile (Honeywell, Morristown, New Jersey, USA) and phase B being 0.1% formic acid in 99:1 acetonitrile:water (Honeywell, Morristown, New Jersey, USA) at 25° C. The injection volume was 5 µl. The mobile phase profile consisted of the following steps and linear gradients: 0 – 5 min from 80 to 65% B; 5 – 7 min from 65 to 20% B; 7 – 9 min constant at 20% B; 9 – 10 min from 20 to 80% B; 10 – 12 min constant at 80% B. An Agilent 6495 ion funnel mass spectrometer was used in positive mode with an electrospray ionization source and the following conditions: ESI spray voltage 2000 V, sheath gas 250° C at 12 l/min, nebulizer pressure 50 psig and drying gas 100° C at 11 l/min. Compounds were identified based on their mass transition and retention time compared to standards. Chromatograms were integrated using MassHunter software (Agilent, Santa Clara, CA, USA). Absolute concentrations of Asp-^{15}N and Asp were calculated based on an external calibration curve of Asp-^{13}C prepared in sample matrix after confirming that the uniformly labelled analyte cannot be detected in the matrix prior to standard addition, and after confirming that the correlation between the signal intensity and concentration of the ^{13}C-labelled analyte equals the correlation of the unlabeled as well as the ^{15}N-labelled amino acid by standard addition. Quantification via an isotopically labelled external standard was required, as the unlabeled analyte that was found in the matrix in high abundance interfered with the measurement.

SDS-PAGE and immunoblot analysis

SDS-PAGE and immunoblot analysis were performed as described in (Laemmli, 1970; Kuhnert et al., 2020). 15 µg total leaf was loaded for SDS-PAGE. For immunoblot analysis monoclonal conjugated horseradish peroxidase anti-HA antibody (Miltenyi Biotech) was used for the detection of AGAT and ISR. Monoclonal conjugated horseradish peroxidase anti-His antibody (Miltenyi Biotech) was used for the detection of BHAA and BHAD.

Plant phenotyping

For fresh weight and dry weight analysis, 12-days-old seedlings were harvested. Seedlings were dried for four days at 65°C before dry weight analysis. Rosette area and rosette diameter were quantified on photographed pots via Fiji.

Chlorophyll fluorescence measurements

Chlorophyll photochemical efficiency of photosystem II in dark-adapted leaves (F_v/F_m) (Krause and Weis, 1991) was measured on 12-days-old seedlings using an imaging chlorophyll fluorometer (Imaging PAM, Walz). Upon dark adaptation for 20 min, seedlings were exposed to a pulsed, blue probe beam and a saturating light flash to measure F_v/F_m values.

Free ammonium quantification

Free ammonium was quantified in plant tissue using a colorimetric assay as described previously (Bräutigam et al., 2007).

Metabolite profiling

Frozen material was grinded using precooled mortar and pistil. Grinded material was aliquoted under continuous liquid nitrogen exposure to avoid sample thawing. Extraction mix, containing water:methanol:chloroform (ratio 1:2.5:1) and 5 µM ribitol as internal standard, were added to frozen material. Samples were vortexed for 20 seconds, rotated for 6 min at 4°C and centrifuged for 2 min at 20,000 x g at room temperature. The supernatant was transferred to a new tube and stored at -80°C before further processing. For metabolite profiling by gas-chromatography time of flight mass spectrometry (GC/MS Q-TOF), 50 µl of extract was dried using a speed vacuum concentrator. Dried samples were placed in the Gerstel MPS 2 XL autosampler for automatic sample derivatization using methoxyamine hydrochloride and N-Methyl-N-(trimethylsilyl) trifluoroacetamide before injection. The GC-MS device is a 7200 accurate mass Q-TOF GC/MS (Agilent). For relative

quantification metabolite peak areas are normalized to the internal extraction standard and the material fresh weight.

Data analysis and software

Data analysis was performed in R. For analysis of gas exchange measurements, the 'plantecophys' package was used (Duursma, 2015).

Supplemental Figures and Tables

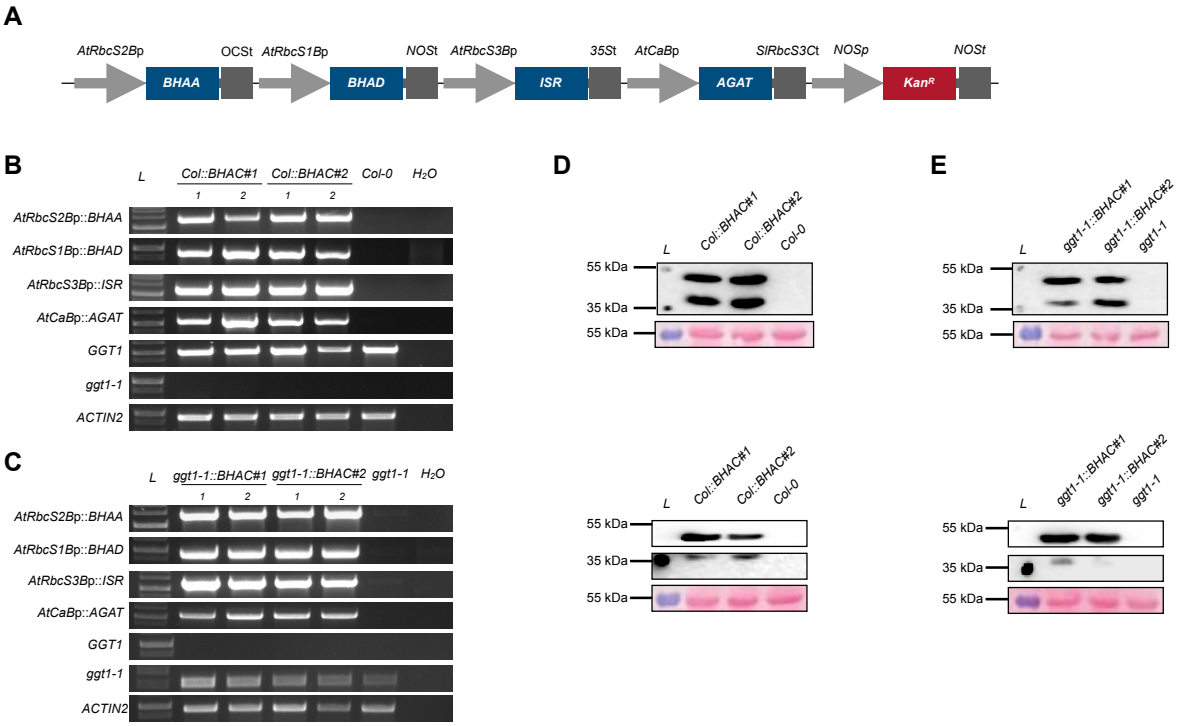

Supplemental Fig. S1: BHAP implementation in *Arabidopsis thaliana* wild type *Col-0* and *ggt1-1* mutant background. A) Schematic representation of the multigene T-DNA construct for BHAC pathway implementation. Aspartate:glyolxyate aminotransferase (AGAT), ß-hydroxyaspartate aldolase (BHAA), ß-hydroxyaspartate dehydratase (BHAD), iminosuccinate reductase (ISR). Kanamycin resistance (KanR). B and C) Genotyping of transgenic homozygous T3 BHAC plants in wild type *Col-0* (B) and *ggt1-1* mutant background (C). D and E) Immunoblot analysis of BHAC enzyme expression in *Col-0* background (D) and *ggt1-1* background (E). Arabidopsis Rubisco large subunit (RbcL) served as loading control and was visualized by ponceau staining. 15 µg total leaf protein of four weeks old air grown plants was loaded per lane. Protein expression was detected using anti-HIS HRP antibody (top) or anti-HA HRP antibody (bottom). AGAT and ISR are HA-tagged and BHAA and BHAD are HIS-tagged.

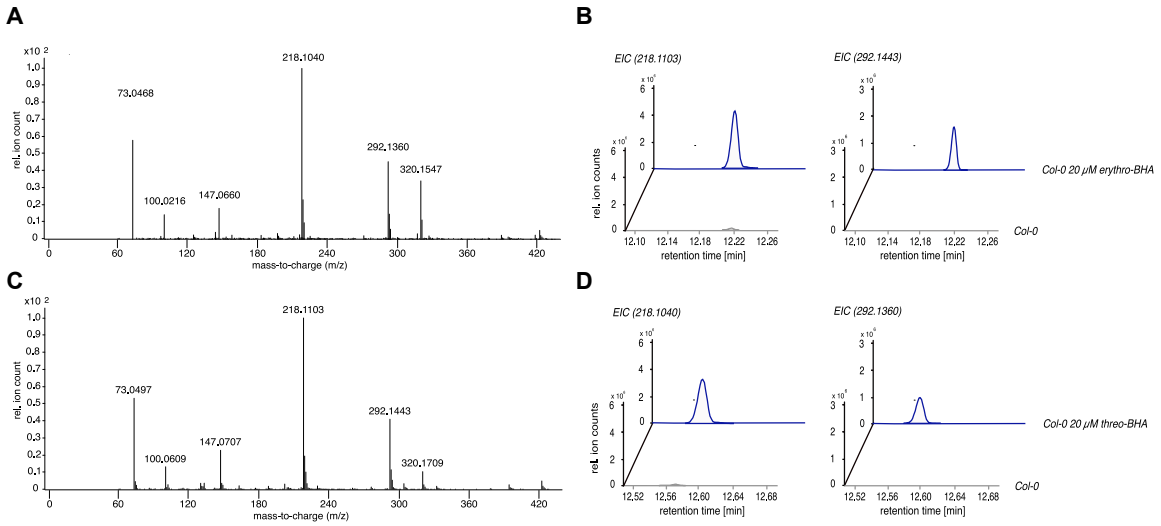

Supplemental Fig. S2: β-hydroxyaspartate detection by GC-MS QTOF. A) Deconvoluted mass spectrum of *erythro*-ß-hydroxyaspartate. B) Extracted ion chromatogram of *erythro*-ß-hydroxyaspartate specific masses in wildtype *Col-0* extract spiked with 20 µM analytical standard of *D-erythro*-ß-hydroxyaspartate. C) Deconvoluted mass spectrum of *threo*-ß-hydroxyaspartate. B) Extracted ion chromatogram of *threo*-ß-hydroxyaspartate specific masses in wild type *Col-0* extract spiked with 20 µM analytical standard of *DL-threo*-ß-hydroxyaspartate.

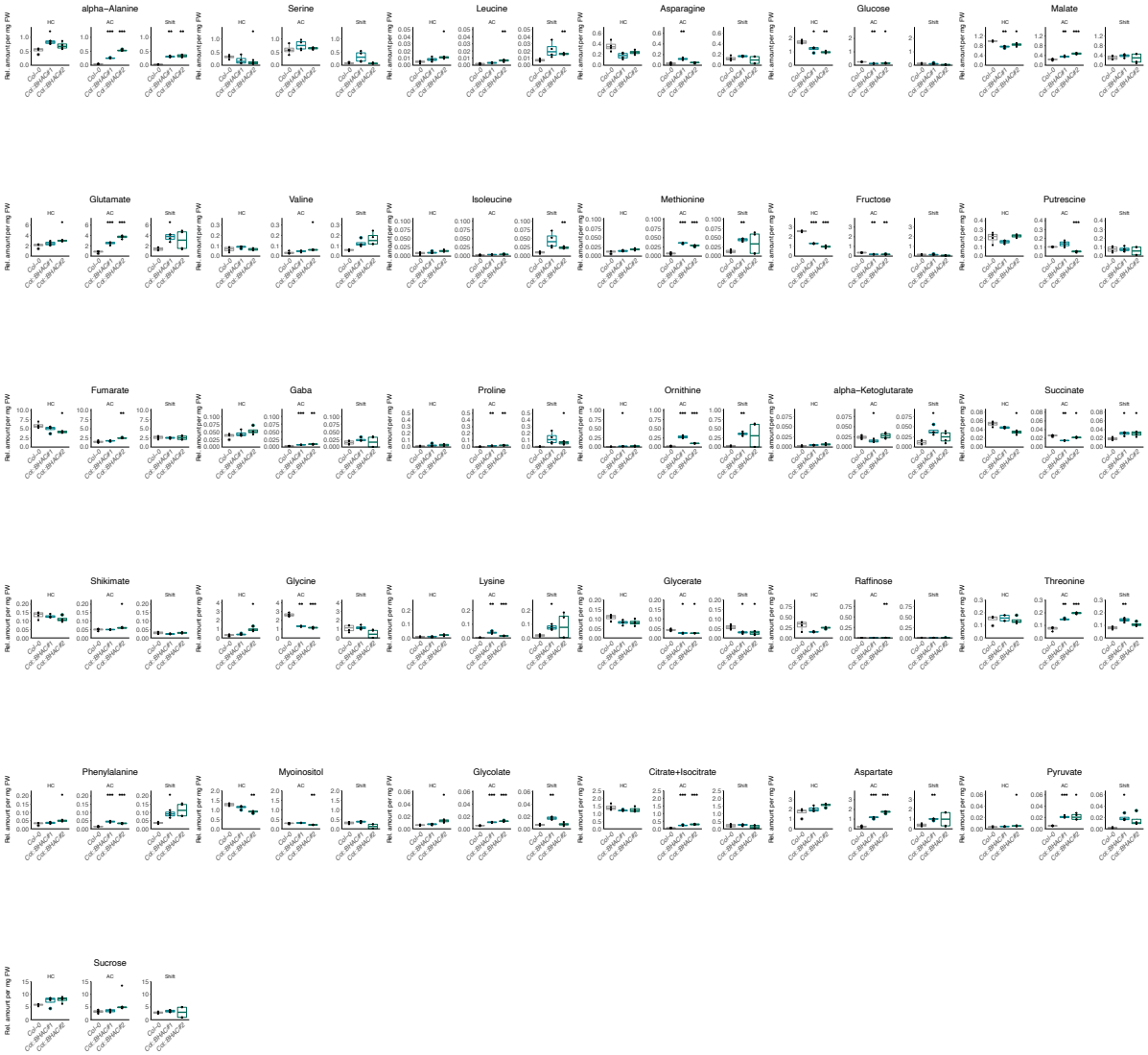

Supplemental Fig. S3: Metabolome profile of BHAC in wild type *Col-0* background. Metabolite profiles were generated using green tissue of 14 days old seedlings grown either in CO_2 enriched air (3000 ppm CO_2, HC), ambient air (400 ppm CO_2, AC) or shifted from HC to AC three days prior to harvest (Shift). Relative metabolite levels of BHAC plants in wild type *Col-0* background. Student's *t*-test against wild type *Col-0*. Asterisks indicate significance after multiple testing correction using Benjamini-Hochberg. $p < 0.05$ = *, < 0.01 = **, < 0.001 = ***. n = 4.

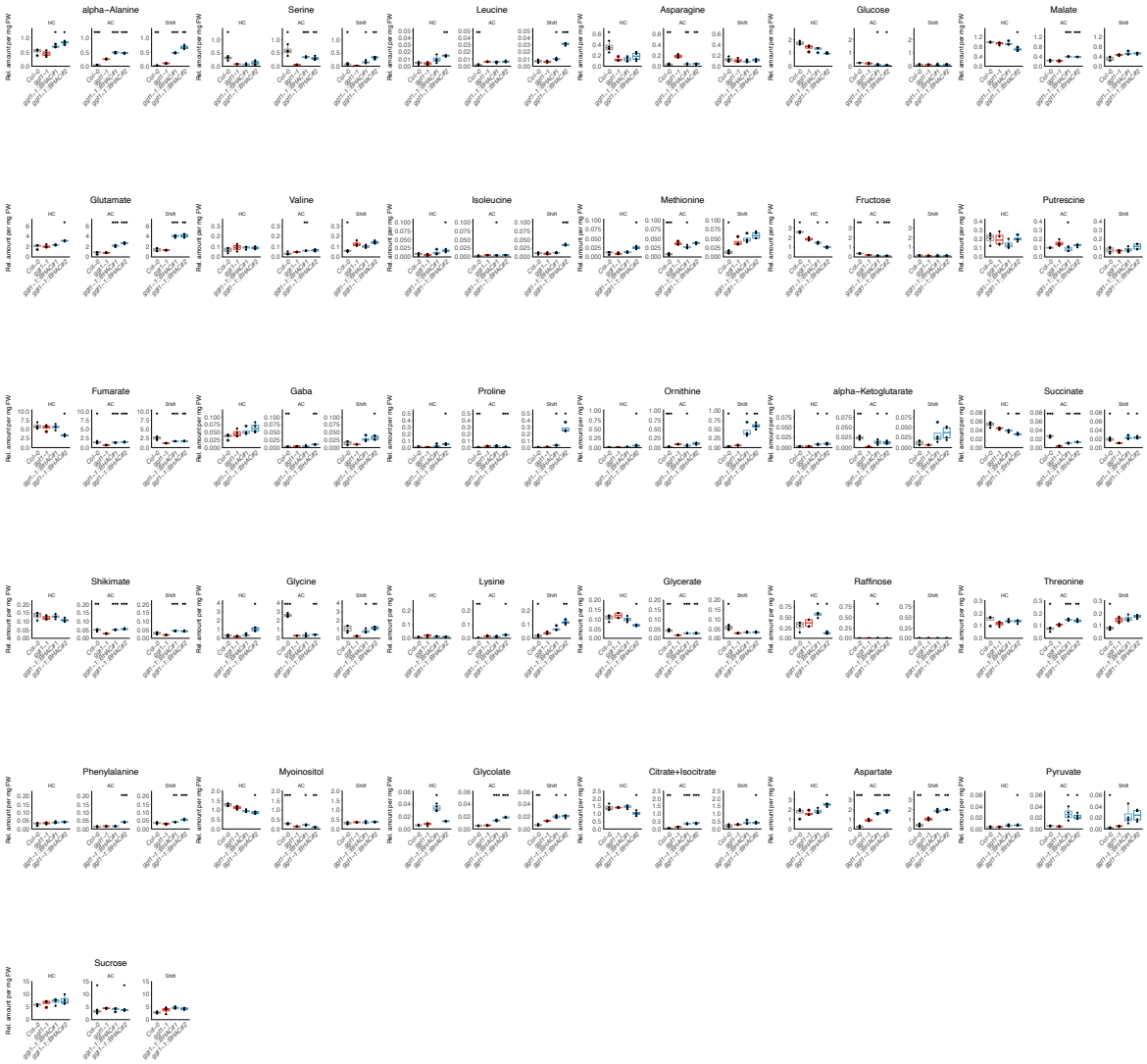

Supplemental Fig. S4: Metabolome profile of BHAC in *ggt1-1* background. Metabolite profiles were generated using green tissue of 14 days old seedlings grown either in CO_2 enriched air (3000 ppm CO_2, HC), ambient air (400 ppm CO_2, AC) or shifted from HC to AC three days prior to harvest (Shift). Relative metabolite levels of BHAC plants in *ggt1-1* background. Student's *t*-test against *ggt1-1* mutant. Asterisks indicate significance after multiple testing correction using Benjamini-Hochberg. $p < 0.05$ = *, < 0.01 = **, < 0.001 = ***. n = 4. Shown wild type *Col-0* is the same as in Supplemental Fig. S3 and added for comparative reasons.

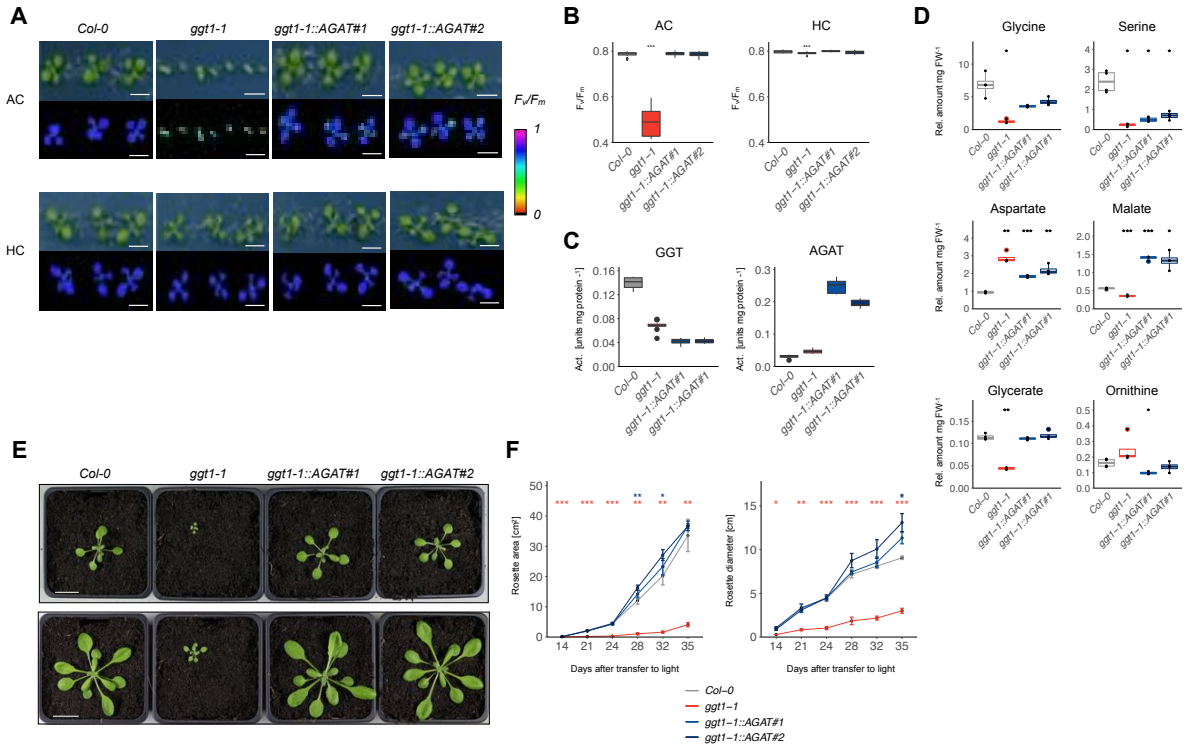

Supplemental Fig. S5: Peroxisomal aspartate:glyoxylate aminotransferase restores canonical photorespiration in the *ggt1-1* mutant. The *ggt1-1* was complemented by expression of aspartate:glyoxylate aminotransferase under the chlorophyll A/B binding protein 1 promoter (*ggt1-1::AGAT*). Numbers indicate independent T-DNA lines. A) Representative images of seedlings for F_v/F_m measurements using twelve days old seedling grown at ambient air (400 ppm CO_2, AC) or in CO_2 enriched air (3000 ppm CO_2, HC). scalebar = 0.5 cm. B) Quantification of F_v/F_m values of plants grown at AC (top) or HC (bottom). Student's *t*-test against wild type *Col-0* $p < 0.05$ = *, < 0.01 = **, < 0.001 = ***. n >25 per genotype per condition. C) *In vitro* glutamate:glyoxylate (GGT) and aspartate:glyoxylate (AGAT) activity. Activity was measured in three biological replicates in technical triplicates using mature rosette leaves of 28 days old air grown plants. D) Relative metabolite levels in *ggt1-1::AGAT* complementation lines grown in air. Student's *t*-test against wild type *Col-0*. Asterisks indicate significance after multiple testing correction using Benjamini-Hochberg. $p < 0.05$ = *, < 0.01 = **, < 0.001 = ***. n = 4. E) Images of plants grown in ambient air (400 ppm CO_2) at 21 days (top) and 28 days (bottom) after transfer to light. F) Rosette area (left) and rosette diameter (right) of ambient air grown plants. Student's *t*-test against wildtype *Col-0*. $p < 0.05$ = *, $p < 0.01$ = **, $p < 0.001$ = ***. Colored asterisks represent the significance for the respective genotype. n = 3. Shown mean ± SD.

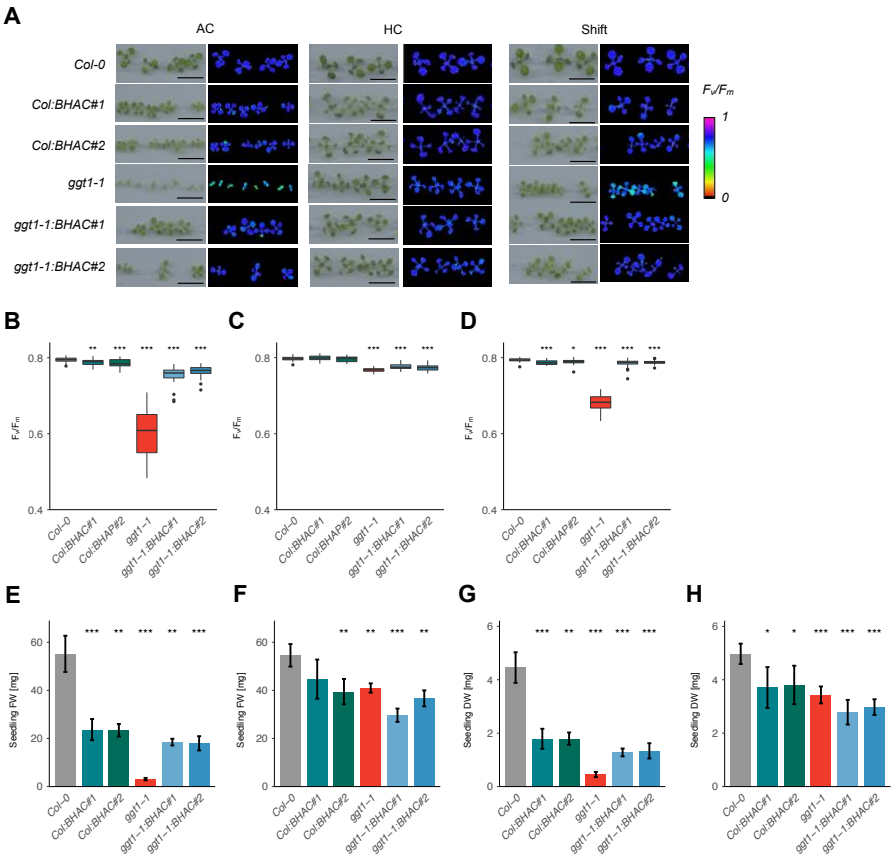

Supplemental Fig. S6: Phenotyping of BHAC plants at seedling stage. A) Representative images of BHAC plants for F_v/F_m measurements using 12-days-old seedling grown in ambient air (400 ppm CO_2, AC), CO_2 enriched air (3000 ppm CO_2, HC) or shifted from HC to AC three days prior measurements and harvest (Shift). scalebar = 0.5 cm. B) Quantification of F_v/F_m values of plants grown at AC (B), HC (C) or Shift (D). Student's *t*-test against wild type *Col-0*. p < 0.05 = *, < 0.01 = **, < 0.001 = ***. n >25 per genotype per condition. E to H) Seedling fresh weight (E and F) and dry weight (G and H) of 12-days-old grown at AC (E and G) or HC (F and H). Student's *t*-test against wildtype *Col-0* p < 0.05 = *, < 0.01 = **, < 0.001 = ***. Shown mean ± SD. n = 4

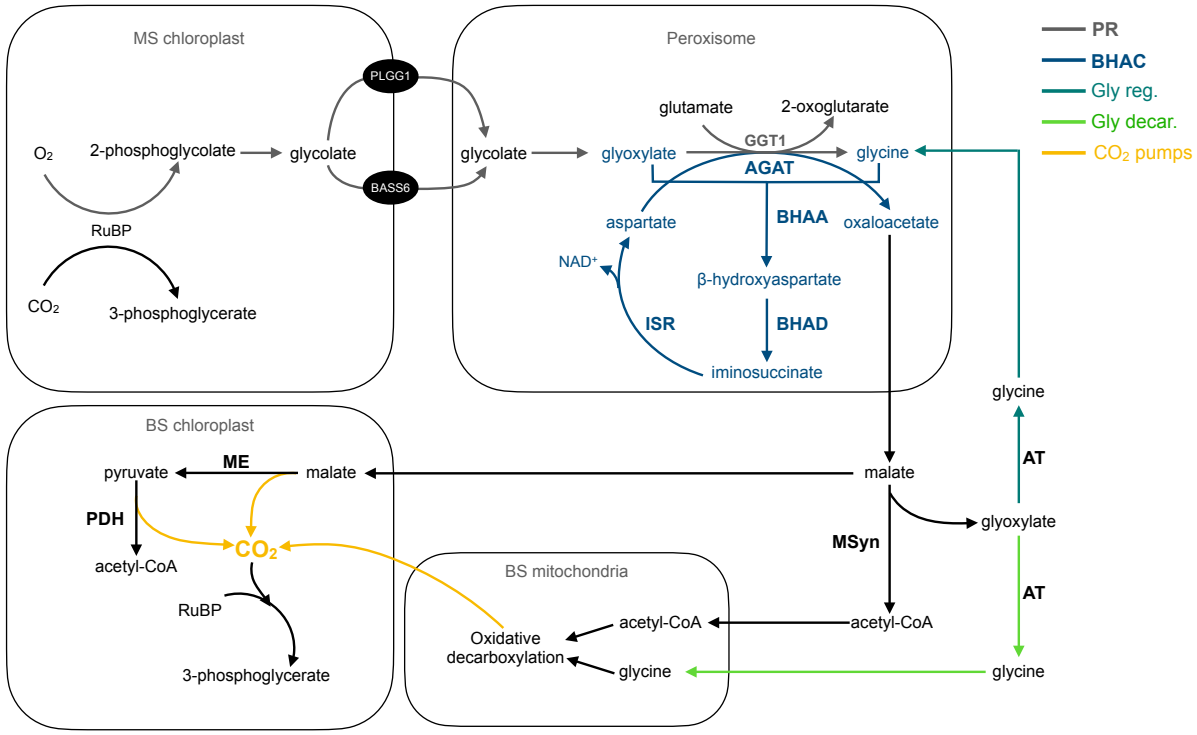

Fig. S7. A BHAC derived synthetic C4 cycle. Schematic representation of plant photorespiration (PR), BHAC and potential routes for a synthetic C4 cycle between mesophyll (MS) and bundle sheath cells (BS). These include the decarboxylation of malate or malate catabolism and acetyl-CoA decarboxylation and glycine decarboxylation (Gly decar.) or regeneration (Gly reg.). Abbreviations: Aspartate:glyolxyate aminotransferase (AGAT), ß-hydroxyasparate aldolase (BHAA), ß-hydroxyaspartate dehydratase (BHAD), iminosuccinate reductase (ISR), glutamate:glyoxylate aminotransferase (GGT1), ribulose-1,5-bisphosphate (RuBP), plastidial glycolate/glycerate transporter 1 (PLGG1), bile-acid sodium symporter 6 (BASS6), malate synthase (MSyn), aminotransferase (AT), malic enzyme (ME), pyruvate dehydrogenase (PDH).

Table S1: List of primer used in this study. Gene specific nucleotides indicated in caps. Abbreviations: GGT1 (glutamate:glyoxylate aminotransferase 1, At1g23310).

Primer sequence	Purpose	Reference
fwd: 5'-CCTTGCCCTTGGCTCTAGAACC-3' rev: 5'-GTCATACCTAAACCGCCTGAAGTC-3'	Genotyping *GGT1*	This Study
fwd: 5'-TAACTCTCCCCACTCTTTGCC-3' rev: 5'-ATATTGACCATCATACTCATTGC-3'	T-DNA primer *ggt1-1*	

Table S2: List of constructs used in this study. Vector backbones, promoters and terminators are described in (Engler et al., 2014). Abbreviations: aspartate:glyolxyate aminotransferase (AGAT), ß-hydroxyasparate aldolase (BHAA), ß-hydroxyaspartate dehydratase (BHAD), iminosuccinate reductase (ISR), peroxisomal target signal 1 (PTS1), peroxisomal target signal 2 (PTS2), ß-hydroxyasparate cycle (BHAC), *Arabidopsis thaliana* (*At*), *Solanum lycopersicum* (*Sl*), Agrobacterium tumefaciens (*Atu*).

Purpose	**Vector**	**Insert**	**Comment**
Localization AGAT	pICH86966	*UBQ10*p::mCherry-AGAT$_{PTS1}$::*Sl*Rbsc3cT	PTS1: serine-lysine-leucine
Localization BHAA	pICH86966	*UBQ10*p::$_{PTS2}$BHAA-mCherry::*Sl*Rbsc3cT	PTS2 from Arabidopsis thaliana Citrate Synthase (At2g42790)
Localization BHAD	pICH86966	*UBQ10*p::mCherry-BHAD$_{PTS1}$::*SlRbsc3c*T	PTS1: serine-lysine-leucine
Localization ISR	pICH86966	*UBQ10*p::eGFP-ISR$_{PTS1}$::*SlRbsc3c*T	PTS1: serine-lysine-leucine
ggt1-1 complementation	pICH86966	*At*CaBp::AGAT$_{PTS1}$:: *Sl*Rbsc3cT	Kanamycin resistance for plants
BHAC T-DNA construct for implementation in plants	pICH75322	Pos. 1: *At*RbcS2Bp::$_{PTS2}$BHAA::*AtuO*csT Pos. 2: *At*RbcS1Bp::BHAD$_{PTS1}$::*Atu*NosT Pos. 3: *At*RbcS3Bp::ISR$_{PTS1}$::35sT Pos. 4: *At*CaBp::AGAT$_{PTS1}$:: *Sl*Rbsc3cT Pos. 5: *Atu*Nosp::NptII::*Atu*OcsT	Kanamycin resistance for plants

European patent application

A method for the production of plants with altered photorespiration and improved CO_2 fixation

The experimental work and underlying ideas described in Manuscript I are part of the pending EU patent application EP 19190404.4 that claims the use of the ß-hydroxyaspartate cycle to alter photorespiration and improve CO_2 fixation in plants.

At the time of submitting this dissertation, the patent application passed the priority year and the final patent application was handed over to the European patent amt for evaluation at the 6th August 2020. The patent application is filled by Dr. Lennart Schada von Borzykowski, Prof. Dr. Tobias J. Erb (both (Max-Planck Institute for Terrestrial Microbiology, Marburg, Germany), Prof. Dr. Andreas P.M. Weber and myself (Institute Plant Biochemistry, Heinrich-Heine University, Düsseldorf, Germany) with support of the Heinrich-Heine University Düsseldorf and the Max-Planck Society.

The claims made in original Patent application are listed below and the complete patent application is available upon request.

1. A method for the production of a transgenic plant with altered photorespiration and improved CO_2 fixation, comprising introducing into a cell or tissue of said plant one or more nucleic acids encoding at least four polypeptides having the enzymatic activities of

    (a) *erythro*-ß-hydroxyaspartate aldolase belonging to the EC class 4.1.3.14,

    (b) *erythro*-ß-hydroxyaspartate dehydratase belonging to the EC class 4.3.1.20,

    (c) iminosuccinate reductase and

    (d) aspartate-glyoxylate transaminase,

    wherein the introduction of said nucleic acid(s) results in a *de novo* expression of the at least four polypeptides having the enzymatic activities of

    (a) *erythro*-ß-hydroxyaspartate aldolase belonging to the EC class 4.1.3.14,

    (b) *erythro*-ß-hydroxyaspartate dehydratase belonging to the EC class 4.3.1.20,

    (c) iminosuccinate reductase and

    (d) aspartate-glyoxylate transaminase,

wherein the polypeptide having the enzymatic activity of (c) iminosuccinate reductase comprises an amino acid sequence selected from SEQ ID NO: 1-299, or an amino acid sequence having at least 80% sequence identity to a sequence selected from SEQ ID NO: 1-299; and the polypeptide having the enzymatic activity of (d) aspartate-glyoxylate transaminase comprises an amino acid sequence selected from SEQ ID NO: 300-599, or an amino acid sequence having at least 80% sequence identity to a sequence selected from SEQ ID NO: 300-599.

2. The method of claim 1, wherein the polypeptide having the enzymatic activity of (c) iminosuccinate reductase comprises an amino acid sequence selected from SEQ ID NO: 1, 7, 22, 25, 26, 39, 47, 58, 75, 123, 135, and 160, or an amino acid sequence having at least 80% sequence identity to a sequence selected from SEQ ID NO: 1, 7, 22, 25, 26, 39, 47, 58, 75, 123, 135, and 160.

3. The method of claim 1 or 2, wherein the polypeptide having the enzymatic activity of (c) iminosuccinate reductase comprises an amino acid sequence as set forth in SEQ ID NO: 135, or an amino acid sequence having at least 80% sequence identity to said sequence; and the polypeptide having the enzymatic activity of (d) aspartate-glyoxylate transaminase comprises an amino acid sequence as set forth in SEQ ID NO: 433, or an amino acid sequence having at least 80% sequence identity to said sequence.

4. The method of any one of claims 1 to 3, wherein the polypeptides having the enzymatic activities (a)-(d) comprise an amino acid sequence targeting said polypeptides to the peroxisomes.

5. The method of claim 4, wherein the (a) *erythro*-ß-hydroxyaspartate aldolase belonging to the EC class 4.1.3.14 is C-terminally fused to a peroxisomal targeting signal 2 of SEQ ID NO: 952 and the polypeptides having the enzymatic activities (b)-(d) are N-terminally fused to a peroxisomal targeting signal 1 of amino acid sequence SKL.

6. The method of any one of claims 1 to 3, wherein the one or more nucleic acids further encode a polypeptide having the enzymatic activity of

    (e) glycolate dehydrogenase belonging to the EC class 1.1.99.14,

    wherein the introduction of said nucleic acid(s) results in a *de novo* expression of at least five polypeptides having the enzymatic activity of

    (a) *erythro*-ß-hydroxyaspartate aldolase belonging to the EC class 4.1.3.14,

(b) *erythro*-ß-hydroxyaspartate dehydratase belonging to the EC class 4.3.1.20,

(c) iminosuccinate reductase,

(d) aspartate-glyoxylate transaminase, and

(e) glycolate dehydrogenase belonging to the EC class 1.1.99.14,

wherein said polypeptides having the enzymatic activities (a)-(e) are localized in cellular mitochondria, and wherein said polypeptides having the enzymatic activities (a)-(e) are N-terminally fused to a serine hydroxymethyltransferase 1 target peptide of SEQ ID NO: 919.

7. The method of any one of claims 1 to 3, wherein the one or more nucleic acids further encode two polypeptides having the enzymatic activities of

(e) glycolate dehydrogenase belonging to the EC class 1.1.99.14,

(f) phosphoenolpyruvate carboxykinase belonging to the EC class 4.1.1.49

wherein the introduction of said nucleic acid(s) results in a *de novo* expression of at least six polypeptides having the enzymatic activities of

(a) *erythro*-ß-hydroxyaspartate aldolase belonging to the EC class 4.1.3.14,

(b) *erythro*-ß-hydroxyaspartate dehydratase belonging to the EC class 4.3.1.20,

(c) iminosuccinate reductase,

(d) aspartate-glyoxylate transaminase,

(e) glycolate dehydrogenase belonging to the EC class 1.1.99.14, and

(f) phosphoenolpyruvate carboxykinase belonging to the EC class 4.1.1.49,

wherein said polypeptides having the enzymatic activities (a) - (f) are localized in cellular chloroplasts, and wherein said polypeptides having the enzymatic activities (a) - (f) are N-terminally fused to *Arabidopsis* Ferredoxin-2 chloroplastic target peptide of SEQ ID NO: 917.

8. A transgenic plant comprising one or more heterologous nucleic acids encoding at least four polypeptides having the enzymatic activities of (a) *erythro*-ß-hydroxyaspartate aldolase belonging to the EC class 4.1.3.14, (b) *erythro*-ß-hydroxyaspartate dehydratase belonging to the EC class 4.3.1.20, (c) iminosuccinate reductase comprising an amino acid sequence selected from SEQ ID NO: 1-299, or

an amino acid sequence having at least 80% sequence identity to a sequence selected from SEQ ID NO: 1-299; and (d) aspartate-glyoxylate transaminase comprising an amino acid sequence selected from SEQ ID NO: 300-599, or an amino acid sequence having at least 80% sequence identity to a sequence selected from SEQ ID NO: 300-599.

9. The transgenic plant of claim 8, wherein the polypeptide having the enzymatic activity of (c) iminosuccinate reductase comprises an amino acid sequence selected from SEQ ID NO: 1, 7, 22, 25, 26, 39, 47, 58, 75, 123, 135, and 160, or an amino acid sequence having at least 80% sequence identity to a sequence selected from SEQ ID NO: 1, 7, 22, 25, 26, 39, 47, 58, 75, 123, 135, and 160.

10. The transgenic plant of claim 8 or 9, wherein the wherein the polypeptide having the enzymatic activity of (c) iminosuccinate reductase comprises an amino acid sequence as set forth in SEQ ID NO: 135, or an amino acid sequence having at least 80% sequence identity to said sequence; and the polypeptide having the enzymatic activity of (d) aspartate-glyoxylate transaminase comprises an amino acid sequence as set forth in SEQ ID NO: 433, or an amino acid sequence having at least 80% sequence identity to said sequence.

11. The transgenic plant of any one of claims 8 to 10, wherein the (a) *erythro*-ß-hydroxyaspartate aldolase belonging to the EC class 4.1.3.14 is C-terminally fused to a peroxisomal targeting signal 2 of SEQ ID NO: 952 and the polypeptides having the enzymatic activities (b)-(d) are N-terminally fused to a peroxisomal targeting signal 1 of amino acid sequence SKL.

12. The transgenic plant of any one of claims 8 to 10, wherein the one or more nucleic acids further encode a polypeptide having the enzymatic activity of (e) glycolate dehydrogenase belonging to the EC class 1.1.99.14, wherein said polypeptides having the enzymatic activities (a)-(e) are localized in cellular mitochondria, and wherein said polypeptides having the enzymatic activity (a) - (e) are N-terminally fused to a serine hydroxymethyltransferase 1 target peptide of SEQ ID NO: 919.

13. The transgenic plant of any one of claims 8 to 10, wherein the one or more nucleic acids further encode two polypeptides having the enzymatic activities of (e) glycolate dehydrogenase belonging to the EC class 1.1.99.14, (f) phosphoenolpyruvate carboxykinase belonging to the EC class 4.1.1.49, wherein said polypeptides having the enzymatic activities (a)-(f) are localized in cellular chloroplasts, and wherein said

polypeptides having the enzymatic activity (a) - (f) are N-terminally fused to *Arabidopsis* Ferredoxin-2 chloroplastic target peptide of SEQ ID NO: 917.

14. The transgenic plant of any one of claims 8 – 13, wherein the plant is selected from *Helianthus annuus, Brassica napus, Camelina sativa, Oryza sativa, Hordeum vulgare, Triticum spp., Avena sativa, Solanum lycopersicum, Solanum tuberosum, Glycine max, Beta vulgaris, Nicotiana tabacum*, and *Arabidopsis thaliana.*

15. A nucleic acid construct comprising nucleic acid sequences encoding at least four polypeptides having the enzymatic activities of (a) erythro-ß-hydroxyaspartate aldolase belonging to the EC class 4.1.3.14, (b) erythro-ß-hydroxyaspartate dehydratase belonging to the EC class 4.3.1.20, (c) iminosuccinate reductase comprising an amino acid sequence selected from SEQ ID NO: 1-299, or an amino acid sequence having at least 80% sequence identity to a sequence selected from SEQ ID NO: 1-299; (d) aspartate-glyoxylate transaminase comprising an amino acid sequence selected from SEQ ID NO: 300-599, or an amino acid sequence having at least 80% sequence identity to a sequence selected from SEQ ID NO: 300-599, a selection marker nucleic acid, wherein the nucleic acid sequences are operably linked to at least one promoter for expression in a plant and are operably linked to at least one terminator.

Manuscript II

CO_2-neutral photorespiration in plants by engineering a cytosolic one carbon unit sink

Marc-Sven Roell,[1] Philipp Westhoff,[1,3] Miguel Miñambres Martin,[1,2,3] Simon Strobbe,[4] Jana Verstraete,[5] Christophe Stove,[5] Dominique Van Der Straeten,[4] Matias D. Zurbriggen,[2,3] Andreas P.M. Weber [1,3]*

[1] Institute of Plant Biochemistry, Heinrich Heine University, Düsseldorf, Germany
[2] Institute of Synthetic Biology, Heinrich Heine University, Düsseldorf, Germany
[3] Cluster of Excellence on Plant Science (CEPLAS), Heinrich Heine University, Düsseldorf, Germany
[4] Laboratory of Functional Plant Biology, Department of Biology, Ghent University, Ghent, Belgium
[5] Laboratory of Toxicology, Department of Bioanalysis, Ghent University, Ghent, Belgium

Status: in preparation

Own contribution:

I designed the T-DNA constructs, including the choice of the promoters and established the transgenic lines that express the cytosolic reductive glycine pathway. All lines were phenotypically analyzed by myself including experiments and the data analysis to assess the metabolome of these plants, except the folate analysis. Further, the concept of the photosynthetic tissue specific CRISPR/Cas9 module was developed by myself as well as the module design and the characterization of the module so far.

CO_2-neutral photorespiration in plants by engineering a cytosolic one carbon unit sink

Marc-Sven Roell,[1,3] Philipp Westhoff,[1,4] Miguel Miñambres Martin,[1,2,4] Simon Strobbe,[5] Jana Verstraete,[6] Christophe Stove,[6] Dominique Van Der Straeten,[5] Matias D. Zurbriggen,[2,4] Andreas P.M. Weber [1,4]*

[1] Institute of Plant Biochemistry, Heinrich Heine University, Düsseldorf, Germany

[2] Institute of Synthetic Biology, Heinrich Heine University, Düsseldorf, Germany

[3] iGRAD Plant Graduate School, Heinrich Heine University, Düsseldorf, Germany

[4] Cluster of Excellence on Plant Science (CEPLAS), Heinrich Heine University, Düsseldorf, Germany

[5] Laboratory of Functional Plant Biology, Department of Biology, Ghent University, Ghent, Belgium

[6] Laboratory of Toxicology, Department of Bioanalysis, Ghent University, Ghent, Belgium

* For correspondence (E-mail: andreas.weber@hhu.de)

ORCID-IDs: 0000-0003-2714-8729 (M.-S.R.); 0000-0003-0970-4672 (A.P.M.W.)

Author contributions

M.-S.R., P.W., M.M.M., S.S., J.V., C.S., D.V.D.S., M.D.Z. and A.P.M.W designed research. M.-S.R., P.W., M.M.M., S.S., J.V. performed research. M.-S.R., P.W., M.M.M., S.S., J.V., C.S., D.V.D.S., M.D.Z. and A.P.M.W analyzed data. M.-S.R., P.W., M.M.M., M.D.Z. and A.P.M.W wrote the manuscript.

Keywords

Synthetic Biology | Photorespiration | Metabolic engineering | Tissue specific knockout

This Manuscript includes:

Main text, 5 figures, supplemental information

Abstract

Rising levels of greenhouse gas emission threaten the global climate and agricultural productivity. Plants naturally sequester atmospheric carbon dioxide (CO_2) and convert it into biomass. However, the primary CO_2-fixing enzyme, ribulose-1,5-bisphosphate carboxylase/oxygenase (Rubisco) also accepts oxygen as substrate and Rubisco-catalyzed oxygenation requires the recycling of photosynthetically fixed carbon by photorespiration. During photorespiration up to 30% of previously fixed carbon is lost and this loss will increase in a climate changing environment of elevated temperature and enhanced drought. Therefore, genetically engineering CO_2-neutral photorespiration will positively impact plant growth. Here, we set the genetic basis for CO_2-neutral photorespiration in plants by module-assisted engineering. Photorespiratory CO_2-release depends on the mitochondrial glycine to serine conversion that requires a one-carbon unit, produced by glycine oxidation via the glycine decarboxylase complex. We implemented the reductive glycine pathway in *Arabidopsis thaliana* to provide a cytosolic sink for one-carbon units by tetrahydrofolate-dependent formate assimilation. The produced one-carbon unit is used for the glycine decarboxylase independent glycine to serine conversion in a CO_2-neutral manner. In order to address limited metabolic flux towards serine biosynthesis, we developed a photosynthetic tissue-specific clustered regularly interspaced short palindromic repeat (CRISPR)/ CRISPR-associated protein 9 (Cas9) [CRISPR/Cas9]) module. This allows to redirect the flux towards the synthetic bypass by knockout out of the glycine decarboxylase P-subunit and formate dehydrogenase, as CO_2-releasing and interfering reactions of canonical plant photorespiration.

Introduction

Two major societal challenges are on one hand the rising atmospheric carbon dioxide (CO_2) concentrations that threaten the balance of the planetary climate, and on the other, innovative strategies to efficiently sequester the released CO_2 (Kim et al., 2020). Currently, chemical CO_2 sequestration into syngas and downstream processing into complex hydrocarbons, is limited by a small product spectrum and low product specificity (Liao et al., 2016). Hybrid systems of physiochemical and biological processes can be optimized for efficient CO_2 sequestration and broad-spectrum utilization (Claassens et al., 2019; Satanowski and Bar-Even, 2020). In a hybrid system, renewable energies are used to activate CO_2 into small molecules, e.g. one-carbon (C_1) compounds like methanol and formate (Claassens et al., 2019). The subsequent microbial utilization of the C_1 molecules into biomass or commercial carbon-based products sets the framework of the microbial C_1

bioeconomy (Satanowski and Bar-Even, 2020). Compared to hybrid systems that require engineered microbes to convert the C_1 molecules, plants (terrestrial and aquatic- including algae) naturally assimilate approximately 170 gigatons atmospheric CO_2 per year by photosynthetic carbon fixation (Bar-On and Milo, 2019). Catalyst of the photosynthetic carbon fixation is ribulose 1,5-bisphophate carboxylase/oxygenase (Rubisco), the most abundant enzyme on earth (Bar-On and Milo, 2019). However, photosynthetic carbon fixation is limited by the Calvin-Benson-Bassham cycle (CBBC) and Rubisco's acceptance of oxygen as substrate (Raines, 2003). Carbon recycling and detoxification of the oxygenation product, 2-phosphoglycolate, by photorespiration releases up to 30% of previously fixed carbon (Walker et al., 2016). Synthetic biology aims to design new-to-nature biological solutions for CO_2 fixation by constructing synthetic pathways, organelles and organisms (Bar-Even et al., 2010; Antonovsky et al., 2016; Schwander et al., 2016; Gleizer et al., 2019; Kim et al., 2020; Miller et al., 2020). The transfer of these approaches to a plant system, either as synthetic photorespiratory bypasses or CBBC/ Rubisco-independent CO_2 fixation via C_1 units (e.g. formate), promises a boost for plant growth (Bar-Even, 2018; Trudeau et al., 2018; Shen et al., 2019; South et al., 2019; Weber and Bar-Even, 2019).

In plants, C_1 metabolism is directly connected with photorespiration (Eisenhut et al., 2019; Busch, 2020). The mitochondrial glycine decarboxylase complex (GDC), produces a C_1 tetrahydrofolate (THF) intermediate by glycine oxidation, thereby releasing NH_3 and CO_2 while producing NADH (Engel et al., 2007; Timm et al., 2012; Timm et al., 2017). In brief, the GDC consists of four subunits (P, T, L and H). The H-protein (GLDH) acts as a mobile element that undergoes a three-step cycle of (1) reductive methylamination, catalyzed by the P-subunit and releasing CO_2, (2) methylamine transfer by the T-protein (GLDT) releasing NH_3 and producing the C_1 THF intermediate 5,10-methylene-THF and finally (3) electron transfer by the L-protein (GLDL) to produce NADH and recycling of the H-protein (Douce et al., 2001; Wittmiß et al., 2020). The produced C_1 unit is then condensed with a second glycine molecule by serine hydroxymethyltransferase 1 (SHM1) to produce serine and subsequent 3-phosphoglycerate regeneration (Fig. 1; Voll et al., 2006; Eisenhut et al., 2019). Instead of utilization for serine biosynthesis, GDC-derived 5-10-methylene-THF is oxidized to produce formate and further CO_2 (Fig. 1). Thereby the THF moiety is recycled, an essential requirement for functional photorespiration, as shown by the photorespiratory phenotype of the 10-formyl-THF deformylase double knockout mutant (Fig. 1; Collakova et al., 2008). Further, the lethality of glycine decarboxylase mutants and mitochondrial serine hydroxymethyltransferase define mitochondria as hub of cellular C_1 metabolism (Engel et al., 2007; Engel et al., 2011a;

Timm et al., 2017). However, unstable and low abundant C_1 metabolites, severe phenotypes of characterized mutants and a high genetic redundancy that requires higher order mutants, limit a conceptualized understanding of C_1 metabolism in plants (Hanson and Roje, 2001; Mehrshahi et al., 2010; Groth et al., 2016). The rise of the clustered regularly interspaced short palindromic repeat (CRISPR)/CRISPR-associated protein 9 (Cas9) [CRISPR/Cas9] system for genome editing now offers the opportunity to characterize these blackspots in primary plant metabolism, in particular by tissue-specific knockout strategies to study constitutive lethal loss-of-function mutants (Decaestecker et al., 2019).

Here, we set the genetic basis for CO_2-neutral photorespiration in plants by module-assisted genetic engineering. Within the first module, we established the cytosolic reductive glycine pathway (cRGP) in *Arabidopsis thaliana* (Arabidopsis) to provide C_1 units by THF-dependent formate assimilation and facilitate GDC/SHM1-independent glycine to serine conversion (Fig. 1). The implementation of the cRGP slightly impaired plant growth, in particular by low cytosolic glycine to serine conversion and elevated methionine biosynthesis. Therefore, we developed a photosynthetic tissue-specific CRISPR/Cas9 module to optimize metabolic flux by knocking out the GDC P-subunit (GLDP) and mitochondrial NAD-dependent formate dehydrogenase (FDH1), the CO_2-releasing reactions of plant photorespiration. Plants with a photosynthetic tissue specific knockout of both *GLDP* genes overcame the seedling-lethal phenotype of previously characterized loss-of-function mutants (Engel et al., 2007), but showed impaired growth under photorespiratory conditions. At a current stage, the combination of both modules did not enhance plant growth, likely because the high photorespiratory flux could not be sustained by low cellular formate levels – a matter that needs to be addressed by a third engineering module.

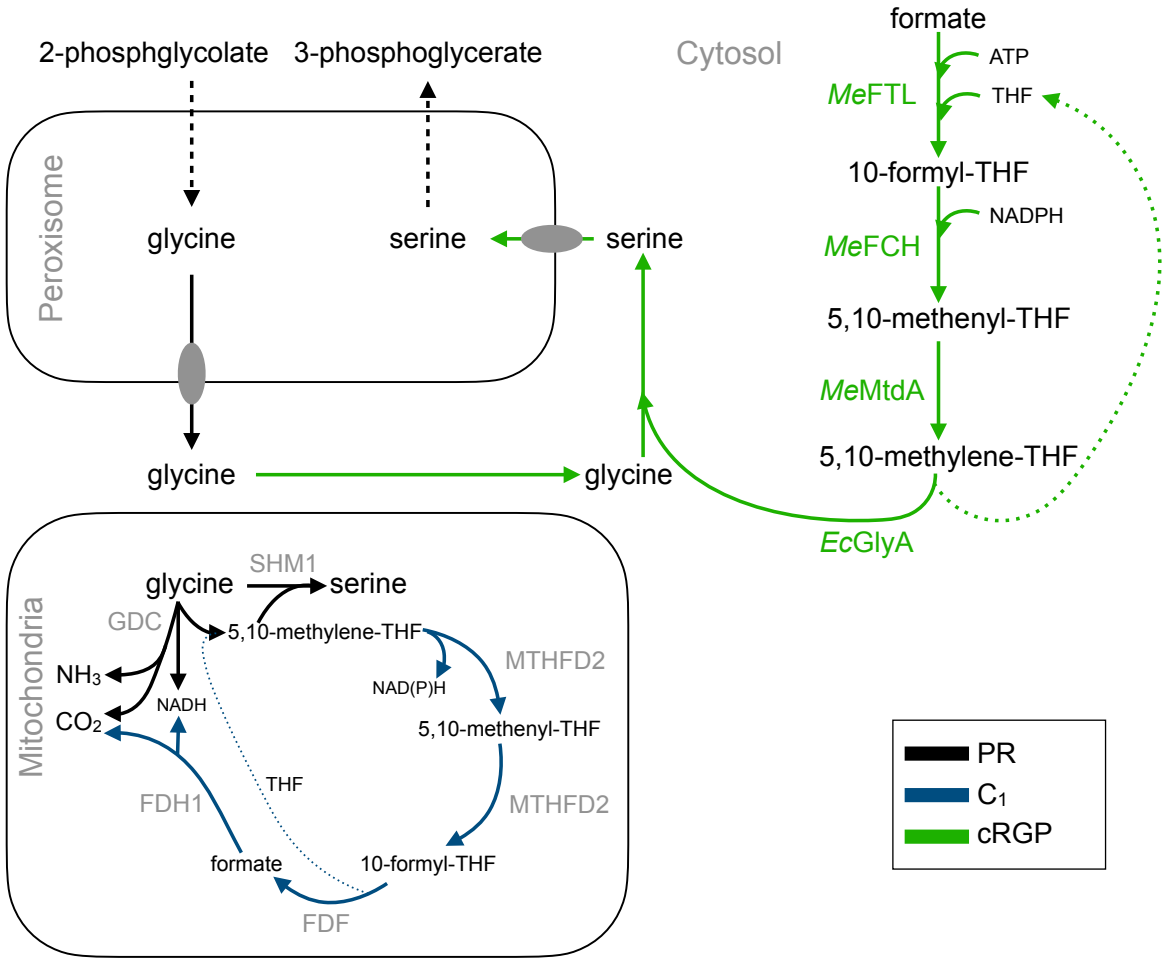

Fig. 1: The reductive glycine pathway to engineer CO_2 neutral photorespiration in plants. Partial schematic representation of plant photorespiration (PR), auxillary one-carbon metabolism (C_1) and the integration of the reductive glycine pathway (cRGP). Abbreviations: *Methylobacterium extorquens AM1* 10-formyl-THF ligase (*Me*FTL), methenyl-THF cyclohydrolase (*Me*FCH) and NADP-dependent methylene-THF dehydrogenase (*Me*MtdA) and *E. coli* serine hydroxymethyl transferase (*Ec*GlyA), serine hydroxymethyltransferase 1 (SHM1), glycine decarboxylase complex (GDC), bifunctional methylenetetrahydrofolate dehydrogenase/cyclohydrolase (MTHDF2), 10-formyl-THF deformylase (FDF), formate dehydrogenase 1 (FDH1). Native Arabidopsis enzymes are indicated in grey. The unknown peroxisomal glycine and serine transport proteins are indicated as grey oval.

Results

Formate assimilation by native C_1 metabolism in plants

Plants encode enzymes for the THF-dependent formate assimilation into serine by 10-formyl-THF synthetase (FTHFS), the bifunctional methylene-THF dehydrogenase/ methenyl-THF cyclohydrolase (MTHFD) and SHM in the cytosol, plastid and mitochondria (Hanson and Roje, 2001; Voll et al., 2006; Zhang et al., 2010; Engel et al., 2011; Groth et al., 2016). The ATP-dependent condensation of formate and THF by FTHS

produces 10-formyl-THF, used in purine- and histidine biosynthesis (Zrenner et al., 2006). Alternatively, 10-formyl-THF is converted into 5,10-methenyl-THF and further 5,10-methylene-THF by the bifunctional methylenetetrahydrofolate dehydrogenase/cyclohydrolase (MTHFD; Groth et al., 2016). At least three metabolic routes are served via the 5,10-methylene-THF pool: (1) cytosolic/plastidial methionine biosynthesis by methyl-THF reductase and methionine synthase, (2) serine biosynthesis by SHM and (3) thymidylate biosynthesis by mitochondrial/cytosolic bifunctional dihydrofolate reductase-thymidylate synthase (Supplemental Fig. S1; Ravanel et al., 1998; Hanson and Roje, 2001; Ravanel et al., 2004; Gorelova et al., 2017).

Formate assimilation by native THF-dependent C_1 metabolism was demonstrated in yeast and mammalian cells, but did not take place in *E. coli* (Ducker et al., 2016; Yishai et al., 2017; Zheng et al., 2018; Gonzalez De La Cruz et al., 2019). We used steady-state formate-^{13}C labeling of Arabidopsis seedlings and assessed the contribution of formate assimilation on methionine-, serine- and histidine biosynthesis (Supplemental Fig. S1). To this extent, five days old seedlings were cultivated on agar with 1 mM sodium formate-^{13}C for five days before harvest. The ^{13}C label enrichment in soluble amino acid pools of serine (3.32 ± 0.84%), methionine (44.45 ± 5.99%) and histidine (6.85 ± 3.55%) demonstrated formate assimilation by native C_1 metabolism in plants (Supplemental Fig. S1). Futher, the disturbance of mitochondrial glycine/serine metabolism in the *shm1* mutant enhanced ^{13}C label incorporation into methionine (1.5-fold), serine (3-fold) and histidine (3-fold, Supplemental Fig. S1).

The cytosolic reductive glycine pathway impairs plant growth

We hypothesized that the low enzyme abundance and unknown regulation of native C_1 metabolism might be insufficient to produce C_1 units for the synthetic bypass. Recently, the reductive glycine pathway (RGP) was employed as the seventh natural CO_2 fixation pathway and used as synthetic route to enable auxotrophic growth of *E. coli* on formate and methanol (Yishai et al., 2017; Kim et al., 2020; Sánchez-Andrea et al., 2020). Core of the synthetic pathway to convert formate into 5,10-methylene-THF are three enzymes from the methylotrophic bacterium *Methylobacterium extorquens* AM1 (10-formyl-THF ligase (*Me*FTL), methenyl-THF cyclohydrolase (*Me*FCH), NADP-dependent methylene-THF dehydrogenase (*Me*MtdA; Crowther et al., 2008)). The final step, the condensation of 5,10-methylene-THF with glycine to serine, is catalyzed by *E. coli* SHM (*Ec*GlyA, Fig. 1). We implemented a cytosolic variant of the RGP (cRGP) into Arabidopsis wild type *Col-0* (WT) via a multi-gene T-DNA construct and photosynthetic tissue specific pathway expression under strong promoters. In detail, the Arabidopsis Rubisco small subunit 1B,

2B, 3B and chlorophyll A binding protein promoters were used to drive cRGP expression in photosynthetic tissue (Supplemental Fig. S2; Dedonder et al., 1993; Mitra et al., 2009). We validated full cRGP implementation on a genomic level and confirmed the abundance of all cRGP enzymes in three independent transgenic lines by immunoblot analysis (Supplemental Fig. S2). The three transgenic lines (Lines #1, #9, #11, hereafter as *Col-0::cRGP#1-3*) showed reduced photosynthetic efficiency, but were not altered in chlorophyll content (Fig. 2B, Supplemental Fig. S2). Further, the cRGP diminished plant growth, independent of growth under photorespiratory conditions in ambient air (400 ppm CO_2) or non-photorespiratory conditions in CO_2 enriched air (3000 ppm CO_2) (Fig. 2C and D, Supplemental Fig. S7). Remarkably, plants with a detectable abundance of only *Me*FTL and *Ec*GlyA showed WT-like phenotype (exemplified by line #17, Fig. 2 and Supplemental Fig. S2).

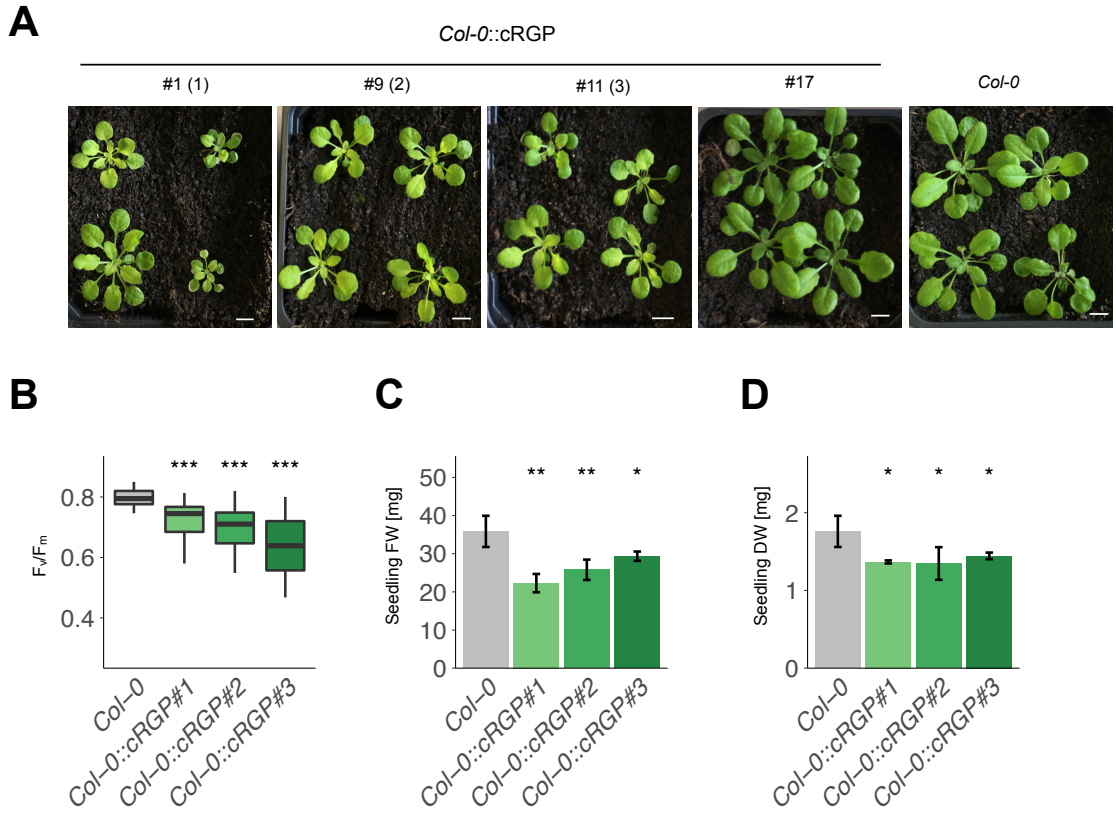

Fig. 2: The reductive glycine pathway impairs plant growth. A) Phenotype of four independent transgenic Arabidopsis lines with an implemented reductive glycine pathway (cRGP) in comparison to wild type *Col-0*. The lines #1, #9 and #11 expressed all four enzymes of the cRGP (Supplemental Fig. S1). Pictures were taken after 28 days of growth in ambient air (400 ppm CO_2, 12h light/ 12h dark). Scalebar = 1 cm. B) F_v/F_m values of twelve days old seedlings grown in ambient air. n >25 per genotype. C) Seedling fresh weight (FW) and D) seedling dry weight (DW) of 12-days-old seedlings grown in ambient air. n = 4. Shown is mean ± SD. Student's *t*-test against wild type *Col-0*, p < 0.05 = *, < 0.01 = **, < 0.001 = ***.

Cytosolic glycine to serine conversion is the limiting step of the cRGP

To understand the metabolic implications of the cRGP that caused the observed phenotype, we used steady-state metabolome profiling on 14-days-old seedlings grown in ambient air (Supplemental Fig. S3). Relative quantification of soluble amino acid pools revealed cRGP-dependent methionine and threonine accumulation, whereas glycine and serine pools did not significantly differ compared to WT (Fig. 3A). In addition, we aimed to understand the effects of the cRGP on C_1 metabolism by quantification of total THF-intermediates (C_1 folates, Fig. 3B). To this extent, the absolute levels of 5-methyl-THF, 5,10-methenyl-THF, 5-formyl-THF as mono- or polyglutamylate C_1 folates were determined in green tissue of 14-days-old seedlings (Fig. 3B). Consistent with the increased methionine levels, total 5-methyl-THF levels are elevated in *Col-0::cRGP#1*, *#3* plants (40.91 ± 1.38 and 42.95 ± 1.91 versus 30.91 ± 2.82 µg 100 g FW^{-1} in *Col-0*, Fig. 3B). Further, mono-glutamylated 5-methyl-THF was elevated in *Col-0::cRGP#1*, #2 (21.46 ± 1.05 and 19.97 ± 1.37 versus 16.64 ± 1.49 µg 100 g FW^{-1} in *Col-0*) and poly-glutamylated 5-methyl-THF *in Col-0::cRGP#3* (23.68 ± 2.79 versus 14.28 ± 2.98 µg 100 g FW^{-1} in *Col-0*). Further the 5,10-methenyl-THF levels are reduced in cRGP plants. Total 5-10-methenyl-THF levels are reduced in *Col-0::cRGP#2*, *#3* (53.45 ± 1.17 and 63.55 ± 2.78 versus 83.88 ± 1.36 µg 100 g FW^{-1} in *Col-0*) and polyglutamylated levels are reduced in all three cRGP lines. The 5-formyl-THF levels did not differ between the genotypes (Fig. 3B).

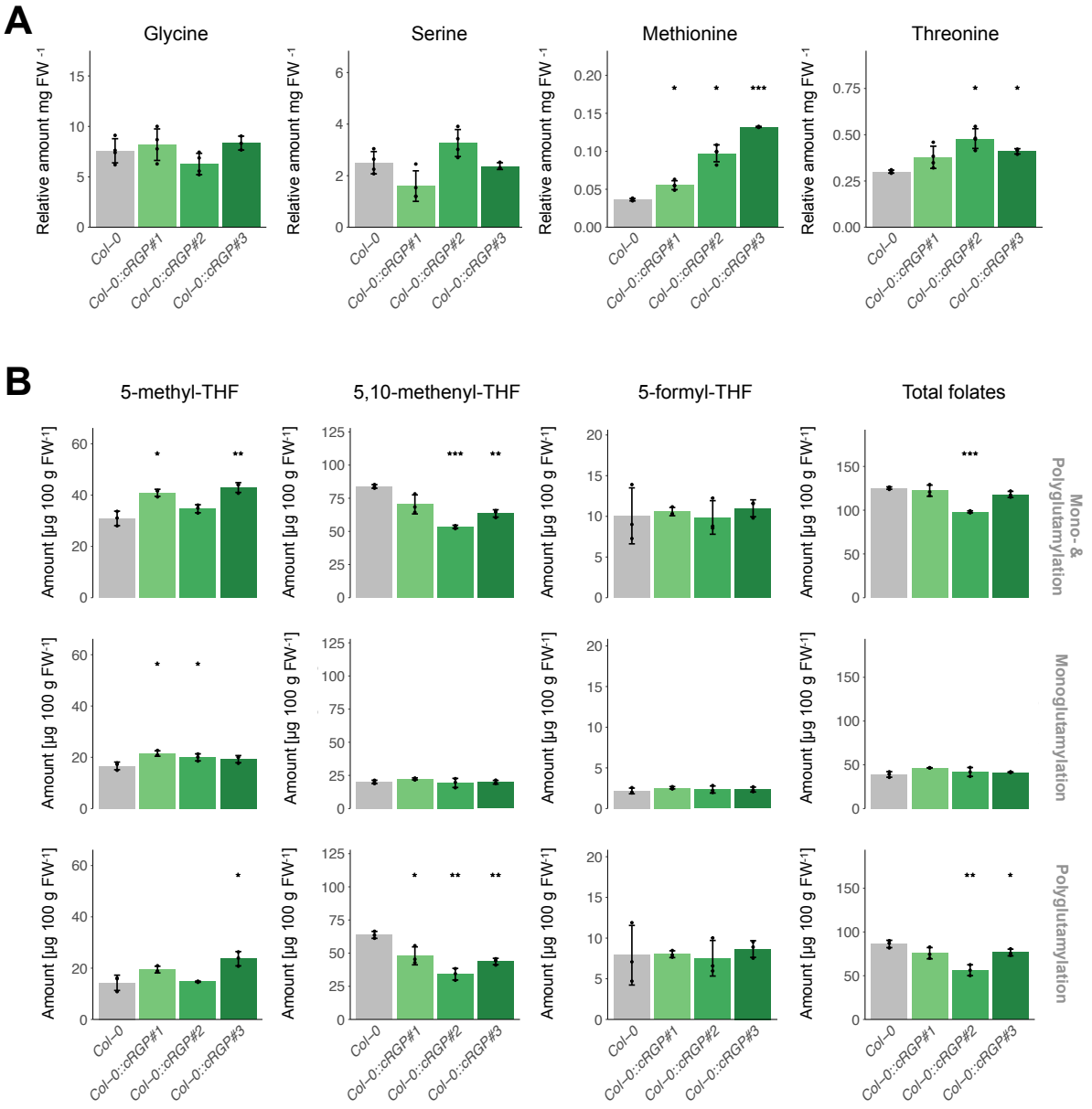

Fig. 3: The cRGP alters soluble amino acid pools and C_1 folate levels. A) Relative metabolite levels of glycine, serine, methionine, threonine in green tissue of 14-days-old seedlings grown in ambient air (400 ppm CO_2). Student's *t*-test against wild type *Col-0*. Asterisks indicate significance after multiple testing correction using Benjamini-Hochberg. p < 0.05 = *, < 0.01 = **, < 0.001 = ***. n = 4, shown mean ± SD, each biological replicate is indicated as point. B) Quantification of cellular C_1 folate levels in green tissue of 14-days-old seedlings grown in ambient air. Total folate represents the sum of all detectable individual C_1 folates and are differentiate in mono- and polyglutamylated C_1 folates. Student's *t*-test against wild type *Col-0*. Asterisks indicate significance p < 0.05 = *, < 0.01 = **, < 0.001 = ***. n = 3, shown mean ± SD and each biological replicate is indicated as point.

A photosynthetic tissue-specific CRISPR/Cas9 module for targeted knockout of cRGP rate limiting steps

Based on the *shm1* amino acid labeling profile (Supplemental Fig. S1) and the metabolome profile of cRGP plants (Fig. 3), we phrased three engineering milestones to be reached to envision the cRGP as CO_2-neutral photorespiratory bypass. First, disturbed photorespiration and mitochondrial C_1 metabolism will favor cytosolic C_1 metabolism and thereby the cRGP as photorespiratory bypass. Second, the cytosolic pools of glycine and serine need to be adjusted to ensure serine production by *Ec*GlyA and avoid 5,10-methylene-THF use for methionine biosynthesis. Third, we assumed that native formate catabolism by mitochondrial NAD-dependent formate dehydrogenase 1 (FDH1) negatively impacts the cRGP by formate oxidation (see for details on FDH1 in plants Manuscript III in this thesis). The knockout out of both *GLDP* genes that encode the GDC P-subunit, addresses two of the defined engineering milestones, (a) disturbed photorespiratory flux and (b) cytosolic glycine accumulation to ensure serine biosynthesis. However, reverse genetic studies on *GLDP1* and *GLDP2* revealed seedling lethality of homozygous *gldp1glp2* loss-of function mutants in Arabidopsis (Engel et al., 2007).

We developed two photosynthetic tissue-specific CRISPR/Cas9 modules to either mutate *GLDP1* and *GLDP2* (tkoG) and or in combination with *FDH1* (tkoGF) to also address the third engineering milestone (Supplemental Fig. S4). The CRISPR/Cas9 module was based on somatic mutations in photosynthetic tissue and should thereby overcome seedling lethality of constitutive *gldp1gldp2* mutants (Engel et al., 2007). The module consisted of four individual genetic parts. A seed-specific expressed turbo eGFP under the *NapinA* promoter and a constitutively overexpressed eGFP under the *UBIQUITIN10* promoter served as fluorescent reporters (Supplemental Fig. S4; Stålberg et al., 1996; Grefen et al., 2010). Functionality of the reporters was tested in tobacco protoplasts and stable transgenic Arabidopsis plants (Supplemental Fig. S4). Photosynthetic tissue specificity of the Cas9 endonuclease was ensured by expression of the *Streptococcus pyogenes* Cas9 protein under the Arabidopsis Rubisco small subunit 2 B promoter (Dedonder et al., 1993). Finally, a transfer RNA–guide RNA multiplexing system was used to target each gene with two guide RNAs (gRNA) respectively (Supplemental Fig. S4). Based on target gene PCR-amplification and Sanger sequencing, we validated that only the respective gRNA2 induced somatic mutations in *GLDP1*, *GLDP2* and *FDH1* genes in leaf tissue and thereby confirmed functionality of the photosynthetic tissue-specific CRISPR/Cas9 module (Supplemental Fig. S5).

Photosynthetic tissue-specific knockout of the GDC overcomes seedling lethality but impairs plants growth under photorespiratory conditions

We established two independent tkoG lines (*tkoG#1* and *#2*) in the WT background to test the developmental consequences of a photosynthetic tissue-specific *gldp1gldp2* knockout. lants were grown either in ambient air or in CO_2 enriched air. The tkoG plants did not differ in germination efficiency compared to WT under both in ambient air or in CO_2 enriched air (Fig. 4A). Upon seedling development in ambient air three distinct phenotypes appeared in tkoG plants. The three phenotypes were classified based on the degree of growth reduction and include a severe growth phenotype (here after as 'strong'), a milder growth phenotype (here after as 'weak') and WT-like growth ('wildtype'; Fig. 4B). Both the 'strong' and 'weak' phenotype occurred at the same frequency of 40% upon growth of tkoG plants in ambient air (Fig 4C). Further, time-dependent imaging of chlorophyll photochemical efficiency of photosystem II in dark-adapted leaves (F_v/F_m) during seedling development demonstrated reduced F_v/F_m values in tkoG seedlings grown in ambient air (Fig. 4D). Both, 'strong' and 'weak' tkoG plants showed a gradual reduction in F_v/F_m values during seedling development in ambient air (Fig. 4E). Growth under non-photorespiratory condition in a CO_2 enriched environment suppressed the observed phenotypes and the reduction in F_v/F_m values during seedling development (Fig. 4E).

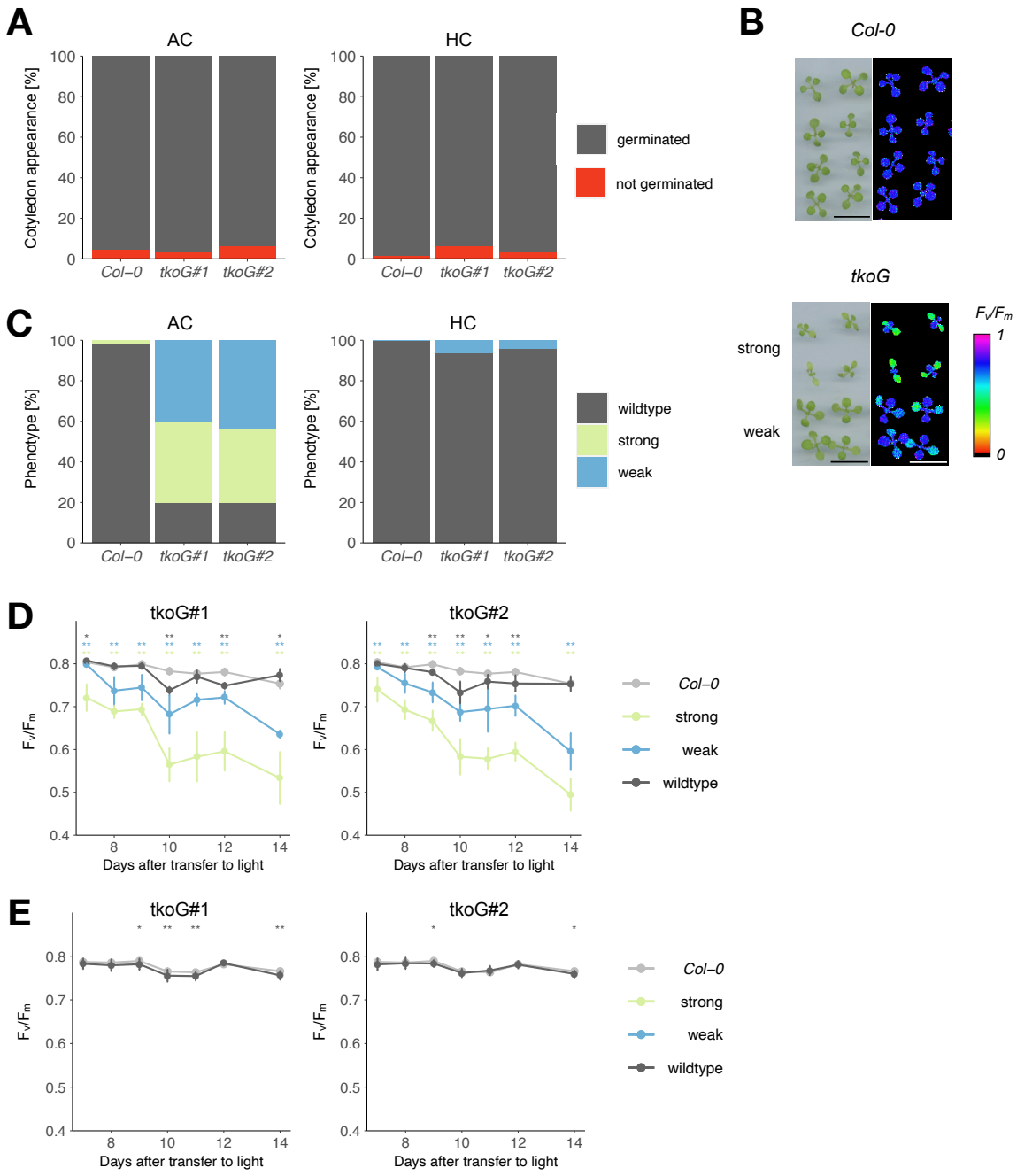

Fig. 4: Photosynthetic tissue-specific knockout of the glycine decarboxylase overcomes seedling lethality. The tkoG module facilitates the knockout of both *GLDP* genes in photosynthetic tissue. Two independent tkoG module containing transgenic Arabidopsis lines were established in the wild type *Col-0* background (*tkoG#1* and *tkoG#2).* A) Germination efficiency of tkoG plants in ambient air (400 ppm CO_2, AC) or in CO_2 enriched air (3000 ppm CO_2, HC). Germination was quantified as cotyledon appearance four days after transfer to light. n > 25. B) Representative image of the phenotypes of tkoG plants grown under ambient CO_2. Images taken 12 days after transfer to light. Brightfield (left) and representative image of a chlorophyll photochemical efficiency of photosystem II in dark-adapted leaves (F_v/F_m) measurement (right). Scalebar = 1 cm. C) Quantification of phenotype appearance of tkoG plants ('strong', 'weak' and 'wildtype'), grown in ambient air (400 ppm CO_2, AC) or in CO_2 enriched air (3000 ppm CO_2, HC). n> 25. D & E) Quantification of F_v/F_m values during seedling establishment in ambient air (D) or in CO_2 enriched air (E). Shown mean ±SD. n > 25. Student's *t*-test against *Col-0*. p > 0.01 = *, p > 0.001 = **. Colored asterisk indicated the student's *t*-test result for the respective phenotypes of tkoG plants. Wild type *Col-0* is indicated in light grey.

Prolonged growth of 'strong' tkoG plants in ambient air caused an 80% reduction in rosette area and rosette diameter respectively (Fig. 5A and B). Further, we validated reduced GLDP protein in mature rosette leaves of four-week-old 'strong' tkoG plants by immunoblot analysis (Fig. 5C). Additionally, we quantified the level of somatic mutations in *GLDP1* and *GLDP2* genes in mature leaves of four-week-old rosettes 'strong' tkoG plants by qPCR (Supplemental Fig. S5). Therefore gene specific primers were designed that span the site of Cas9 induced double strand breaks at the gRNA site to quantify the degree of induced indel mutations (Yu et al., 2014). In 'strong' tkoG plants the presence of WT *GLDP1* and *GLDP2* is diminished by 85% and 50% on average respectively (Fig. 5D). Considering each leaf as a chimera of different induced mutations in *GLDP* genes, the overall degree of somatic mutations remained constant between leaves of independent plants of *tkoG#1* and *#2* plants (Fig. 5D). In addition to the tkoG module, we also implemented the tkoGF module in the WT background to simultaneously mutate *GLDP1*, *GLDP2* and *FDH1* (Supplemental Figure S4). Two independent transgenic lines were established (*tkoGF#1* and *#2*). Compared to WT, 'strong' tkoGF plants were 50% reduced in rosette area and rosette diameter (Fig. 5E and F). Growth of tkoG and tkoGF plants CO_2 enriched air repressed the observed growth phenotypes and plants were indistinguishable from WT regarding rosette area and diameter (Fig. 5, Supplemental Fig. S6).

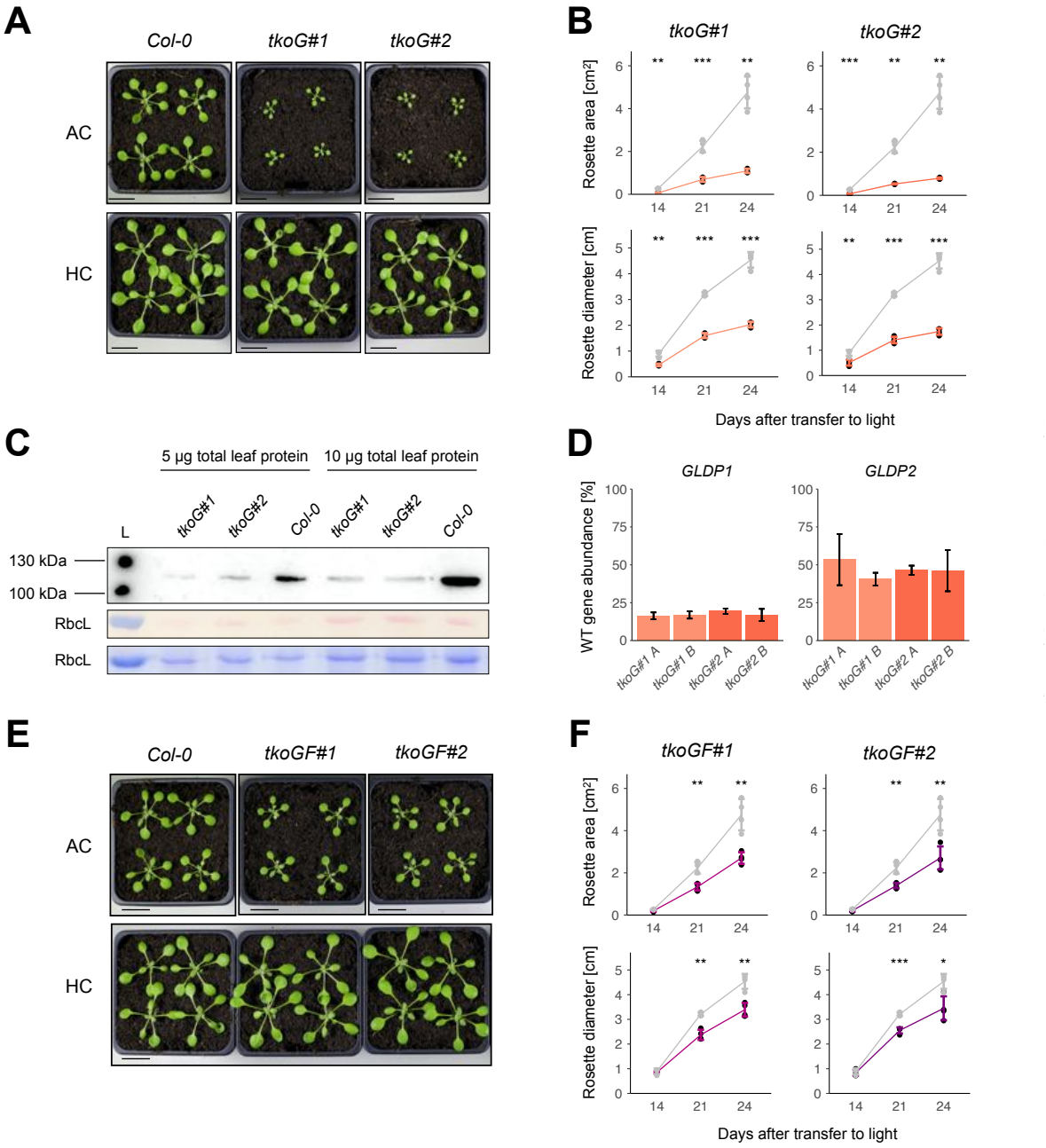

Fig. 5: Photosynthetic tissue specific knockout of the glycine decarboxylase affects plants growth under photorespiratory conditions. A) Phenotype of three-weeks-old 'strong' tkoG plants grown in ambient air (400 ppm CO_2, AC) or in CO_2 enriched air (3000 ppm CO_2, HC). Scalebar = 2 cm. B) Rosette area (top row) and rosette diameter (bottom row) were quantified in AC grown 'strong' tkoG plants. Wild type *Col-0* is indicated in light grey. Shown mean ± SD. n= 4. C) GLDP protein abundance in tkoG plants was quantified by immunoblot analysis. Total leaf protein from the fourth leaf of four-week-old AC grown rosettes was loaded. Rubisco large subunit (RbcL) detected by ponceau- and coomassie staining served as loading control. D) Quantification of wild type (WT) *GLDP1* and *GLDP2* abundance by qPCR. Genomic DNA from the fourth mature leaf of two independent plants (A & B) was isolated. Wild type *Col-0* was set to 100 %. Shown mean ± SD. n_{tech} = 4. E) Phenotype of three-weeks-old 'strong' tkoGF plants grown in AC or in HC. Scalebar = 2 cm. F) Rosette area (top row) and rosette diameter (bottom row) was quantified in AC grown 'strong' tkoGF plants. Wild type *Col-0* is indicated in light grey. Shown mean ± SD. n= 4. Line connects means. For B) and F) Student's *t*-test against *Col-0*. p <0.05 = *, < 0.01 = **, p < 0.001 = ***.

Setting the genetic basis for CO_2-neutral photorespiration

Finally, we combined the cRGP module with the photosynthetic tissue specific CRISPR/Cas9 module to set the genetic basis for CO_2-neutral photorespiration via a cytosolic C_1 unit sink. Therefore, we established independently the tkoG and tkoGF modules in *Col-0::cRGP#1* and *#3* backgrounds. Per cRGP background genotype two independent transgenic lines were established for each photosynthetic tissue specific CRISPR/Cas9 module. Initially, we quantified plant growth in ambient air, CO_2 enriched air, or shifted from CO_2 enriched air to ambient air three days before harvest. The combination of the cRGP and tkoG module did not significantly recover growth compared to tkoG plants and overall growth was considerably reduced compared to WT (Supplemental Fig. S7). Further the combination of tkoGF and cRGP modules reduced plant growth in the *Col-0::cRGP#1 background* and but remained unaltered in the *Col-0::cRGP*#3 background compared to tkoGF plants. Both, growth in CO_2 enriched air and a three days shift from CO_2 enriched air to ambient air showed a cRGP-dependent growth reduction (Supplemental Fig. S7).

Discussion

Photorespiratory CO_2 release lowers plant growth and reduces the extent atmospheric CO_2 sequestration into biomass. Bypasses of photorespiration have been proven as a valid approach to accelerate plant growth and plant carbon use efficiency (Kebeish et al., 2007; Maier et al., 2012; Shen et al., 2019; South et al., 2019). However, the validation of a metabolic bypass that addresses the hub of photorespiratory CO_2 release, the mitochondrial GDC, in plants is not described. Photorespiratory glycine oxidation by the GDC yields the C_1 unit 5,10-methylene-THF, that is condensed with a second glycine molecule by SHM1 to produce serine (Fig. 1). The underlying biochemistry implies that a potential CO_2-neutral bypass of photorespiration requires an alternative supply of 5,10-methylene-THF for GDC/SHM1-independent glycine to serine conversion in a CO_2-neutral manner. For this purpose, we combined the cRGP, for cytosolic C_1 unit provision based on THF-dependent formate assimilation, with a photosynthetic tissue specific CRISPR/Cas9 module to eliminate CO_2-releasing reactions of photorespiration (GDC and FDH1).

The cornerstone of our approach is the assimilation of formate into serine (Fig. 1). Although a small contribution of native formate assimilation to cellular serine production was shown, the direct use of formate derived C_1 units in auxiliary pathways has not been clarified (Prabhu et al., 1996; Prabhu et al., 1998; Li et al., 2003). Based on formate-^{13}C labeling of Arabidopsis seedlings, we demonstrated that formate derived C_1 units were

predominantly used for histidine- and methionine- rather than serine biosynthesis (Supplementary Fig. S1). We note that, the ^{13}C-label quantification did not consider the cellular pool sizes and the ^{13}C-label abundance in the large serine pool might be underestimated. However, it is assumed that cytosolic and plastidial SHM produce 5,10-methylene-THF for C_1 metabolism by hydroxymethyl transfer to THF rather than serine biosynthesis (Zhang et al., 2010). The cytosol and plastid contribute to 55% of the soluble cellular methionine pool and are autonomous for methionine *de novo* biosynthesis (Ravanel et al., 1998; Ravanel et al., 2004; Szecowka et al., 2013). An average ^{13}C-label enrichment of 44% in methionine indicates that formate assimilation took place in both the cytosol and plastid (Supplementary Fig. S1). This is further supported by ^{13}C-label incorporation in histidine, a consequence of plastidial purine *de-novo* synthesis (Zrenner et al., 2006; Witte and Herde, 2020). This observation supports the hypothesis of intracellular formate dependent C_1 unit provision since the transport of C_1 folates across biological membranes is unlikely (Cybulski and Fisher, 1981; Zrenner et al., 2006; Witte and Herde, 2020; see Manuscript III in this thesis).

Although Arabidopsis is capable to assimilate formate by native C_1 metabolism, we implemented the cRGP to avoid unknown catalytic and regulatory deficits of native plant C_1 metabolism (Yishai et al., 2017; Kim et al., 2020). Based on metabolome profiling we identified glycine to serine conversion as the rate-limiting step of the cRGP (Fig. 3). A low cytosolic glycine/serine ratio would favor the reverse reaction of the final enzyme *Ec*GlyA and in plants the combined C_1 part of the cRGP and the *Ec*GlyA reaction contributed to C1 folate pools (Fig. 3B; Szecowka et al., 2013). In line, the 5,10-methylene-THF and 5-methyl-THF levels increased in cRGP plants (Fig. 3B). In Arabidopsis methylene-THF reductase is not allosterically regulated by *S*-adenosyl-*L*-methionine and would allow a constant metabolic flux towards methionine biosynthesis and the SAM cycle (Fig. 3A; Roje et al., 2002). Remarkably, the cRGP did not influence the cellular 5-formyl-THF levels, which is critical to avoid inhibition of SHM activity by 5-formyl-THF accumulation (Goyer et al., 2005). Further, the large cellular glycine and serine pools were not significantly altered in cRGP plants (Fig. 3), but threonine and branch-chain amino acid levels were elevated and could be explained by increased cytosolic threonine aldolase and methionine γ-lyase activity (Joshi et al., 2006; Joshi and Jander, 2009). Although, the aldol reaction of plants threonine aldolases seems unlikely, direct evidence by glycine-^{13}C labeling is lacking (Prabhu et al., 1996; Prabhu et al., 1998). Taken together, the observed changes in the metabolome of cRPG plants might contribute to the reduced growth phenotype (Fig. 2). However, downstream effects like DNA hypermethylation by increased SAM cycle activity and altered cytosolic redox metabolism are not assessed so far and could be

alternative explanations of the phenotype (Groth et al., 2016; Gorelova et al., 2017; Meng et al., 2018).

A GDC knockout seemed the rational solution to redirect photorespiratory flux towards the cRGP and alter the cytosolic glycine/serine ratio to favor *Ec*GlyA dependent serine production (Fig. 1). The dual role of the GDC in photorespiration and C_1 metabolism prevents traditional reverse genetic approaches due to seedling lethality of loss-of-function mutants (Engel et al., 2007; Timm et al., 2017). Further, a limited understanding on the integration of the GDC in cellular metabolism restricts metabolic engineering approaches and the underlying reasons for the growth supporting effects of GDC subunit overexpression are mysterious (Timm et al., 2012; Timm et al., 2015; Lopez-Calcagno et al., 2019). We developed a tissue specific CRISPR/Cas9 module to knockout both *GLDP* genes in photosynthetic tissue. The use of tissue-specific knockouts is a novel approach to study conditional lethal genes and pioneering work on Arabidopsis root caps, the stomatal lineage and lateral roots demonstrated the potential to induce somatic mutations and study the effects in a defined cell type or tissue (Decaestecker et al., 2019). The role of the GDC in photorespiration explains the reduced growth of tkoG plants in ambient air that is suppressed under non-photorespiratory conditions (Fig. 5, Supplemental Fig. S7). However, the quantity of homozygous *gldp1gldp2* cells within a chimeric leaf, consisting of WT, *gldp1*, *gldp2*, *gldp1glpd2* cells, remained unknown and challenging to determine. Single cell RNA sequencing (scRNA-seq) offers a novel tool to decipher transcriptional changes at the cellular level (Rich-Griffin et al., 2020). We propose that scRNA-seq could be used to identify *gldp1gldp2* cells in tkoG plants and thereby elucidate the transcriptome of a homozygous *GLDP* knockout in plants. The mix of CRISPR/Cas9 genome editing with scRNA-seq is already used in mammalian cells in randomized gRNA screens to identify genetic circuits of epigenetic gene regulation and immune response (Jaitin et al., 2016; Datlinger et al., 2017; Alda-Catalinas et al., 2020). The combination of tissue-specific knockouts in plants with scRNA-seq will be a powerful tool to understand the role of lethal loss-of-function genes in photorespiration, e.g. the peroxisomal serine:glyoxylate aminotransferase (Modde et al., 2017).

In comparison to the observed growth reduction in tkoG plants, the simultaneous knockout of *GLDP1, GLDP2* and *FDH1* affected plant growth less (Fig. 5). It is appealing to believe that reduced formate catabolism increased the formate pool and partially complemented the GDC loss by enhanced cytosolic formate to serine conversion (see Manuscript III in this thesis). However, it remains to be determined if the tkoGF growth

phenotype is based on a metabolic consequence or a result of lower editing efficiency in the *GLDP* genes.

Based on the current understanding of photorespiration, we established the genetic basis for CO_2-neutral photorespiration in plants. However, a growth promoting effect was not observed by combining the cRGP and tkoG or tkoGF modules (Supplemental Fig. S7). Likely, the low intracellular formate concentration (~100 nmol g FW^{-1}) is not sufficient to sustain the high serine demands of photorespiration (Igamberdiev et al., 1999; Wingler et al., 1999). A third engineering module will focus on enhancing *in vivo* formate production. One potential strategy includes the direct conversion of CO_2 into formate by formate dehydrogenase and requires a high reduction potential and/or metal-dependent enzymes (Hartmann and Leimkühler, 2013; Cotton et al., 2018; Nielsen et al., 2019). Alternatively, an acetyl-CoA/malony-CoA shuttle could enable *in vivo* production of formate from bicarbonate (personal communication with Tobias Erb, Max-Planck Institute for Terrestrial Microbiology, Marburg, Germany). It should be noted, that the direct production of formate from CO_2 and the subsequent assimilation by the cRGP will transform plant photorespiration into a carbon positive process (Weber and Bar-Even, 2019).

Conclusion

In summary, the genetic basis for CO_2-neutral photorespiration was set by implementing the cRGP to engineer a cytosolic C_1 unit sink for GDC/SHM1-independent glycine to serine conversion. In addition, the developed photosynthetic tissue specific CRISPR/Cas9 module can be used as a novel tool to redirect the metabolic flux towards a synthetic bypass and eliminate interfering reactions of native plant metabolism. Future work will elucidate the potential of a combined photosynthetic tissue specific knockout with scRNA-seq to understand the role of conditional lethal genes in the photorespiratory cycle. Given the role of the GDC in photorespiration, picturing the transcriptome of a *gldp1gldp2* knockout at the single cell levels will benefit fundamental research and engineering approaches of photorespiration.

Materials and Methods

Gene synthesis

The coding sequences of *Methylobacterium extorquens AM1* 10-formyl-THF ligase (*Me*FTL, EC: 6.3.4.3), methenyl-THF cyclohydrolase (*Me*FCH, EC: 3.5.4.9), NADP-dependent methylene-THF dehydrogenase (*Me*MtdA, EC: 1.5.1.5) and *E. coli* serine

hydroxymethyltransferase (*Ec*GlyA, EC: 2.1.2.1) were codon optimized for expression in Arabidopsis by gene synthesis (ThermoFisher Scientific, Waltham, USA) and matured for golden-gate cloning.

Plasmid construction

All plasmids were generated with the golden-gate based MoClo tool kit, including vector backbones and genetic parts (Engler et al., 2014). Plasmids used for the CRISPR/Cas9 based tool for tissue specific knockouts in photosynthetic tissue were modified from (Xie et al., 2015) and provided by Claus-Peter Witte (University of Hannover, Hannover, Germany). Plasmids were sequenced by Sanger sequencing (Microsynth, Balgach, Switzerland). Generated plasmids and primers used in this study are listed in Supplemental Table S1 and S2, respectively.

Plant material and cultivation conditions

The Arabidopsis ecotype *Col-0* was used as reference wild type and genetic background for transgenic plants. Seeds were surface-sterilized using the vapor-phase sterilization method (Clough and Bent, 1998). Seeds were grown on half-strength Murashige and Skoog medium (pH 5.7) supplemented with 0.8% (w/v) agar (½ MS plates). Seeds were cold stratified for two days at 4°C. After germination, seedlings were grown for 14 days at 100 µmol m^{-2} s^{-1} light intensity, at atmospheric CO_2 concentration (400 ppm) or in CO_2 enriched air (3000 ppm) in 12 hours light/12 hours dark photoperiod prior transfer to soil and cultivation under similar conditions.

For stable isotope labeling experiments with formate-^{13}C, seedlings were grown on ½ MS plates for five days and afterwards transferred to ½ MS plates supplemented with 1 mM sodium formate-^{13}C (Cambridge Isotope Laboratories, Tewksbury, USA). Plates were placed in the growth chamber for five additional days and whole seedlings were harvested in the middle of the light phase.

Generation of transgenic *Arabidopsis* lines

T-DNA constructs were introduced into *Agrobacterium tumefaciens* strain GV3101::pMP90 (Koncz and Schell, 1986) and Arabidopsis *Col-0* plants were transformed via agrobacterium-mediated transformation (Clough and Bent, 1998). Homozygous T3 plants were used for further analysis.

Chlorophyll fluorescence and chlorophyll measurements

F_v/F_m values were measured using an imaging chlorophyll fluorometer (Imaging PAM, Walz, Effeltrich, Germany). Upon dark adaptation for 20 min, seedlings were exposed to

a pulsed, blue probe beam and a saturating light flash to measure F_v/F_m values. Chlorophyll was extracted in 80% acetone and rotating at 4°C in the dark before photometric measurement. Chlorophyll was calculated based on (Inskeep and Bloom, 1985).

Plant phenotyping

For fresh weight and dry weight analysis, either 12- or 14-days old seedlings were harvested and weight for fresh weight analysis. Seedlings were dried for four days at 65°C before dry weight analysis. Germination was quantified as cotyledon appearance four days after transfer to light.

Immunoblot analysis

SDS-PAGE and immunoblot analysis was performed as described in (Laemmli, 1970; Kuhnert et al., 2020). Monoclonal conjugated horseradish peroxidase anti-His antibody (Miltenyi Biotech, Bergisch Gladbach, Germany), polyclonal glycine decarboxylase P protein antibody (Agrisera, Vännäs, Sweden) and goat anti-rabbit IgG horse radish peroxidase (Miltenyi Biotech, Bergisch Gladbach, Germany) were used for immunoblot analysis.

Quantitative real time PCR (qPCR)

Genomic DNA (gDNA) of mature Arabidopsis leaves was extracted by precipitation with isopropanol (Weigel and Glazebrook, 2009). The qRT-PCR was carried out using Luna Universal qPCR Master Mix (New England Biolabs, Ipswich, USA) and a StepOnePlus Real-Time PCR thermocycle (Applied Biosystems, Foster City, USA**).** PCR conditions were as followed: an initial denaturation step at 95°C for 10 min, followed by 45 cycles of 95°C for 15 s, and 60°C for 60 s, followed by a melting curve. Per assay 50 ng of extracted gDNA was used. In order to quantify the degree of mutations gene specific primer were designed that span the Cas9 cleavage site three nucleotides before the PAM (Yu et al., 2014). Primer sequences are listed in Supplemental Table S1 and the primer efficiency for each pair was determined (Supplemental Fig. S5). *ACTIN2* (*ACT2*) served as reference gene. The relative abundance was calculated as described in (Simon, 2003) and for comparison WT levels were set to 100%.

Transient expression in *Nicotiana benthamiana*

Overnight grown *Agrobacterium tumefaciens* GV3101::pMP90 cells, carrying the T-DNA construct were diluted in infiltration medium (10 mM $MgCl_2$, 10 mM MES [pH 5.7], 100 µM acetosyringone) to an OD_{600} of 0.4. Leaves of four-week old greenhouse-grown

Nicotiana benthamiana (*N. benthamiana*) plants were infiltrated using a syringe without a needle.

Protoplast isolation

N. benthamiana protoplasts were isolated two days post infection. Leaves were sliced into small pieces, vacuum-infiltrated with protoplast digestion solution (1.5% [w/v] cellulase R-10, 0.4% [w/v] macerozyme R-10, 0.4 M mannitol, 20 mM KCl, 20 mM MES [pH 5.7], 10 mM $CaCl_2$, 0.1% [w/v] bovine serum albumin) and incubated for two hours at 28°C. Sedimented protoplasts were resuspended in W5 solution (154 mM NaCl, 125 mM $CaCl_2$, 5 mM KCl, 2 mM MES [pH5.7]) and analyzed by confocal laser scanning microscopy.

Confocal laser scanning microscopy

Zeiss LSM780 confocal microscope and Zeiss ZEN software (Zeiss, Jena, Germany) was used for confocal laser scanning microscopy. Excitation/ emission wavelengths were as followed: green fluorescent protein (488 nm/490 to 550 nm), chlorophyll A (488 nm/ 640 to 710 nm). Images were processed with Fiji (Schindelin et al., 2012).

Reversed-phase liquid chromatography/ mass spectrometry analysis of mono- and polyglutamylated C_1 folates

Levels of mono- and polyglutamylated C_1 folates were quantified in 200 mg material of green tissue of 14-days-old Arabidopsis seedlings grown under atmospheric CO_2 concentration (400 ppm). Absolute quantification was performed by reverse-phase liquid chromatography with tandem mass spectrometry detection as described previously (De Brouwer et al., 2010; Blancquaert et al., 2013).

Metabolite profiling by gas-chromatography time of flight mass spectrometry

For metabolite profiling green tissue of 14-days-old seedlings was harvested by liquid nitrogen dousing at the middle of the light phase. Frozen material was ground using precooled mortar and pistil. Ground material was aliquoted under continuous liquid nitrogen exposure to avoid sample thawing. Metabolites were extracted by one-phase extraction as previously described (Fiehn et al., 2000). In detail, the extraction mix, containing water:methanol:chloroform (ratio 1:2.5:1) and 5 µM ribitol as internal standard, was added to frozen material. Samples were vortexed for 20 seconds, rotated for 6 minutes at 4 °C and centrifuged for 2 minutes at 20,000 x g at room temperature. The supernatant was transferred to a new tube and stored at -80 °C before further processing. For metabolite profiling by gas chromatography-time of flight mass spectrometry (GC/MS

QTOF, Agilent, Santa Clara, USA). 50 µl of extract was dried using a speed vacuum concentrator. Dried samples were placed in the Gerstel MPS 2 XL autosampler for automatic sample derivatization using methoxyamine hydrochloride and N-Methyl-N-(trimethylsilyl) trifluoroacetamide before injection. The GC-MS device is a 7200 accurate mass Q-TOF GC/MS (Agilent, Santa Clara, USA). For relative quantification metabolite peak areas are normalized to the internal extraction standard and the material fresh weight.

Reversed-phase liquid chromatography/mass spectrometry analysis of amino acids

Soluble amino acids in whole seedlings were quantified using a 6530 quadrupole-time-of-flight mass spectrometer (Agilent, Santa Clara, USA) coupled to a 1290 HPLC system (Agilent, Santa Clara, USA). For chromatographic separation a Waters Symmetry C18 column (2.1 × 100 mm, 3.5-µm particle size) was used with column oven temperature at 30°C. The injection volume was set to 10 µl, and the HPLC flow rate was 0.3 ml/min using the following mobile phases and gradient: Starting conditions were 98% mobile phase A (1 mM aqueous perfluoroheptanoic acid) and 2% mobile phase B (100% Acetonitrile). Within 0.1 min B increased to 20%, following a 40% increase after 2.3 min. This was hold until 4 min before dropping down to 2% until 4.1 min. Equilibration time with start conditions was 4 min. Mass spectra were acquired using electrospray ionization in positive ion mode. The source parameters were set as follows: capillary voltage 3500V, gas temperature 250°C, drying gas flow of 5 l/min, nebulizer pressure 25 psig, sheath gas temperature 350°C, and a sheath gas flow of 10 l/min. The fragmentor was set to 100 V, the skimmer to 65 V and the Oct1 RF Vpp to 750 V. Data were acquired with MassHunter Workstation Data Aqusition (Version B.08.00; Agilent) and processed and analyzed for quantification with MassHunter Quantitative Analysis (Version B.08.00; Agilent). Retention times of target metabolites were verified with standard compounds as reference. The peak area of the isotopomers was corrected for the natural abundance to quantify ^{13}C label enrichment (Supplementary Table S3).

Data analysis and software

Data analysis was performed in R. The respective code and the primary data are available upon request from the corresponding author.

Accession Numbers

The protein accession numbers used in this study are as followed: FDH1 (AT5G14780, Q56X34), GLDP1 (AT4G33010, Q94B78), GLDP2 (AT2G26080, O80988), *Me*FCH (P55818), *Me*FTL (Q83WS0), *Me*MtdA (P55818) , *Ec*GlyA (P0A825)

Acknowledgment

We would like to thank Elisabeth Klemp, Maria Graf and Katrin Weber from the CEPLAS Metabolomics facility for technical assistance, Steffen Köhler (Center for Advacned Imaging, Heinrich-Heine University Düsseldorf, Germany) for photography and Dr. Alisandra Denton for proof reading of the manuscript. Further, we would like to thank Dr. Arren Bar-Even (Max-Planck Institute for Molecular Plant Physiology, Golm, Germany) for teaching us that everything is possible unless thermodynamics restricts you.

Funding Information

This study was supported by the German Research Foundation (DFG) under Germany's Excellence Strategy (CEPLAS – EXC-2048/1 – Project ID 390686111 to P.W., M.M.M., M.D.Z. and A.P.M.W), the iGRAD Plant Graduate School (DFG/GRK1525 to M.-S.R.) and the Federal Ministry of Education and Research (BMBF/Project: Format Plant-031B0194C to A.P.M.W. and M.-S.R.).

Literature Cited

Alda-Catalinas C, Bredikhin D, Hernando-Herraez I, Santos F, Kubinyecz O, Eckersley-Maslin MA, Stegle O, Reik W (2020) A single-cell transcriptomics CRISPR-activation screen identifies epigenetic regulators of the zygotic genome activation program. Cell Syst **11**: 25–41

Antonovsky N, Gleizer S, Noor E, Zohar Y, Herz E, Barenholz U, Zelcbuch L, Amram S, Wides A, Tepper N, et al (2016) Sugar synthesis from CO_2 in *Escherichia coli*. Cell **166**: 115–125

Bar-Even A (2018) Daring metabolic designs for enhanced plant carbon fixation. Plant Science **273**: 71–83

Bar-Even A, Noor E, Lewis NE, Milo R (2010) Design and analysis of synthetic carbon fixation pathways. Proc Natl Acad Sci USA **107**: 8889–8894

Bar-On YM, Milo R (2019) The global mass and average rate of rubisco. Proc Natl Acad Sci USA **116**: 4738–4743

Blancquaert D, Van Daele J, Storozhenko S, Stove C, Lambert W, Van Der Straeten D (2013) Rice folate enhancement through metabolic engineering has an impact on rice seed metabolism, but does not affect the expression of the endogenous folate biosynthesis genes. Plant Mol Biol **83**: 329–349

Busch FA (2020) Photorespiration in the context of Rubisco biochemistry, CO_2 diffusion and metabolism. Plant J **101**: 919–939

Claassens NJ, Cotton CAR, Kopljar D, Bar-Even A (2019) Making quantitative sense of electromicrobial production. Nat Catal **2**: 437–447

Clough SJ, Bent AF (1998) Floral dip: a simplified method for Agrobacterium-mediated transformation of *Arabidopsis thaliana*. Plant J **16**: 735–743

Collakova E, Goyer A, Naponelli V, Krassovskaya I, Gregory JF, Hanson AD, Shachar-Hilla Y (2008) Arabidopsis 10-formyl tetrahydrofolate deformylases are essential for photorespiration. Plant Cell **20**: 1818–1832

Cotton CA, Edlich-Muth C, Bar-Even A (2018) Reinforcing carbon fixation: CO_2 reduction replacing and supporting carboxylation. Curr Opin Biotechnol **49**: 49–56

Crowther GJ, Kosály G, Lidstrom ME (2008) Formate as the main branch point for methylotrophic metabolism in *Methylobacterium extorquens* AM1. J Bacteriol **190**: 5057–5062

Datlinger P, Rendeiro AF, Schmidl C, Krausgruber T, Traxler P, Klughammer J, Schuster LC, Kuchler A, Alpar D, Bock C (2017) Pooled CRISPR screening with single-cell transcriptome readout. Nat Methods **14**: 297–301

De Brouwer V, Storozhenko S, Stove CP, Van Daele J, Van Der Straeten D, Lambert WE (2010) Ultra-performance liquid chromatography-tandem mass spectrometry (UPLC-MS/MS) for the sensitive determination of folates in rice. J Chromatogr B Analyt Technol Biomed Life Sci **878**: 509–513

Decaestecker W, Buono RA, Pfeiffer ML, Vangheluwe N, Jourquin J, Karimi M, Van Isterdael G, Beeckman T, Nowack MK, Jacobs TB (2019) CRISPR-Tsko: A technique for efficient mutagenesis in specific cell types, tissues, or organs in Arabidopsis. Plant Cell **31**: 2868–2887

Dedonder A, Rethy R, Fredericq H, Van Montagu M, Krebbers E (1993) Arabidopsis *rbcS* genes are differentially regulated by light. Plant Physiol **101**: 801–808

Douce R, Bourguignon J, Neuburger M, Rébeillé F (2001) The glycine decarboxylase system: a fascinating complex. Trends Plant Sci **6**: 167–176

Ducker GS, Chen L, Morscher RJ, Ghergurovich JM, Esposito M, Teng X, Kang Y, Rabinowitz JD (2016) Reversal of cytosolic one-carbon flux compensates for loss of the mitochondrial folate pathway. Cell Metab **23**: 1140–1153

Eisenhut M, Roell M-S, Weber APM (2019) Mechanistic understanding of photorespiration paves the way to a new green revolution. New Phytol **223**: 1762–1769

Engel N, Ewald R, Gupta KJ, Zrenner R, Hagemann M, Bauwe H (2011) The presequence of Arabidopsis serine hydroxymethyltransferase SHM2 selectively prevents import into mesophyll mitochondria. Plant Physiol **157**: 1711–1720

Engel N, Van Den Daele K, Kolukisaoglu Ü, Morgenthal K, Weckwerth W, Pärnik T, Keerberg O, Bauwe H (2007) Deletion of glycine decarboxylase in Arabidopsis is lethal under nonphotorespiratory conditions. Plant Physiol **144**: 1328–1335

Engler C, Youles M, Gruetzner R, Ehnert T-M, Werner S, Jones JDG, Patron NJ, Marillonnet S (2014) A golden gate modular cloning toolbox for plants. ACS Synth Biol **3**: 839–843

Fiehn O, Kopka J, Dörmann P, Altmann T, Trethewey RN, Willmitzer L (2000) Metabolite profiling for plant functional genomics. Nat Biotechnol **18**: 1157–1161

Gleizer S, Ben-Nissan R, Bar-On YM, Antonovsky N, Noor E, Zohar Y, Jona G, Krieger E, Shamshoum M, Bar-Even A, et al (2019) Conversion of *Escherichia coli* to generate all biomass carbon from CO_2. Cell **179**: 1255–1263

Gonzalez De La Cruz J, Machens F, Messerschmidt K, Bar-Even A (2019) Core Catalysis of the Reductive Glycine Pathway Demonstrated in Yeast. ACS Synth Biol **8**: 911–917

Gorelova V, De Lepeleire J, Van Daele J, Pluim D, Meï C, Cuypers A, Leroux O, Rébeillé F, Schellens JHM, Blancquaert D, et al (2017) Dihydrofolate reductase/thymidylate synthase fine-tunes the folate status and controls redox homeostasis in plants. Plant Cell **29**: 2831–2853

Goyer A, Collakova E, Díaz de la Garza R, Quinlivan EP, Williamson J, Gregory JF, Shachar-Hill Y, Hanson AD (2005) 5-Formyltetrahydrofolate is an inhibitory but well tolerated metabolite in Arabidopsis leaves. J Biol Chem **280**: 26137–26142

Grefen C, Donald N, Hashimoto K, Kudla J, Schumacher K, Blatt MR (2010) A ubiquitin-10 promoter-based vector set for fluorescent protein tagging facilitates temporal stability and native protein distribution in transient and stable expression studies. Plant J **64**: 355–365

Groth M, Moissiard G, Wirtz M, Wang H, Garcia-Salinas C, Ramos-Parra PA, Bischof S, Feng S, Cokus SJ, John A, et al (2016) MTHFD1 controls DNA methylation in Arabidopsis. Nat Commun **7**: 11640

Hanson AD, Roje S (2001) One-carbon metabolism in higher plants. Annu Rev Plant Physiol **52**: 119–137

Hartmann T, Leimkühler S (2013) The oxygen-tolerant and NAD^+-dependent formate dehydrogenase from *Rhodobacter capsulatus* is able to catalyze the reduction of CO_2 to formate. FEBS J **280**: 6083–6096

Igamberdiev AU, Bykova NV, Kleczkowski LA (1999) Origins and metabolism of formate in higher plants. Plant Physiol Biochem **37**: 503–513

Inskeep WP, Bloom PR (1985) Extinction coefficients of chlorophyll a and b in n,n-dimethylformamide and 80% acetone. Plant Physiol **77**: 483–485

Jaitin DA, Weiner A, Yofe I, Lara-Astiaso D, Keren-Shaul H, David E, Salame TM, Tanay A, van Oudenaarden A, Amit I (2016) Dissecting immune circuits by linking CRISPR-pooled screens with single-cell RNA-seq. Cell **167**: 1883–1896.e15

Joshi V, Jander G (2009) Arabidopsis methionine γ-lyase is regulated according to isoleucine biosynthesis needs but plays a subordinate role to threonine deaminase. Plant Physiol **151**: 367–378

Joshi V, Laubengayer KM, Schauer N, Fernie AR, Jander G (2006) Two Arabidopsis threonine aldolases are nonredundant and compete with threonine deaminase for a common substrate pool. Plant Cell **18**: 3565–3575

Kebeish R, Niessen M, Thiruveedhi K, Bari R, Hirsch H-J, Rosenkranz R, Stäbler N, Schönfeld B, Kreuzaler F, Peterhänsel C (2007) Chloroplastic photorespiratory bypass increases photosynthesis and biomass production in *Arabidopsis thaliana*. Nat Biotechnol **25**: 593–599

Kim S, Lindner SN, Aslan S, Yishai O, Wenk S, Schann K, Bar-Even A (2020) Growth of *E. coli* on formate and methanol via the reductive glycine pathway. Nat Chem Biol **332**: 805–8

Koncz C, Schell J (1986) The promoter of TL-DNA gene 5 controls the tissue-specific expression of chimaeric genes carried by a novel type of Agrobacterium binary vector. Mol Gen Genet **204**: 383–396

Kuhnert F, Stefanski A, Overbeck N, Drews L, Reichert AS, Stühler K, Weber APM (2020) Rapid single-step affinity purification of HA-tagged plant mitochondria. Plant Physiol **182**: 692–706

Laemmli UK (1970) Cleavage of structural proteins during the assembly of the head of bacteriophage T4. Nature **227**: 680–685

Li R, Moore M, King J (2003) Investigating the regulation of one-carbon metabolism in *Arabidopsis thaliana*. Plant Cell Physiol **44**: 233–241

Liao JC, Mi L, Pontrelli S, Luo S (2016) Fueling the future: Microbial engineering for the production of sustainable biofuels. Nat Rev Microbiol **14**: 288–304

Lopez-Calcagno PE, Fisk S, Brown KL, Bull SE, South PF, Raines CA (2019) Overexpressing the H-protein of the glycine cleavage system increases biomass yield in glasshouse and field-grown transgenic tobacco plants. Plant Biotechnol J **17**: 141–151

Maier A, Fahnenstich H, Caemmerer von S, Engqvist MKM, Weber APM, Flügge U-I, Maurino VG (2012) Transgenic introduction of a glycolate oxidative cycle into *A. thaliana* chloroplasts leads to growth improvement. Front Plant Sci **3**: 38

Mehrshahi P, Gonzalez-Jorge S, Akhtar TA, Ward JL, Santoyo-Castelazo A, Marcus SE, Lara-Núñez A, Ravanel S, Hawkins ND, Beale MH, et al (2010) Functional analysis of folate polyglutamylation and its essential role in plant metabolism and development. Plant J **64**: 267–279

Meng J, Wang L, Wang J, Zhao X, Cheng J, Yu W, Jin D, Li Q, Gong Z (2018) METHIONINE ADENOSYLTRANSFERASE4 mediates DNA and histone methylation. Plant Physiol **177**: 652–670

Miller TE, Beneyton T, Schwander T, Diehl C, Girault M, McLean R, Chotel T, Claus P, Cortina NS, Baret J-C, et al (2020) Light-powered CO_2 fixation in a chloroplast mimic with natural and synthetic parts. Science **368**: 649–654

Modde K, Timm S, Florian A, Michl K, Fernie AR, Bauwe H (2017) High serine:glyoxylate aminotransferase activity lowers leaf daytime serine levels, inducing the phosphoserine pathway in Arabidopsis. J Exp Bot **68**: 643–656

Nielsen CF, Lange L, Meyer AS (2019) Classification and enzyme kinetics of formate dehydrogenases for biomanufacturing via CO_2 utilization. Biotechnol Adv **37**: 107408

Prabhu V, Chatson KB, Abrams GD, King J (1996) ^{13}C nuclear magnetic resonance detection of interactions of serine hydroxymethyltransferase with C_1-tetrahydrofolate synthase and glycine decarboxylase complex activities in Arabidopsis. Plant Physiol **112**: 207–216

Prabhu V, Chatson KB, Lui H, Abrams GD, King J (1998) Effects of sulfanilamide and methotrexate on ^{13}C fluxes through the glycine decarboxylase/serine hydroxymethyltransferase enzyme system in Arabidopsis. Plant Physiol **116**: 137–144

Raines CA (2003) The Calvin cycle revisited. Photosyn Res **75**: 1–10

Ravanel S, Block MA, Rippert P, Jabrin S, Curien G, Rébeillé F, Douce R (2004a) Methionine metabolism in plants: chloroplasts are autonomous for de novo methionine synthesis and can import S-adenosylmethionine from the cytosol. J Biol Chem **279**: 22548–22557

Ravanel S, Gakiere B, Job D, Douce R (1998) The specific features of methionine biosynthesis and metabolism in plants. Proc Natl Acad Sci USA **95**: 7805–7812

Rich-Griffin C, Stechemesser A, Finch J, Lucas E, Ott S, Schäfer P (2020) Single-cell transcriptomics: A high-resolution avenue for plant functional genomics. Trends Plant Sci **25**: 186–197

Roje S, Chan SY, Kaplan F, Raymond RK, Horne DW, Appling DR, Hanson AD (2002) Metabolic engineering in yeast demonstrates that S-adenosylmethionine controls flux through the methylenetetrahydrofolate reductase reaction *in vivo*. J Biol Chem **277**: 4056–4061

Satanowski A, Bar-Even A (2020) A one-carbon path for fixing CO_2: C_1 compounds, produced by chemical catalysis and upgraded via microbial fermentation, could become key intermediates in the valorization of CO_2 into commodity chemicals. EMBO Reports **21**: e50273

Sánchez-Andrea I, Guedes IA, Hornung B, Boeren S, Lawson CE, Sousa DZ, Bar-Even A, Claassens NJ, Stams AJM (2020) The reductive glycine pathway allows autotrophic growth of *Desulfovibrio desulfuricans*. Nat Commun **11**: 5090

Schindelin J, Arganda-Carreras I, Frise E, Kaynig V, Longair M, Pietzsch T, Preibisch S, Rueden C, Saalfeld S, Schmid B, et al (2012) Fiji: an open-source platform for biological-image analysis. Nat Methods **9**: 676–682

Schwander T, Schada von Borzyskowski L, Burgener S, Cortina NS, Erb TJ (2016) A synthetic pathway for the fixation of carbon dioxide *in vitro*. Science **354**: 900–904

Shen B-R, Wang L-M, Lin X-L, Yao Z, Xu H-W, Zhu C-H, Teng H-Y, Cui L-L, Liu EE, Zhang J-J, et al (2019) Engineering a new chloroplastic photorespiratory bypass to increase photosynthetic efficiency and productivity in rice. Molecular Plant **12**: 199–214

Simon P (2003) Q-Gene: Processing quantitative real-time RT-PCR data. Bioinformatics **19**: 1439–1440

South PF, Cavanagh AP, Liu HW, Ort DR (2019) Synthetic glycolate metabolism pathways stimulate crop growth and productivity in the field. Science **363**: eaat9077

Stålberg K, Ellerström M, Ezcurra I, Ablov S, Rask L (1996) Disruption of an overlapping E-box/ABRE motif abolished high transcription of the napA storage-protein promoter in transgenic *Brassica napus* seeds. Planta **199**: 515–519

Szecowka M, Heise R, Tohge T, Nunes-Nesi A, Vosloh D, Huege J, Feil R, Lunn J, Nikoloski Z, Stitt M, et al (2013) Metabolic fluxes in an illuminated Arabidopsis rosette. Plant Cell **25**: 694–714

Timm S, Florian A, Arrivault S, Stitt M, Fernie AR, Bauwe H (2012) Glycine decarboxylase controls photosynthesis and plant growth. FEBS Lett **586**: 3692–3697

Timm S, Giese J, Engel N, Wittmiß M, Florian A, Fernie AR, Bauwe H (2017) T-protein is present in large excess over the other proteins of the glycine cleavage system in leaves of Arabidopsis. Planta **301**: 1–11

Timm S, Wittmiß M, Gamlien S, Ewald R, Florian A, Frank M, Wirtz M, Hell R, Fernie AR, Bauwe H (2015) Mitochondrial dihydrolipoyl dehydrogenase activity shapes photosynthesis and photorespiration of *Arabidopsis thaliana*. Plant Cell **27**: 1968–1984

Trudeau DL, Edlich-Muth C, Zarzycki J, Scheffen M, Goldsmith M, Khersonsky O, Avizemer Z, Fleishman SJ, Cotton CAR, Erb TJ, et al (2018) Design and *in vitro* realization of carbon-conserving photorespiration. Proc Natl Acad Sci USA **115**: E11455–E11464

Voll LM, Jamai A, Renné P, Voll H, McClung CR, Weber APM (2006) The photorespiratory Arabidopsis *shm1* mutant is deficient in SHM1. Plant Physiol **140**: 59–66

Walker BJ, VanLoocke A, Bernacchi CJ, Ort DR (2016) The costs of photorespiration to food production now and in the future. Annu Rev Plant Biol **67**: 107–129

Weber APM, Bar-Even A (2019) Update: Improving the efficiency of photosynthetic carbon reactions. Plant Physiol **179**: 803–812

Weigel D, Glazebrook J (2009) Quick miniprep for plant DNA isolation. Cold Spring Harb Protoc **4**: pdb.prot5179

Wingler A, Lea PJ, Leegood RC (1999) Photorespiratory metabolism of glyoxylate and formate in glycine-accumulating mutants of barley and *Amaranthus edulis*. Planta **207**: 518–526

Witte C-P, Herde M (2020) Nucleotide metabolism in plants. Plant Physiol **182**: 63–78

Wittmiß M, Mikkat S, Hagemann M, Bauwe H (2020) Stoichiometry of two plant glycine decarboxylase complexes and comparison with a cyanobacterial glycine cleavage system. Plant J **103**: 801–813

Xie K, Minkenberg B, Yang Y (2015) Boosting CRISPR/Cas9 multiplex editing capability with the endogenous tRNA-processing system. Proc Natl Acad Sci USA **112**: 3570–3575

Yishai O, Goldbach L, Tenenboim H, Lindner SN, Bar-Even A (2017) Engineered assimilation of exogenous and endogenous formate in *Escherichia coli*. ACS Synth Biol **6**: 1722–1731

Yu C, Zhang Y, Yao S, Wei Y (2014) A PCR based protocol for detecting Indel mutations induced by TALENs and CRISPR/Cas9 in zebrafish. PLoS ONE **9**: e98282–7

Zhang Y, Sun K, Sandoval FJ, Santiago K, Roje S (2010) One-carbon metabolism in plants: characterization of a plastid serine hydroxymethyltransferase. Biochem J **430**: 97–105

Zheng Y, Lin T-Y, Lee G, Paddock MN, Momb J, Cheng Z, Li Q, Fei DL, Stein BD, Ramsamooj S, et al (2018) Mitochondrial one-carbon pathway supports cytosolic folate integrity in cancer cells. Cell **175**: 1546–1560.e17

Zrenner R, Stitt M, Sonnewald U, Boldt R (2006) Pyrimidine and purine biosynthesis and degradation in plants. Annu Rev Plant Biol **57**: 805–836

Supplemental Information

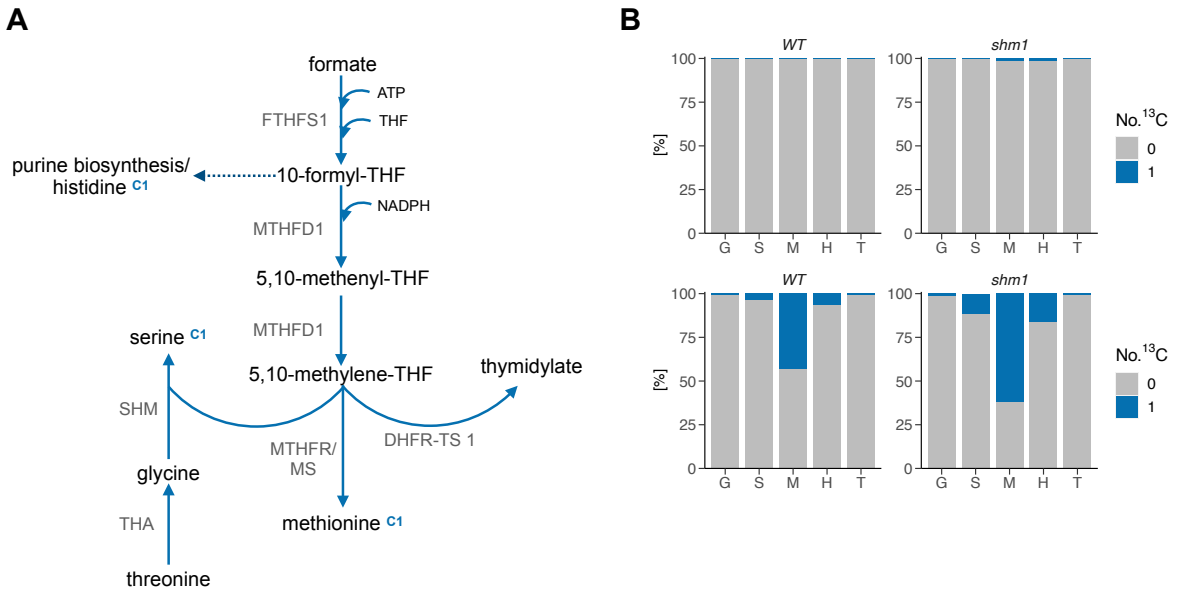

Supplemental Fig. S1: Formate-^{13}C labeling with Arabidopsis seedlings. A) Schematic representation of cytosolic C_1 metabolism in plants. B) Reversibility of cytosolic C_1 metabolism in Arabidopsis by formate-^{13}C feeding. Five days old seedlings of Arabidopsis wild type or the serine hydroxymethyltransferase 1 mutant (*shm1*) were grown in CO_2 enriched air (3000 ppm CO_2) either on 1 mM sodium formate (top) or 1 mM sodium formate-^{13}C (bottom) for five days before harvesting. The ^{13}C label enrichment in soluble amino acids pools of glycine (G), serine (S), methionine (M), histidine (H) and threonine (T) was quantified. n = 6. Abbreviations: 10-formyl-THF synthetase (FTHFS), bifunctional methylenetetrahydrofolate dehydrogenase/cyclohydrolase (MTHFD), serine hydroxymethyltransferase (SHM), bifunctional dihydrofolate reductase-thymidylate synthase (DHFR-TS), methylene-THF reductase (MTHFR), methionine synthase (MS), threonine aldolase (THA).

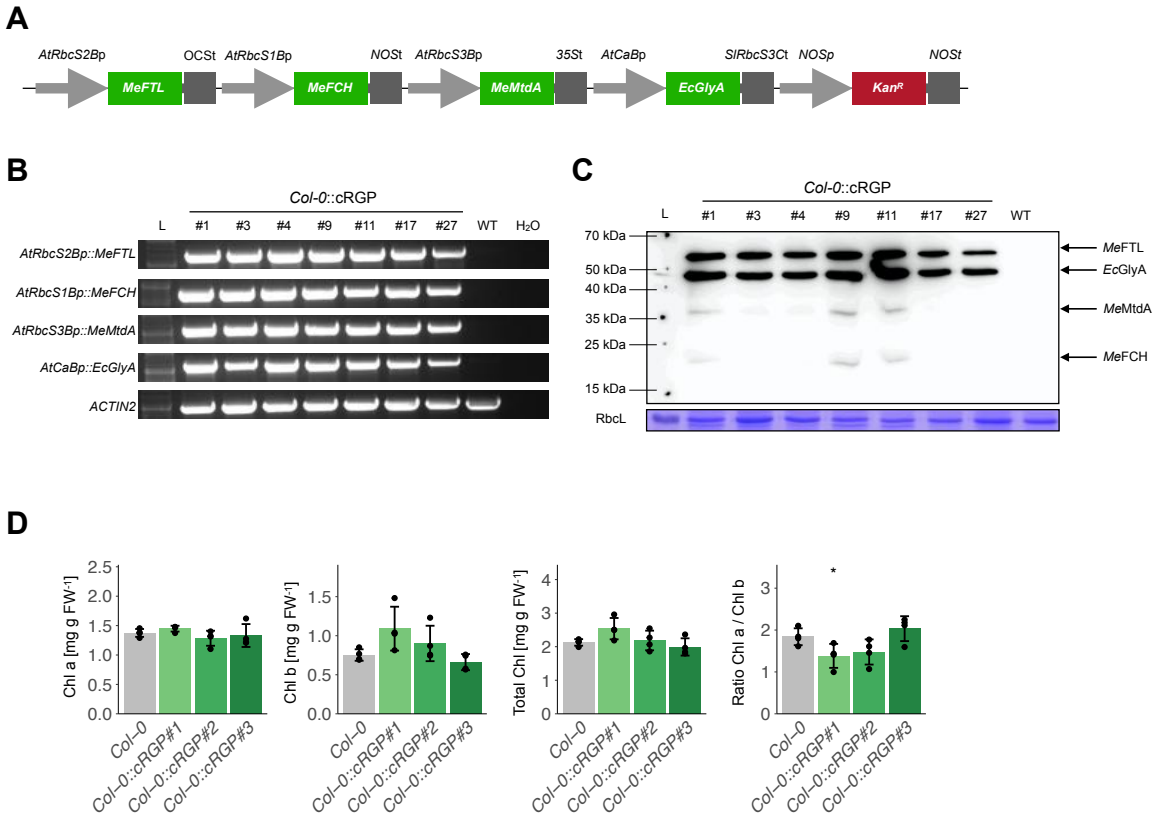

Supplemental Fig. S2: Implementation of the cRGP in Arabidopsis. A) Schematic representation of the multigene T-DNA construct for cRGP pathway implementation. Kanamycin (Kan^R) was used as antibiotic selection marker. B) Genotyping of transgenic T1 cRGP plants in wild type *Col-0. C)* Immunoblot analysis of cRGP enzyme abundance. Arabidopsis Rubisco large subunit (RbcL) served as loading control, shown by coomassie staining. 12 µg leaf protein of four-weeks-old air-grown plants was loaded per lane. Protein abundance was detected using a monoclonal anti-HIS HRP antibody for all four cRGP enzymes, separated based on size. D) Chlorophyll (Chl) content in rosettes of four-weeks-old plants. Chlorophyll a, chlorophyll b, total chlorophyll content, ratio chlorophyll a/b was determined. n = 4. Shown mean ± SD. Biological replicates are indicated as points. Students *t*-test against wild type *Col-0.* p > 0.05 = *,> 0.01 = **, > 0.001 = ***.

Supplemental Fig. S3: Metabolome profile of cRGP plants. Green tissue of 14-days-old seedlings was harvested in the middle of the light phase. Plants were grown in ambient air (400 ppm CO_2) and metabolite levels were analyzed by GC-MS QTOF. Student's *t*-test against wild type *Col-0*. Asterisks indicate significance after multiple testing correction using Benjamini-Hochberg. $p < 0.05$ = *, < 0.01 = **, < 0.001 = ***. n = 4. UK indicates detected metabolites by GC-MS QTOF, that were identified based on NIST-library searches but not verified with analytical standards.

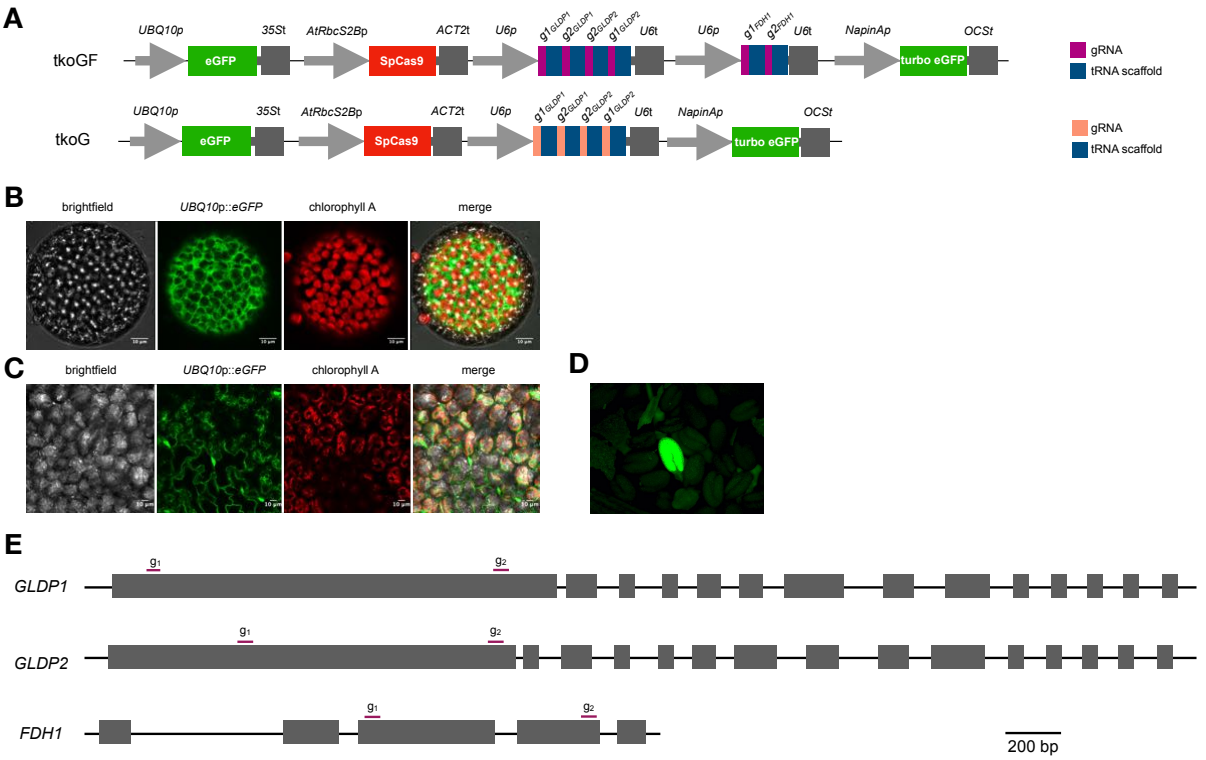

Supplemental Fig. S4: A CRISPR/Cas9 based module for photosynthetic tissue specific knockouts. A) Schematic representation of the T-DNA constructs for photosynthetic tissue specific knockouts (tko). Two T-DNA constructs were designed to simultaneously knockout both glycine decarboxylase P-subunit encoding genes (*GLPD1* and *GLDP2)* and formate dehydrogenase 1 (*FDH1*, tkoGF). Alternatively, only *GLPD1* and *GLDP2* are knocked out (tkoG). The guide RNAs (g1 and g2) are indicated with the respective target subscripted. B) The constitutive eGFP marker (*UBQ10*p::eGFP) was tested in *N. benthamiana* protoplasts and transgenic Arabidopsis lines. Images are representative for both the tkoGF and tkoG module. Red = chlorophyll A autofluorescence. Confocal microscopy images were analyzed using Fiji. D) Arabidopsis seed expressing the turbo eGFP under the NapinA promoter. E) Schematic representation of the *GLDP1* (At4g33010), *GLDP2* (At2g26080) and *FDH1* (At5g14780) genomic loci with position of the used guide RNAs (g) indicated in purple. Exons are indicated in grey.

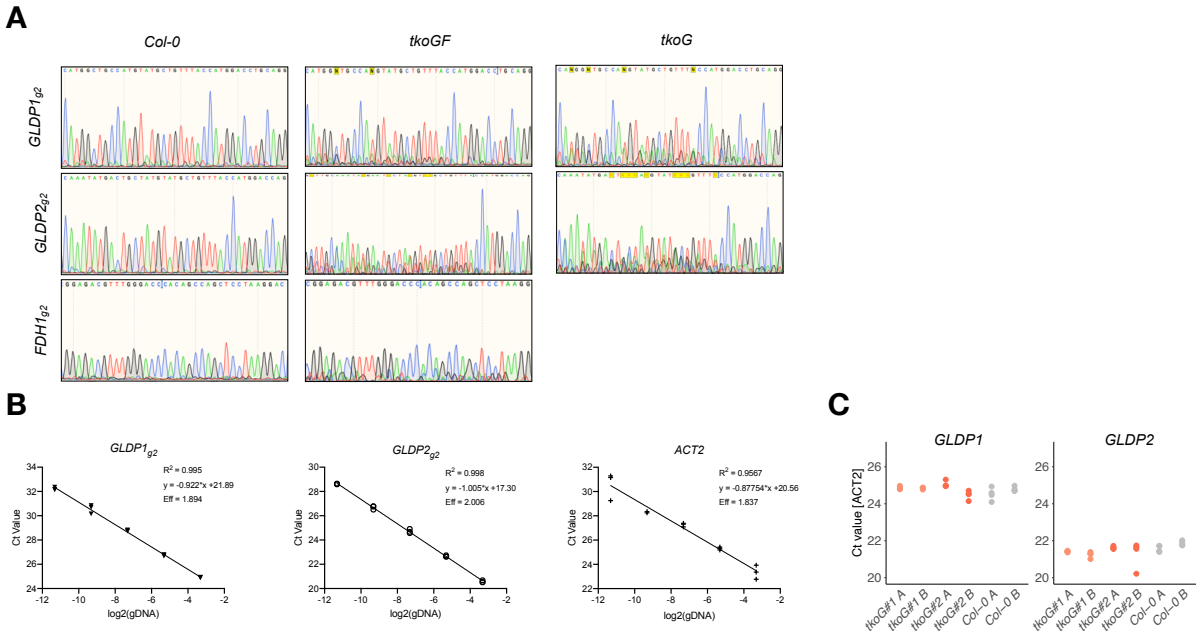

Supplemental Fig. S5: Functionality of the CRISPR/Cas9 module. A) Verification of CRISPR/Cas9 dependent editing in *GLDP1*, *GLDP2* and *FDH1* genes by the respective used guide RNA 2 (g2). Genomic DNA was isolated from mature leaves of four weeks old plants grown in CO_2 enriched air. Target genes were amplified by PCR and PCR fragments were sequenced by Sanger sequencing. B) Primer efficiency of qPCR primers, determined by genomic DNA dilution series. *GLDP1* and *GLDP2* primers were specific for the position of g2. Linear equation and R^2 were determined based on the regression line. n_{tech}= 3. C) Ct-values for the *ACT2* reference gene to quantify wild type *GLDP1* and *GLDP2* abundance by qPCR. Genomic DNA from the fourth leaf of four-week-old air grown rosettes of two independent plants (A & B) per genotype was isolated. n_{tech}= 4.

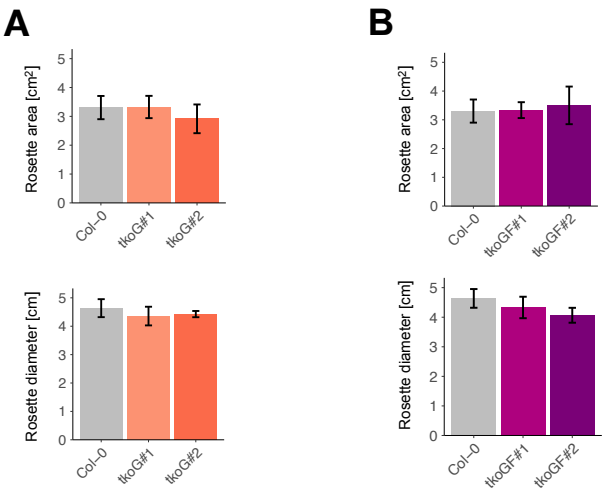

Supplemental Fig. S6: Growth of tkoG and tkoGF plants in CO_2 enriched air. A and B) Rosette area (top) and rosette diameter (bottom) of three weeks old tkoG (A) and tkoGF plants grown in CO_2 enriched air (3000 ppm CO_2) was quantified. Shown mean ± SD. n= 4. Student's *t*-test against *Col-0*. $p > 0.05$ = not significant.

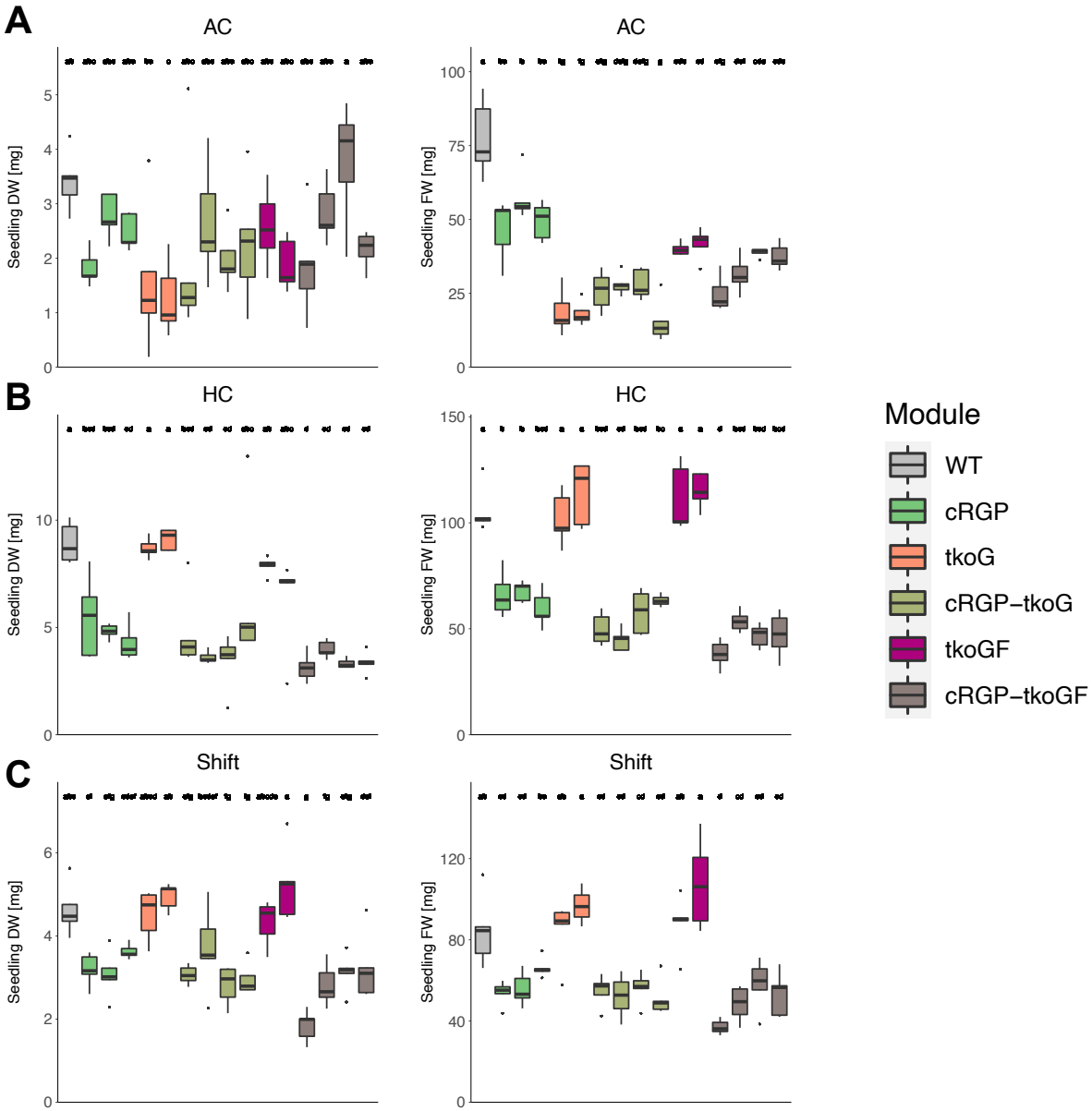

Supplemental Figure S7: Growth of plants with the cRGP and the CRISPR/Cas9 module. Quantification of seedlings fresh weight (FW, top) and dry weight (DW, bottom) of the combined cRGP and photosynthetic tissue-specific CRISPR/Cas9 modules tkoG and tkoGF. Plant growth was quantified on 14-days-old seedlings grown in ambient air (400 ppm CO_2, A), in CO_2 enriched air (3000 ppm CO_2, B) or shifted from CO_2 enriched air to ambient air three days before harvest (C). n per genotype = 5. One-way ANOVA with a post-hoc Tukey HSD test.

Supplemental Table S1: List of primer used in this study. Gene specific nucleotides are indicated in caps. Abbreviations: guide RNA (gRNA). *Arabidopsis Formate Dehydrogenase 1* (*FDH1*, At5g14780), Arabidopsis *Glycine decarboxylase P-protein 1* (*GLDP1*, At4g33010), Arabidopsis *Glycine decarboxylase P-protein 2* (*GLDP2*, At2g26080), *Arabidopsis ACTIN2* (*ACT2*, At3g18780).

Primer sequence	Purpose	Reference
fwd: 5'-CTGGTACTGAAGGTGAAGTCTTG-3' rev: 5'-CAACACTCACAGGCTTGC-3'	Sequencing primer *GLDP1*	This study
fwd: 5'-GTTCCGAAATCGATTCGGTTAG-3' rev: 5'-CTCACAGTGTTGGAGTCCAC-3'	Sequencing primer *GLDP2*	This study
fwd: 5'-GCCAACGAATACGCTACC-3' rev: 5'-CGATGTAATTCTCAGTAGGGAAG-3'	Sequencing primer *FDH1*	This study
fwd: 5' GAGTATAAGAGAATGATGCCTGGGAGG-3' rev: 5'-CTTGAGCAGTACAGATGTTGCTAGTG-3'	qPCR gRNA1 *GLDP1*	This study
fwd: 5'-CTTCATCTTTTCATTTTCCTGCAGGCG-3' rev: 5'-GCAGGTCCATGGTAAACAGCATAC-3'	qPCR gRNA2 *GLDP1*	This study
fwd: 5'-GTGACGGTTGATATTAAGGATGTGG-3' rev: 5'-GTCAAAGCCAACAAATCCGTAGCC-3'	qPCR gRNA1 *GLDP2*	This study
fwd: 5'-GAGGTACCGAGAGAGCAGTACC-3' rev: 5'-GGTCCATGGTAAACAGCATACATAGC-3'	qPCR gRNA2 *GLDP2*	This study
fwd: 5'-CCGGATCTTCACGTCCTAATCTCC-3' rev: 5'-CAATATGATCCGAGCCAATACCAGC-3'	qPCR gRNA1 *FDH1*	This study
fwd: 5'-GAACAACGCAAGAGGAGCCATC-3' rev: 5'-TTAGGAGCTGGCTGTGGGTC-3'	qPCR gRNA2 *FDH1*	This study
fwd: 5'-CCAAGCTGTTCTCTCCTTGTACGC-3' rev: 5'-GTGAGACACACCATCACCAGAATCC-3'	qPCR *ACT2*	This study
fwd: 5'-CTGGTACTGAAGGTGAAGTCTTG-3'	Sequence gRNA1 *GLDP1*	This study
fwd: 5'-CTGGTACTGAAGGTGAAGTCTTG-3'	Sequence gRNA2 *GLDP1*	This study
fwd: 5'-CTGGTACTGAAGGTGAAGTCTTG-3'	Sequence gRNA1 *GLDP2*	This study
fwd: 5'-CTGGTACTGAAGGTGAAGTCTTG-3'	Sequence gRNA2 *GLDP2*	This study
fwd: 5'-CTGGTACTGAAGGTGAAGTCTTG-3'	Sequence gRNA1 *FDH1*	This study
fwd: 5'-CTGGTACTGAAGGTGAAGTCTTG-3'	Sequence gRNA2 *FDH1*	This study

Supplemental Table S2: List of constructs used in this study. Vector backbones, promoters and terminators are described in (Engler et al., 2014). Abbreviations: *Methylobacterium extorquens AM1* 10-formyl-THF ligase (MeFTL), methenyl-THF cyclohydrolase (MeFCH) and NADP-dependent methylene-THF dehydrogenase (MeMtdA) and *E. coli* serine hydroxymethyl transferase (EcGlyA). *Streptococcus pyogenes* Cas9 (*Sp*Casp). *Arabidopsis Formate Dehydrogenase 1* (*FDH1*, At5g14780), Arabidopsis *Glycine decarboxylase P-protein 1* (*GLDP1*, At4g33010), Arabidopsis *Glycine decarboxylase P-protein 2* (*GLDP2*, At2g26080), *Arabidopsis ACTIN2* (*ACT2*, At3g18780). *Arabidopsis thaliana* (*At*), *Solanum lycopersicum* (*Sl*), Agrobacterium tumefaciens (*Atu*). The CRISPR/Cas9 multiplexing system was adapted based on (Xie et al., 2015).

Purpose	**Vector**	**Insert**	**Comment**
cRGP T-DNA construct for implementation in plants	pICH75322	Pos. 1: *At*rbcS2Bp::*Me*FTL::*AtuOCS*t Pos. 2: *At*rbcS1Bp::*Me*FCH::*Atu*NOSt Pos. 3: *At*rbcS3Bp::*Me*MtdA::35St Pos. 4: *At*CABp::*Me*GlyA:: *SlRbcS3C*t Pos. 5: *Atu*Nosp::NptII::*Atu*OCSt	Implementation of the cytosolic reductive glycine pathway
tkoG T-DNA construct for implementation in plants	pICH86966	*Pos. 1: UBQ10*p::eGFP::*35St* *Pos. 2:* AtrbcS2Bp::SpCas9::ACT2t *Pos. 3: U6p::gRNAs-GLDP::U6t* *Pos. 4: NapinAp::turbo eGFP::OCSt*	Tissue knockout (tko) in photosynthetic tissue of both glycine decarboxylase P-protein genes, *GLPD1* and *GLDP2*.
tkoGF T-DNA construction for implementation in plants	pICH86966	*Pos. 1: UBQ10*p::eGFP::*35St* *Pos. 2:* AtrbcS2Bp::SpCas9::ACT2t *Pos. 3: U6p::gRNAs-GLDP::U6t* *Pos. 4: U6p::gRNAs-GLDP::U6t* *Pos. 5: NapinAp::turbo eGFP::OCSt*	Tissue knockout (tko) in photosynthetic tissue of both glycine decarboxylase P-protein genes, *GLPD1* and *GLDP2* and formate dehydrogenase 1 (*FDH1*)

Supplemental Table S3: Masses and natural abundance used for LC-MS QTOF based amino acid profiling and ^{13}C label quantification.

Metabolite	Molecular mass [g mol^{-1}]	^{13}C-label	Formula	Natural abundance [%]
Glycine	76.0393	0	$C_2H_5NO_2$	
	77.0419	1		26.73
	78.0436	2		4.34
Serine	106.0498	0	$C_3H_7NO_3$	
	107.0527	1		3.81
	108.0542	2		0.67
Methionine	150.0583	0	$C_5H_{11}NO_2S$	
	151.0610	1		6.77
	152.0552	2		5.08
Histidine	156.0767	0	$C_6H_9N_3O_2$	
	157.0792	1		7.77
Threonine	120.0655	0	$C_4H_9NO_3$	
	121.0684	1		4.92
	122.0699	2		0.71

Manuscript III

Formate dehydrogenase regulates the one carbon shunt in plants

Marc-Sven Roell,[1,2,a] Franziska Kuhnert,[1,2,a] Sompop Saeheng,[4] Philipp Westhoff,[1,3] Sanja Roje,[4] Andreas P.M. Weber [1,2] *

[1] Institute of Plant Biochemistry, Heinrich Heine University, Düsseldorf, Germany
[2] iGRAD Plant Graduate School, Heinrich Heine University, Düsseldorf, Germany
[3] Cluster of Excellence on Plant Science (CEPLAS), Heinrich Heine University, Düsseldorf, Germany
[4] Institute of Biological Chemistry, Washington State University, Pullman, WA, USA

[a] Contributed equally to this work.

Status: in preparation

Own contribution:

I designed and generated constructs for the biochemical characterization as well as the CRISPR/Cas9 mutant establishment, overexpression and localization constructs. I established the mutants and overexpression lines and performed the phenotypical analysis as well as transcript assessment and jointly with Franziska Kuhnert the metabolomics experiment.

Formate dehydrogenase regulates the one carbon shunt in plants

Marc-Sven Roell,[1,2,a] Franziska Kuhnert,[1,2,a] Sompop Saeheng,[4] Philipp Westhoff,[1,3] Sanja Roje,[4] Andreas P.M. Weber [1,2] *

[1] Institute of Plant Biochemistry, Heinrich Heine University, Düsseldorf, Germany

[2] iGRAD Plant Graduate School, Heinrich Heine University, Düsseldorf, Germany

[3] Cluster of Excellence on Plant Science (CEPLAS), Heinrich Heine University, Düsseldorf, Germany

[4] Institute of Biological Chemistry, Washington State University, Pullman, WA, USA

[a] Contributed equally to this work.

* For correspondence (E-mail: andreas.weber@hhu.de)

ORCID-IDS: 0000-0003-2714-8729 (M.-S.R.); 0000-0002-0374-6671 (F.K.); 0000-0003-0970-4672 (A.P.M.W.)

Author contributions

M.-S.R., F.K., S.S., P.W., S.R. and A.P.M.W. designed research. M.-S.R., F.K., S.S. and P.W. performed research. M.-S.R., F.K., S.S. and P.W. analyzed data. M.-S.R., F.K., S.S., P.W., S.R. and A.P.M.W. wrote the manuscript.

Keywords

Photorespiration | One carbon metabolism | Formate dehydrogenase

This Manuscript includes:

Main text, 5 figures, supplemental information

Abstract

The transfer of one carbon (C_1) units is an integral part of cellular metabolism and essential for nucleotide-, amino acid-, and cofactor biosynthesis as well as cellular methylation reactions. Within the plant cell, mitochondria are considered the hub of one carbon metabolism, but mechanisms and fluxes to distribute C_1 units from the mitochondria within the cell are unknown. Formate, the anion of formic acid, is an intermediate of C_1 metabolism and is converted into C_1-tetrahydrofolate intermediates (C_1 folates) or oxidized to CO_2 by formate dehydrogenase. In plants, the existence of formate dehydrogenase questions formate exchange between mitochondria and the cytosol, a basic principle of eukaryotic cellular and organellar C_1 metabolism. Based on biochemical and physiological characterization of *Arabidopsis thaliana* formate dehydrogenase 1 (FDH1), we propose a FDH1-regulated C_1 shunt that connects mitochondrial and cytosolic C_1 metabolism by formate exchange. Finally, we give a perspective on a cellular serine/formate shuttle that allows the distribution and transfer of C_1 units according to the redox state within the compartments.

Introduction

One carbon (C_1) metabolism is essential to all living organisms (Hanson et al., 2000). In plants, folate (vitamin B_9) co-enzymes, supply activated C_1 units for a variety of metabolic processes. The biosynthesis of nucleotides (purine and thymidylate) mitochondrial and chloroplastic proteins, vitamin as well as amino acid metabolism and methylation reactions all depend on the provision of C_1 units (Hanson and Roje, 2001). Within the cell, tetrahydrofolate (THF) functions as carrier for C_1 units via C_1 THF (C_1 folates; Hanson and Roje, 2001). C_1 folates exist in several oxidation states (10-formyl-THF as most oxidized and 5-methyl-THF as most reduced form) and are reversibly converted between the different oxidation states (Hanson and Gregory, 2011).

Since the transport of C_1 folates across organellar membranes is unlikely, different mechanisms need to exist that allow the distribution of C_1 units between compartments (Cybulski and Fisher, 1981). Heterotrophic eukaryotes use a C_1 shunt based on formate exchange to connect mitochondrial and cytosolic C_1 metabolism (Christensen and MacKenzie, 2006) Ducker:2016kk, Zheng:2018fj}. In mammalian cells, mitochondrial derived formate fuels cytosolic C_1 metabolism for 10-formyl-THF formation and thereby maintains cellular redox homeostasis and folate integrity (Ducker et al., 2016) (Zheng et al., 2018). However in plants, a comparable C_1 shunt between mitochondria and the cytosol is questioned by the existence of a mitochondrial formate dehydrogenase (Li et al., 2000).

In leaf mitochondria, photorespiration and C_1 metabolism interact by glycine to serine conversion catalyzed by the combined activity of the glycine decarboxylase complex (GDC) and serine hydroxymethyltransferase (SHM). Both enzymes catalyze THF-dependent reactions and are major soluble proteins of leaf mitochondria (Eisenhut et al., 2019; Busch, 2020; Fuchs et al., 2020; Wittmiß et al., 2020). The lethal phenotypes of the *gldp1gldp2* (GDC P-protein), *gldt1* (GDC T-protein) and *shm1shm2* mutants in *Arabidopsis thaliana* (Arabidopsis) are explained by the dual role of GDC and SHM in C_1 metabolism and define mitochondria as the cellular hub for the provision of C_1 units within the plant cell (Engel et al., 2007; Engel et al., 2011; Timm et al., 2017). The central C_1 intermediate of the GDC/SHM catalyzed reactions is 5,10-methylene-THF, that either derives from glycine oxidation or reversible hydroxymethyl group transfer from serine. Besides glycine/serine metabolism, 5,10-methylene-THF is also oxidized in the mitochondrial THF cycle (Eisenhut et al., 2019; Busch, 2020). The final step of the cycle, catalyzed by 10-formyl-deformylase (FDF), releases THF and produces a single formate molecule (Collakova et al., 2008; Eisenhut et al., 2019). The photorespiratory phenotype and progeny lethality of the 10-formyl-deformylase double knockout mutant is additional evidence on the role of mitochondrial C_1 metabolism in photorespiration and plant development (Collakova et al., 2008). Further, the THF-cycle together the non-enzymatic glyoxylate decarboxylation, methanol metabolism and oxalate catabolism contributes to the cellular formate pool (Igamberdiev et al., 1999; Wingler et al., 1999; Foster et al., 2012).

At least two metabolic routes exist that determine the fate of formate and imply either a role as intermediate of folate-dependent C_1 metabolism or the oxidation to CO_2 (Hanson and Roje, 2001). Plants possess enzymes for the THF-dependent conversion of formate into 5,10-methylene-THF and isoforms exist in the plastid, mitochondria and cytosol (Hanson and Roje, 2001). In the cytosol 5,10-methylene-THF is allocated between thymidylate- and methionine biosynthesis (Groth et al., 2016; Gorelova et al., 2017). Methionine is integral part of the methyl cycle to produce *S*-adenosyl-*L*-methionine (SAM), the cellular methyl group donor(Ranocha et al., 2001; Sauter et al., 2013). Although plastids are autonomous for methionine biosynthesis, they depend on the import of SAM as methyl donor by the SAMT1 transporter (Ravanel et al., 2004; Bouvier et al., 2006). The essentiality of cytosolic C_1 metabolism was shown by characterization of the hypomorphic and dwarfed mutant of the cytosolic methylenetetrahydrofolate dehydrogenase/methenyltetrahydrofolate cyclohydrolase activity (MTHFD1). Loss of MTHFD1 activity abolishes the SAM cycle and causes genome-wide DNA hypomethylation and loss of histone H3K9 methylation (Groth et al., 2016). However, given by the existence of mitochondrial NAD-dependent formate dehydrogenase (FDH), formate could also be oxidized to CO_2 while reducing a pyridine co-

factor, preferentially NADH. The existence of FDH was demonstrated in several plant species (potato, rice, *Arabidopsis*) and a role as stress inducible protein was hypothesized (Colas des Francs-Small et al., 1993; Hourton-Cabassa et al., 1998; Li et al., 2000; Shiraishi et al., 2000; Alekseeva et al., 2011; Choi et al., 2014; Lou et al., 2016). Further, FDH is regulated via post-translational modifications, including phosphorylation and acetylation, but the consequences on FDH activity remain unknown (Bykova et al., 2003; Kuhnert et al., 2020; Møller et al., 2020). In *Arabidopsis*, FDH is encoded by a single gene (hereafter as FDH1) and several studies at the beginning of the century reported on the biochemical characterization of FDH1 and dual targeting of the enzyme to mitochondria and the chloroplast (Li et al., 2000; Olson, 2000; Li et al., 2002; Baack et al., 2003).

Here, we address the limited understanding of C_1 metabolism in plants by characterization of Arabidopsis FDH1. Based on this, we propose that plants use a C_1 shunt based on formate exchange to connect mitochondrial and cytosolic C_1 metabolism and regulate flux via the shunt by FDH1. To this extent, we analyzed the kinetic constants of recombinant FDH1 and define the enzyme as NAD-dependent FDH. In addition, we confirmed that FDH1 is localized to plant mitochondria and not dual-targeted to the chloroplast as previously described (Li et al., 2000; Olson, 2000; Li et al., 2002; Baack et al., 2003). Further, we assessed the *in planta* role of FDH1 by generated loss-of function mutants and overexpression plants. The loss of *FDH1* reduced plant growth and altered chlorophyll biosynthesis whereas overexpression increased plant growth. Finally, we picture a potential serine/formate shuttle to mediate C_1 unit transfer between compartments according to the cellular and/or organellar redox state.

Results

FDH1 is a NAD-dependent formate dehydrogenase

Biochemical characterization of FDH1 reported kinetic constants that differ by one order of magnitude with respect to the affinity for formate, ranging from 1.4 mM to 10 mM (Li et al., 2000) (Olson, 2000). In order to accurately determine the kinetic constants of FDH1, we heterologously expressed FDH1 in *E. coli* and purified the protein by immobilized metal affinity chromatography based on an N-terminal 6xHis-tag. Recombinant FDH1 had a K_m value of 3.85 ± 0.14 mM for formate and a V_{max} of 1.02 ± 0.01 µmol min^{-1} mg^{-1} protein determined by Michaelis-Menten kinetics (Supplemental Fig. S1). In a recently published mitochondrial proteomic dataset, we identified the first 30 N-terminal amino acids of FDH1 as mitochondrial target peptide that is cleaved upon mitochondrial import (Kuhnert et al., 2020). Comparison of FDH1 activity with a variant lacking the

mitochondrial target peptide (FDH1$^{\Delta 1\text{-}30}$), revealed no significant differences in total FDH activity (Fig. 1A), although both, the K_m value for formate (4.11 ± 0.1 mM) and V_{max} (1.47 ± 0.02 µmol min^{-1} mg^{-1} protein) increased (Supplemental Fig. S1).

We only considered FDH1 for further biochemical characterization and determined a pH optimum of 7.5 (Fig. 1B). Formate was the preferred substrate of FDH1, since no activity was detected with glutamate, glycolate, acetate or oxalate (Fig. 1C). However, glyoxylate was accepted as a secondary substrate with 4% activity compared to formate (Fig. 1C). In addition, FDH1 was neither allosterically regulated by photorespiratory metabolites (glycine, serine, glycolate, glyoxylate), glutamate and oxalate (Fig. 1D), nor did oxidized or reduced conditions alter the activity (Fig. 1E and F).

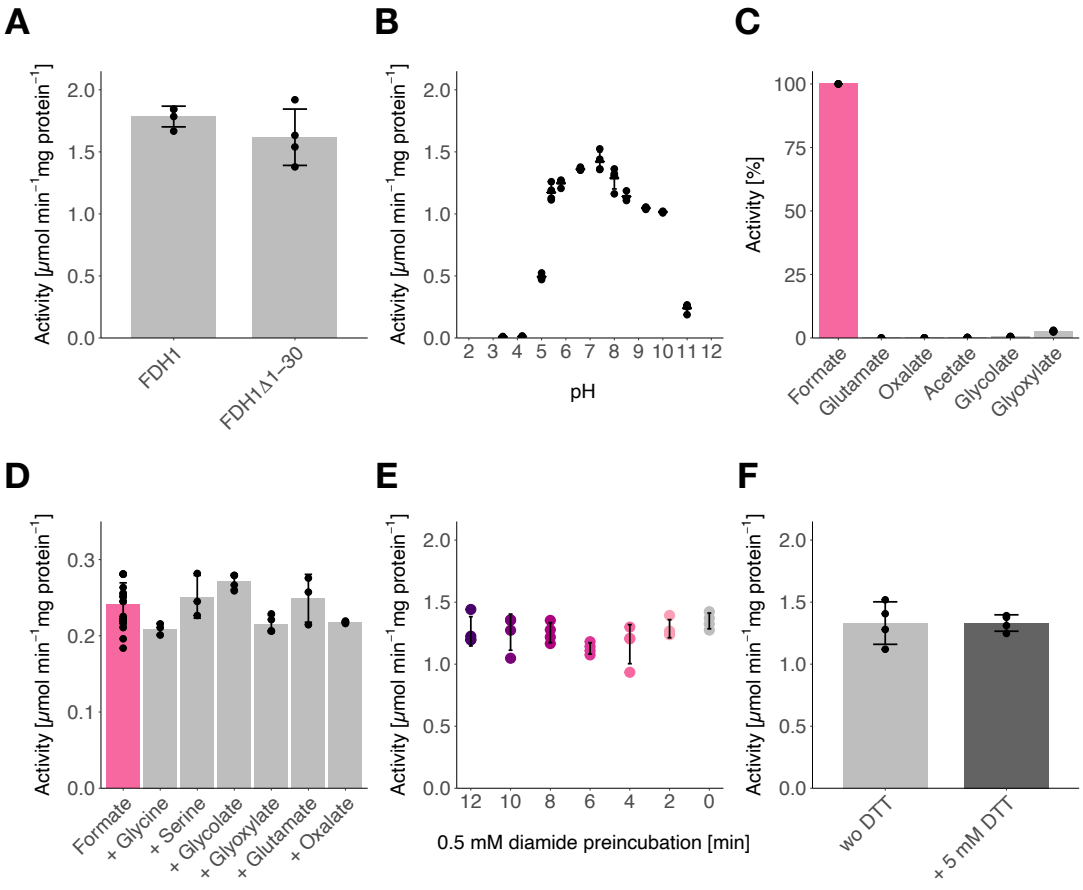

Fig. 1: Biochemical characterization of Arabidopsis formate dehydrogenase 1. Arabidopsis formate dehydrogenase 1 (FDH1) was N-terminally 6xHis-tagged, heterologously expressed in *E. coli* and purified by immobilized metal affinity chromatography. All enzymatic assays were performed with 50 mM sodium formate, if not stated otherwise. A) Activity of FDH1 and FDH1$^{\Delta 1\text{-}30}$. B) pH-optimum of FDH1, C) Substrate specificity of FDH1. Activity with formate was set to 100%. D) Allosteric regulation of FDH1. Assays performed with 1 mM formate in the presence of 10 mM allosteric inhibitor. E) FDH1 under oxidized conditions. Recombinant FDH1 protein was preincubated with 0.5 mM diamide before enzymatic assays. F) FDH1 activity under reduced conditions in the presence of 5 mM DTT. For all experiments: n ≥ 3. Shown = mean ± SD, replicates shown as points.

FDH1 is a mitochondrial enzyme

It was previously hypothesized that FDH1 is dual localized to mitochondria and chloroplasts (Olson, 2000; Herman et al., 2002). Based on subcellular fluorescence studies we demonstrated that FDH1 is only localized in mitochondria (Fig. 2A and B and Supplemental Fig. S2). Initially, we generated GFP fusions of FDH1 N-termini and analyzed the subcellular localization in tobacco protoplasts by confocal laser scanning microscopy. The GFP-fusion of the N-terminal 60 amino acids ($FDH1^{1-60}$) resulted in mitochondrial protein localization, whereas shorter FDH1 N-termini fusions ($FDH1^{1-30, 1-40, 1-50}$) localized in the cytosol (Supplemental Fig. S2). In order to independently validate the mitochondrial localization of FDH1, we generated stable Arabidopsis plants. Therefore, full-length FDH1 was C-terminally fused with mCherry and overexpressed under the constitutive active *UBQ10* promoter (Grefen et al., 2010). The respective FDH1-mCherry fusion localized to mitochondria in leaves and roots and remained FDH activity when heterologously expressed in *E. coli* (Fig. 2C).

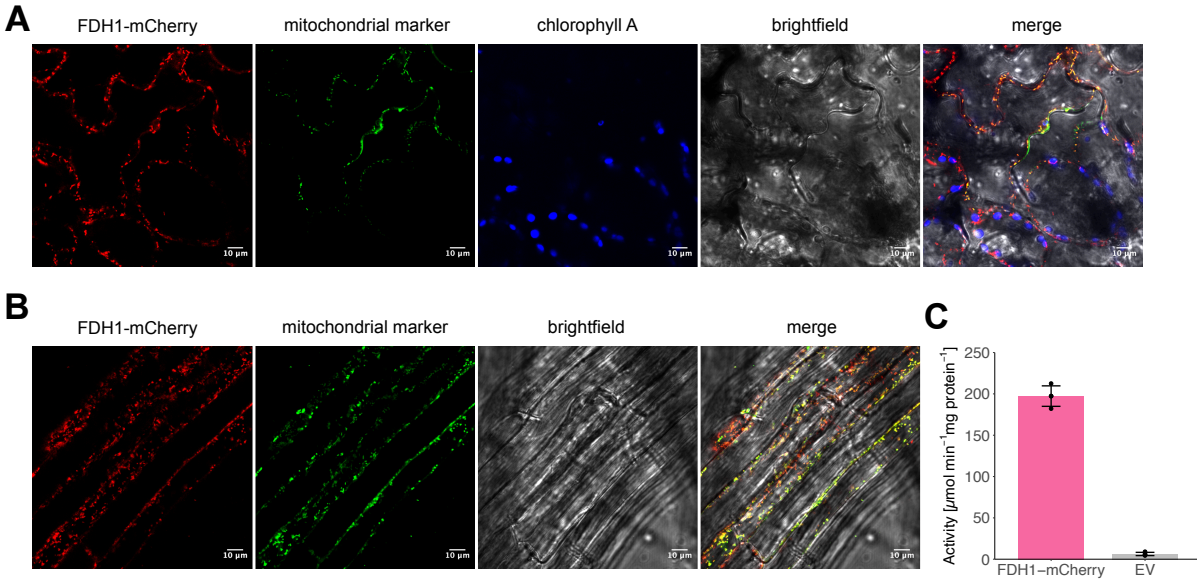

Fig. 2: Localization of Arabidopsis formate dehydrogenase 1. A and B) Arabidopsis formate dehydrogenase 1 (FDH1) was C-terminally fused with mCherry. Transgenic Arabidopsis lines expressing *FDH1-mCherry* under the constitutive *UBQ10* promoter were generated. Leaves (epidermal cell layer, A) and roots (root cortex, B) of 14 days old seedlings were analyzed by confocal laser scanning microscopy. Red = FDH1-mCherry signal, Green = MitoTracker Green FM as mitochondrial marker, in A) Blue = chlorophyll A autofluorescence. (C) FDH activity of FDH1-mCherry fusion. FDH1-mCherry was heterologously expressed in *E. coli*. The respective lysate was measured for FDH activity and compared to the empty vector control (EV). n = 3, Shown = mean ± SD, replicates shown as points.

Generation of *fdh1* mutants by genome editing

Although previous studies hypothesized on a role of plant FDHs in stress response, direct evidence by mutant characterization is lacking (Hourton-Cabassa et al., 1998; Choi et al., 2014; Møller et al., 2020). We generated three independent *fdh1* (hereafter *fdh1-1*, *fdh1-2* and *fdh1-3)* loss-of function mutants in Arabidopsis using the clustered regularly interspaced short palindromic repeat (CRISPR)/ CRISPR-associated protein 9 (Cas9) [CRISPR/Cas9] system for genome editing (Hahn et al., 2017b). Two guide RNAs (gRNA) were designed, targeting the 4th exon of the *FDH1* gene, encoding for the NAD-binding site (Fig. 3). The induced genomic mutations and homozygosity of the *fdh1* mutants were confirmed by Sanger-sequencing of the *FDH1* genomic locus upon PCR-based amplification (Supplemental Fig. S3). The *fdh1* mutants harbor 34, ten and seven base pair deletions, respectively, either at the position of gRNA1 (*fdh1-1* and *fdh1-2*) or gRNA2 (*fdh1-3*) (Fig. 3A and B). FDH activity measurements, using isolated mitochondria, confirmed all three *fdh1* mutants as loss function mutants, since FDH activity was not detectable, whereas mitochondrial NAD-dependent malate dehydrogenase activity, remained unaltered between wild type (WT) and *fdh1* mutants (Fig. 3C). To independently validate the *fdh1* mutants as loss of function mutants, the primary *FDH1* transcript from each *fdh1* mutant was isolated. Based on the respective transcript, recombinant protein was synthesized *in vitro* and FDH activity was measured (Fig. 3D). Recombinant FDH1 proteins from the *fdh1* mutants did not catalyze FDH activity and immunoblot analysis confirmed truncated FDH1 protein of 84 and 64 amino acids in the *fdh1-2* and *fdh1-3* mutant, respectively (Fig. 3D, Supplemental Fig. S3). Although a 100 amino acid ablated FDH1 protein was expected in the *fdh1-1* mutant, mis-splicing of the *FDH1* transcript resulted in an early stop codon 120 base pairs after the start codon (Supplemental Fig. S3).

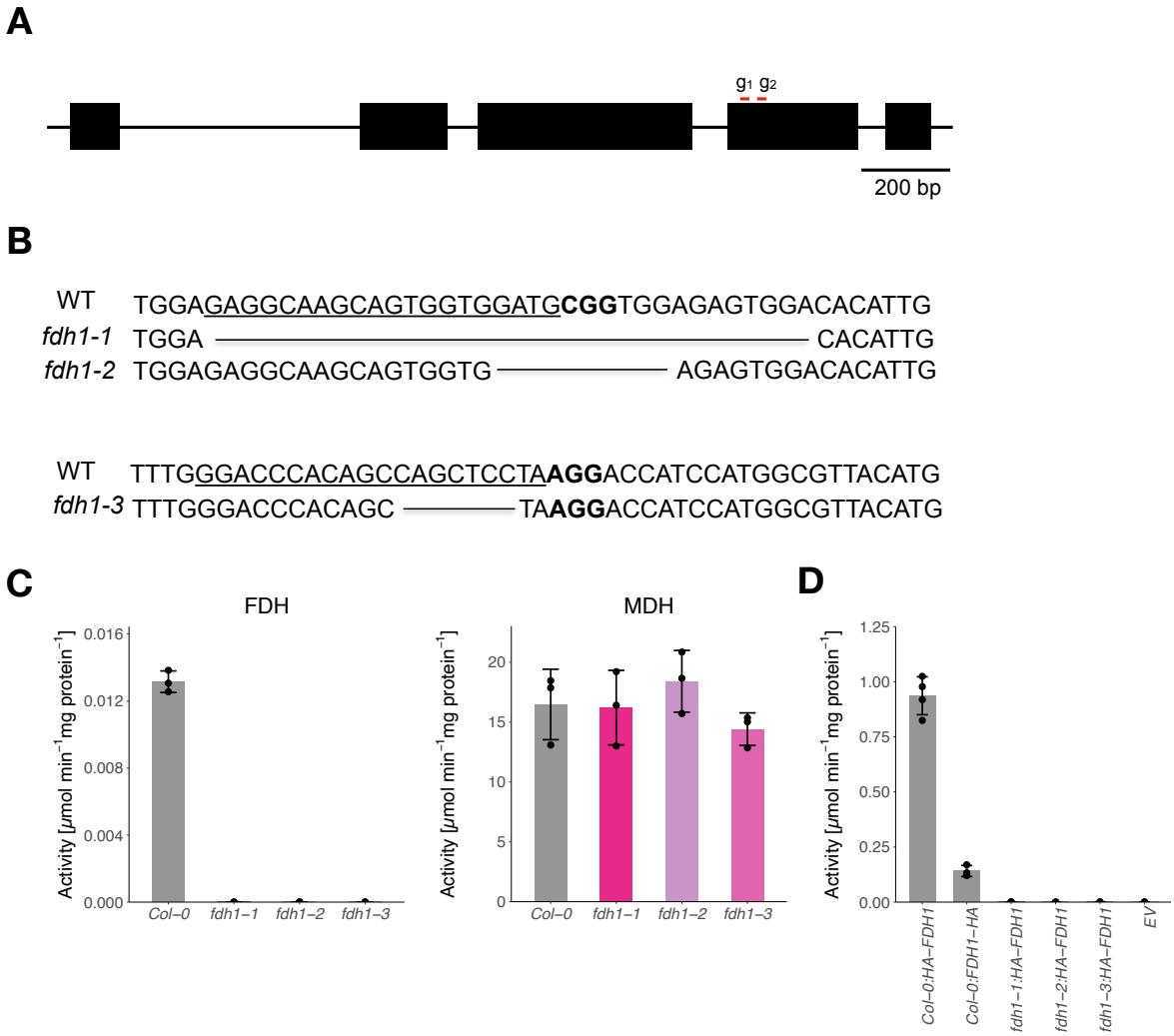

Fig. 3: Generation *FDH1* knockout mutants. A) Schematic representation of the Arabidopsis *FDH1* genomic locus. Red lines indicate the position of the guide RNAs (g1 & g2) used for genome editing by the CRISPR/Cas9 system. B) Genomics mutations in the *fdh1* mutants. Within the wild type (WT) *FDH1* sequence the 20 base pairs target sequence of the guide RNAs (g1 top, g2 bottom panel) is underlined. The protospacer adjacent motif is indicated in bold. C) FDH activity in isolated leaf mitochondria. Mitochondrial NAD-dependent malate dehydrogenase (MDH) was measured as control. Shown = mean ± SD, replicates shown as points, n = 3. D) FDH activity of *in vitro* synthesized recombinant FDH1 protein based on the primary *FDH1* transcript of the *fdh1* mutant (*fdh1-1*, *fdh1-2*, *fdh1-3*). Wild type (*Col-0*) FDH1 protein, N- and C-terminally HA tagged (HA-FDH1, FDH1-HA respectively) served as positive controls. Empty vector (EV) served as negative control. Shown = mean ± SD, replicates shown as points, n = 4.

The lack of FDH1 causes hypersensitivity to exogenously supplied formate

To characterize the physiological role of FDH1, we combined the *fdh1* mutants with three independent overexpression lines (*OEX:FDH1#1-3*). The *OEX:FDH1* plants express the *FDH1-mCherry* fusion under the constitutive *UBQ10* promoter and the *FDH1* transcript is eightfold (#1), 13-fold (#2) and 14-fold (#3) more abundant compared to WT (Supplemental Fig. S4). Millimolar concentrations of exogenously supplied formate reduce

plant growth and photosynthetic electron transport in isolated chloroplasts (Stemler, 1980; Blubaugh and Govindjee, 1988). Competitive inhibition of the bicarbonate binding site within photosystem II by formate, prevents proton donation to the plastoquinone reductase site (Blubaugh and Govindjee, 1988; Li et al., 2002). To initially verify the effect of exgenously supplied formate on plant growth and development, we quantified seedling establishment of *fdh1* mutants and *OEX:FDH1* plants in the presence of 5 mM formate. Even without formate treatment the *fdh1-2* and *fdh1-3* mutants are reduced in germination compared to WT, whereas *fdh1-1* is not altered ($\chi^2 = 0.16$). All *OEX:FDH1* plants germinated WT-like in the absence of formate. Plant cultivation in the presence of 5 mM formate impaired germination and development of the *fdh1* mutants compared to WT (Fig. 4A and B). Chlorophyll photochemical efficiency of photosystem II in dark-adapted leaves (F_v/F_m) is a key parameter reflecting photosystem II efficiency and a common marker of plant stress (Krause and Weis, 1991). To test the inhibitory effect of formate on photosystem II, we quantified F_v/F_m values (Fig. 4B). Even under control conditions *fdh1* mutants showed reduced F_v/F_m values compared to WT (Fig. 4B). Growth on 5 mM formate reduced F_v/F_m values of all genotypes but severely affected *fdh1* mutants, whereas the overexpression plants were less affected in comparison to WT (Fig. 4B and C). This highlights that *fdh1* mutants are hypersensitive to exogenously supplied formate, whereas overexpression of *FDH1* conferred resistance.

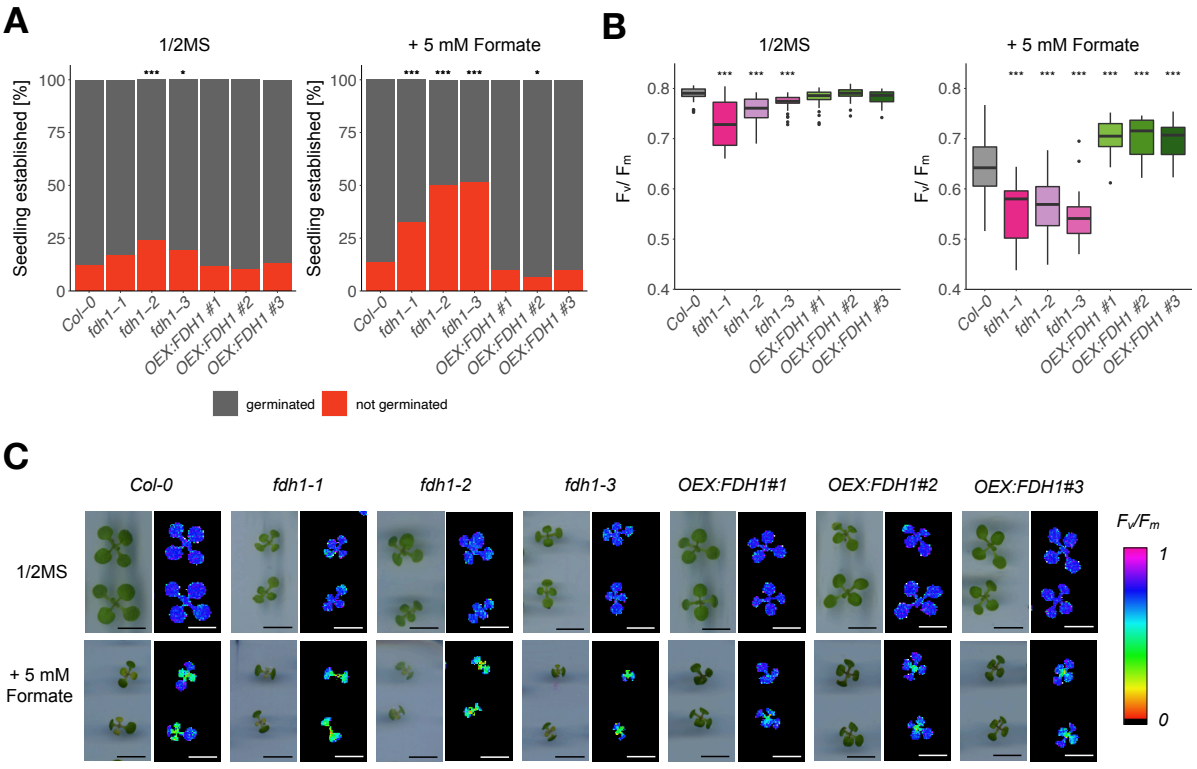

Fig. 4: Sensitivity of *fdh1* mutants and *FDH1* overexpression plants to exogenously supplied formate. A) Seedling establishment, quantified on twelve days after transfer to light. Seedlings grown at ambient CO_2 on agar plates (1/2MS) or agar plates supplemented with 5 mM sodium formate (+ 5 mM Formate). n > 25. Chi-square test χ^2 > 0.05 = *,> 0.01 = **, > 0.001 = ***. B) Quantification of chlorophyll photochemical efficiency of photosystem II in dark-adapted leaves (F_v/F_m). Students *t*-test against wild type *Col-0*. p > 0.05 = *,> 0.01 = **, > 0.001 = ***. $n_{1/2MS}$ > 25, $n_{+5\ mM\ Formate}$ > 10. C) Representative image of F_v/F_m measurement of twelve days old seedlings. Scale bar = 0.5 cm.

Mitochondrial formate dehydrogenase activity is required for plant growth

The absence of mitochondrial FDH1 activity impaired growth of air grown plants, whereas *FDH1* overexpression accelerated growth and an earlier completion of the life cycle (Fig. 5, Supplemental Fig. S4). Consistently, fresh weight and dry weight of 12-d-old seedlings were reduced in the *fdh1* mutants and increased in the *OEX:FDH1* plants (Fig. 5B and C). In addition, both, mutants and overexpression plants were reduced in primary root length (Fig. 5D).

Recent evidence shows that an integral folate status is required for functional chlorophyll biosynthesis (Van Wilder et al., 2009). Chlorophyll synthesis requires the conversion of Mg-protoporphyrin IX into Mg-protoporphyrin IX monomethyl ester. The enzyme, Mg-protoporphyrin IX methyltransferase catalyzing this reaction uses the universal methyl-donor Ado-Met as substrate. Chlorophyll analysis indicated an altered chlorophyll a to chlorophyll b ratio in the *fdh1* mutants (Fig. 5H). An opposite trend was found in the

overexpression lines. Total chlorophyll a content was significantly reduced in two out of three *fdh1* mutants and unaltered in the overexpression lines (Fig. 5G). In contrast, chlorophyll b content was increased in the *fdh1* mutants (Fig. 5F; $p < 0.05$ for *fdh1-1* and *fdh1-2*). However, despite the visible growth effects, soluble metabolite pools linked to C_1 metabolism (glycine, serine, methionine) were not altered (Supplemental Fig. S5).

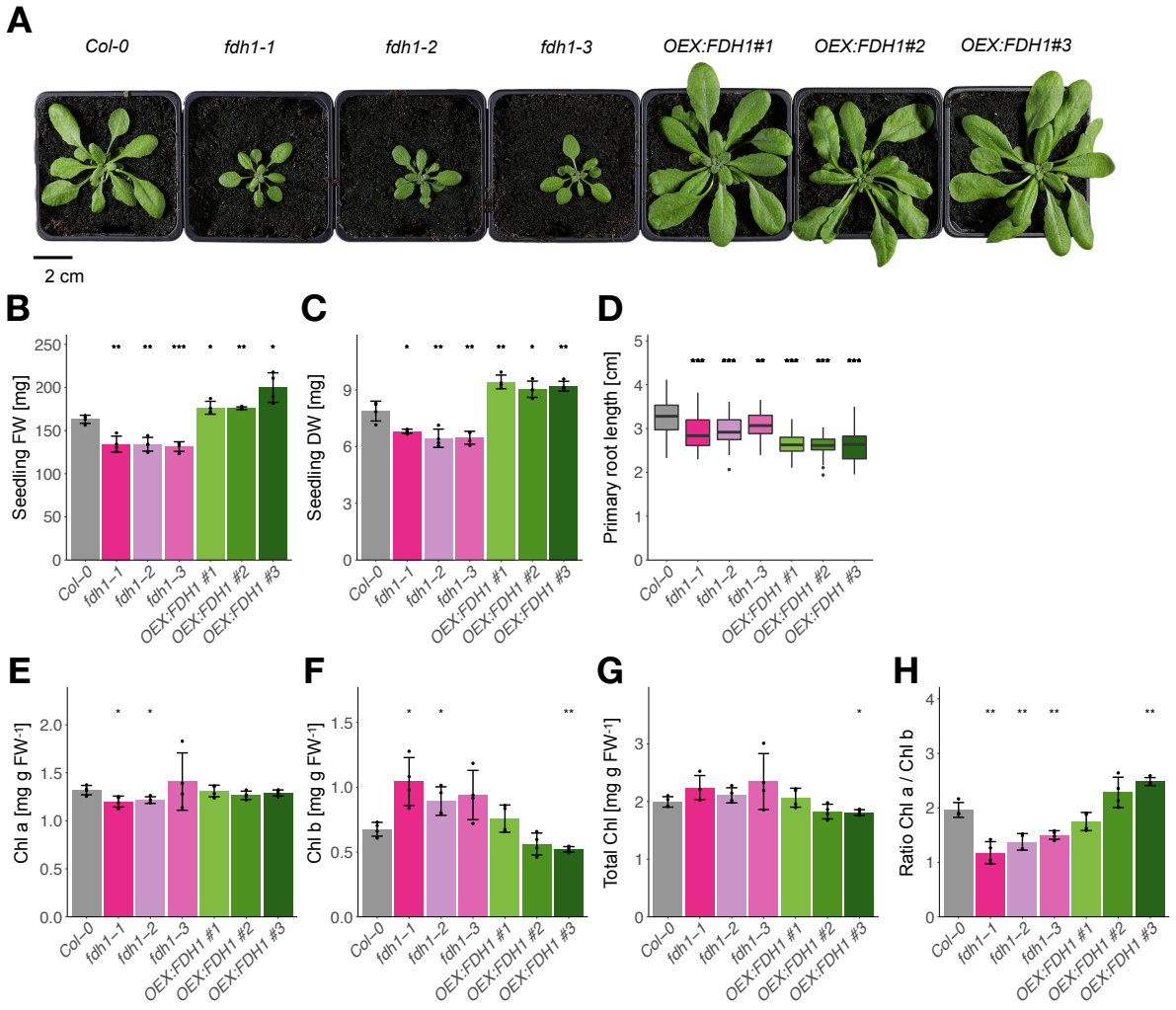

Fig. 5: Phenotype of *fdh1* mutants and overexpression plants. A) Representative image of phenotypes of four weeks old plants grown at ambient CO_2. B and C) Fresh weight (B) and dry weight C) of twelve days old seedlings. n = 4. Shown mean ± SD. Biological replicates are indicated as points. D) Primary root length of twelve days old seedlings. n > 30. E-H) Chlorophyll content in rosettes of four weeks old plants. Chlorophyll a (E), chlorophyll b (F), total chlorophyll content (G), ratio chlorophyll a/ chlorophyll b (H) was determined. n = 4. Shown mean ± SD. Biological replicates are indicated as points. For all: Students *t*-test against wild type *Col-0*. p > 0.05 = *,> 0.01 = **, > 0.001 = ***.

Discussion

Underlying fundamental principles of C_1 metabolism in plants are marginally defined, caused by a high genetic redundancy, low metabolic flux, metabolite instability and mutant lethality (Hanson and Roje, 2001). Formate, an intermediate of C_1 metabolism, is

either used in folate-dependent C_1 metabolism or oxidized to CO_2 (Ducker and Rabinowitz, 2017). In mammalian cells, formate exchange between mitochondria and the cytosol is essential for compartmentalized folate-dependent C_1 metabolism (Fan et al., 2014; Ducker et al., 2016; Zheng et al., 2018). However, a comparable C_1 shunt in plants, is questioned by the existence of mitochondrial FDH, that is putatively dual localized to the chloroplast (Olson, 2000; Herman et al., 2002; Alekseeva et al., 2011). Based on characterizing the role of Arabidopsis FDH1, we propose that in plants, FDH regulates the flux of the C_1 shunt that mediates formate exchange between mitochondria and the cytosol to maintain homeostatic C_1 metabolism.

In Arabidopsis, FDH is encoded by a single gene (*FDH1*) and localized to mitochondria (Fig. 2, Supplemental Fig. S2). Given the expected low intracellular formate levels in the plant cell, the high K_m for formate of recombinant FDH1 was surprising ((Wingler et al., 1999) Supplemental Fig. S1). However, it implies either underestimated cellular formate levels or a small pool size, that is maintained below a toxicity threshold (Fig. 4, (Stemler, 1980; Blubaugh and Govindjee, 1988; Igamberdiev et al., 1999)). Further, *in vitro* determined kinetic constants could differ from *in vivo* scenarios based on the cellular environment and regulation of the enzyme. Indeed, redox regulation of the plastidial glucose-6-phosphate dehydrogenase, the first enzyme of the glucose-6-phosphate shunt, increases the K_m of the enzyme under reduced conditions (Scheibe et al., 1989; Hauschild and Schaewen, 2003; Sharkey and Weise, 2016). Although FDH1 activity was not influenced by oxidized or reduced conditions (Fig. 1), posttranslational modification, by phosphorylation and/or acetylation, could play a role in regulating FDH activity and kinetics (Bykova et al., 2003; Kuhnert et al., 2020; Møller et al., 2020). We note, that FDH1 was identified in a mitochondrial lysine (Lys) acetylome study of Arabidopsis (König et al., 2014). In a recent study on the mitochondrial carrier protein A BOUT DE SOUFFLE from Arabidopsis, FDH1 was differentially abundant between the WT and the mutant but unchanged in activity, indicating *in vivo* regulation of the enzyme by posttranslational modifications (Kuhnert et al., 2020). However, a recombinant $FDH1^{K184R}$ mimicking mutant, with the mutated lysine in the NAD-binding pocket did not show altered activity and kinetics (data not shown).

The photorespiratory phenotype of the 10-deformylase double knockout mutant indicates that 5,10-methylene-THF produced by the GDC is oxidized in the mitochondrial THF cycle and formate is produced (Collakova et al., 2008). This implies that in an illuminated leaf, the GDC is one source of mitochondrial derived formate. In line with the hypothesis of mitochondrial formate export via the shunt for cytosolic folate-dependent C_1 metabolism,

the transcriptional abundance of *FDH1* within a light phase behaved acyclic to *GLDT* (Supplemental Fig. S6). The *GLDT* gene encodes the GDC T-protein that is required to produce 5,10-methylene-THF that is oxidized by the THF-cycle to produce formate. However, a quantitative estimate on the fate and flux of photorespiratory C_1 metabolism is lacking (Busch, 2020). Stable-isotope tracing by $^{13}CO_2$ and ^{33}sulfur using the soluble methionine pool as readout of C_1 fluxes, do not differentiate between cytosolic and/or plastidial SHM and formate-dependent folate metabolism that both contribute to the 5,10-methylene-THF pool used for methionine synthesis (Gauthier et al., 2010; Abadie and Tcherkez, 2019).

In order to provide *in planta* evidence on the C_1 shunt and the associated regulatory role of FDH1, we generated *FDH1* knockout mutants and overexpression plants (Fig. 3 and 5, Supplemental Fig. S4). The stunted growth of the *fdh1* mutants indicates impaired C_1 metabolism, that has to be addressed by the quantification of cellular formate, folate and SAM levels. Indeed, dysfunctional cytosolic C_1 metabolism in a hypomorphic and dwarfed *mthfd1* mutant, caused DNA hypomethylation and reduced folate levels (Groth et al., 2016). Further, chlorophyll biosynthesis depends on the integrity of the cellular folate pool. Depletion of the THF pool by methotrexate caused decreased chlorophyll biosynthesis, whereas the altered chlorophyll a/b ratio in the *fdh1* mutants might be a consequence of an altered folate pool (Fig. 5H; Van Wilder et al., 2009). Remarkably, *FDH1* overexpression accelerated plant growth (Fig. 5, Supplemental Fig. S4). At least three effects could explain the observed phenotype. First, overcoming the rate limiting steps of photorespiration by overexpression of the GDCH protein was shown to increase plant growth (Timm et al., 2012; Timm et al., 2015; Lopez-Calcagno et al., 2019). So far, it remains to be proven, that higher mitochondrial FDH activity by *FDH1* overexpression expedites THF recycling and the GDC catalyzed reaction of photorespiration because glycine and serine pools remained unaltered (Supplemental Fig. S5). Further, produced NADH by formate oxidation could be used in the redox shuttles and the respiratory chain to positively affect the cytosolic ATP/ADP ratio, as well as NADH/NAD ratio (Gardeström and Wigge, 1988; Wigge et al., 1993; Igamberdiev and Gardeström, 2003; Tomaz et al., 2010; Tcherkez et al., 2012). Finally, a positive effect of respired CO_2 on the Calvin-Benson-Bassham cycle seems possible and can be addressed by gas-exchange measurements (Busch et al., 2013).

However, all three explanations imply a plastic system to ensure integrity of C_1 metabolism. Based on comparison to mammalian C_1 metabolism and the unlikely transport of C_1 folates across organellar membranes, we propose a formate/serine shuttle

between the compartments in the plant cell (Cybulski and Fisher, 1981; Ducker et al., 2016; Zheng et al., 2018; Li et al., 2020; Yang et al., 2020). Such a shuttle allows the inter-compartment distribution of C_1 units and enables to adapt the fluxes according to the redox status in the respective compartment. It should be noted that the specificity for NAD or NADP of the plant enzymes in C_1 metabolism remain unknown. Therefore, the following hypothesis is based on specificity of mammalian counterparts and considers the ratio of reduced/oxidized NAD(P) in the compartments of the plant cell.

In an illuminated leaf, photorespiration and within combined GDC and SHM1 activity represent the primary route of serine biosynthesis (Prabhu et al., 1996; Prabhu et al., 1998; Voll et al., 2006; Igamberdiev and Kleczkowski, 2018). However, GDC derived 5,10-methylene-THF is also oxidized in the THF cycle, producing NADH, used by the respiratory chain or redox shuttles (Gardeström and Wigge, 1988; Wigge et al., 1993; Douce et al., 2001; Tomaz et al., 2010; Selinski and Scheibe, 2019; Shameer et al., 2019). The NADH-dependency of the mammalian mitochondrial MTHFD and the slightly oxidized mitochondrial NAD pool support NADH production by C_1 metabolism (Christensen et al., 2005; Fan et al., 2014). Generated formate is assimilated in the cytosol and reduced to 5,10-methylene-THF under NADPH consumption, given a NADPH/NAPD ratio of 1.5 in the cytosol (Gardeström and Wigge, 1988; Igamberdiev and Gardeström, 2003). This implies only a minor role of cytosolic SHM in C_1 unit provision or a regulatory role in mediating flux between SAM- and thymidylate biosynthesis (Herbig et al., 2002). Depending on the redox state, the fluxes could be reversed and formate produced in the cytosol is oxidized in the mitochondria to produce NADH and CO_2, if necessary.

In the chloroplast, formate is used to produce 10-formyl-THF for purine biosynthesis or 5,10-methylene-THF for methionine biosynthesis (Hanson and Roje, 2001; Ravanel et al., 2004; Zrenner et al., 2006). So far, the plastidial SHM3 was biochemically characterized, but a respective mutant is not described (Zhang et al., 2010). Therefore, conclusion on the extend of plastidial SHM to the 5,10-methylen-THF pool are hard to make at this point and requires *shm3* mutant establishment and characterization to understand plastidial C_1 metabolism and associated genes.

In contrast to an illuminated leaf, the phosphoserine pathway is the dominant route of serine biosynthesis in the night and in heterotrophic tissue (Benstein et al., 2013; Cascales-Miñana et al., 2013; Wulfert and Krueger, 2018). In mitochondria, serine catabolism by SHM2 and the GDC produces two 5,10-methylene-THF molecules per serine and one NADH. The subsequent complete oxidation of the 5,10-methylene-THF produces four additional NADH molecules, which might be particularly important under energy

limiting conditions to maintain respiration (Mouillon et al., 1999; Engel et al., 2011; Nunes-Nesi et al., 2014; Yang et al., 2020).

In general, the plasticity of the proposed formate/serine shuttle ensures C_1 unit distribution between compartments. Further, C_1 metabolic fluxes can be rapidly adjusted according to the cellular and organellar redox state. The experimental proof of the C_1 shunt and the formate/serine shuttle requires a dynamic flux analysis by formate-^{13}C feeding. The first step towards this was made by elucidating the time to reach isotopic steady-state labeling in the pools of glycine, serine and methionine (Supplemental Fig. S7). Now, dynamic metabolite profiling in the established *fdh1* mutants and overexpression plants as well as established mutants of *shm1*, *shm2* and a necessary *shm3* mutant will contribute to understand C_1 metabolic fluxes within the plant cell (Voll et al., 2006; Zhang et al., 2010; Engel et al., 2011).

Conclusion

Taken together, mitochondrial FDH1 seems crucial to maintain homeostatic C_1 metabolism by controlling the flux via the C_1 shunt that connects the mitochondria and the cytosol. Hypothetically, the low metabolic flux of the C_1 shunt prevents alterations in whole cell pool sizes, detected by steady-state metabolomics. Therefore, the quantification of cellular formate, C_1 folates and SAM levels, dynamic formate-^{13}C labeling in combination with flux analysis and gas-exchange measurement will provide further proof of the C_1 shunt in plants.

Material and Methods

Chemicals

All chemicals were purchased from Sigma Aldrich (St. Louis, USA) unless otherwise stated.

Plasmid construction

The *Arabidopsis thaliana* (Arabidopsis) *FDH1* coding sequence (At5g14780) was cloned into pET-16b (Merck, Darmstadt, Germany) by Gibson Assembly for heterologous protein expression (Gibson et al., 2009). Plasmids used for localization studies were made using the MoClo GoldenGate cloning system (Engler et al., 2014). Internal *BsaI* and *BpiI* restriction sites of the *FDH1* coding sequence were removed by gene synthesis (ThermoFisher Scientific, Waltham, USA). FDH1 localization constructs were assembled in pICH86966 (Addgene #46967). Sites and plasmids for targeted mutagenesis of the *FDH1* gene by CRISPR/Cas9 were designed and cloned as described in (Hahn et al.,

2017a). All constructs were verified by Sanger sequencing (Microsynth, Balgach, Switzerland). Primers and constructs used in this study are listed in Supplemental Tables S1 and S2 respectively.

In vitro protein synthesis, heterologous expression in *E. coli* and purification of FDH1

In vitro protein synthesis was performed using the PURE system according to the manufacturer (New England Biolabs, Ipswich, USA) (Shimizu et al., 2001). FDH1 and FDH1 $^{\Delta 1\text{-}30}$ was expressed in *E. coli* BL-21(DE3) Rosetta cells (Novagen, Wisconsin, USA). Cells were grown at 37°C and 140 rpm in liquid lysogeny broth medium containing 200 µg mL^{-1} ampicillin and 25 µg mL^{-1} chloramphenicol to an OD_{600} of 0.6. Cultures were cooled to 30°C, protein expression was induced with isopropyl ß-d-1-thiogalactopyranoside to a final concentration of 0.5 mM, and the cultures were incubated at 30°C and 200 rpm for 2 h. Cells were pelleted by centrifugation at 4,000 x *g* for 15 min and stored at -20°C. Pellets containing recombinant protein were resuspended in cell lysis buffer (50 mM NaP_i [pH 7.5], 1 mM EDTA, 0.5 M NaCl, 10 mM Imidazole, 10% [v/v] Glycerol, 1 mM DTT, 0.5 mM PMSF, 100 µM AEBSF, 1 µM Pepstatin, 1 mg mL^{-1} Lysozyme) at a ratio of 5 mL per gram wet weight cells and incubated for 30 min with gentle shaking. After 30 min, 6 mM 3-[(3-Cholamidopropyl)-dimethylammonio]-1-propanesulfonate (CHAPS) was added and the mixture was incubated for a further 30 min with gentle shaking. Subsequently, 10 mM $MgCl_2$, 5 mM ATP and a few DNase crystals were added and the mixture was incubated for 20 min at room temperature with gentle shaking, followed by centrifugation for 10 min at 3,000 x *g* at 4°C. The supernatant was collected and incubated for 1 h at 4°C with Ni-NTA resin pre-equilibrated with 50 mM NaP_i (pH 7.5) and 0.5 M NaCl. The Ni-NTA resin was washed twice with wash buffer I (50 mM NaP_i [pH 7.5], 20 mM Imidazole) followed by one washing step with wash buffer II (50 mM NaP_i [pH 7.5], 50 mM Imidazole). The recombinant protein was eluted with 50 mM NaP_i (pH 7.5) containing 500 mM imidazole. Imidazole was removed and protein samples concentrated using Amicon® Ultra Centrifugal Filter units (cutoff 30 kDa, Merck Millipore) according to the manufacturer's instruction. Protein concentration of the purified FDH1 was determined using the Quick Start™ Bradford Protein Assay Kit (Bio-Rad), with gamma-globulin as the standard.

Enzyme assays

FDH activity was measured in a plate-reader spectrophotometer by following the absorbance at 340 nm. The standard activity assay contained 100 mM potassium phosphate buffer (pH 7.5), 1 mM NAD, 50 mM sodium formate, 1–3 µg purified recombinant protein or 5 µg isolated mitochondria, and was conducted at 30°C. For determination of substrate specificity, the following substrates were tested at a final concentration of 50 mM: sodium glutamate, sodium oxalate, sodium acetate, glycolate, and glyoxylate. Inhibition of enzyme activity was determined at 1 mM sodium formate and 10 mM of the following inhibitors: glycine, serine, glycolate, glyoxylate, sodium glutamate, and sodium oxalate. The influence of pH on enzyme activity was determined at 50 mM sodium formate and 1 mM NAD using 100 mM citrate buffer (pH 3.4–5.8), 100 mM potassium phosphate (pH 5.8–8.0), 100 mM Tris buffer (8.0–9.3), and 100 mM N-cyclohexyl-3-aminopropanesulfonic acid buffer (pH 10–11). Redox regulation of FDH was tested in the presence or absence of 5 mM DTT and 0.5 mM diamide. To fully oxidize the enzyme purified recombinant FDH was preincubated with 0.5 mM diamide 0–12 min. Kinetic constants (K_m and V_{max}) for sodium formate were determined at pH 7.5 over a concentration range of 0.1–50 mM sodium formate. Assays were conducted at least in triplicates. Activities were calculated from initial velocities. Mitochondrial malate dehydrogenase activity was measured as described previously (Tomaz et al., 2010; Kuhnert et al., 2020).

SDS-PAGE and immunoblot analysis

Successful protein purification was confirmed by SDS-PAGE using standard protocols (Laemmli, 1970). 20 µg of *in vitro* synthesized protein was heated at 96°C in SDS-PAGE loading buffer for 10 min and separated on 12% SDS-polyacrylamide gels (Laemmli, 1970). Proteins were transferred onto 0.45 µm nitrocellulose membranes (Thermo Scientific) using the semi-dry blotting procedure. Membranes were blocked in Tris-buffered saline containing 0.1% (v/v) Tween 20 (TBST) and 5% (w/v) non-fat milk powder, washed with TBST and subsequently incubated with a monoclonal conjugated horseradish peroxidase anti-HA antibody (Miltenyi Biotech) overnight at 4°C. Membranes were washed five times with TBST and visualized using a chemiluminescence detection system (Immobilon Western HRP Substrate, Merck Millipore).

Plant material and growth conditions

Arabidopsis ecotype *Col-0* was used in this study. Seeds were surface-sterilized using the vapor-phase sterilization method (Clough and Bent, 1998). Seeds were grown on half-

strength Murashige and Skoog medium (pH 5.7) supplemented with 0.8% (w/v) agar (½ MS plates). Seeds were cold stratified for 2 d at 4°C. After germination, seedlings were grown for 14 d at 100 µmol m^{-2} s^{-1} light intensity, ambient CO_2 atmosphere (0.04% [v/v] CO_2) and a 12-h light/12-h dark photoperiod unless otherwise stated.

Generation of transgenic Arabidopsis lines

T-DNA constructs were introduced into *Agrobacterium tumefaciens* strain GV3101::pMP90 (Koncz and Schell, 1986) and Arabidopsis *Col-0* plants were transformed via Agrobacterium-mediated transformation (Clough and Bent, 1998). Homozygous T3 plants were used for physiological analysis.

Transient expression in *Nicotiana benthamiana* and protoplast isolation

For transient expression in *Nicotiana benthamiana*, overnight-grown *Agrobacterium tumefaciens* cells harboring the T-DNA construct were diluted in infiltration medium (10 mM $MgCl_2$, 10 mM MES [pH 5.7], 100 µM acetosyringone) to an OD_{600} of 0.4. Leaves of 4-weeks-old greenhouse-grown *Nicotiana benthamiana* plants were infiltrated using a syringe without a needle. The pIVD145-eqFP611 plasmid (Forner and Binder, 2007) was co-infiltrated as mitochondrial mCherry marker. Protoplasts were isolated 2 d post infection. Leaves were sliced into small pieces, vacuum-infiltrated with protoplast digestion solution (1.5% [w/v] cellulase R-10, 0.4% [w/v] macerozyme R-10, 0.4 M mannitol, 20 mM KCl, 20 mM MES [pH 5.7], 10 mM $CaCl_2$, 0.1% [w/v] bovine serum albumin) and incubated for 2 h at 28°C. Sedimented protoplasts were resuspended in W5 solution (154 mM NaCl, 125 mM $CaCl_2$, 5 mM KCl, 2 mM MES [pH5.7]).

Mitochondria isolation

Mitochondria were isolated from 4-weeks-old Arabidopsis *Col-0*, *fdh1-1*, *fdh1-2*, and *fdh1-3* rosette leaves via differential centrifugation and Percoll gradient purification, as described previously (Kühn et al., 2015). BSA was omitted from all solutions.

Chlorophyll fluorescence and chlorophyll measurements

F_v/F_m values of 12-days-old seedlings were measured using an imaging chlorophyll fluorometer (Imaging PAM, Walz, Effeltrich, Germany). Upon dark adaptation for 20 min, seedlings were exposed to a pulsed, blue probe beam and a saturating light flash to measure F_v/F_m values. Chlorophyll was extracted from 4-week-old leaves in 80% acetone and rotating at 4°C in the dark before photometric measurement. Chlorophyll content was calculated based on (Inskeep and Bloom, 1985).

Quantification of germination efficiency, primary root length, fresh weight and dry weight

Germination efficiency was quantified as seedlings establishment twelve days after transfer to light. For primary root length measurements, seeds were spotted on ½ MS plates and grown in vertical position for 12 d. Seedlings were photographed and primary root length was measured using Fiji (Schindelin et al., 2012). Fresh weight and dry weight were analyzed using 12-d-old seedlings. Seedlings were collected in a 1.5 mL microcentrifuge tube and immediately weighted for fresh weight analysis. The same samples were dried at 65°C for 4 d and tubes were weighted again for dry weight analysis.

Quantitative real time PCR

Total RNA from Arabidopsis tissue was extracted with Universal RNA kit (Roboklon). 2 µg of total RNA was DNase treated with RNA-free DNase RQ1 (Promega). 1 µg DNase-treated RNA was reverse-transcribed into cDNA using LunaScript™ RT SuperMix Kit (New England Biolabs). The quantitative real time PCR was carried out using Luna® Universal qPCR Master Mix (New England Biolabs) and a StepOnePlus™ Real-Time PCR thermocycle (Applied Biosystems, Foster City, USA**).** PCR conditions were as followed: an initial denaturation step at 95°C for 10 min, followed by 45 cycles of 95°C for 15 s, and 60°C for 60 s, followed by a melting curve. Gene specific primers are listed in Supplemental Table S1. Transcript abundance was normalized to the reference gene *Protein Phosphatase 2A Subunit A3* (*PP2A*, At1g13320) (Czechowski et al., 2005). Relative transcript abundance was calculated as described by (Simon, 2003).

Confocal laser scanning microscopy

Zeiss LSM780 confocal microscope and Zeiss ZEN software (Zeiss, Jena, Germany) was used for confocal laser scanning microscopy. In Arabidopsis, mitochondria were stained with the MitoTracker™ Green FM (ThermoFisher Scientific, Waltham, USA) and imaged according to the manufacturer's instructions. Excitation/ emission wavelengths were as followed: mCherry (561 nm/580 to 625 nm), eGFP (488 nm/490 to 550 nm), chlorophyll A (488 nm/ 640 to 710 nm). Images were processed with Fiji (Schindelin et al., 2012).

Stable isotope labeling

For stable isotope labeling experiments with formate-^{13}C, seedlings were grown on ½ MS plates for 5 d and afterwards transferred to new ½ MS plates supplemented with 1 mM sodium formate-^{13}C (Cambridge Isotope Laboratories, Tewksbury, USA). Plates were

placed in the growth chamber for five additional days and whole seedlings were harvested in the middle of the light phase.

Metabolite profiling by gas-chromatography time of flight mass spectrometry

For metabolite profiling green tissue of 14-days-old seedlings was harvested by liquid nitrogen dousing at the middle of the light phase. Frozen material was grinded using precooled mortar and pestil. Grinded material was aliquoted under continuous liquid nitrogen exposure to avoid sample thawing. Metabolites were extracted by one-phase extraction as previously described and normalized to ribitol as internal standard and the sample freshweight (Fiehn et al., 2000).

Data Analysis

Data analysis was performed in R. The respective code and the primary data are available upon request from the corresponding author. The Michaelis-Menten constants of recombinant FDH1 were calculated using Michaelis-Menten plot (GraphPad PRISM 8).

Accession Numbers

The protein accession numbers used in this study are as followed: Formate dehydrogenase 1 (FDH1, At5g14780, Q56X34), Glycine decarboxylase T-protein (GLDT, At1g11860, A0A2H1ZEA9)

Acknowledgment

We would like to thank Elisabeth Klemp, Maria Graf and Katrin Weber from the CEPLAS Metabolomics facility for technical assistance, Steffen Köhler (Center for Advanced Imaging, Heinrich-Heine University Düsseldorf, Germany) for photography. We also would like to acknowledge Balraj Singh who assisted in establishing the *fdh1* mutants.

Funding Information

This study was supported by the German Research Foundation (DFG) under Germany's Excellence Strategy (CEPLAS – EXC-2048/1 – Project ID 390686111 to P.W. and A.P.M.W), the iGRAD Plant Graduate School (DFG/GRK1525 to M.-S.R. and F.K.) and the Federal Ministry of Education and Research (BMBF/Project: Format Plant-031B0194C to A.P.M.W. and M.-S.R.).

Literature Cited

Abadie C, Tcherkez G (2019) Plant sulphur metabolism is stimulated by photorespiration. Commun Biol **2**: 379–7

Alekseeva AA, Savin SS, Tishkov VI (2011) NAD (+) -dependent formate dehydrogenase from plants. Acta Naturae **3**: 38–54

Baack RD, Markwell J, Herman PL, Osterman JC (2003) Kinetic behavior of the *Arabidopsis thaliana* leaf formate dehydrogenase is thermally sensitive. Journal of Plant Physiology **160**: 445–450

Benstein RM, Ludewig K, Wulfert S, Wittek S, Gigolashvili T, Frerigmann H, Gierth M, Flügge U-I, Krueger S (2013) Arabidopsis phosphoglycerate dehydrogenase1 of the phosphoserine pathway is essential for development and required for ammonium assimilation and tryptophan biosynthesis. Plant Cell **25**: 5011–5029

Blubaugh DJ, Govindjee (1988) The molecular mechanism of the bicarbonate effect at the plastoquinone reductase site of photosynthesis. Photosyn Res **19**: 85–128

Bouvier F, Linka N, Isner J-C, Mutterer J, Weber APM, Camara B (2006) Arabidopsis SAMT1 defines a plastid transporter regulating plastid biogenesis and plant development. Plant Cell **18**: 3088–3105

Busch FA (2020) Photorespiration in the context of Rubisco biochemistry, CO_2 diffusion and metabolism. Plant J **101**: 919–939

Busch FA, Sage TL, Cousins AB, Sage RF (2013) C3 plants enhance rates of photosynthesis by reassimilating photorespired and respired CO_2. Plant Cell Environ **36**: 200–212

Bykova NV, Stensballe A, Egsgaard H, Jensen ON, Møller IM (2003) Phosphorylation of formate dehydrogenase in potato tuber mitochondria. J Biol Chem **278**: 26021–26030

Cascales-Miñana B, Muñoz-Bertomeu J, Flores-Tornero M, Anoman AD, Pertusa J, Alaiz M, Osorio S, Fernie AR, Segura J, Ros R (2013) The phosphorylated pathway of serine biosynthesis is essential both for male gametophyte and embryo development and for root growth in Arabidopsis. Plant Cell **25**: 2084–2101

Choi DS, Kim NH, Hwang BK (2014) Pepper mitochondrial formate dehydrogenase 1 regulates cell death and defense responses against bacterial pathogens. Plant Physiol **166**: 1298–1311

Christensen KE, MacKenzie RE (2006) Mitochondrial one-carbon metabolism is adapted to the specific needs of yeast, plants and mammals. Bioessays **28**: 595–605

Christensen KE, Mirza IA, Berghuis AM, MacKenzie RE (2005) Magnesium and phosphate ions enable NAD binding to methylenetetrahydrofolate dehydrogenase-methenyltetrahydrofolate cyclohydrolase. J Biol Chem **280**: 34316–34323

Clough SJ, Bent AF (1998) Floral dip: a simplified method for Agrobacterium-mediated transformation of *Arabidopsis thaliana*. Plant J **16**: 735–743

Colas des Francs-Small C, Ambard-Bretteville F, Small ID, Remy R (1993) Identification of a major soluble protein in mitochondria from nonphotosynthetic tissues as NAD-dependent formate dehydrogenase. Plant Physiol **102**: 1171–1177

Collakova E, Goyer A, Naponelli V, Krassovskaya I, Gregory JF, Hanson AD, Shachar-Hilla Y (2008) Arabidopsis 10-formyl tetrahydrofolate deformylases are essential for photorespiration. Plant Cell **20**: 1818–1832

Cybulski RL, Fisher RR (1981) Uptake of oxidized folates by rat liver mitochondria. Biochim Biophys Acta **646**: 329–333

Czechowski T, Stitt M, Altmann T, Udvardi MK, Scheible W-R (2005) Genome-wide identification and testing of superior reference genes for transcript normalization in Arabidopsis. Plant Physiol **139**: 5–17

Douce R, Bourguignon J, Neuburger M, Rébeillé F (2001) The glycine decarboxylase system: a fascinating complex. Trends Plant Sci **6**: 167–176

Ducker GS, Chen L, Morscher RJ, Ghergurovich JM, Esposito M, Teng X, Kang Y, Rabinowitz JD (2016) Reversal of cytosolic one-carbon flux compensates for loss of the mitochondrial folate pathway. Cell Metab **23**: 1140–1153

Ducker GS, Rabinowitz JD (2017) One-carbon metabolism in health and disease. Cell Metab **25**: 27–42

Eisenhut M, Roell M-S, Weber APM (2019) Mechanistic understanding of photorespiration paves the way to a new green revolution. New Phytol **223**: 1762–1769

Engel N, Ewald R, Gupta KJ, Zrenner R, Hagemann M, Bauwe H (2011) The presequence of Arabidopsis serine hydroxymethyltransferase SHM2 selectively prevents import into mesophyll mitochondria. Plant Physiol **157**: 1711–1720

Engel N, Van Den Daele K, Kolukisaoglu Ü, Morgenthal K, Weckwerth W, Pärnik T, Keerberg O, Bauwe H (2007) Deletion of glycine decarboxylase in Arabidopsis is lethal under nonphotorespiratory conditions. Plant Physiol **144**: 1328–1335

Engler C, Youles M, Gruetzner R, Ehnert T-M, Werner S, Jones JDG, Patron NJ, Marillonnet S (2014) A golden gate modular cloning toolbox for plants. ACS Synth Biol **3**: 839–843

Fan J, Ye J, Kamphorst JJ, Shlomi T, Thompson CB, Rabinowitz JD (2014) Quantitative flux analysis reveals folate-dependent NADPH production. Nature **510**: 298–302

Fiehn O, Kopka J, Dörmann P, Altmann T, Trethewey RN, Willmitzer L (2000) Metabolite profiling for plant functional genomics. Nat Biotechnol **18**: 1157–1161

Forner J, Binder S (2007) The red fluorescent protein eqFP611: application in subcellular localization studies in higher plants. BMC Plant Biol **7**: 28–12

Foster J, Kim HU, Nakata PA, Browse J (2012) A previously unknown oxalyl-CoA synthetase is important for oxalate catabolism in Arabidopsis. Plant Cell **24**: 1217–1229

Fuchs P, Rugen N, Carrie C, Elsässer M, Finkemeier I, Giese J, Hildebrandt TM, Kühn K, Maurino VG, Ruberti C, et al (2020) Single organelle function and organization as estimated from Arabidopsis mitochondrial proteomics. Plant J **101**: 420–441

Gardeström P, Wigge B (1988) Influence of photorespiration on ATP/ADP ratios in the chloroplasts, mitochondria, and cytosol, studied by rapid fractionation of barley (*Hordeum vulgare*) protoplasts. Plant Physiol **88**: 69–76

Gauthier PPG, Bligny R, Gout E, Mahé A, Nogués S, Hodges M, Tcherkez GGB (2010) *In folio* isotopic tracing demonstrates that nitrogen assimilation into glutamate is mostly independent from current CO_2 assimilation in illuminated leaves of *Brassica napus*. New Phytol **185**: 988–999

Gibson DG, Young L, Chuang R-Y, Venter JC, Hutchison CA, Smith HO (2009) Enzymatic assembly of DNA molecules up to several hundred kilobases. Nat Methods **6**: 343–345

Gorelova V, De Lepeleire J, Van Daele J, Pluim D, Meï C, Cuypers A, Leroux O, Rébeillé F, Schellens JHM, Blancquaert D, et al (2017) Dihydrofolate reductase/thymidylate synthase fine-tunes the folate status and controls redox homeostasis in plants. Plant Cell **29**: 2831–2853

Grefen C, Donald N, Hashimoto K, Kudla J, Schumacher K, Blatt MR (2010) A ubiquitin-10 promoter-based vector set for fluorescent protein tagging facilitates temporal stability and native protein distribution in transient and stable expression studies. Plant J **64**: 355–365

Groth M, Moissiard G, Wirtz M, Wang H, Garcia-Salinas C, Ramos-Parra PA, Bischof S, Feng S, Cokus SJ, John A, et al (2016) MTHFD1 controls DNA methylation in Arabidopsis. Nat Commun **7**: 11640

Hahn F, Eisenhut M, Mantegazza O, Weber A (2017a) Generation of Targeted Knockout Mutants in Arabidopsis thaliana Using CRISPR/Cas9. BIO-PROTOCOL. doi: 10.21769/BioProtoc.2384

Hahn F, Mantegazza O, Greiner A, Hegemann P, Eisenhut M, Weber APM (2017b) An efficient visual screen for CRISPR/CAS9 activity in *Arabidopsis thaliana*. Front Plant Sci **8**: 39

Hanson AD, Gage DA, Shachar-Hill Y (2000) Plant one-carbon metabolism and its engineering. Trends Plant Sci **5**: 206–213

Hanson AD, Gregory JF (2011) Folate biosynthesis, turnover, and transport in plants. Annu Rev Plant Biol **62**: 105–125

Hanson AD, Roje S (2001) One-carbon metabolism in higher plants. Annu Rev Plant Physiol **52**: 119–137

Hauschild R, Schaewen von A (2003) Differential regulation of glucose-6-phosphate dehydrogenase isoenzyme activities in potato. Plant Physiol **133**: 47–62

Herbig K, Chiang E-P, Lee L-R, Hills J, Shane B, Stover PJ (2002) Cytoplasmic serine hydroxymethyltransferase mediates competition between folate-dependent deoxyribonucleotide and S-adenosylmethionine biosynthesis. J Biol Chem **277**: 38381–38389

Herman PL, Ramberg H, Baack RD, Markwell J, Osterman JC (2002) Formate dehydrogenase in *Arabidopsis thaliana*: overexpression and subcellular localization in leaves. Plant Science **163**: 1137–1145

Hourton-Cabassa C, Ambard-Bretteville F, Moreau F, De Virville JD, Rémy R, Colas Des Francs-Small C (1998) Stress induction of mitochondrial formate dehydrogenase in potato leaves. Plant Physiol **116**: 627–635

Igamberdiev AU, Bykova NV, Kleczkowski LA (1999) Origins and metabolism of formate in higher plants. Plant Physiol Biochem **37**: 503–513

Igamberdiev AU, Gardeström P (2003) Regulation of NAD- and NADP-dependent isocitrate dehydrogenases by reduction levels of pyridine nucleotides in mitochondria and cytosol of pea leaves. Biochimica et Biophysica Acta (BBA) - Bioenergetics **1606**: 117–125

Igamberdiev AU, Kleczkowski LA (2018) The glycerate and phosphorylated pathways of serine synthesis in plants: The branches of plant glycolysis linking carbon and nitrogen metabolism. Front Plant Sci **9**: 318

Inskeep WP, Bloom PR (1985) Extinction coefficients of chlorophyll a and B in n,n-dimethylformamide and 80% acetone. Plant Physiol **77**: 483–485

Koncz C, Schell J (1986) The promoter of TL-DNA gene 5 controls the tissue-specific expression of chimaeric genes carried by a novel type of Agrobacterium binary vector. Mol Gen Genet **204**: 383–396

König A-C, Hartl M, Boersema PJ, Mann M, Finkemeier I (2014) The mitochondrial lysine acetylome of Arabidopsis. Mitochondrion **19**: 252–260

Krause GH, Weis E (1991) Chlorophyll fluorescence and photosynthesis - the basics. Annu Rev Plant Physiol **42**: 313–349

Kuhnert F, Stefanski A, Overbeck N, Drews L, Reichert AS, Stühler K, Weber APM (2020) Rapid single-step affinity purification of HA-tagged plant mitochondria. Plant Physiol **182**: 692–706

Kühn K, Obata T, Feher K, Bock R, Fernie AR, Meyer EH (2015) Complete mitochondrial complex I deficiency induces an up-regulation of respiratory fluxes that is abolished by traces of functional complex I. Plant Physiol **168**: 1537–1549

Laemmli UK (1970) Cleavage of structural proteins during the assembly of the head of bacteriophage T4. Nature **227**: 680–685

Li AM, Ducker GS, Li Y, Seoane JA, Xiao Y, Melemenidis S, Zhou Y, Liu L, Vanharanta S, Graves EE, et al (2020) Metabolic profiling reveals a dependency of human metastatic breast cancer on mitochondrial serine and one-carbon unit metabolism. Mol Cancer Res **18**: 599–611

Li R, Moore M, Bonham-Smith PC, King J (2002) Overexpression of formate dehydrogenase in *Arabidopsis thaliana* resulted in plants tolerant to high concentrations of formate. Journal of Plant Physiology **159**: 1069–1076

Li R, Ziola B, King J (2000) Purification and characterization of formate dehydrogenase from *Arabidopsis thaliana*. Journal of Plant Physiology **157**: 161–167

Lopez-Calcagno PE, Fisk S, Brown KL, Bull SE, South PF, Raines CA (2019) Overexpressing the H-protein of the glycine cleavage system increases biomass yield in glasshouse and field-grown transgenic tobacco plants. Plant Biotechnol J **17**: 141–151

Lou HQ, Gong YL, Fan W, Xu JM, Liu Y, Cao MJ, Wang M-H, Yang JL, Zheng SJ (2016) A formate dehydrogenase confers tolerance to aluminum and low pH. Plant Physiol **171**: 294–305

Mouillon JM, Aubert S, Bourguignon J, Gout E, Douce R, Rébeillé F (1999) Glycine and serine catabolism in non-photosynthetic higher plant cells: Their role in C_1 metabolism. Plant J **20**: 197–205

Møller IM, Igamberdiev AU, Bykova NV, Finkemeier I, Rasmusson AG, Schwarzländer M (2020) Matrix redox physiology governs the regulation of plant mitochondrial metabolism through posttranslational protein modifications. Plant Cell **32**: 573–594

Nunes-Nesi A, Florian A, Howden A, Jahnke K, Timm S, Bauwe H, Sweetlove L, Fernie AR (2014) Is there a metabolic requirement for photorespiratory enzyme activities in heterotrophic tissues? Molecular Plant **7**: 248–251

Olson B (2000) Formate dehydrogenase in *Arabidopsis thaliana*: characterization and possible targeting to the chloroplast. Plant Science **159**: 205–212

Prabhu V, Chatson KB, Abrams GD, King J (1996) ^{13}C nuclear magnetic resonance detection of interactions of serine hydroxymethyltransferase with C_1-tetrahydrofolate synthase and glycine decarboxylase complex activities in Arabidopsis. Plant Physiol **112**: 207–216

Prabhu V, Chatson KB, Lui H, Abrams GD, King J (1998) Effects of sulfanilamide and methotrexate on ^{13}C fluxes through the glycine decarboxylase/serine hydroxymethyltransferase enzyme system in Arabidopsis. Plant Physiol **116**: 137–144

Ranocha P, McNeil SD, Ziemak MJ, Li C, Tarczynski MC, Hanson AD (2001) The S-methylmethionine cycle in angiosperms: ubiquity, antiquity and activity. Plant J **25**: 575–584

Ravanel S, Block MA, Rippert P, Jabrin S, Curien G, Rébeillé F, Douce R (2004) Methionine metabolism in plants: chloroplasts are autonomous for *de novo* methionine synthesis and can import S-adenosylmethionine from the cytosol. J Biol Chem **279**: 22548–22557

Sauter M, Moffatt B, Saechao MC, Hell R, Wirtz M (2013) Methionine salvage and S-adenosylmethionine: essential links between sulfur, ethylene and polyamine biosynthesis. Biochemical Journal **451**: 145–154

Scheibe R, Geissler A, Fickenscher K (1989) Chloroplast glucose-6-phosphate-dehydrogenase - Km shift upon light-modulation and reduction. Archives of Biochemistry and Biophysics **274**: 290–297

Schindelin J, Arganda-Carreras I, Frise E, Kaynig V, Longair M, Pietzsch T, Preibisch S, Rueden C, Saalfeld S, Schmid B, et al (2012) Fiji: an open-source platform for biological-image analysis. Nat Methods **9**: 676–682

Selinski J, Scheibe R (2019) Malate valves: old shuttles with new perspectives. Plant Biol (Stuttg) **21**: 21–30

Shameer S, Ratcliffe RG, Sweetlove LJ (2019) Leaf energy balance requires mitochondrial respiration and export of chloroplast NADPH in the light. Plant Physiol **180**: 1947–1961

Sharkey TD, Weise SE (2016) The glucose 6-phosphate shunt around the Calvin-Benson cycle. J Exp Bot **67**: 4067–4077

Shimizu Y, Inoue A, Tomari Y, Suzuki T, Yokogawa T, Nishikawa K, Ueda T (2001) Cell-free translation reconstituted with purified components. Nat Biotechnol **19**: 751–755

Shiraishi T, Fukusaki EI, Kobayashi A (2000) Formate dehydrogenase in rice plant: growth stimulation effect of formate in rice plant. J Biosci Bioeng **89**: 241–246

Simon P (2003) Q-Gene: Processing quantitative real-time RT-PCR data. Bioinformatics **19**: 1439–1440

Stemler A (1980) Inhibition of photosystem II by formate. Possible evidence for a direct role of bicarbonate in photosynthetic oxygen evolution. Biochim Biophys Acta **593**: 103–112

Tcherkez G, Boex-Fontvieille E, Mahé A, Hodges M (2012) Respiratory carbon fluxes in leaves. Curr Opin Plant Biol **15**: 308–314

Timm S, Florian A, Arrivault S, Stitt M, Fernie AR, Bauwe H (2012) Glycine decarboxylase controls photosynthesis and plant growth. FEBS Lett **586**: 3692–3697

Timm S, Giese J, Engel N, Wittmiß M, Florian A, Fernie AR, Bauwe H (2017) T-protein is present in large excess over the other proteins of the glycine cleavage system in leaves of Arabidopsis. Planta **301**: 1–11

Timm S, Wittmiß M, Gamlien S, Ewald R, Florian A, Frank M, Wirtz M, Hell R, Fernie AR, Bauwe H (2015) Mitochondrial dihydrolipoyl dehydrogenase activity shapes photosynthesis and photorespiration of *Arabidopsis thaliana*. Plant Cell **27**: 1968–1984

Tomaz T, Bagard M, Pracharoenwattana I, Lindén P, Lee CP, Carroll AJ, Ströher E, Smith SM, Gardeström P, Millar AH (2010) Mitochondrial malate dehydrogenase lowers leaf respiration and alters photorespiration and plant growth in Arabidopsis. Plant Physiol **154**: 1143–1157

Van Wilder V, De Brouwer V, Loizeau K, Gambonnet B, Albrieux C, Van Der Straeten D, Lambert WE, Douce R, Block MA, Rébeillé F, et al (2009) C_1 metabolism and chlorophyll synthesis: the Mg-protoporphyrin IX methyltransferase activity is dependent on the folate status. New Phytol **182**: 137–145

Voll LM, Jamai A, Renné P, Voll H, McClung CR, Weber APM (2006) The photorespiratory Arabidopsis *shm1* mutant is deficient in SHM1. Plant Physiol **140**: 59–66

Wigge B, Krömer S, Gardeström P (1993) The redox levels and subcellular distribution of pyridine nucleotides in illuminated barley leaf protoplasts studied by rapid fractionation. Physiol Plant **88**: 10–18

Wingler A, Lea PJ, Leegood RC (1999) Photorespiratory metabolism of glyoxylate and formate in glycine-accumulating mutants of barley and *Amaranthus edulis*. Planta **207**: 518–526

Wittmiß M, Mikkat S, Hagemann M, Bauwe H (2020) Stoichiometry of two plant glycine decarboxylase complexes and comparison with a cyanobacterial glycine cleavage system. Plant J **103**: 801–813

Wulfert S, Krueger S (2018) Phosphoserine aminotransferase1 is part of the phosphorylated pathways for serine biosynthesis and essential for light and sugar-dependent growth promotion. Front Plant Sci **871**: 1712

Yang L, Garcia Canaveras JC, Chen Z, Wang L, Liang L, Jang C, Mayr JA, Zhang Z, Ghergurovich JM, Zhan L, et al (2020) Serine catabolism feeds NADH when respiration is impaired. Cell Metab **31**: 809–821.e6

Zhang Y, Sun K, Sandoval FJ, Santiago K, Roje S (2010) One-carbon metabolism in plants: characterization of a plastid serine hydroxymethyltransferase. Biochem J **430**: 97–105

Zheng Y, Lin T-Y, Lee G, Paddock MN, Momb J, Cheng Z, Li Q, Fei DL, Stein BD, Ramsamooj S, et al (2018) Mitochondrial one-carbon pathway supports cytosolic ffolate integrity in cancer cells. Cell **175**: 1546–1560.e17

Zrenner R, Stitt M, Sonnewald U, Boldt R (2006) Pyrimidine and purine biosynthesis and degradation in plants. Annu Rev Plant Biol **57**: 805–836

Supplemental Information

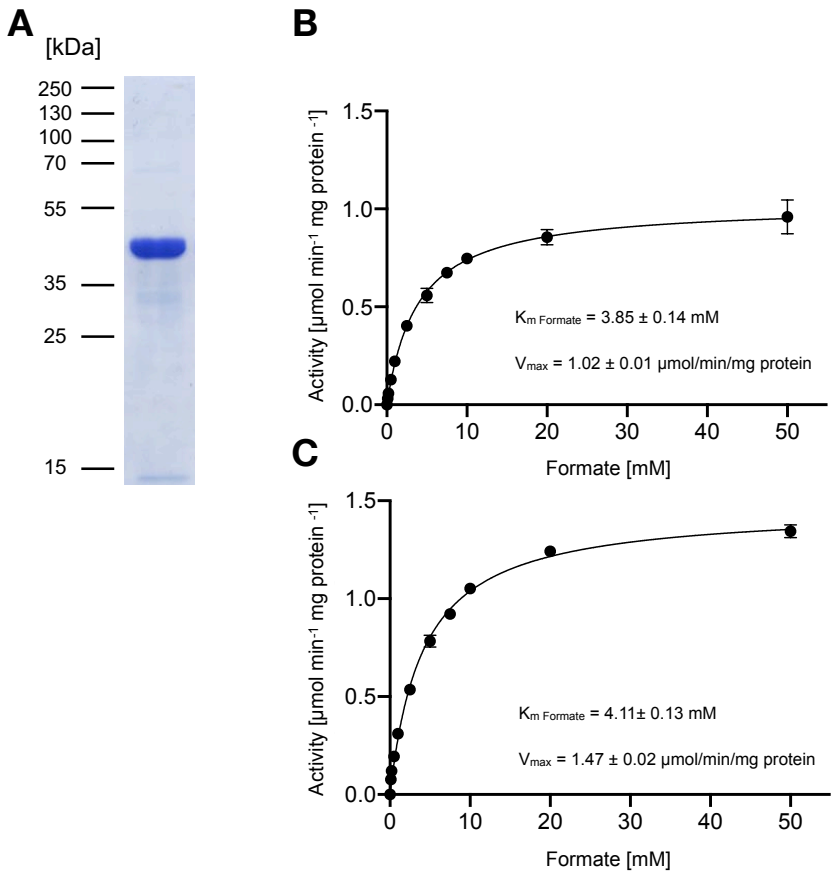

Supplemental Fig. S1: Michaelis-Menten kinetics of recombinant FDH1 protein. A) SDS-PAGE and coomassie staining of purified recombinant *6x*His-tagged FDH1 protein. B and C) Michaelis-Menten kinetics were determined using recombinant purified protein B) recombinant FDH1, C) recombinant FDH1$^{\Delta 1\text{-}30}$. $Km_{Formate}$ and V_{max} were calculated based on fitting the measured activities with the Michaelis-Menten equation. $n \geq 4$.

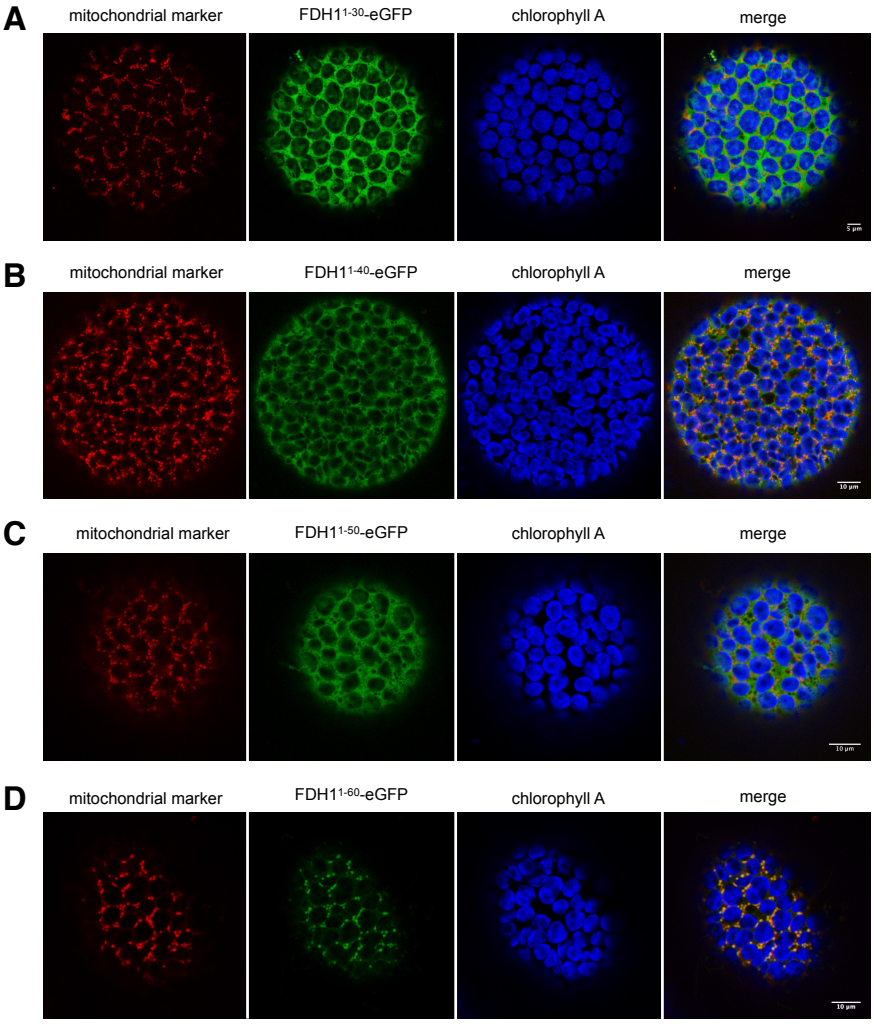

Supplemental Fig. S2: Localization of Arabidopsis formate dehydrogenase 1 N-termini. Four different N-terminal length of *Arabidopsis* formate dehydrogenase 1 (FDH1): A) FDH1$^{1\text{-}30}$, B) FDH1$^{1\text{-}40}$, C) FDH1$^{1\text{-}50}$, D) FDH1$^{1\text{-}60}$ were used and C-terminally fused with enhanced green fluorescent protein (eGFP). Fusion proteins were expressed under the *UBQ10* promoter. Protoplasts from *N. benthamiana* leaves were isolated two days post infection and imaged by confocal laser scanning microscopy. Red = mitochondrial marker (Forner and Binder, 2007). Blue = chlorophyll A autofluorescence.

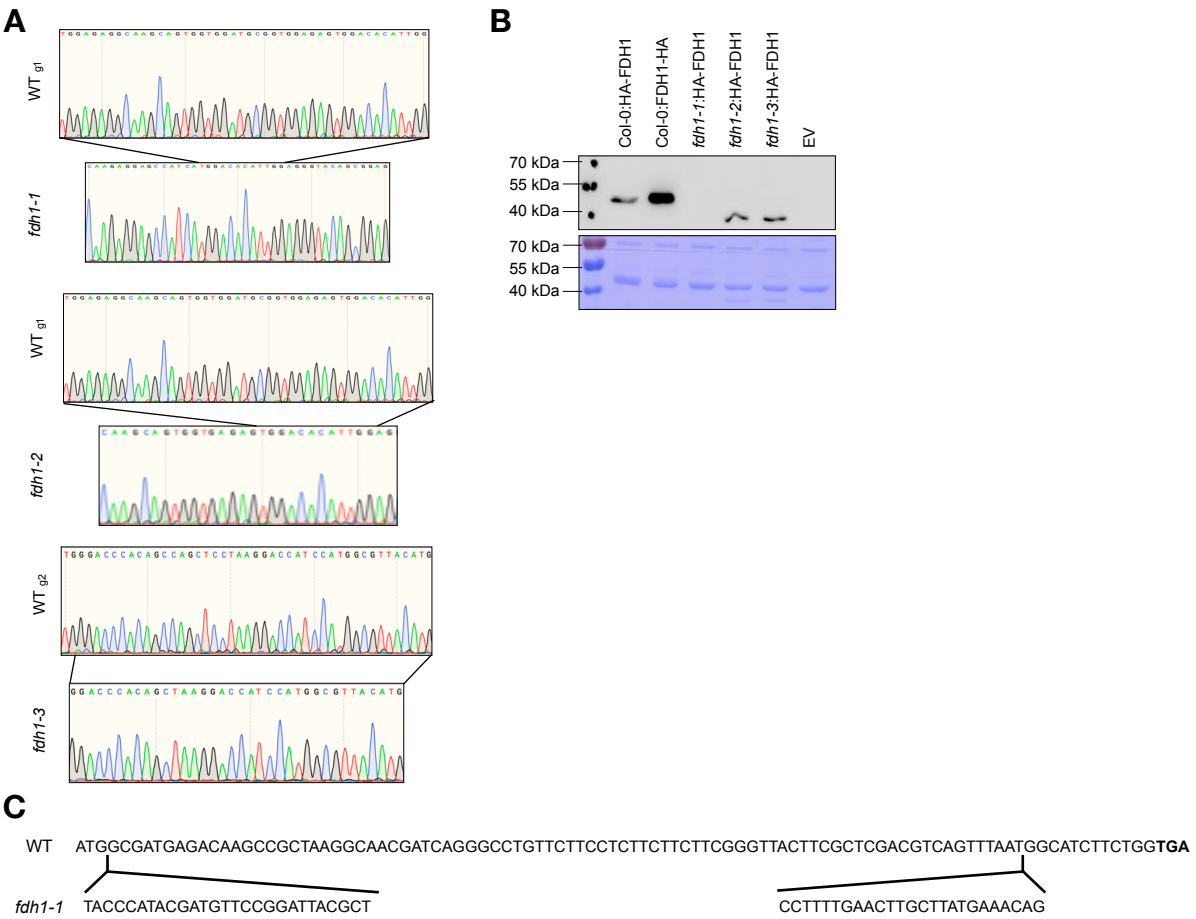

Supplemental Fig. S3: Verification of *fdh1* mutants. A) *FDH1* genomic locus was amplified by PCR and sequenced. Chromatograms of respective wild type (WT) sequence for the position of guide RNA 1 and 2 (g1 & g2) is shown. Chromatograms of sequencing results for each *fdh1* mutant is shown below the wild type. B) Immunoblot of *E. coli* cell-free produced FDH1 protein used for FDH activity measurements (Figure 3D). 20 µg of total protein was loaded per lane and protein was detected using HA-HRP single step antibody. C) Detected missplicing of the primary *FDH1* transcript in the *fdh1-1* mutant. Early stop codon is highlighted in bold.

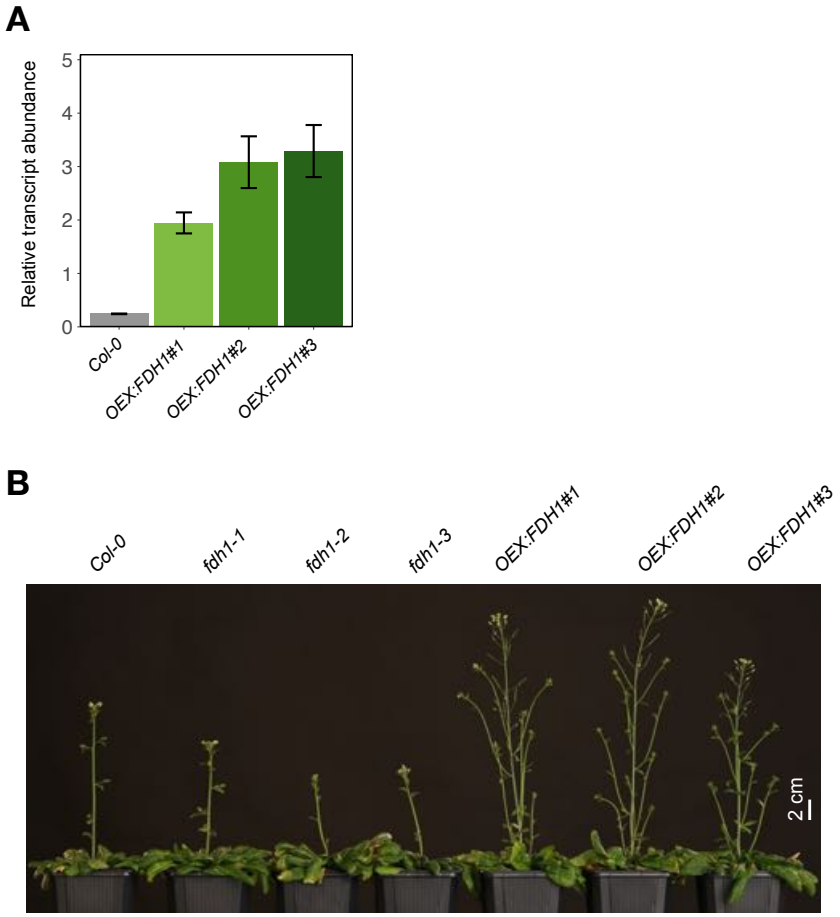

Supplemental Fig. S4: *FDH1* transcript abundance in overexpression lines and phenotype of six weeks old plants. A) *FDH1* transcript abundance in mature rosette leaves of four weeks old plants. Shown are mean ± SEM of four biological replicates measured in technical triplicates. B) Phenotype of plants six weeks after transfer to light, grown at ambient CO_2.

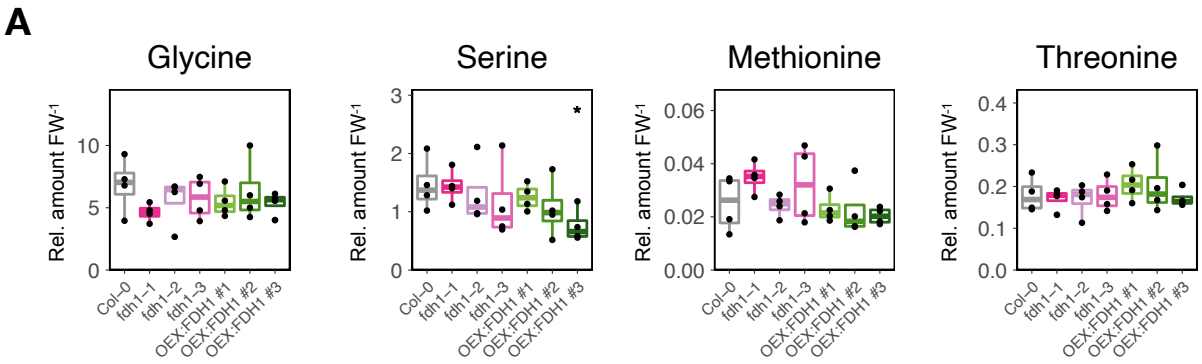

Supplemental Fig. S5: Steady state metabolite levels. A) Soluble metabolites in green tissue of 14 days old seedlings grown under ambient CO_2 were analyzed. Samples were taken midday. n = 4. Students *t*-test against wild type *Col-0*. p > 0.05 = *,> 0.01 = **, > 0.001 = ***.

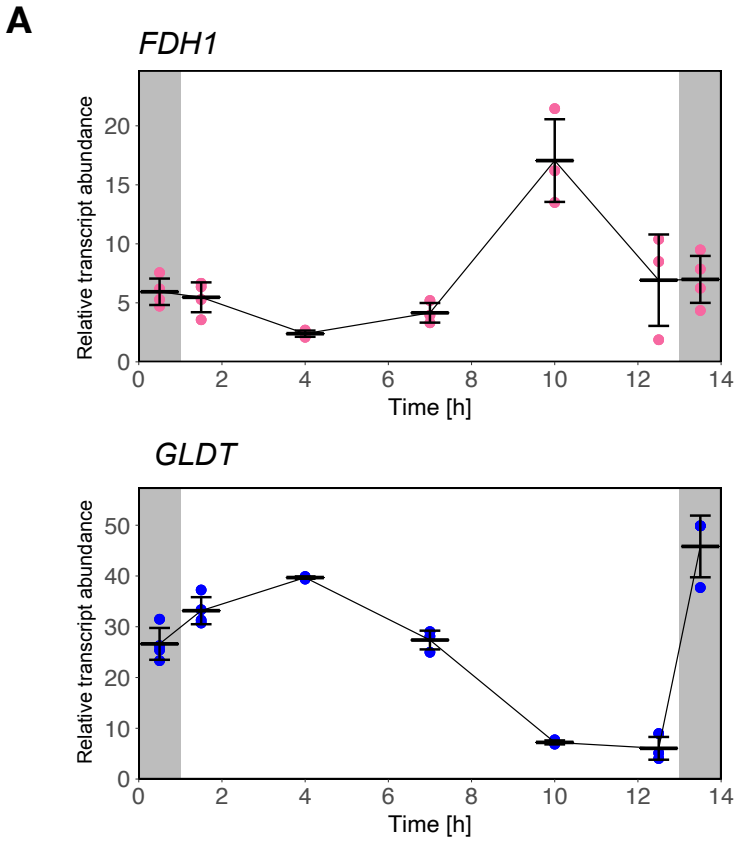

Supplemental Fig. S6: *FDH1* and *GLDT* transcript levels during a light period. A) Normalized transcript level during a light period of formate dehydrogenase 1 (*FDH1*) and glycine decarboxylase T-protein (*GLDT*). Green tissue of 14 days old seedlings was harvested per time point. Night periods are indicated in grey. Transcript abundance was normalized against *PP2A* (Czechowski et al., 2005). Shown is mean of three technical replicates per biological replicate (dots). Shown mean ± SD, n = 4 per timepoint. Line connects the mean.

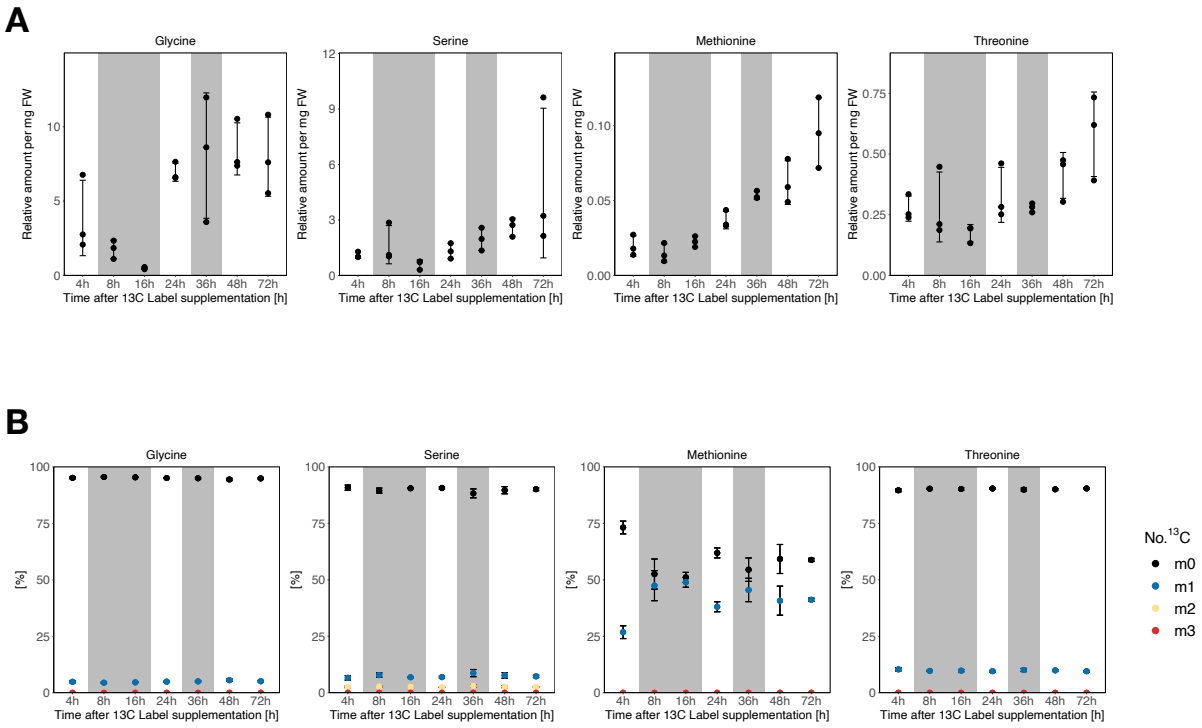

Supplemental Fig. S7: Time-dependent formate-^{13}C pulse-chase labeling. For stable isotope labeling experiments with formate-^{13}C, seedlings were grown on agar plates for eight days and afterwards transferred to new agar plates supplemented with 1 mM sodium formate-^{13}C. Samples were taken over three consecutive days. Night periods are indicated in grey. A) Relative metabolite levels of soluble glycine, serine, methionine, threonine pools. Metabolite pools were quantified as sum of all isotopomers. n = 3. Each biological replicate shown as point. Error bar = SD. B) Percentual ^{13}C label abundance in the soluble metabolite pools of glycine, serine methionine and threonine. ^{13}C label was corrected for natural isotope abundance of the detected fragment. n = 3. Shown: mean ± SD.

Supplemental Table S1: List of primer used in this study. Gene specific nucleotides indicated in caps. Abbreviations: hemagglutinin A (HA), coding sequence (CDS), *formate dehydrogenase 1* (*FDH1*, At5g14780, g*lycine decarboxylase T-protein* (*GLDT*, At1g11860), *Arabidopsis Protein Phosphatase 2A Subunit A3* (*PP2A*, AT1G13320). Superscripted numbers indicated base pairs.

Primer sequence	Purpose	Reference
fwd: 5'-actttaagaaggagatatacatgcatcaccatcaccaccacGCGATGAGACAAGCCGCTAAG-3' rev: 5'-tcgggctttgttagcagccgTTACCGGTACTGAGGAGCAAG-3'	*FDH1* CDS in pET-16b N-term 6xHis	This Study
fwd: 5'-actttaagaaggagatatacatgcatcaccatcaccaccacTCTTCTGGTGATAGCAAAAAG-3' rev: 5'-tcgggctttgttagcagccgTTACCGGTACTGAGGAGC-3'	FDH1$^{\Delta 1\text{-}90}$ CDS in pET-16b N-term 6xHis	This Study
fwd: 5'-actttaagaaggagatatacATGGCGATGAGACAAGCC-3' rev: 5'- tcgggctttgttagcagccgttaagcgtaatccggaacatcgtatgggtaCCGGTACTGAGGAGCAAG-3'	*FDH1* CDS in pET-16b with C-term HA-tag	This Study
fwd: 5'- actttaagaaggagatatacatgtacccatacgatgttccggattacgctGCGATGAGACAAGCCGCTAAG-3' rev: 5'-tcgggctttgttagcagccgTTACCGGTACTGAGGAGCAAG-3'	*FDH1* CDS in pET-16b with N-term HA-tag	This Study
fwd: 5'-GCCAACGAATACGCTACC-3' rev: 5'-CGATGTAATTCTCAGTAGGGAAG-3'	Sequencing primer *fdh1* CRISPR/Cas9 mutants	This Study
fwd: 5'-CATGCCTAACCAGGCTATG-3' rev: 5'-CTCTCCAACATGTCTTTCGTC-3'	qRT-PCR *FDH1*	This Study
fwd: 5'- GGATATGTGAAGTCAGGTCAGCAC-3' rev: 5'- GGTTTGTAGTATTTGGTGGCCACG-3'	qRT-PCR *GLDT*	This Study
fwd: 5'-TAACGTGGCCAAAATGATGC-3' rev: 5'-GTTCTCCACAACCGCTTGGT-3'	qRT-PCR *PP2A*	(Czechowski et al., 2005)
fwd: 5'- GAGGCAAGCAGTGGTGGATG-3'	Sequence gRNA1	This Study
fwd: 5'- CCTTAGGAGCTGGCTGTGGG-3'	Sequence gRNA2	This Study

Supplemental Table S2: List of constructs used in this study. Abbreviations: hemagglutinin A (HA), coding sequence (CDS), *Arabidopsis formate dehydrogenase 1* (*FDH1*, At5g14780). Superscripted numbers indicated base pairs.

Purpose	**Vector**	**Insert**	**Comment**	**Reference**
Heterologous expression of FDH1 in *E. coli*	*pET-16b*	*FDH1* CDS	N-term 6xHis	
		FDH1$^{\Delta 1\text{-}90}$ CDS	N-term 6xHis	
Cell-free expression of FDH1	pET-16b	*FDH1* CDS	N-term HA	
		FDH1 CDS	C-term HA	
		FDH1 CDS *fdh1-1*	N-term HA	
		FDH1 CDS *fdh1-2*	N-term HA	
		FDH1 CDS *fdh1-3*	N-term HA	
Localization of FDH1	*pICH86966*	FDH1 CDS	C-term mCherry	*Vector from* (Engler et al., 2014)
		FDH1$^{1\text{-}90}$ CDS	C-term eGFP	
		FDH1$^{1\text{-}120}$ CDS	C-term eGFP	
		FDH1$^{1\text{-}150}$ CDS	C-term eGFP	
		FDH1$^{1\text{-}180}$ CDS	C-term eGFP	
Generation of *fdh1* mutants by CRISPR/Cas9	pUB-Cas9	gRNA1 $_{FDH1}$ + gRNA2 $_{FDH1}$		*Vector from* (Hahn et al., 2017b)

Supplemental Table S3: Masses and natural abundance used for GC-MS QTOF based ^{13}C label quantification.

Metabolite	Molecular mass [g mol^{-1}]	^{13}C-label	Formula	Natural abundance [%]
Glycine	174.113	0	$C_7H_{20}NSi_2$	
	175.115	1		18.32
Serine	204.124	0	$C_8H_{22}NOSi_2$	
	205.125	1		9.46
	206.122	2		8.50
Methionine	176.092	0	$C_7H_{18}NSSi$	
	177.094	1		14.01
Threonine	219.111	0	$C_8H_{21}NO_2Si_2$	
	220.112	1		19.4958

Journal version of published articles

Mechanistic understanding of photorespiration paves the way to a new green revolution

New Phytologist

Review

Tansley insight

Mechanistic understanding of photorespiration paves the way to a new green revolution

Author for correspondence:
Andreas P. M. Weber
Tel: +49 211 8112347
Email: andreas.weber@hhu.de

Received: *13 February 2019*
Accepted: *11 April 2019*

Marion Eisenhut, Marc-Sven Roell and Andreas P. M. Weber

Institute of Plant Biochemistry, Cluster of Excellence on Plant Science (CEPLAS), Heinrich Heine University, Universitätsstrasse 1, Düsseldorf 40225, Germany

Contents

New Phytologist (2019)
doi: 10.1111/nph.15872

Key words: C_1 metabolism, CO_2 assimilation, crop yield, metabolic interdependency, oxygenation, photosynthetic efficiency, RubisCO, synthetic bypass.

Summary

Photorespiration is frequently considered a wasteful and inefficient process. However, mutant analysis demonstrated that photorespiration is essential for recycling of 2-phosphoglycolate in C_3 and C_4 land plants, in algae, and even in cyanobacteria operating carboxysome-based carbon (C) concentrating mechanisms. Photorespiration links photosynthetic C assimilation with other metabolic processes, such as nitrogen and sulfur assimilation, as well as C_1 metabolism, and it may contribute to balancing the redox poise between chloroplasts, peroxisomes, mitochondria and cytoplasm. The high degree of metabolic interdependencies and the pleiotropic phenotypes of photorespiratory mutants impedes the distinction between core and accessory functions. Newly developed synthetic bypasses of photorespiration, beyond holding potential for significant yield increases in C_3 crops, will enable us to differentiate between essential and accessory functions of photorespiration.

I. Introduction

Photorespiration designates an essential metabolic pathway that occurs in all organisms that perform oxygenic photosynthesis. Photorespiration recycles 2-phosphoglycolate (2PG), a dead-end metabolite that inhibits enzymes needed for CO_2 assimilation, into the Calvin–Benson cycle (CBC) intermediate 3-phosphoglycerate (3PGA). 2PG is formed because ribulose 1,5-bisphosphate carboxylase/oxygenase (RubisCO) cannot fully discriminate between CO_2 and O_2, and thus catalyzes not only the carboxylation of its substrate, ribulose 1,5-bisphosphate (RuBP), but also its oxygenation. The ratio of carboxylation and oxygenation reactions depends on the kinetic properties of the enzyme, temperature and the $CO_2 : O_2$ ratio at the site of Rubisco. During glycine decarboxylation in mitochondria, previously assimilated carbon (C) and nitrogen (N) is lost as CO_2 and NH_3. ATP and NAD(P)H are consumed in the process. Photorespiration constrains the rate of CO_2 assimilation because Rubisco is partially occupied with unproductive oxygenation reactions and part of the CBC flux is wasted to produce RuBP for the counterproductive oxygenation reactions (reviewed in Hagemann & Bauwe, 2016). Photorespiration hence reduces the CO_2 assimilation efficiency and biomass production. In C_3-type land plants, losses due to photorespiration can be in the range of 30–50%. For the US corn belt alone, this means an estimated minus of *c.* 322 trillion calories per year (Walker *et al.*, 2016).

New Phytologist

II. The core photorespiratory pathway and its metabolic interdependency

Plant core photorespiratory metabolism

Photorespiration means 'respiration in light' and describes the observation that plants consume O_2 and release CO_2 in the light. The core reactions of photorespiratory metabolism comprise nine enzymatic reactions distributed over the three compartments chloroplast, peroxisome and mitochondrion (Fig. 1a; Table 1; Bauwe *et al.*, 2010). The initial pathway metabolite is 2PG, which results from the oxygenase activity of Rubisco. 2PG is dephosphorylated by phosphoglycolate phosphatase (PGLP) in the chloroplast. The resulting glycolate is exported by the plastid glycolate/glycerate transporter1 (PLGG1; Pick *et al.*, 2013) and the bile acid sodium symporter6 (BASS6; South *et al.*, 2017), and then imported into the peroxisome by an unknown transport or channel protein. Glycolate is oxidized to glyoxylate by glycolate oxidase (GOX). In this step O_2 serves as electron acceptor and H_2O_2 is formed, which is decomposed by catalase (CAT). Glyoxylate is then transaminated into glycine by the action of glutamate: glyoxylate aminotransferase (GGAT). Glycine is exported from peroxisomes and taken up into mitochondria by unknown transporters. In the mitochondria, glycine is converted into serine, CO_2 and NH_3 by the joint activities of the multienzyme system glycine decarboxylase (GDC) and serine hydroxymethyl transferase (SHMT; reviewed in Bauwe & Kolukisaoglu, 2003). Serine is shuttled back into the peroxisome for deamination by serine: glyoxylate aminotransferase (SGAT) to generate hydroxypyruvate. This metabolite is reduced by hydroxypyruvate reductase1 (HPR1) into glycerate. Glycerate is taken up by PLGG1 into the chloroplast for phosphorylation, which is catalyzed by glycerate kinase (GLYK). The final metabolite of the photorespiratory pathway is 3PGA, which can enter the CBC.

Photorespiratory metabolism is essential for all organisms performing oxygenic photosynthesis, including cyanobacteria, algae, mosses and vascular plants, as evidenced by the observation that deletion of involved enzymes results in a photorespiratory phenotype (Fig. 1b). That is, mutants can grow only under elevated CO_2 concentrations. Current ambient CO_2 concentrations (0.041%) impair growth and some mutants are even lethal in ambient air. This also holds for photosynthetic organisms that employ a C-concentrating mechanism, such as cyanobacteria (Eisenhut *et al.*, 2008) and C_4 plants (Levey *et al.*, 2019). It is likely that photorespiratory metabolism co-evolved with oxygenic photosynthesis in cyanobacteria as an essential consequence to thrive in an O_2-containing atmosphere (Eisenhut *et al.*, 2008) In addition to detoxification of 2PG, which acts as an inhibitor of CBC enzymes, multiple functions of photorespiratory metabolism have been proposed: protection from photoinhibition by dissipation of excess energy; biosynthesis of amino acids glycine and serine; and source of activated one-carbon (C_1) units (Bauwe *et al.*, 2010).

The photorespiratory core enzymes and corresponding genes (Fig. 1a; Table 1) have been identified during the past four decades mostly using *Arabidopsis thaliana* (*A. thaliana*) as model organism (reviewed in Bauwe *et al.*, 2010). Importantly, photorespiratory metabolism is not a closed metabolic cycle, but interacts with N assimilation (Bloom, 2015), respiration and the TCA cycle (reviewed in Obata *et al.*, 2016), C_1 metabolism (Hodges *et al.*, 2016) and sulfur (S) metabolism (Samuilov *et al.*, 2018). In the following, we describe steps/reactions demonstrating metabolic interdependencies with the core photorespiratory pathway in *A. thaliana*. The genes assigned to these are specified in Fig. 1a and Table 1.

Photorespiration and N metabolism

Glycine decarboxylation by the mitochondrial multi-subunit enzyme system GDC releases NH_3 and CO_2. NH_3 must be re-assimilated utilizing ATP- and reducing power consumption by glutamine synthetase (GS2) and the ferredoxin-dependent glutamine:oxoglutarate aminotransferase (Fd-GOGAT; Coschigano *et al.*, 1998) in chloroplasts. Two chloroplastic transport proteins are essential for photorespiratory N metabolism. The 2-oxoglutarate/malate transporter Dit1 imports the C backbone required for glutamate production (Kinoshita *et al.*, 2011). Produced glutamate is exported from the chloroplast by the glutamate/malate transporter Dit2.1 (Renné *et al.*, 2003). Glutamate is required for the peroxisomal conversion of glyoxylate to glycine by GGAT1. Alternatively, alanine might serve as amino group donors for the GGAT1-mediated transamination reaction (Liepman & Olsen, 2003; Dellero *et al.*, 2015). The conditional lethal phenotype of the *sgat1* knockout mutants indicates its predominant role in maintaining photorespiratory flux by glyoxylate transamination and hydroxypyruvate production. (Liepman & Olsen, 2001).

Photorespiration, respiration and the TCA cycle

Photorespiration represents the highest metabolic flux during photosynthesis in mitochondria. Rapid fractionation of barley protoplasts under photorespiratory or nonphotorespiratory conditions demonstrated that the NADH produced in the GDC reaction is oxidized by the respiratory chain, leading to increased cytosolic ATP/ADP and higher mitochondrial NADH : NAD ratio under photorespiratory conditions (Gardeström & Wigge, 1988; Wigge *et al.*, 1993). Uncoupling protein 1 (UCP1) supports photorespiratory flux by modulating the mitochondrial redox status (Sweetlove *et al.*, 2006). Recently, UCP1 and UCP2 were biochemically characterized as metabolite carriers for aspartate, glutamate and dicarboxylates, and proposed to function in exporting reducing power by supplying the mitochondrial and cytosolic glutamate:oxaloacetate transaminase reactions with their respective substrates (see Monné *et al.*, 2018, for details).

Photorespiration and C_1 metabolism

Mutant analyses emphasized the importance of photorespiration in C_1 metabolism. C_1 metabolism is essential for the synthesis of nucleic acids, proteins, pantothenate and methylated molecules,

New Phytologist

Tansley insight Review 3

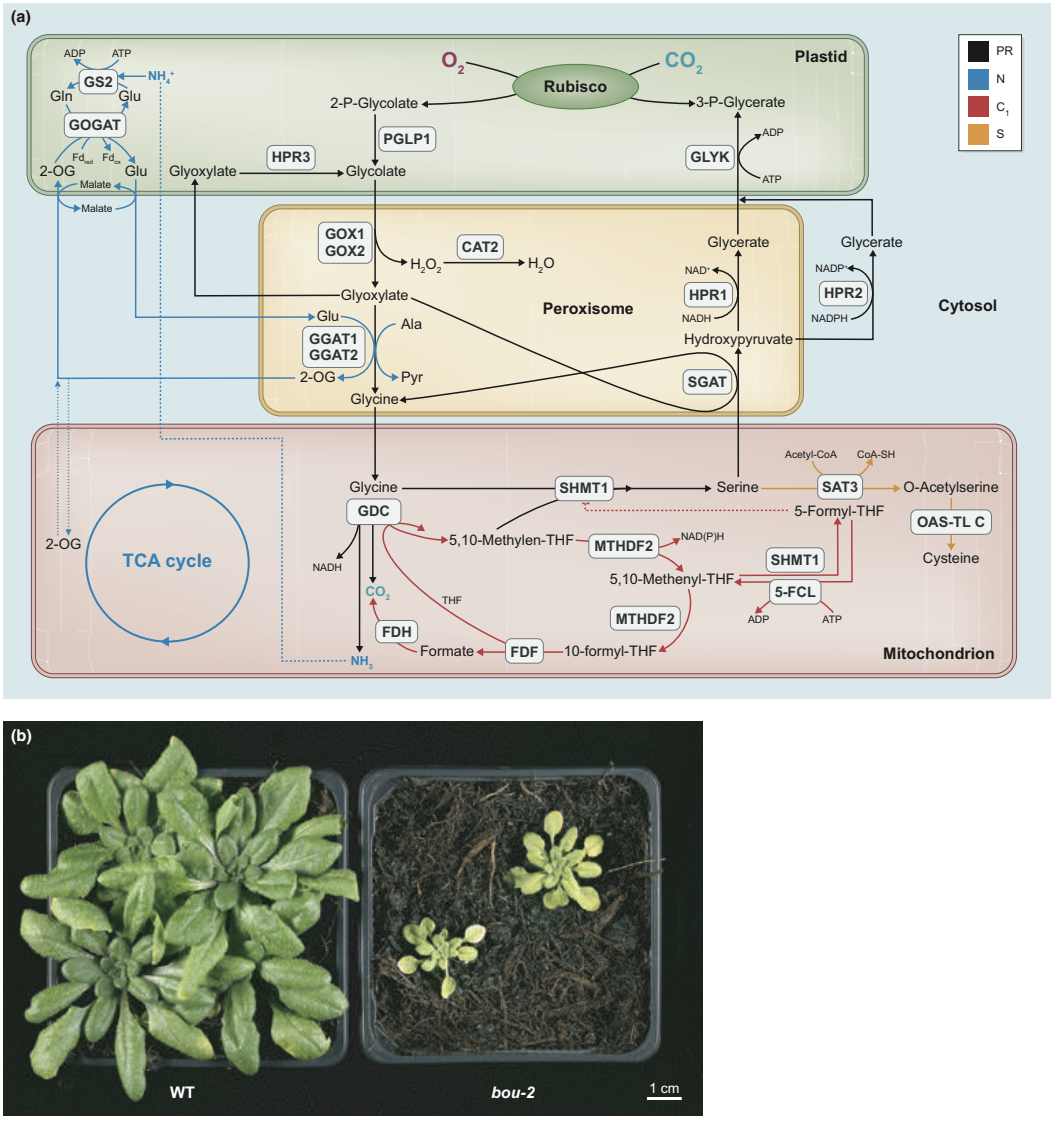

Fig. 1 Photorespiratory metabolism in *Arabidopsis thaliana*. (a) Interdependency of photorespiration with nitrogen, C_1 and sulfur metabolism. (b) Photorespiratory phenotype of the *bou-2* mutant. The plants, *A. thaliana* wild-type (WT) and *bou-2*, were grown under elevated CO_2 conditions (0.3% CO_2) for 3 weeks and then shifted for 12 d to ambient CO_2 conditions (0.03% CO_2) before the picture was taken. Abbreviations: PGLP1, phosphoglycolate phosphatase 1; GOX1, glycolate oxidase 1; GOX2, glycolate oxidase 2; CAT2, catalase 2; GGAT1, glutamate:glyoxylate aminotransferase 1; GGAT2, glutamate:glyoxylate aminotransferase 2; GDC, glycine decarboxylase complex; SHMT1, serine hydroxymethyltransferase 1; SGAT, serine:glyoxylate aminotransferase; HPR1, hydroxypyruvate reductase 1; HPR2, hydroxypyruvate reductase 2; HPR3, hydroxypyruvate reductase 3, GLYK, glycerate kinase, GS2, glutamine synthetase 2; GOGAT, glutamine:oxoglutarate aminotransferase; THF, tetrahydrofolate; MTHDF2, bifunctional 5,10-methylene-THF dehydrogenase/5,10-methenyl-THF cyclohydrolase; 5-FCL, 5-formyl-THF cycloligase; FDF, 10-formyl-THF deformylase; FDH, formate dehydrogenase; SAT3, serine *o*-acetyltransferase; OAS-TL C, *o*-acetylserine lyase isoform C.

Table 1 Genes that have been associated with photorespiration in *Arabidopsis thaliana*.

Name	EC	AGI locus	Function	PR phenotype	Reference
Core photorespiratory metabolism					
PGLP1	EC 3.1.3.18	At5g36700	Phosphoglycolate phosphatase 1	Yes	Schwarte & Bauwe (2007)
GOX1	EC 1.1.3.15	At3g14420	Glycolate oxidase 1	Redundancy,	Dellero *et al.* (2016)
GOX2		At3g14415	Glycolate oxidase 2	double k.d. yes	
CAT2	EC 1.11.1.6	At4g35090	Catalase 2	Yes	Queval *et al.* (2007)
GGAT1	EC 2.6.1.4	At1g23310	Glutamate:glyoxylate aminotransferase	Mutant in *GGAT1*: yes	Dellero *et al.* (2015)
GGAT2		At1g70580		*GGAT2*: no mutant report	Igarashi *et al.* (2003)
GDC-P1	EC 1.4.4.2	At4g33010	P protein, glycine decarboxylase	Redundancy,	Engel *et al.* (2007)
GDC-P2		At2g26080		double k.o. lethal	
GDC-T	EC 2.1.2.10	At1g11860	T protein, aminomethyl transferase	Lethal	Timm *et al.* (2018)
GDC-H1		At2g35370	H protein, lipoamide (5[3-(1,2) dithiolanyl]	Redundancy, no	Bauwe & Kolukisaoglu
GDC-H2		At2g35120	pentanoic acid) protein	mutant report	(2003)
GDC-H3		At1g32470			
GDC-L1	EC 1.8.1.4	At3g17240	L protein, dihydrolipoamide dehydrogenase	Redundancy, no	Bauwe & Kolukisaoglu
GDC-L2		At1g48030		mutant report	(2003)
SHMT1	EC 2.1.2.1	At4g37930	Serine hydroxymethyltransferase 1	Yes	Voll *et al.* (2006)
SGAT	EC 2.6.1.45	At2g13360	Serine:glyoxylate aminotransferase	Yes	Liepman & Olsen (2001)
HPR1	EC 1.1.1.29	At1g68010	Hydroxypyruvate reductase 1 (peroxisomal)	Redundancy, double k.o. *hpr1hpr2* yes	Timm *et al.* (2008)
HPR2	EC 1.1.1.81	At1g79870	Hydroxypyruvate reductase 2 (cytosolic)	Redundancy, double k.o. *hpr1hpr2* yes	Timm *et al.* (2008)
GLYK	EC 2.7.1.31	At1g80380	Glycerate kinase	Yes	Boldt *et al.* (2005)
PLGG1		At1g32080	Plastid glycolate glycerate transporter 1	Yes	Pick *et al.* (2013)
BASS6		At4g22840	Bile acid sodium symporter 6, plastid glycolate importer	Yes	South *et al.* (2017)
BOU		At5g46800	A bout de souffle, mitochondrial transporter involved in photorespiratory metabolism (substrate undefined, possibly glutamate)	Yes	Eisenhut *et al.* (2013) Porcelli *et al.* (2018)
Nitrogen metabolism					
GS2	EC 6.1.3.2	At5g35630	Glutamine synthetase 2	No mutant report	
Fd-GOGAT	EC 1.4.7.1	At5g04140	Ferredoxin-dependent glutamine:oxoglutarate aminotransferase	Yes	Coschigano *et al.* (1998)
DiT1		At5g12860	Plastidial dicarboxylate (2-oxoglutarate/malate) transporter	Yes	Kinoshita *et al.* (2011)
DiT2.1		At5g64290	Plastidial dicarboxylate	Yes	Renné *et al.* (2003)
DCT			(2-oxoglutarate/malate) transporter		
Sulfur metabolism					
SAT3	EC 2.3.1.30	At3g13110	Serine o-acetyltransferase (mitochondrial)	Redundancy, no	Watanabe *et al.* (2008)
OAS-TL C	EC 2.5.1.47	At3g59760	O-acetylserine lyase (mitochondrial)	Not tested, retarded growth	Heeg *et al.* (2008)
C_1 metabolism					
MTHDF2	EC 1.5.1.5 EC 3.5.4.9	At2g38660	Bifunctional 5,10-methylene-THF dehydrogenase/5,10-methenyl-THF cyclo-hydrolase	No	Collakova *et al.* (2008)
5-FCL	EC 6.3.3.2	At5g13050	5-formyltetrahydrofolate cycloligase	Weak	Goyer *et al.* (2005)
FDF1	EC 3.5.1.10	At4g17360	10-formyl-THF deformylase	Redundancy,	Collakova *et al.* (2008)
FDF2		At5g47435		double k.o. yes	
PurU					
FDH	EC 1.2.1.2	At5g14780	Formate dehydrogenase	No mutant report	

PR phenotype, photorespiratory phenotype, knock-out mutant shows growth impairment under ambient CO_2 conditions (0.041% in air) that can be alleviated under elevated CO_2 conditions (> 0.3% CO_2 in air); k.o., knockout; k.d., knock-down.

including DNA (Hanson & Roje, 2001). The lethal phenotypes of the *gldp1gldp2* (GDC P-protein), *gldt1* (GDC T-protein) and *shm1shm2* mutants, even under nonphotorespiratory conditions, demonstrate that GDC and SHMT are essential for cellular C_1 metabolism (Engel *et al.*, 2007, 2011; Timm *et al.*, 2018). GDC links the co-factor tetrahydrofolate (THF), *de novo* synthesized in mitochondria, with the produced C_1 unit. However, under photorespiratory conditions THF re-cycling by mitochondrial C_1 metabolism is required to maintain photorespiratory flux via the GDC-SHMT complex. In particular, 10-formyl deformylase (FDF) releases THF and thereby maintains the mitochondrial THF pool (Collakova *et al.*, 2008). A second catalytic activity of SHMT produces the SHMT-inhibitory C_1 compound 5-formyl-THF from 5,10-methenyl-THF in the presence of glycine. This 5-formyl-THF is re-converted into 5,10-methenyl by 5-formyl-THF cycloligase (5-FCL; Goyer *et al.*, 2005). Fluctuating 5-formyl-THF concentrations might regulate the metabolic flux between C_1 metabolism and serine biosynthesis in plant mitochondria. The mitochondrial transporter A bout de souffle (BOU) contributes to GDC activity and is essential under photorespiratory conditions

(Eisenhut *et al.*, 2013). Recent work showed that BOU is a glutamate transporter (Porcelli *et al.*, 2018). Polyglutamylation of THF enhances co-enzyme affinity and THF stability (Mehrshahi *et al.*, 2010). Whether altered co-enzyme affinity or overall reduced THF concentrations in BOU mitochondria cause the photorespiratory phenotype remains to be tested.

Photorespiration and S metabolism

The majority of serine in illuminated leaves of C_3 plants is produced by mitochondrial SHMT1 (Li *et al.*, 2003). Serine is converted into *o*-acetylserine by serine *o*-acyltransferase. *O*-acetylserine is required for cysteine and glutathione metabolism. Indeed, it was shown that the *bou* mutant displays reduced serine concentrations and shows altered transcription in S metabolism associated genes (Samuilov *et al.*, 2018).

III. Synthetic approaches modulating photorespiratory metabolism

Photorespiration decreases the rate of CO_2 fixation and increases the energy costs of photosynthesis. This results in a yield penalty of 20-50% in C_3 plants, depending on environmental conditions (Bauwe *et al.*, 2010). These losses define photorespiratory metabolism as a prime target in biotechnological efforts aiming at increased crop productivity (reviewed in Weber & Bar-Even, 2019). Here, we focus on two different metabolic engineering strategies: eliminating enzymatic bottlenecks and introducing synthetic bypasses.

Flux through a metabolic pathway is controlled by the capacity of the enzymes involved. It was suggested that flux through the photorespiratory pathway in plants is limited by the rate of mitochondrial glycine-to-serine conversion (Hagemann & Bauwe, 2016). Overexpression of different subunits of the GDC system in *A. thaliana* supports this assumption. Increasing the activities of the H (Timm *et al.*, 2012) or L proteins (Timm *et al.*, 2015), respectively, was associated with decreased CO_2 compensation points and enhanced plant performance. The T protein apparently is not a limiting factor because neither down- nor upregulation of its activity affected photosynthetic CO_2 uptake and plant growth (Timm *et al.*, 2018). By contrast to those neutral to beneficial effects, overexpression of peroxisomal SGAT negatively affects plant performance. Elevated SGAT amounts caused reduced photosynthetic CO_2 uptake under ambient air conditions, enhanced serine and asparagine consumption, and thus disturbed the C/N balance, leading to diminished growth (Modde *et al.*, 2017). Obviously, the tight interaction with other metabolic pathways, such as N metabolism, does not allow arbitrary manipulation of every photorespiratory enzyme but requires careful examination and better understanding of regulation and interdependency of these metabolic routes.

Synthetic bypasses to photorespiration aim at avoiding mitochondrial glycine decarboxylation and the release of NH_3 that is associated with this reaction. Instead, current synthetic bypasses metabolize glycolate in the chloroplast stroma and release CO_2 from glycolate metabolization next to Rubisco. The first synthetic bypasses implemented into *A. thaliana* were inspired by the glycolate oxidizing pathway occurring naturally in *E. coli* (Kebeish *et al.*, 2007). Alternatively, photorespiratory enzymes from other compartments were re-targeted to the chloroplasts, thereby shortening the pathway (Maier *et al.*, 2012). In both cases, an increase in biomass was observed under controlled low-light and short-day environmental conditions. Several modifications to these bypasses recently have been engineered into the crop model tobacco and into rice. South and colleagues (South *et al.*, 2019) designed an alternative plastid glycolate oxidizing pathway that requires only two transgenes plus the repression of one transporter activity. Glycolate dehydrogenase from mitochondria of the green alga *Chlamydomonas reinhardtii* and malate synthase from peroxisomes of *Cucurbita maxima* were redirected to chloroplasts of tobacco plants. In these transgenic tobacco lines, 2PG is converted to glycolate by native PGLP. Glycolate is then oxidized to glyoxylate by the glycolate dehydrogenase inside the chloroplast. Catalyzed by malate synthase, the second introduced enzyme, glyoxylate reacts with acetyl-CoA to form malate. The resulting malate is then converted to acetyl-CoA and two molecules of CO_2 by the native chloroplast enzymes malic enzyme and pyruvate dehydrogenase (Fig. 2a). Overall, glycolate is converted into CO_2 while acetyl-CoA for renewed malate biosynthesis is regenerated. Importantly, to restrict export of glycolate from the chloroplast, the plastidial glycolate exporter PLGG1 was silenced. The synthetic bypass led to a biomass increase of 40% in the field, as compared to tobacco wild-type (WT) plants (South *et al.*, 2019).

An alternative full decarboxylation strategy was implemented by Shen and colleagues in rice (Shen *et al.*, 2019). The GOC bypass requires three additional enzymes in the chloroplast stroma: glycolate oxidase, oxalate oxidase and catalase. The native enzymes localize to peroxisomes in rice and hence had to be redirected to the chloroplast. There, they catalyze the complete decarboxylation of glycolate to CO_2. By contrast to the approach by South *et al.* (2019), efflux of glycolate from the chloroplast was not restricted (Fig. 2b). The GOC rice plants outperformed the WT in field trials with respect to biomass yield. The grain yield, however, strongly varied depending on the seeding season (Shen *et al.*, 2019). It is not fully understood why full decarboxylation of glycolate inside chloroplasts is associated with higher yields because computational modelling indicated that such pathways would decrease photosynthetic efficiency (see Box 1 for details).

The actual flux distribution between native photorespiration and the various synthetic bypasses remains elusive. However, even a reduced metabolic flux through endogenous photorespiration in the presence of a bypass is apparently sufficient to meet the metabolic demands in associated processes, such as C_1-, N and S metabolism. Advanced engineering strategies that fully replace endogenous photorespiration with synthetic pathways will be required to resolve whether photorespiration fulfils other essential functions beyond the recycling 2PG.

IV. Conclusions and future perspectives

The enzymes catalyzing the core reactions of photorespiration have been identified. However, most of the involved transporters and

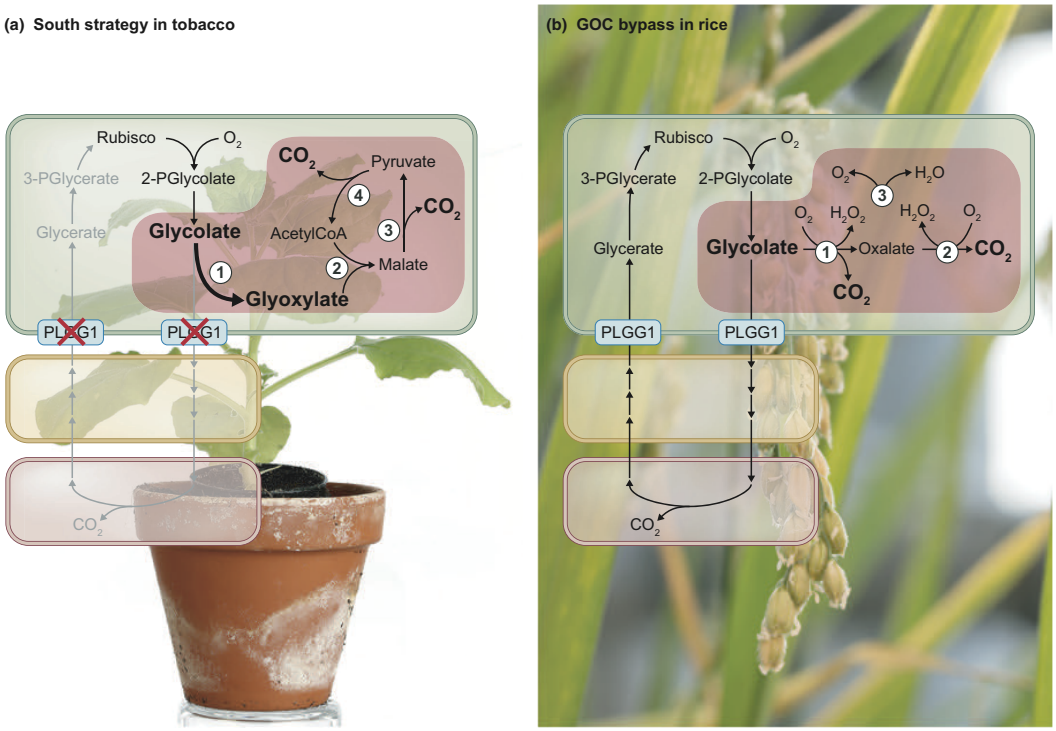

Fig. 2 Synthetic bypasses for alternative glycolate oxidation in crop plants. Engineered glycolate oxidation inside the chloroplast (red) releases CO_2, consequently promoting the carboxylation reaction of Rubisco and enhancing crop yield. (a) The South strategy employs glycolate dehydrogenase from *Chlamydomonas reinhardtii* (1), malate synthase from *Cucurbita maxima* (2), and endogenous malic enzyme (3) and pyruvate dehydrogenase (4) for glycolate oxidation with release of CO_2 inside the chloroplast. Knock-down (red crosses) of the plastidial glycolate/glycerate transporter 1 (PLGG1) reduces the export of glycolate from the chloroplast and thus enhances glycolate consumption by the alternative bypass. This bypass was tested in tobacco plants (South *et al.*, 2019). (b) The GOC bypass utilizes the activities of glycolate oxidase (1), oxalate oxidase (2) and catalase (3) for the consecutive decarboxylation of glycolate with production of CO_2. The GOC bypass was tested in rice plants (Shen *et al.*, 2019).

channels, respectively, from peroxisomes (glycine, serine, glycerate, glycolate) and mitochondria (glycine, serine) are still unknown. The difficulties in identifying the still missing shuttle proteins might be due to genetic redundancy or to an essential role of these proteins in other cellular functions, which would lead to lethality in corresponding mutants. The generation of higher order mutants will likely be required to identify the missing transport and channel proteins involved in photorespiration. Also, a clear demarcation of core photorespiratory metabolism from other metabolic pathways remains a challenge.

Another less understood aspect of photorespiration is the mechanisms that distinguish dynamic, short- and long-term regulation of photorespiration. Transcriptional regulation and redox-regulation via thioredoxins is believed to play a crucial role in adapting photorespiration to fluctuating environmental conditions. Post-translational modification via S-nitrosylation, amino acid oxidation and phosphorylation likely play roles in regulating photorespiratory core enzymes (reviewed in Hodges *et al.*, 2016, and references therein). Obviously, transcriptional, post-transcriptional and post-translational regulation of photorespiration will be important focii of future research.

Newly established synthetic approaches that shortcut photorespiratory metabolism have produced intriguing yield increases. However, the discrepancies between theoretical expectations and results observed in crops expressing glycolate-decarboxylating bypasses remain to be resolved. These and more advanced synthetic approaches hold the potential to spur a new green revolution.

Acknowledgements

APMW appreciates funding by the Deutsche Forschungsgemeinschaft (DFG, German Research Foundation) under Germany's Excellence Strategy – EXC-2048/1 – project ID: 390686111, the Federal Ministry of Education and Research, project FormatPlant (FKZ: 031B0194), and the EU H2020 project CropBooster-P (grant agreement 817690).

Box 1 Synthetic bypasses to photorespiration – predictions and reality

Several alternative synthetic bypasses to photorespiration have been designed and some of these have been implemented in the model plant *Arabidopsis thaliana*, as well as in crops such as potato, camelina, tobacco (reviewed in: Weber & Bar-Even, 2019; Eisenhut & Weber, 2019) and rice (Shen *et al.*, 2019). In all cases, growth stimulation, and in the case of crops, yield increases, have been reported, in particular for bypasses that fully convert glycolate to CO_2 (Shen *et al.*, 2019; South *et al.*, 2019). However, computational modelling of various bypass designs (*e.g.* Xin *et al.*, 2015) predicted that full decarboxylation of glycolate would perform worse than wild-type (WT) photorespiration. Also, the decreased photocompensation point (Γ*) observed in some of these works is unexpected, given that two molecules of CO_2 are released per oxygenation event in glycolate decarboxylating bypasses, as compared to half a molecule of CO_2 per oxygenation in native photorespiration. The reasons for these unexpected results are unclear. Some clues might come from pleiotropic effects observed in *A. thaliana* and rice lines expressing glycolate decarboxylating pathways. In *A. thaliana* lines expressing a glycolate decarboxylation pathway, leaves were flatter and thinner (leaf thickness was reduced by 20%) and chl as well as other pigments were reduced on a FW basis (Maier *et al.*, 2012). In rice lines expressing the GOC pathway (Fig. 2b), the size of mesophyll cells was increased by 40% and chl size was nearly doubled (Shen *et al.*, 2019). The authors noted that the leaf ultrastructure of the GOC rice lines resembled that of WT plants grown under elevated CO_2 concentrations. This hypothesis was further supported by RNA-Seq analysis (Shen *et al.*, 2019). These findings might indicate that increased metabolization of glycolate in chloroplasts (or reduced export from chloroplasts) affects the regulation of gene expression, which in turn leads to altered growth behaviour and yield. It is possible that reduced production of hydrogen peroxide in peroxisomes or a lower rate of NADH production from glycine in mitochondria exerts a signalling function. In this context, it will be interesting to observe the effects of more advanced bypasses that recycle 2PG to CBC intermediates without releasing CO_2, such as the recently developed glycoly-CoA synthetase-based bypasses (Trudeau *et al.*, 2018), which have not yet been tested in plants. We point the readers to the excellent Supplemental Computational Analysis accompanying this paper, which provides a comprehensive computational analysis of various bypass designs.

Author contributions

ME, MSR, and APMW jointly developed the concept for this Tansley insight and jointly wrote the manuscript.

ORCID

Marion Eisenhut https://orcid.org/0000-0002-2743-8630
Marc-Sven Roell https://orcid.org/0000-0003-2714-8729
Andreas P. M. Weber https://orcid.org/0000-0003-0970-4672

References

Bauwe H, Hagemann M, Fernie AR. 2010. Photorespiration: players, partners and origin. *Trends in Plant Science* **15**: 330–336.

Bauwe H, Kolukisaoglu U. 2003. Genetic manipulation of glycine decarboxylation. *Journal of Experimental Botany* **54**: 1523–1535.

Bloom AJ. 2015. Photorespiration and nitrate assimilation: a major intersection between plant carbon and nitrogen. *Photosynthesis Research* **123**: 117–128.

Boldt R, Edner C, Kolukisaoglu U, Hagemann M, Weckwerth W, Wienkoop S, Morgenthal K, Bauwe H. 2005. D-GLYCERATE 3-KINASE, the last unknown enzyme in the photorespiratory cycle in Arabidopsis, belongs to a novel kinase family. *Plant Cell* **17**: 2413–2420.

Collakova E, Goyer A, Naponelli V, Krassovskaya I, Gregory JF 3rd, Hanson AD, Shachar-Hill Y. 2008. Arabidopsis 10-formyl tetrahydrofolate deformylases are essential for photorespiration. *Plant Cell* **20**: 1818–1832.

Coschigano KT, Melo-Oliveira R, Lim J, Coruzzi GM. 1998. Arabidopsis *gls* mutants and distinct Fd-GOGAT genes. Implications for photorespiration and primary nitrogen assimilation. *Plant Cell* **10**: 741–752.

Dellero Y, Jossier M, Glab N, Oury C, Tcherkez G, Hodges M. 2016. Decreased glycolate oxidase activity leads to altered carbon allocation and leaf senescence after a transfer from high CO_2 to ambient air in *Arabidopsis thaliana*. *Journal of Experimental Botany* **67**: 3149–3163.

Dellero Y, Lamothe-Sibold M, Jossier M, Hodges M. 2015. *Arabidopsis thaliana ggt1* photorespiratory mutants maintain leaf carbon/nitrogen balance by reducing RuBisCO content and plant growth. *The Plant Journal* **83**: 1005–1018.

Eisenhut M, Planchais S, Cabassa C, Guivarc'h A, Justin A-M, Taconnat L, Renou J-P, Linka M, Gagneul D, Timm S *et al.* 2013. Arabidopsis *A BOUT DE SOUFFLE* is a putative mitochondrial transporter involved in photorespiratory metabolism and is required for meristem growth at ambient CO_2 levels. *The Plant Journal* **73**: 836–849.

Eisenhut M, Ruth W, Haimovich M, Bauwe H, Kaplan A, Hagemann M. 2008. The photorespiratory glycolate metabolism is essential for cyanobacteria and might have been conveyed endosymbiontically to plants. *Proceedings of the National Academy of Science, USA* **105**: 17199–17204.

Eisenhut M, Weber APM. 2019. Improving crop yield. *Science* **363**: 32–33.

Engel N, Ewald R, Gupta KJ, Zrenner R, Hagemann M, Bauwe H. 2011. The presequence of Arabidopsis serine hydroxymethyltransferase SHM2 selectively prevents import into mesophyll mitochondria. *Plant Physiology* **157**: 1711–1720.

Engel N, Van Den Daele K, Kolukisaoglu Ü, Morgenthal K, Weckwerth W, Pärnik T, Keerberg O, Bauwe H. 2007. Deletion of glycine decarboxylase in Arabidopsis is lethal under nonphotorespiratory conditions. *Plant Physiology* **144**: 1328–1335.

Gardeström P, Wigge B. 1988. Influence of photorespiration on ATP/ADP ratios in the chloroplasts, mitochondria, and cytosol, studied by rapid fractionation of barley (*Hordeum vulgare*) protoplasts. *Plant Physiology* **88**: 69–76.

Goyer A, Collakova E, Díaz de la Garza R, Quinlivan EP, Williamson J, Gregory JF 3rd, Shachar-Hill Y, Hanson AD. 2005. 5-Formyltetrahydrofolate is an inhibitory but well tolerated metabolite in Arabidopsis leaves. *Journal of Biological Chemistry* **280**: 26137–26142.

Hagemann M, Bauwe H. 2016. Photorespiration and the potential to improve photosynthesis. *Current Opinion in Chemical Biology* **35**: 109–116.

Hanson AD, Roje S. 2001. One-carbon metabolism in higher plants. *Annual Review of Plant Physiology and Plant Molecular Biology* **52**: 119–137.

Heeg C, Kruse C, Jost R, Gutensohn M, Ruppert T, Wirtz M, Hell R. 2008. Analysis of the Arabidopsis O-acetylserine(thiol)lyase gene family demonstrates compartment-specific differences in the regulation of cysteine synthesis. *Plant Cell* **20**: 168–185.

Hodges M, Dellero Y, Keech O, Betti M, Raghavendra AS, Sage R, Zhu X-G, Allen DK, Weber APM. 2016. Perspectives for a better understanding of the metabolic integration of photorespiration within a complex plant primary metabolism network. *Journal of Experimental Botany* **67**: 3015–3026.

Igarashi D, Miwa T, Seki M, Kobayashi M, Kato T, Tabata S, Shinozaki K, Ohsumi C. 2003. Identification of photorespiratory glutamate:glyoxylate aminotransferase(GGAT) gene in Arabidopsis. *The Plant Journal* **33**: 975–987.

Kebeish R, Niessen M, Thiruveedhi K, Bari R, Hirsch HJ, Rosenkranz R, Stäbler N, Schönfeld B, Kreuzaler F, Peterhänsel C. 2007. Chloroplastic photorespiratory bypass increases photosynthesis and biomass production in *Arabidopsis thaliana*. *Nature Biotechnology* **25**: 593–599.

Kinoshita H, Nagasaki J, Yoshikawa N, Yamamoto A, Takito S, Kawasaki M, Sugiyama T, Miyake H, Weber APM, Taniguchi M. 2011. The chloroplastic 2-

oxoglutarate/malate transporter has dual function as the malate valve and in carbon/nitrogen metabolism. *The Plant Journal* **65**: 15–26.

Levey M, Timm S, Mettler-Altmann T, Luca Borghi G, Koczor M, Arrivault S, Pm Weber A, Bauwe H, Gowik U, Westhoff P. 2019. Efficient 2-phosphoglycolate degradation is required to maintain carbon assimilation and allocation in the C_4 plant *Flaveria bidentis*. *Journal of Experimental Botany* **70**: 575–587.

Li R, Moore M, King J. 2003. Investigating the regulation of one-carbon metabolism in *Arabidopsis thaliana*. *Plant & Cell Physiology* **44**: 233–241.

Liepman AH, Olsen LJ. 2001. Peroxisomal alanine:glyoxylate aminotransferase (AGT1) is a photorespiratory enzyme with multiple substrates in *Arabidopsis thaliana*. *The Plant Journal* **25**: 487–498.

Liepman AH, Olsen LJ. 2003. Alanine aminotransferase homologs catalyze the glutamate:glyoxylate aminotransferase reaction in peroxisomes of Arabidopsis. *Plant Physiology* **131**: 215–227.

Maier A, Fahnenstich H, von Caemmerer S, Engqvist MK, Weber AP, Flügge UI, Maurino VG. 2012. Transgenic introduction of a glycolate oxidative cycle into *A. thaliana* chloroplasts leads to growth improvement. *Frontiers in Plant Science* **3**: 38.

Mehrshahi P, Gonzalez-Jorge S, Akhtar TA, Ward JL, Santoyo-Castelazo A, Marcus SE, Lara-Núñez A, Ravanel S, Hawkins ND, Beale MH *et al.* 2010. Functional analysis of folate polyglutamylation and its essential role in plant metabolism and development. *The Plant Journal* **64**: 267–279.

Modde K, Timm S, Florian A, Michl K, Fernie AR, Bauwe H. 2017. High serine: glyoxylate aminotransferase activity lowers leaf daytime serine levels, inducing the phosphoserine pathway in Arabidopsis. *Journal of Experimental Botany* **68**: 643–656.

Monné M, Daddabbo L, Gagneul D, Obata T, Hielscher B, Palmieri L, Miniero DV, Fernie AR, Weber APM, Palmieri F. 2018. Uncoupling proteins 1 and 2 (UCP1 and UCP2) from *Arabidopsis thaliana* are mitochondrial transporters of aspartate, glutamate, and dicarboxylates. *Journal of Biological Chemistry* **293**: 4213–4227.

Obata T, Florian A, Timm S, Bauwe H, Fernie AR. 2016. On the metabolic interactions of (photo)respiration. *Journal of Experimental Botany* **67**: 3003–3014.

Pick TR, Bräutigam A, Schulz MA, Obata T, Fernie AR, Weber AP. 2013. *PLGG1*, a plastidic glycolate glycerate transporter, is required for photorespiration and defines a unique class of metabolite transporters. *Proceedings of the National Academy of Science, USA* **10**: 3185–3190.

Porcelli V, Vozza A, Calcagnile V, Gorgoglione R, Arrigoni R, Fontanesi F, Marobbio CMT, Castegna A, Palmieri F, Palmieri L. 2018. Molecular identification and functional characterization of a novel glutamate transporter in yeast and plant mitochondria. *Biochimica et Biophysica Acta - Bioenergetics* **1859**: 1249–1258.

Queval G, Issakidis-Bourguet E, Hoeberichts FA, Vandorpe M, Gakière B, Vanacker H, Miginiac-Maslow M, Van Breusegem F, Noctor G. 2007. Conditional oxidative stress responses in the Arabidopsis photorespiratory mutant *cat2* demonstrate that redox state is a key modulator of daylength-dependent gene expression, and define photoperiod as a crucial factor in the regulation of H_2O_2-induced cell death. *The Plant Journal* **52**: 640–657.

Renné P, Dressen U, Hebbeker U, Hille D, Flügge UI, Westhoff P, Weber AP. 2003. The Arabidopsis mutant *dct* is deficient in the plastidic glutamate/malate translocator DiT2. *The Plant Journal* **35**: 316–331.

Samuilov S, Brilhaus D, Rademacher N, Flachbart S, Arab L, Alfarraj S, Kuhnert F, Kopriva S, Weber APM, Mettler-Altmann T *et al.* 2018. The photorespiratory *BOU* gene mutation alters sulfur assimilation and its crosstalk with carbon and nitrogen metabolism in *Arabidopsis thaliana*. *Frontiers in Plant Science* **871**: 1709.

Schwarte S, Bauwe H. 2007. Identification of the photorespiratory 2-phosphoglycolate phosphatase, PGLP1, in Arabidopsis. *Plant Physiology* **144**: 1580–1586.

Shen BR, Wang LM, Lin XL, Yao Z, Xu HW, Zhu CH, Teng HY, Cui LL, Liu EE, Zhang JJ *et al.* 2019. Engineering a new chloroplastic photorespiratory bypass to increase photosynthetic efficiency and productivity in rice. *Molecular Plant* **12**: 199–214.

South PF, Cavanagh AP, Liu HW, Ort DR. 2019. Synthetic glycolate metabolism pathways stimulate crop growth and productivity in the field. *Science* **363**: eaat9077.

South PF, Walker BJ, Cavanagh AP, Rolland V, Badger M, Ort DR. 2017. Bile acid sodium symporter BASS6 can transport glycolate and is involved in photorespiratory metabolism in *Arabidopsis thaliana*. *Plant Cell* **29**: 808–823.

Sweetlove LJ, Lytovchenko A, Morgan M, Nunes-Nesi A, Taylor NL, Baxter CJ, Eickmeier I, Fernie AR. 2006. Mitochondrial uncoupling protein is required for efficient photosynthesis. *Proceedings of the National Academy of Science, USA* **103**: 19587–19592.

Timm S, Florian A, Arrivault S, Stitt M, Fernie AR, Bauwe H. 2012. Glycine decarboxylase controls photosynthesis and plant growth. *FEBS Letters* **586**: 3692–3697.

Timm S, Giese J, Engel N, Wittmiß M, Florian A, Fernie AR, Bauwe H. 2018. T-protein is present in large excess over the other proteins of the glycine cleavage system in leaves of Arabidopsis. *Planta* **301**: 1–11.

Timm S, Nunes-Nesi A, Pärnik T, Morgenthal K, Wienkoop S, Keerberg O, Weckwerth W, Kleczkowski LA, Fernie AR, Bauwe H. 2008. A cytosolic pathway for the conversion of hydroxypyruvate to glycerate during photorespiration in Arabidopsis. *Plant Cell* **20**: 2848–2859.

Timm S, Wittmiß M, Gamlien S, Ewald R, Florian A, Frank M, Wirtz M, Hell R, Fernie AR, Bauwe H. 2015. Mitochondrial dihydrolipoyl dehydrogenase activity shapes photosynthesis and photorespiration of *Arabidopsis thaliana*. *Plant Cell* **27**: 1968–1984.

Trudeau DL, Edlich-Muth C, Zarzycki J, Scheffen M, Goldsmith M, Khersonsky O, Avizemer Z, Fleishman SJ, Cotton CAR, Erb TJ *et al.* 2018. Design and *in vitro* realization of carbon-conserving photorespiration. *Proceedings of the National Academy of Science, USA* **115**: E11455–E11464.

Voll LM, Jamai A, Renné P, Voll H, McClung CR, Weber AP. 2006. The photorespiratory Arabidopsis *shm1* mutant is deficient in SHM1. *Plant Physiology* **140**: 59–66.

Walker BJ, VanLoocke A, Bernacchi CJ, Ort DR. 2016. The costs of photorespiration to food production now and in the future. *Annual Review of Plant Biology* **67**: 107–129.

Watanabe M, Mochida K, Kato T, Tabata S, Yoshimoto N, Noji M, Saito K. 2008. Comparative genomics and reverse genetics analysis reveal indispensable functions of the serine acetyltransferase gene family in Arabidopsis. *Plant Cell* **20**: 2484–2496.

Weber APM, Bar-Even A. 2019. Improving the efficiency of photosynthetic carbon reactions. *Plant Physiology* **179**: 803–812.

Wigge B, Krömer S, Gardeström P. 1993. The redox levels and subcellular distribution of pyridine nucleotides in illuminated barley leaf protoplasts studied by rapid fractionation. *Physiologia Plantarum* **88**: 10–18.

Xin CP, Tholen D, Devloo V, Zhu XG. 2015. The benefits of photorespiratory bypasses: how can they work? *Plant Physiology* **167**: 574–585.

The impact of synthetic biology for future agriculture and nutrition

Available online at www.sciencedirect.com

ScienceDirect

Current Opinion in Biotechnology

The impact of synthetic biology for future agriculture and nutrition

Marc-Sven Roell[a,b] and Matias D Zurbriggen[b,c]

Global food production needs to be increased by 70% to meet demands by 2050. Current agricultural practices cannot cope with this pace and furthermore are not ecologically sustainable. Innovative solutions are required to increase productivity and nutritional quality. The interdisciplinary field of synthetic biology implements engineering principles into biological systems and currently revolutionizes fundamental and applied research. We review the diverse spectrum of synthetic biology applications that started impacting plant growth and quality. We focus on latest advances for synthetic carbon-conserving pathways *in vitro* and *in planta* to improve crop yield. We highlight strategies improving plant nutrient usage and simultaneously reduce fertilizer demands, exemplified with the engineering of nitrogen fixation in crops or of synthetic plant-microbiota systems. Finally, we address engineering approaches to increase crop nutritional value as well as the use of photoautotrophic organisms as autonomous factories for the production of biopharmaceuticals and other compounds of commercial interest.

Addresses
[a] Institute of Plant Biochemistry, University of Düsseldorf, Universitätsstrasse 1, 40225 Düsseldorf, Germany
[b] iGRAD Plant Graduate School, University of Düsseldorf, Düsseldorf, Germany
[c] Institute of Synthetic Biology and CEPLAS-Cluster of Excellence on Plant Sciences, University of Düsseldorf, Universitätsstrasse 1, 40225 Düsseldorf, Germany

Corresponding author:
Zurbriggen, Matias D (matias.zurbriggen@uni-duesseldorf.de)

Current Opinion in Biotechnology 2020, **61**:102–109
This review comes from a themed issue on **Plant biotechnology**
Edited by **Ralf Reski**, **Ed Rybicki** and **Gary Foster**
For a complete overview see the Issue and the Editorial
Available online 5th December 2019
https://doi.org/10.1016/j.copbio.2019.10.004

Introduction

An estimated population increase of about 2 billion people until 2050 will require novel and innovative solutions to improve agricultural productivity and ensure food security [1]. Several factors pose extra challenges, for example the loss of arable land by rapid urbanization, erosion, and climate warming. In addition, changes in living standards, specifically higher meat consumption, require increased plant-based protein production for animal feed. The development and massive implementation of synthetic and natural fertilizers-nitrogen, phosphorous and potassium in particular- and the Green Revolution — including breeding strategies to maximize plant architecture and light harvesting — resulted in higher yields. This is however currently not sufficient, and in order to meet food demands of the growing world population crop yield has to double in the next 30 years, representing an annual yield increase of 2.2% [2,3]. However, within the last years the yield-increase rate of major crop plants plateaued and the possibility to increase arable land is limited. Genetically engineering plant performance towards improving growth and yield is a potential solution to overcome upcoming problems [4,5]. Classical plant biotechnology rather focuses on modulating individual components, but improving complex multigenic traits requires rational and systematic engineering strategies. The revolutionizing field of synthetic biology applies principles of modern engineering to biological systems. Modular genetic parts are the cornerstone and are combined to construct synthetic biological systems, supported by mathematical model guided design and quantitative functional characterization of the individual parts [6].

Currently, plant synthetic biology is lagging behind bacterial, yeast and mammalian systems, where these approaches are already reshaping fundamental research and the biotechnological/biopharmaceutical industries [7,8]. Within the plant field the standardization of genetic parts and establishment of modular cloning tools were the first steps towards a more generalized implementation of synthetic biology strategies [9,10•]. Synthetic tools for controlling gene expression and cellular processes, in particular chemically inducible systems and optogenetics [6,11,12], CRISPR/Cas9-based technologies and other advances in genome engineering are fundamental for future progress of plant synthetic biology [13].

Here, we discuss current applications and the potential of synthetic biology approaches for improving agriculture productivity, food quality and production, ideally attaining a sustainable and cost-effective practice (Figure 1). In particular, we focus on strategies to: i) develop synthetic metabolic routes for improved CO_2 fixation and carbon-conservation; ii) reduce the usage of natural and synthetic fertilizer in agriculture by engineering nitrogen fixation in

Figure 1

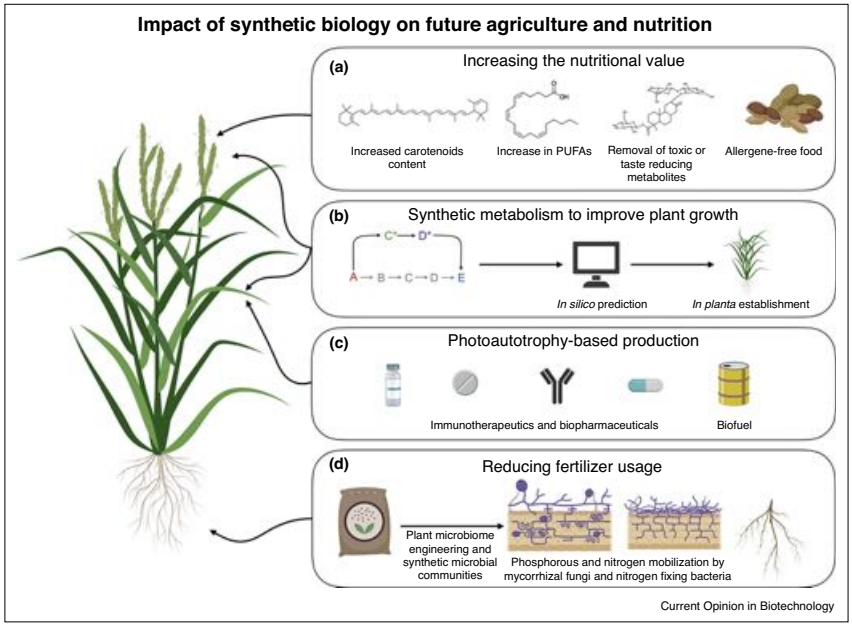

Impact of synthetic biology on future agriculture and nutrition. **(a)** Enhancing the nutritional value of plants includes increasing the content of diverse carotenoids (exemplified by provitamin A) and very-long polyunsaturated fatty acids (PUFAs, exemplified by arachidonic acid). Steviosid (shown), the major component of *Stevia rebaudiana*, is used as natural sweetener, but its bitter aftertaste limits its application in food. **(b)** The construction of synthetic metabolism in plants will contribute to plant growth improvement. Synthetic metabolic pathway design and *in silico* prediction of its function in the context of the endogenous plant network will contribute to a successful implementation *in planta*. **(c)** Photoautotrophy-based platforms are employed for the production of vaccines, immunotherapeutics, antibodies, biopharmaceuticals and biofuels (from left to right). **(d)** Reducing fertilizer usage can be achieved by plant microbiome engineering and the construction of synthetic microbial communities using arbuscular and/or ectomycorrhizal symbioses as well as nodule forming nitrogen-fixing bacteria (from left to right).

crop plants and the construction of synthetic plant microbiome consortia; iii) increase the nutritional value of crop plants; and finally iv) use photoautotrophic organisms as production platforms for commercially interesting compounds. We would like to emphasize that this work focuses on synthetic biology approaches, as needed to improve such complex traits, rather than classical biotechnological approaches which are thoroughly reviewed elsewhere [14].

Synthetic metabolism to increase plant growth and agricultural yield

Agricultural yield is mostly influenced by three major components: the efficiency of light energy capture and of light conversion into biomass, and the harvest index — fraction of total energy in plant biomass contained in the harvestable organs. Whereas, the efficiency of light energy capture and the harvest index have reached their biological limits, the conversion efficiency represents only 20% of its theoretical maximum, constituting therefore a potential engineering target [4]. However, manipulation of such multicomponent traits is still cumbersome. Optimizing and re-designing carbon metabolism using novel synthetic pathways including tailored-engineered enzymes are promising approaches as described below (Figure 1, [reviewed in Ref. 15]). The *in silico* accurate and fast prediction of the behavior of the synthetic metabolic routes integrated within the endogenous metabolic networks will facilitate *in planta* implementation (Figure 1), supported by recent advances in computational tools (Box 1, [reviewed in Ref. 16]).

We discuss here three major targets for enhancing plant carbon efficiency: i) improving carboxylation efficiency, minimizing ii) photorespiratory and iii) respiratory CO_2 loss (summarized in Table 1).

Box 1 Computational tools for synthetic metabolism in plants

Applying principles of engineering to the field of biology requires computational tools for *in silico* predictions. The realization of synthetic pathways not only requires assessing the thermodynamic feasibility [53], but also predicting its behavior in the context of the endogenous metabolic network and identifying potential bottlenecks by flux balance analysis (FBA) [16]. The construction of metabolic networks for cyanobacteria [54], *Chlamydomonas reinhardtii* [55,56] and plants [summarized in Ref. 16] were major achievements aided by the prediction of the behavior of synthetic pathways in phototrophic organisms. Further, classical biochemical models of C3 and C4 photosynthesis [57,58] and cross-scale models connecting leaf photosynthesis with crop field performance can be assessed to predict the effects of photosynthesis manipulation [59]. Integrating these advanced computational tools to the engineering approach will facilitate the realization of synthetic metabolism in plants.

The CO_2-fixing enzyme ribulose-1,5-bisphosphate carboxylase/oxygenase (Rubisco) has been an engineering target for several years. However, attempts to increase its activity and substrate specificity to minimize oxygenase activity were not successful [5]. Instead, engineering carbon concentrating mechanisms, such as C4 photosynthesis, pyrenoids or cyanobacterial carboxysomes are currently preferentially addressed for improving carboxylation efficiency (Table 1). The exploration of rather radical engineering strategies aims at developing synthetic, more efficient routes of CO_2 fixation besides the Calvin-Benson-Bassham cycle (CBBC). The first steps towards this goal are exemplified by the construction of a complete synthetic route for CO_2 fixation *in vitro*, namely the crotonyl–coenzyme A (CoA)/ ethylmalonyl-CoA/ hydroxybutyryl-CoA (CETCH) cycle [17••]. Extensive computational analysis is needed to identify the most efficient enzymes for *de novo* engineering efficient CO_2 fixation, improve their activity and integrate them into a balanced network including precursors and intermediates. All these constraints considered, a final version of the engineered CETCH cycle yielded comparable CO_2 fixation rates to the CBBC (5 nmol CO_2 min^{-} mg^{-1} versus 1–3 nmol CO_2 min^{-1} mg^{-1}) [17••].

The engineering of chloroplastic photorespiratory bypasses to reduce photorespiratory CO_2 loss has been demonstrated as a suitable approach to improve plant growth [reviewed in 18]. For example, the chloroplastic oxidation of glycolate into two molecules of CO_2 upon expression of two enzymes (glycolate dehydrogenase and malate synthase) resulted in a 40% biomass increase in tobacco plants under field conditions [19••]. Inhibition of glycolate export from the chloroplast upon transcriptional downregulation by RNA interference of the plastidic glycerate/glycolate transporter 1 (PLGG1) improved the phenotypic effect of the synthetic pathway [19••]. Glycolate seems to be the most promising substrate for redesigning photorespiration without CO_2 and ammonia release as by products (carbon-conserving photorespiration). Recently, CO_2-neutral synthetic bypasses of photorespiration based on the conversion of glycolate into glycolyl-CoA and re-assimilation into the CBBC were identified computationally [20]. Kinetic-stoichiometric modelling supported the impact of these pathways on plant growth. Engineering of an acetyl-CoA synthetase to convert glycolate into glycolyl-CoA and of a propionyl-CoA reductase for higher glycolyl-CoA selectivity and NADPH specificity, was performed and pathway functionality was demonstrated *in vitro* [20].

Finally, as up to 60% of assimilated carbon is lost by respiration, minimizing respiratory CO_2 losses would be a breakthrough to improve plant productivity. Although engineering respiratory metabolism has been overlooked within the last years, recently four main targets for manipulation were identified in order to reduce respiratory costs. These include, i) optimize protein turnover, ii) redesign respiratory metabolism, iii) avoid futile cycles, and iv) engineering efficient ion transport [21•]. However, negative side effects of these approaches need careful evaluation. A detailed overview about engineering strategies regarding respiration is provided in [21•].

Besides the engineering and implementation of synthetic metabolic pathways in plants, the manipulation of stomatal kinetics [22•] and accelerated recovery from photoprotection [23] are strategies of current interest (Table 1).

Reducing fertilizer usage in agriculture

The massive use of (synthetic) fertilizers — ~140 kg per hectare of arable land — sustains western agricultural productivity today. In developing countries, the high costs pose a limitation, ergo low fertilization leads to lower yields. However, current heavy fertilization practices are not sustainable due to low nitrogen utilization efficiency of crop plants, contamination of ground waters, energy-intensive fertilizer production and finite phosphorous resources [24–26]. Therefore, strategies to improve plant nutrient use efficiency, uptake or assimilation mechanisms are needed.

Previous attempts to improve nitrogen and phosphorous use efficiency in plants, which have shown limited success, mostly focused on genetically modifying individual components involved in nutrient uptake, allocation, metabolism or transcriptional regulation. Current limitations can be overcome by differentiating between nutrient uptake and nutrient utilization [25,26].

Promising efforts towards reducing nitrogen fertilization involve complex synthetic biology strategies for the engineering of a nitrogenase into plants, or establishing symbiotic nitrogen fixation in major crop plants, otherwise only present in legumes [24]. The implementation of a functional multi-subunit nitrogenase is challenging due to the high number of involved genes, oxygen-sensitivity and metal co-factor dependence (iron and molybdenum)

Table 1

Synthetic biology applications for future agriculture and food

Approach	Description	Species	Reference
Improving plant growth and agricultural yield			
Improving carboxylation reactions			
C4 photosynthesis in C3 plants	Implementation of C4 photosynthesis in C3 species includes biochemical and developmental (Kranz-Anatomy) engineering with the most prominent example of the C4 Rice Project (https://c4rice.com).	C3 crop plants (e.g. *Oryza sativa*)	[60]
Implementation of carbon-concentrating-microcompartments	Implementation of algae (pyrenoid) or cyanobacterial (carboxysomes) carbon concentrating mechanism in plant chloroplasts to suppress RubisCO oxygenase activity	C3 crop plants (e.g. *Oryza sativa*)	[61,62]
Synthetic pathways for CO_2 assimilation	*In vitro* CO_2 fixation using a synthetic pathway composed of 17 enzymes (CETCH cycle)		[17••]
Minimizing (photo)–respiratory CO_2losses			
Chloroplastic photorespiratory bypass	Oxidation of glycolate in the chloroplast to release two CO_2 molecules and native photorespiratory flux knockdown resulted in a 40% biomass increase under field conditions	*Nicotiana tabacum*	[19••]
Synthetic CO_2 neutral photorespiration	*In vitro* conversion of glycolate into glycoly-CoA and re-assimilation into the CBBC without CO_2 and nitrogen release. Two enzymes were engineered for substrate and co-factor specificity		[20]
Minimizing respiratory CO_2 loss	Potential targets: i) optimize protein turnover ii) redesign respiratory metabolism, iii) avoid futile cycle, iv) efficient ion transport		[21•]
Improving water use efficiency and photosynthetic light reactions			
Optogenetic manipulation of stomatal kinetics	Guard-cell specific of a synthetic blue light-gated K^+-channel to allow rapid response of stomatal opening under fluctuating light conditions	*Arabidopsis thaliana*	[22•]
Accelerating recovery from photoprotection	Overexpression of *PsbS* and xanthophyll cycle enzymes resulted in a faster restoration of maximum CO_2 assimilation from nonphotochemical quenching of chlorophyll fluorescence	*Nicotiana tabacum*	[23]
Design Breeding			
De novo domestication	Genetic manipulation of several domestication genes in wild type plants enables a timesaving domestication process	*Solanum lycopersicum*	[63••]
Reducing synthetic fertilizer usage in agriculture			
Establish functional nitrogenase or symbiotic nitrogen fixation in crop plants			
Functional nitrogenase in plants	Expression of 16 nitrogenase genes in plant mitochondria	*Nicotiana benthamiana*	[29•]
Symbiotic nitrogen fixation in crop plants	Requires the expression of four regulatory programs. The SynSym international consortia addresses questions regarding synthetic nitrogen fixation (https://synthsym.org)	Several crop plants	[24]
Synthetic microbiota for improved nutrient utilization			
Cultivation with growth promoting plant microbiome bacteria	Different Rhizobiales isolated supported growth of *Arabidopsis*. In particular, taxonomic groups containing nitrogen-fixing nodule symbionts	*Arabidopsis thaliana*	[32••]
Plant microbiome composition	Identification of root-associated fungus in non-mycorrhizal plants to improve phosphorous utilization	*Arabis alpina*	[64]
Construction of synthetic microbiota for crops	Within the private sector engineering the microbiome of crops is already addressed	Several crop plants	[52]
Increasing the nutrional value of crop plants			
Increase provitamin A content	GoldenRice project (http://www.goldenrice.org)	Oryza sativa	[35]

Table 1 (*Continued*)

Approach	Description	Species	Reference
Increase VLC-PUFA content	Seed-specifically expression of VLC-PUFAs biosynthetic genes	*Brassica napus Canola sativa*	[41•,42]
Remove cyanogenic glycosides	RNA interference targeting two cytochrome P450 genes	*Manihot esculenta* Crantz	[43]
Increased anthocyanin content	Fruit-specific expression of two transcription factors (*Del* and *Ros1*) inducing anthocyananin biosynthesis	*Solanum lycopersicum*	[65]
Reduced gluten content in wheat	CRISPR/Cas9 mediated knockout of up to 45 genes in wheat to lower gluten content	*Triticum aestivum*	[66•]
Vitamin B_{12} biosynthesis in plants	Engineering *E. coli* for *de novo* vitamin B_{12} biosynthesis		[67]
Photoautotrophic organisms as production platform			
Vaccine and cosmetic production	Use mosses as green cell factory for the production of vaccines and cosmetics	*Physcomitrella patens*	[48•]
Scalable production of artemisinin in biomass crops	Chloroplastic expression of the core artemisinic acid biosynthesis pathway and additional enzymes to improve flux through the pathway	*Nicotiana tabacum*	[68]
Improving saccharification efficiency	TALEN-mediated mutagenesis of more than 100 caffeic acid O-methyltransferase alleles in polyploid sugarcane to improve the saccharification efficiency for biofuel production	*Saccharum officinarum*	[69]
Synthetic or biohybrid systems	Construction of artificial leaves and synthetic photosynthetic cell as solar energy driven production platforms		[50,51]

Abbreviations: VLC-PUFAs: very long poly-unsaturated fatty acids; CETCH cycle: crotonyl–coenzyme A (CoA)/ethylmalonyl-CoA/hydroxybutyryl-CoA; CBBC: Calvin-Benson-Bassham cycle; TALEN: transcriptional activator like effector nuclease.

[27 and references therein]. To achieve spatiotemporal separation of photosynthesis and N_2 fixation, the mitochondrion is suggested as the suitable target compartment for implementing the nitrogenase. However, it still remains to be analyzed how to achieve correct mitochondrial targeting, functionality of the nitrogenase subunits and nitrogenase metal cluster assembly [28]. First steps made in this direction comprise the transient expression and correct targeting of 16 nitrogenase subunit proteins in *Nicotiana benthamiana* [29•].

An alternative strategy requires the establishment of the rhizobium-legume symbiosis in crop plants. This requires the coordinated engineering of four genetic regulatory programs: i) Nod factor perception, ii) root nodule organogenesis, iii) bacterial infection, and iv) establishing nitrogenase activity inside the nodule [24].

In contrast to the before mentioned approaches, bottom-up construction of synthetic plant microbiota is a suitable strategy to concurrently improving the utilization of nitrogen and phosphorous in plants [30]. Tremendous efforts in understanding the plant microbiome pinpoint to its engineering potential [31••,32••,33], and will probably soon be reflected in a generalized implementation of such synthetic consortia.

Establishing plant microbe interactions depends on phytohormones. In particular strigolactones play an essential role in mediating the symbiosis with arbuscular mycorrhizal fungi and nitrogen fixing bacteria [34]. Engineering of targeted and regulated strigolactone secretion or the production and release of metabolites able to recruit useful microorganisms for plant nutrition might represent a simple strategy towards improved nutrition [34].

Increasing the nutritional value of crop plants

Reaching the limits of productivity implies that agriculture needs to increase the nutritional value of crop plants to secure sufficient food supply and tackle issues of malnutrition (Figure 1). The most prominent example of the biotech-era is the Golden Rice Project [35]. Vitamin A deficiency causes major health problems, an issue overrepresented in countries where rice is the staple food and diet diversity is limited. Implementation of two carotenoid biosynthesis genes, phytoene synthase and carotene desaturase, lead to the biosynthesis and accumulation of beta-carotene (provitamin A) in rice plants [35]. However, in order to engineer complex, multigenic traits and multi-enzymatic pathways as those needed to produce other vitamins and secondary metabolites, synthetic biology strategies are needed [36]. Of interest are several carotenoids and their oxygen containing derivatives, xanthophylls. They are associated with major health benefits, like eye-health and cardiovascular-health, functional immune system, cognitive function and antioxidant activity [36]. The red ketocarotenoid astaxanthin is of high commercial value as food supplement in particular for the fish industry. However, most of the astaxanthin used in salmon and trout farming is currently of synthetic origin and plant-based sources would represent a cheap alternative as fish feed [37]. Understanding the regulatory mechanisms coordinating astaxanthin and fatty acid biosynthesis would facilitate future engineering strategies. Indeed, it was shown that

astaxanthin esterification is a prerequisite for astaxanthin accumulation in algae [38].

Very-long-chain polyunsaturated fatty acids (VLC-PUFAs) such as arachidonic acid (AA; C20:4 Δ5,8,11,14), eicosapentaenoic acid (EPA; C20:5 Δ5,8,11,14,17) and docosahexaenoic acid (DHA; C22:6 Δ4,7,10,13,16,19) are associated with brain development and are beneficial for reducing cardiovascular disease prevalence. The consumption of microalgae by marine fish represents the primary, but non-sustainable source of VLC-PUFAs in human diet. While flowering plants contain low amounts of VLC-PUFAs [39], several moss species are known to accumulate higher levels [40]. The introduction of VLC-PUFA biosynthetic genes, including moss genes, has shown success in improving the VLC-PUFA content in model plants [39 and references therein]. In oil crops the expression of VLC-PUFA biosynthetic genes resulted in a 15% VLC-PUFA content in *Camelina sativa* [41•]. Further, in canola (*Brassica napus*) the seed-specific expression of VLC-PUFA biosynthetic genes caused an increased VLC-PUFA content of 12%. These transgenic plants are expected to have full regulatory approval in the US soon [42].

Increasing the nutritional value of food also comprises the elimination of undesired secondary metabolites and proteins. The presence of toxic cyanogenic glycosides is a major issue for cassava (*Manihot esculenta* Crantz) based diets, as it is the case in Sub-Saharan countries [35]. Engineering efforts to reduce cyanogenic glycoside content are limited to RNA interference approaches targeting two cytochrome P450 genes, *CYP79D1* and *CYP79D2*, encoding the first enzymes in linamarin and lotaustralin synthesis [43]. *Stevia rebaudiana*, naturally found in South America, is a source of steviol glycosides which have attracted the attention of the food industry as natural sweetener. However, its organoleptic qualities, namely a bitter aftertaste limit their generalized consumer/food industry acceptance [44]. Within the private sector the recent advances in genome-editing are already used to facilitate the targeted elimination of undesired traits. These approaches will further contribute to reducing the allergenicity of plant-based food, which is of relevance due to severe health risks. In particular peanuts, a high protein containing plant-based food source, cause severe allergies [45]. Therefore, elimination of the major allergens — Ara proteins — would make these crops available to a wider market. Table 1 includes several other approaches recently developed to increase the nutritional value in crop plants (Table 1).

Harnessing photoautotrophy as a bioproduction platform

Photoautrophic organisms are well-suited systems for the large-scale production of immunotherapeutics, biopharmaceuticals and biofuels due to their low cost, highly scalable biomass production and no endotoxin synthesis (Table 1). Furthermore, the native post-translational modification machinery can be further engineered to achieve humanized *N*-glycan structure as exemplified in [46]. For a thorough overview on higher plants as production platform we refer the reader to [47]. The moss *Physcomitrella patens* emerged as an efficient green cell factory, with moss-made pharmaceuticals currently in clinical trial and moss-product cosmetics already on the market [48•]. Aquatic phototrophic organism, such as cyanobacteria and green algae, are in turn of industrial relevance for biofuel production [reviewed in Ref. 49]. Besides phototrophic organisms, complete synthetic or biohybrid systems are emerging using solar energy as driving force, as exemplified by artificial leaves [50] and synthetic photosynthetic cells [51].

Conclusions and future perspectives

Recent advances in the engineering of complex traits in plants as illustrated here indicate the potential of plant synthetic biology to tackle some of the urgent nutritional and ecological demands. Some of the mentioned approaches have already entered the market as for example the engineering of synthetic microbiota to reduce fertilizer use in agriculture [52]. However, many of the associated technologies still need to mature and a regulatory framework to be in place before a generalized commercial application can finally ensue. The suitability of the approaches within the regulatory framework, in particular in the EU, needs to be carefully evaluated in the future (for detailed information see article in this issue). In accordance with the fast, widespread and successful implementation of synthetic biology strategies witnessed in the biomedical field and the white and red high-value compounds and biopharmaceutical industries, we foresee the game changing effects of plant synthetic biology for agriculture and nutrition.

Author's contribution

MSR and MDZ jointly developed the concept and wrote the manuscript.

Conflict of interest statement

Nothing declared.

Acknowledgements

This study was supported by the German Research Foundation (DFG) under Germany's Excellence Strategy (CEPLAS – EXC-2048/1 – Project ID 390686111 to MDZ) and the iGRAD Plant Graduate School (DFG/GRK1525 to MSR). The figure was made with BioRender.io (Toronto, Canada).

References and recommended reading

Papers of particular interest, published within the period of review, have been highlighted as:

- • of special interest
- •• of outstanding interest

1. Food and Agriculture Organization of the United Nations: *The State of Food Security and Nutrition in the World 2017: Building Resilience for Peace and Food Security*. 2017.

2. Tilman D, Clark M: **Global diets link environmental sustainability and human health**. *Nature* 2014, **515**:518-522.

3. Walker BJ, VanLoocke A, Bernacchi CJ, Ort DR: **The costs of photorespiration to food production now and in the future**. *Annu Rev Plant Biol* 2016, **67**:107-129.

4. Long SP, Marshall-Colon A, Zhu X-G: **Meeting the global food demand of the future by engineering crop photosynthesis and yield potential**. *Cell* 2015, **161**:56-66.

5. Ort DR, Merchant SS, Alric J, Barkan A, Blankenship RE, Bock R, Croce R, Hanson MR, Hibberd JM, Long SP *et al.*: **Redesigning photosynthesis to sustainably meet global food and bioenergy demand**. *Proc Natl Acad Sci U S A* 2015, **112**:8529-8536.

6. Andres J, Blomeier T, Zurbriggen MD: **Synthetic switches and regulatory circuits in plants**. *Plant Physiol* 2019, **179**:862-884.

7. Toda S, Blauch LR, Tang SKY, Morsut L, Lim WA: **Programming self-organizing multicellular structures with synthetic cell-cell signaling**. *Science* 2018, **361**:156-162.

8. Shaw WM, Yamauchi H, Mead J, Gowers G-OF, Bell DJ, Öling D, Larsson N, Wigglesworth M, Ladds G, Ellis T: **Engineering a model cell for rational tuning of GPCR signaling**. *Cell* 2019, **177**:782-796.e27.

9. Sarrion-Perdigones A, Falconi EE, Zandalinas SI, Juárez P, Fernández-del-Carmen A, Granell A, Orzaez D: **GoldenBraid: an iterative cloning system for standardized assembly of reusable genetic modules**. *PLoS One* 2011, **6**:e21622.

10. • Engler C, Youles M, Gruetzner R, Ehnert T-M, Werner S, Jones JDG, Patron NJ, Marillonnet S: **A golden gate modular cloning toolbox for plants**. *ACS Synth Biol* 2014, **3**:839-843

In this study the authors develop a golden gate based toolkit for synthetic biology in plants and thereby setting the standards within the plant synthetic biology community.

11. Müller K, Siegel D, Rodriguez Jahnke F, Gerrer K, Wend S, Decker EL, Reski R, Weber W, Zurbriggen MD: **A red light-controlled synthetic gene expression switch for plant systems**. *Mol Biosyst* 2014, **10**:1679-1688.

12. Chatelle C, Ochoa-Fernandez R, Engesser R, Schneider N, Beyer HM, Jones AR, Timmer J, Zurbriggen MD, Weber W: **A green-light-responsive system for the control of transgene expression in mammalian and plant Cells**. *ACS Synth Biol* 2018, **7**:1349-1358.

13. Kumlehn J, Pietralla J, Hensel G, Pacher M, Puchta H: **The CRISPR/Cas revolution continues: From efficient gene editing for crop breeding to plant synthetic biology**. *J Integr Plant Biol* 2018, **60**:1127-1153.

14. Varshney RK, Bansal KC, Aggarwal PK, Datta SK, Craufurd PQ: **Agricultural biotechnology for crop improvement in a variable climate: Hope or hype?** *Trends Plant Sci* 2011, **16**:363-371.

15. Weber APM, Bar-Even A: **Update: improving the efficiency of photosynthetic carbon reactions**. *Plant Physiol* 2019, **179**:803-812.

16. Küken A, Nikoloski Z: **Computational approaches to design and test plant synthetic metabolic pathways**. *Plant Physiol* 2019, **179**:894-906.

17. •• Schwander T, Schada von Borzyskowski L, Burgener S, Cortina NS, Erb TJ: **A synthetic pathway for the fixation of carbon dioxide in vitro**. *Science* 2016, **354**:900-904

This study demonstrates the construction of a novel, complete synthetic pathway for the *in vitro* fixation of carbon dioxide. The pioneering study is the first to show synthetic CO_2 fixation *in vitro*.

18. Eisenhut M, Roell MS, Weber APM: **Mechanistic understanding of photorespiration paves the way to a new green revolution**. *New Phytol* 2019, **15**:330-338 http://dx.doi.org/10.1111/nph.15872.

19. •• South PF, Cavanagh AP, Liu HW, Ort DR: **Synthetic glycolate metabolism pathways stimulate crop growth and productivity in the field**. *Science* 2019, **363**

In this study the authors demonstrate a biomass increase of 40% in tobacco plants under field conditions using a chloroplastic bypass of photorespiration. It is the first study to demonstrate the positive impact of bypasses of photorespiration under field conditions.

20. Trudeau DL, Edlich-Muth C, Zarzycki J, Scheffen M, Goldsmith M, Khersonsky O, Avizemer Z, Fleishman SJ, Cotton CAR, Erb TJ *et al.*: **Design and in vitro realization of carbon-conserving photorespiration**. *Proc Natl Acad Sci U S A* 2018, **115**:E11455-E11464.

21. • Amthor JS, Bar-Even A, Hanson AD, Millar AH, Stitt M, Sweetlove LJ, Tyerman SD: **Engineering strategies to boost crop productivity by cutting respiratory carbon loss**. *Plant Cell* 2019, **31**:297-314

In this study the authors outline the importance of respiratory CO_2 loss as engineering target and propose different approaches that are of future interest.

22. • Papanatsiou M, Petersen J, Henderson L, Wang Y, Christie JM, Blatt MR: **Optogenetic manipulation of stomatal kinetics improves carbon assimilation, water use, and growth**. *Science* 2019, **363**:1456-1459

In this study a synthetic blue light regulated potassium channel was expressed in *Arabidopsis* guard cells to accelerate the response of stomatal behavior causing a growth-promoting phenotype.

23. Kromdijk J, Głowacka K, Leonelli L, Gabilly ST, Iwai M, Niyogi KK, Long SP: **Improving photosynthesis and crop productivity by accelerating recovery from photoprotection**. *Science* 2016, **354**:857-861.

24. Rogers C, Oldroyd GED: **Synthetic biology approaches to engineering the nitrogen symbiosis in cereals**. *J Exp Bot* 2014, **65**:1939-1946.

25. Heuer S, Gaxiola R, Schilling R, Herrera-Estrella L, López-Arredondo D, Wissuwa M, Delhaize E, Rouached H: **Improving phosphorus use efficiency: a complex trait with emerging opportunities**. *Plant J* 2017, **90**:868-885.

26. Perchlik M, Tegeder M: **Improving plant nitrogen use efficiency through alteration of amino acid transport processes**. *Plant Physiol* 2017, **175**:235-247.

27. Vicente EJ, Dean DR: **Keeping the nitrogen-fixation dream alive**. *Proc Natl Acad Sci U S A* 2017, **114**:3009-3011.

28. Burén S, Rubio LM: **State of the art in eukaryotic nitrogenase engineering**. *FEMS Microbiol Lett* 2018, **365**:1.

29. • Allen RS, Tilbrook K, Warden AC, Campbell PC, Rolland V, Singh SP, Wood CC: **Expression of 16 nitrogenase proteins within the plant mitochondrial matrix**. *Front Plant Sci* 2017, **8**:287

In this paper the authors demonstrate the transient expression of 16 nitrogenase subunits in *Nicotiana benthamiana* and the successful targeting of these subunits to plant mitochondria.

30. Vorholt JA, Vogel C, Carlström CI, Müller DB: **Establishing causality: opportunities of synthetic communities for plant microbiome research**. *Cell Host Microbe* 2017, **22**:142-155.

31. •• Hiruma K, Gerlach N, Sacristán S, Nakano RT, Hacquard S, Kracher B, Neumann U, Ramírez D, Bucher M, O'Connell RJ *et al.*: **Root endophyte Colletotrichum tofieldiae confers plant fitness benefits that ere phosphate status dependent**. *Cell* 2016, **165**:464-474

In this study the plant fitness promoting effect of root endophytes regarding phosphorous utilization was demonstrated. Defining mycorrhizal fungi and root endophytes as engineering targets for improved phosphorous utilization within the plant microbiome.

32. •• Garrido-Oter R, Nakano RT, Dombrowski N, Ma K-W, AgBiome Team, McHardy AC, Schulze-Lefert P: **Modular traits of the Rhizobiales root microbiota and their evolutionary relationship with symbiotic Rhizobia**. *Cell Host Microbe* 2018, **24**:155-167.e5

In this paper the authors characterize Rhizobiales as major constituent of the plant microbiome in non-legume plants. Further, the plant growth-promoting effects of Rhizobiales are demonstrated.

33. Sarkar D, Rovenich H, Jeena G, Nizam S, Tissier A, Balcke GU, Mahdi LK, Bonkowski M, Langen G, Zuccaro A: **The inconspicuous gatekeeper: endophytic Serendipita vermifera acts as extended plant protection barrier in the rhizosphere**. *New Phytol* 2019, **224**:886-901 http://dx.doi.org/10.1111/nph.15904.

34. Waters MT, Gutjahr C, Bennett T, Nelson DC: **Strigolactone signaling and evolution**. *Annu Rev Plant Biol* 2017, **68**:291-322.

35. Beyer P: **Golden Rice and "Golden" crops for human nutrition**. *Nat Biotechnol* 2010, **27**:478-481.

36. Wurtzel ET: **Changing form and function through carotenoids and synthetic biology**. *Plant Physiol* 2019, **179**:830-843.

37. Breitenbach J, Nogueira M, Farre G, Zhu C, Capell T, Christou P, Fleck G, Focken U, Fraser PD, Sandmann G: **Engineered maize as a source of astaxanthin: processing and application as fish feed**. *Transgenic Res.* 2016, **25**:785-793.

38. Chen G, Wang B, Han D, Sommerfeld M, Lu Y, Chen F, Hu Q: **Molecular mechanisms of the coordination between astaxanthin and fatty acid biosynthesis in *Haematococcus pluvialis* (Chlorophyceae)**. *Plant J* 2015, **81**:95-107.

39. Dyer JM, Stymne S, Green AG, Carlsson AS: **High-value oils from plants**. *Plant J* 2008, **54**:640-655.

40. Beike AK, Jaeger C, Zink F, Decker EL, Reski R: **High contents of very long-chain polyunsaturated fatty acids in different moss species**. *Plant Cell Rep* 2014, **33**:245-254.

41. • Ruiz-Lopez N, Haslam RP, Napier JA, Sayanova O: **Successful high-level accumulation of fish oil omega-3 long-chain polyunsaturated fatty acids in a transgenic oilseed crop**. *Plant J* 2014, **77**:198-208
In this study the seed specific expression of VLC-PUFA biosynthetic genes resulted in *Camelina sativa* plants with 15% increased VLC-PUFA content.

42. Napier JA, Olsen RE, Tocher DR: **Update on GM canola crops as novel sources of omega-3 fish oils**. *Plant Biotechnol J* 2019, **17**:703-705.

43. Jørgensen K, Bak S, Busk PK, Sørensen C, Olsen CE, Puonti-Kaerlas J, Møller BL: **Cassava plants with a depleted cyanogenic glucoside content in leaves and tubers. Distribution of cyanogenic glucosides, their site of synthesis and transport, and blockage of the biosynthesis by RNA interference technology**. *Plant Physiol* 2005, **139**:363-374.

44. Prakash I, Markosyan A, Bunders C: **Development of next generation stevia sweetener: Rebaudioside M**. *Foods* 2014, **3**:162-175.

45. Palladino C, Breiteneder H: **Peanut allergens**. *Mol Immunol* 2018, **100**:58-70.

46. Reski R, Parsons J, Decker EL: **Moss-made pharmaceuticals: from bench to bedside**. *Plant Biotechnol J* 2015, **13**:1191-1198.

47. Tschofen M, Knopp D, Hood E, Stöger E: **Plant molecular farming: much more than medicines**. *Annu Rev Anal Chem (Palo Alto Calif)* 2016, **9**:271-294.

48. • Reski R, Bae H, Simonsen HT: **Physcomitrella patens, a versatile synthetic biology chassis**. *Plant Cell Rep* 2018, **37**:1409-1417
In this review the authors elucidate the tremendous potential of *Physcomitrella patens* as a photoautotrophic production platform and as suitable species for synthetic biology approaches.

49. Wijffels RH, Kruse O, Hellingwerf KJ: **Potential of industrial biotechnology with cyanobacteria and eukaryotic microalgae**. *Curr Opin Biotechnol* 2013, **24**:405-413.

50. Nocera DG: **The artificial leaf**. *Acc Chem Res* 2012, **45**:767-776.

51. Berhanu S, Ueda T, Kuruma Y: **Artificial photosynthetic cell producing energy for protein synthesis**. *Nat Commun* 2019, **10**:1325.

52. Waltz E: **A new crop of microbe startups raises big bucks, takes on the establishment**. *Nat Biotechnol* 2017, **35**:1120-1122.

53. Noor E, Bar-Even A, Flamholz A, Reznik E, Liebermeister W, Milo R: **Pathway thermodynamics highlights kinetic obstacles in central metabolism**. *PLoS Comput Biol* 2014, **10**:e1003483.

54. Knoop H, Gründel M, Zilliges Y, Lehmann R, Hoffmann S, Lockau W, Steuer R: **Flux balance analysis of cyanobacterial metabolism: the metabolic network of *Synechocystis* sp. PCC 6803**. *PLoS Comput Biol* 2013, **9** e1003081.

55. Boyle NR, Sengupta N, Morgan JA: **Metabolic flux analysis of heterotrophic growth in *Chlamydomonas reinhardtii***. *PLoS One* 2017, **12** e0177292.

56. Salguero DAM, Fernández-Niño M, Serrano-Bermúdez LM, Melo DOP, Winck FV, Caldana C, Barrios AFG: **Development of a *Chlamydomonas reinhardtii* metabolic network dynamic model to describe distinct phenotypes occurring at different CO_2 levels**. *PeerJ* 2018, **2018** e5528.

57. Farquhar GD, Caemmerer von S, Berry JA: **A biochemical model of photosynthetic CO_2 assimilation in leaves of C3 species**. *Planta* 1980, **149**:78-90.

58. Caemmerer von S: *Biochemical Models of Leaf Photosynthesis*. 2000.

59. Wu A, Hammer GL, Doherty A, Caemmerer von S, Farquhar GD: **Quantifying impacts of enhancing photosynthesis on crop yield**. *Nat Plants* 2019, **5**:380-388.

60. Schuler ML, Mantegazza O, Weber APM: **Engineering C4 photosynthesis into C3 chassis in the synthetic biology age**. *Plant J* 2016, **87**:51-65.

61. Mackinder LCM, Meyer MT, Mettler-Altmann T, Chen VK, Mitchell MC, Caspari O, Rosenzweig ESF, Pallesen L, Reeves G, Itakura A *et al.*: **A repeat protein links Rubisco to form the eukaryotic carbon-concentrating organelle**. *Proc Natl Acad Sci U S A* 2016, **113**:5958-5963.

62. Long BM, Hee WY, Sharwood RE, Rae BD, Kaines S, Lim Y-L, Nguyen ND, Massey B, Bala S, Caemmerer von S *et al.*: **Carboxysome encapsulation of the CO_2-fixing enzyme Rubisco in tobacco chloroplasts**. *Nat Commun* 2018, **9**:3570.

63. •• Zsögön A, Cermak T, Naves ER, Notini MM, Edel KH, Weinl S, Freschi L, Voytas DF, Kudla J, Peres LEP: **De novo domestication of wild tomato using genome editing**. *Nat Biotechnol* 2018, **36**:1211-1216
In this paper wild tomato was *de novo* domesticated by CRISPR/Cas9 genome editing of six loci. The study illustrates how genome editing can be efficiently used for speeding up plant breeding.

64. Almario J, Jeena G, Wunder J, Langen G, Zuccaro A, Coupland G, Bucher M: **Root-associated fungal microbiota of nonmycorrhizal *Arabis alpina* and its contribution to plant phosphorus nutrition**. *Proc Natl Acad Sci U S A* 2017, **114**:E9403-E9412.

65. Butelli E, Titta L, Giorgio M, Mock H-P, Matros A, Peterek S, Schijlen EGWM, Hall RD, Bovy AG, Luo J *et al.*: **Enrichment of tomato fruit with health-promoting anthocyanins by expression of select transcription factors**. *Nat Biotechnol* 2008, **26**:1301-1308.

66. • Sánchez-León S, Gil-Humanes J, Ozuna CV, Giménez MJ, Sousa C, Voytas DF, Barro F: **Low-gluten, nontransgenic wheat engineered with CRISPR/Cas9**. *Plant Biotechnol J* 2018, **16**:902-910
This study demonstrates the tremendous potential of genome editing to modulate complex traits by knocking out of up to 45 genes to engineering low-gluten wheat.

67. Fang H, Li D, Kang J, Jiang P, Sun J, Zhang D: **Metabolic engineering of Escherichia coli for de novo biosynthesis of vitamin B 12**. *Nat Commun* 2018, **9**:4917.

68. Fuentes P, Zhou F, Erban A, Karcher D, Kopka J, Bock R: **A new synthetic biology approach allows transfer of an entire metabolic pathway from a medicinal plant to a biomass crop**. *eLife* 2016, **5**.

69. Kannan B, Jung JH, Moxley GW, Lee S-M, Altpeter F: **TALEN-mediated targeted mutagenesis of more than 100 COMT copies/alleles in highly polyploid sugarcane improves saccharification efficiency without compromising biomass yield**. *Plant Biotechnol J* 2018, **16**:856-866.

Phosphoregulation within the photorespiratory cycle: Regulate smarter, adapt better?

News and Views

Phosphoregulation within the Photorespiratory Cycle: Regulate Smarter, Adapt Better?

To cope with various abiotic and biotic stress factors, plants must be facile in adapting cellular metabolism. In particular, they have to adjust photosynthesis and balance associated metabolism. Heat and drought stress strengthen plant photorespiration, a metabolic process resulting from Rubisco oxygenase activity (Busch, 2020). Rubisco oxygenase activity results in the production of 2-phosphoglycolate, a toxic intermediate that needs to be rapidly detoxified via the photorespiratory cycle to avoid inhibition of several Calvin-Benson-Bassham cycle enzymes (Fernie and Bauwe, 2020). The interconnection with associated metabolism, in particular the nitrogen cycle, demands a precise regulation of photorespiration depending on the environmental circumstances (Eisenhut et al., 2019). In order to achieve short-term regulation of photorespiratory fluxes, the activities of several photorespiratory enzymes are regulated by posttranslational modifications, including *S*-nitrosylation and phosphorylation (Hodges et al., 2016).

In this issue of *Plant Physiology*, Liu et al. (2020) demonstrate a novel regulatory mechanism that depends on cofactor switching mediated by phosphorylation of the photorespiratory enzyme hydroxypyruvate reductase 1 (HPR1) in Arabidopsis (*Arabidopsis thaliana*; Fig. 1). Under changing environmental conditions, the phosphorylation-dependent changes in HPR1 cofactor specificity allow the regulation of photorespiratory fluxes.

HPR catalyzes the second to last step of photorespiration, converting hydroxypyruvate into glycerate, while oxidizing a pyridine cofactor, preferentially NADH. In photosynthetic leaves, peroxisomal HPR1 accounts for up to 80% of HPR activity (Liu et al., 2020). The central role of HPR1 in photorespiration is supported by the retarded growth phenotype of the *hpr1-1* loss-of function mutant in air (Fig. 1).

Based on previous knowledge of the likely HPR1 phosphorylation site, Liu et al. (2020) demonstrate that mimicking HPR1 phosphorylation at Thr-335 (HPR1^{T335D}) shifted HPR activity toward NADPH dependency. Speaking in numbers, the catalytic efficiency for NADPH-dependent HPR1 activity was increased by 35%, while the NADH-dependent activity was reduced by 50%. Consequently, HPR1^{T335D} was more specific for hydroxypyruvate as substrate for HPR activity in the presence of NADPH (31% increase) compared with NADH (56% reduction). Homology-based modeling revealed that the position of the phosphorylated Thr residue is within an α-helix connecting the substrate-binding and cofactor-binding domains. Structural changes upon Thr phosphorylation can explain the observed effects regarding cofactor and substrate specificity (Fig. 1).

Liu et al. (2020) complemented the *hpr1-1* photorespiratory phenotype in planta to assess the effects of HPR1 phosphorylation at Thr-335. Whereas wild-type HPR1 and nonphosphorylated HPR1 fully complemented the photorespiratory *hpr1-1* mutant phenotype in air, HPR1^{T335D} only partially rescued the phenotype (Fig. 1). In planta, HPR1^{T335D} also preferentially catalyzed NADPH-dependent HPR activity, consistent with the biochemical data using purified HPR1^{T335D} protein. The partial complementation of the

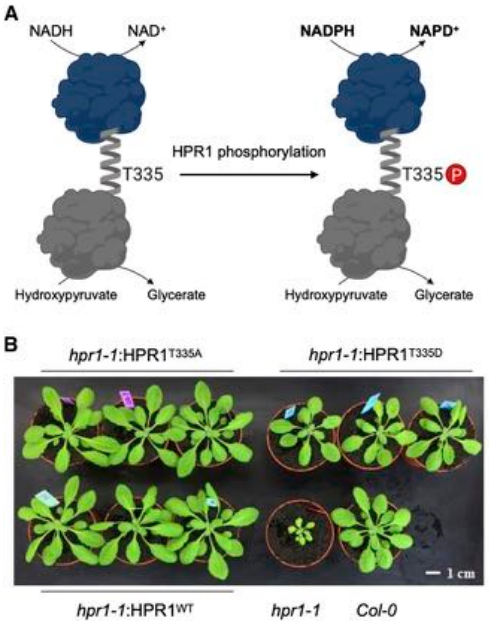

Figure 1. Phosphorylation of HPR1 at Thr-335 alters cofactor specificity and impacts Arabidopsis growth in air. A, HPR1 catalyzes the reduction of hydroxypyruvate to glycerate upon NADH oxidation. Phosphorylation at Thr-335 shifts HPR1 cofactor specificity toward NADPH. B, Complementation of the *hpr1-1* mutant with a nonphosphorylated HPR1 (HPR1^{T335A}), a mimicked phosphorylation HPR1 (HPR1^{T335D}), and wild-type HPR1 (HPR1^{WT}). Columbia-0 (Col-0) served as the wild-type control. A was generated with BioRender and B was adapted from Liu et al. (2020).

[1]Author for contact: marc-sven.roell@hhu.de.
[2]Senior author.
www.plantphysiol.org/cgi/doi/10.1104/pp.20.00330

hpr1-1 phenotype implies that constitutive HPR1 phosphorylation is obstructive under optimal growth conditions in air.

Indeed, HPR1 phosphorylation negatively influenced photosynthetic CO_2 assimilation due to disturbed photorespiration, shown by decreased levels of photorespiratory metabolites (glycerate, Gly, and glyoxylate). It remains to be proven if the reduced levels of photorespiratory metabolite are due to a feedback inhibition of the peroxisomal Ser:glyoxylate aminotransferase or reduced chloroplastic export of glycolate via the plastidial glycolate/glycerate transporter1 (Pick et al., 2013).

The study by Liu et al. (2020) provides evidence for a novel regulatory mechanism within the photorespiratory cycle. In contrast to previous studies that focused on altered enzymatic activity of photorespiratory enzymes upon posttranslational modifications, phosphorylation of HPR1 changes cofactor specificity. The shift from NADH toward NADPH for the HPR1-catalyzed step of photorespiration allows the adaptation of photorespiratory fluxes in response to altered environmental conditions that directly influence cellular NADH/NADPH ratios. Moreover, cofactor switching allows the cell to modulate the peroxisomal NADH/NADPH ratio by HPR1 activity. However, the advantages of altering cofactor specificity as an adaptive mechanism under changing environmental conditions have to be proven. Furthermore, open questions remain regarding the in vivo functions of the other HPR isoforms (Timm et al., 2011) as well as the regulation of both isoforms in the context of photorespiration.

Marc-Sven Roell[1,2]
ORCID ID: 0000-0003-2714-8729
Institute of Plant Biochemistry,
Heinrich-Heine University, 40225 Duesseldorf,
Germany

LITERATURE CITED

Busch FA (2020) Photorespiration in the context of Rubisco biochemistry, CO_2 diffusion and metabolism. Plant J **101:** 919–939

Eisenhut M, Roell MS, Weber APM (2019) Mechanistic understanding of photorespiration paves the way to a new Green Revolution. New Phytol **223:** 1762–1769

Fernie AR, Bauwe H (2020) Wasteful, essential, evolutionary stepping stone? The multiple personalities of the photorespiratory pathway. Plant J doi:10.1111/tpj.14669

Hodges M, Dellero Y, Keech O, Betti M, Raghavendra AS, Sage R, Zhu XG, Allen DK, Weber APM (2016) Perspectives for a better understanding of the metabolic integration of photorespiration within a complex plant primary metabolism network. J Exp Bot **67:** 3015–3026

Liu Y, Guérard F, Hodges M, Jossier M (2020) Phospho-mimetic T335D HPR1 modifies cofactor specificity and impacts Arabidopsis growth in air. Plant Physiol **183:** 194–205

Pick TR, Bräutigam A, Schulz MA, Obata T, Fernie AR, Weber APM (2013) PLGG1, a plastidic glycolate glycerate transporter, is required for photorespiration and defines a unique class of metabolite transporters. Proc Natl Acad Sci USA **110:** 3185–3190

Timm S, Florian A, Jahnke K, Nunes-Nesi A, Fernie AR, Bauwe H (2011) The hydroxypyruvate-reducing system in Arabidopsis: Multiple enzymes for the same end. Plant Physiol **155:** 694–705

Terpenes in cannabis: Solving the puzzle how to predict taste and smell

News and Views

Terpenes in Cannabis: Solving the Puzzle of How to Predict Taste and Smell

Cannabis sativa (cannabis) is the cornerstone of the multibillion-dollar legal marijuana industry. Cannabis plants are industrially used for fiber and oilseed production, but are primarily known for their resin, which is produced from glandular trichomes covering the surface of female flowers and is rich in cannabinoids and terpenes. The medicinal and psychoactive properties of cannabis depend on the total cannabinoid amount and the ratio of tetrahydrocannabinolic acid to cannabidiolic acid. However, fragrance and flavor are affected by terpene composition (Booth et al., 2017). To predict and design cannabis smell and taste to meet consumer demands, two milestones have to be reached. First, a comprehensive understanding of terpene composition is required, which can be achieved by using quantitative terpene profiling in existing cultivars. Second, the underlying molecular and biochemical mechanisms leading to these distinct profiles need to be understood.

In this issue of *Plant Physiology*, Booth et al. (2020) provide the framework for future breeding efforts to produce cannabis fragrance and flavor features demanded by consumers. Specifically, they analyzed terpene profiles of eight cannabis cultivars and characterized 13 new cannabis terpene synthases. In plants, terpenes form a diverse group of hydrocarbon-based metabolites estimated to encompass thousands of different molecules (Pichersky and Raguso, 2018). Terpenes have diverse roles. They function as primary cellular components, e.g. as hormones or antioxidants, and they are indispensable for ecological interactions, e.g. signaling and defense against herbivores (Pichersky and Raguso, 2018). In cannabis, more than 100 different terpenes have been identified that define odor and flavor of different cultivars (Rothschild et al., 2005; Andre et al., 2016).

Terpene- and cannabinoid-biosynthesis depend on the five carbon building block isopentenyl pyrophosphate (IPP; Fig. 1). IPP is produced by the plastidial methylerythritol phosphate pathway and the cytosolic mevalonate pathway. Metabolic fluxes within both pathways contribute to the substrate pools available for terpene synthases (TPSs). TPSs produce the diversity of cyclic and acyclic terpene core structures, using geranyl diphosphate or farnesyl diphosphate for monoterpene or sesquiterpene synthesis, respectively (Fig. 1).

The accurate predicting and design of cannabis terpene profiles requires understanding of TPS, the key enzyme in terpene biosynthesis (Fig. 1). Booth et al. (2020) identified 19 *TPS* gene models in the 'Purple Kush' cannabis reference genome. *TPS* genes show multicopy gene clustering, a common phenomenon previously observed for genes of the IPP and cannabinoid biosynthetic pathways (Taura et al., 2009). Foliar terpene profiling of eight cannabis cultivars revealed a total of 48 different terpenes with three monoterpenes (myrcene, α-pinene, and limonene) and two sesquiterpenes (β-caryophyllene and α-humulene) present in all cultivars. In six selected cultivars, monoterpenes accumulated during the life cycle, in tissues including leaves, juvenile flowers, and adult flowers. Using trichome transcriptome profiling, Booth et al. (2020) identified 33 *TPS* genes among the selected six cultivars. Further, 13 new TPSs were biochemically characterized regarding product formation using both geranyl diphosphate and farnesyl diphosphate as substrates. Overall TPS specificity varied between the production of a single mono- or sesquiterpene to as

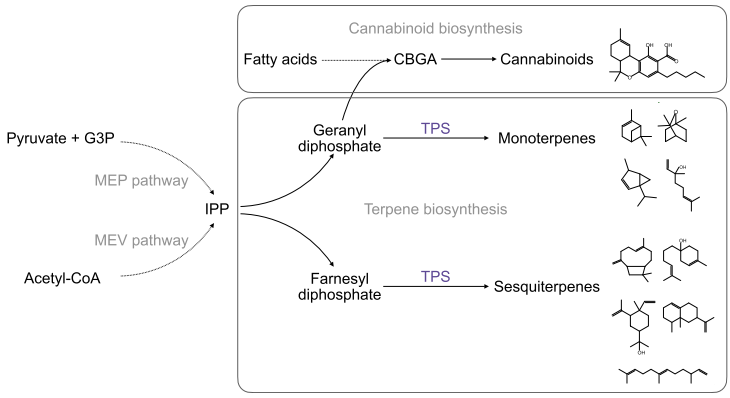

Figure 1. Simplified scheme of terpene biosynthesis. IPP is produced either by the methylerythritol phosphate (MEP) pathway or the mevalonate (MEV) pathway. TPSs catalyze the last step of terpene biosynthesis. G3P, Glyceraldehyde 3-phosphate; CBGA, cannabigerolic acid. Adapted from figure 1 of Booth et al. (2020).

many as 13 different sesquiterpenes produced by a single TPS enzyme.

With these results, simple assumptions regarding *TPS* transcript abundance and terpene profiles can be made. However, spatiotemporal profiling of *TPS* transcript levels and terpene quantities will be necessary for more accurate predictions. Integrating the 13 TPSs characterized in this study with previously characterized TPS brings the total number to 30 known TPSs across 14 different cannabis cultivars (Booth et al., 2017; Zager et al., 2019; Livingston et al., 2020). Harmonizing trichome transcriptomics tools, knowledge of TPS function, and terpene profiling sets the framework for cannabis breeders to predictively shape and design terpene composition on demand.

Marc-Sven Roell[1,2]
ORCID ID: 0000-0003-2714-8729
Institute of Plant Biochemistry, Heinrich-Heine University Düsseldorf, 40225 Düsseldorf, Germany

LITERATURE CITED

Andre CM, Hausman J-F, Guerriero G (2016) *Cannabis sativa*: The plant of the thousand and one molecules. Front Plant Sci **7:** 19

Booth JK, Page JE, Bohlmann J (2017) Terpene synthases from *Cannabis sativa*. PLoS One **12:** e0173911

Booth JK, Yuen MMS, Jancsik S, Madilao L, Page J, Bohlmann J (2020) Terpene synthases and terpene variation in *Cannabis sativa*. Plant Physiol **184:** 130–147

Livingston SJ, Quilichini TD, Booth JK, Wong DCJ, Rensing KH, Laflamme-Yonkman J, Castellarin SD, Bohlmann J, Page JE, Samuels AL (2020) Cannabis glandular trichomes alter morphology and metabolite content during flower maturation. Plant J **101:** 37–56

Pichersky E, Raguso RA (2018) Why do plants produce so many terpenoid compounds? New Phytol **220:** 692–702

Rothschild M, Bergström G, Wängberg SÅ (2005) *Cannabis sativa*: Volatile compounds from pollen and entire male and female plants of two variants, Northern Lights and Hawaian Indica. Bot J Linn Soc **147:** 387–397

Taura F, Tanaka S, Taguchi C, Fukamizu T, Tanaka H, Shoyama Y, Morimoto S (2009) Characterization of olivetol synthase, a polyketide synthase putatively involved in cannabinoid biosynthetic pathway. FEBS Lett **583:** 2061–2066

Zager JJ, Lange I, Srividya N, Smith A, Lange BM (2019) Gene networks underlying cannabinoid and terpenoid accumulation in cannabis. Plant Physiol **180:** 1877–1897

[1]Author for contact: marc-sven.roell@hhu.de.
[2]Senior author.
www.plantphysiol.org/cgi/doi/10.1104/pp.20.00919

A novel trojan horse for molecule delivery into plants

News and Views

A Novel Trojan Horse for Molecule Delivery into Plants

The agronomic application of nanotechnology harbors huge potential for future agriculture (Landry and Mitter, 2019). Within the last years, nanocarriers have emerged as vehicles for the delivery of cargo (RNA, DNA, protein, and plant protection substances) into the plant cell (Wang et al., 2016). RNA-induced gene silencing (also known as RNA interference) is a reliable method to study and alter the genetic form and function of plants. Nanocarriers offer the possibility to directly deliver small interfering RNAs (siRNAs; double-stranded RNAs of 20–25 bp) into the plant cell without involving a biological carrier (e.g. viruses) or genetic transformation (Cunningham et al., 2018).

Carbon-based nanostructures such as carbon dots and single-walled carbon nanotubes (Demirer et al., 2019, 2020) are valuable alternatives to common transformation methods, since they do not require genetic transformation (Wang et al., 2016) and avoid heavy metal nanoparticles, usually used for biolistic transformation (Klein et al., 1987). Although single-walled carbon nanotubes and carbon dots share most beneficial properties, they differ in size. Single-walled carbon nanotubes are ~1 nm in diameter and up to 1,000 nm in length; in contrast, carbon dots are on average ~3 nm in size (Demirer et al., 2020; Schwartz et al., 2020). The benefits of carbon-based nanostructures are a high aspect ratio (i.e. the ratio of length to width), good biocompatibility (especially compared with metal nanoparticles), and the ability to protect bound biomolecules from cellular metabolism and degradation (Demirer et al., 2019; Kwak et al., 2019). Furthermore, tissue-specific tracking based on their fluorescent properties and intracellular on-demand cargo release holds great promise for broad application (Wang et al., 2016;

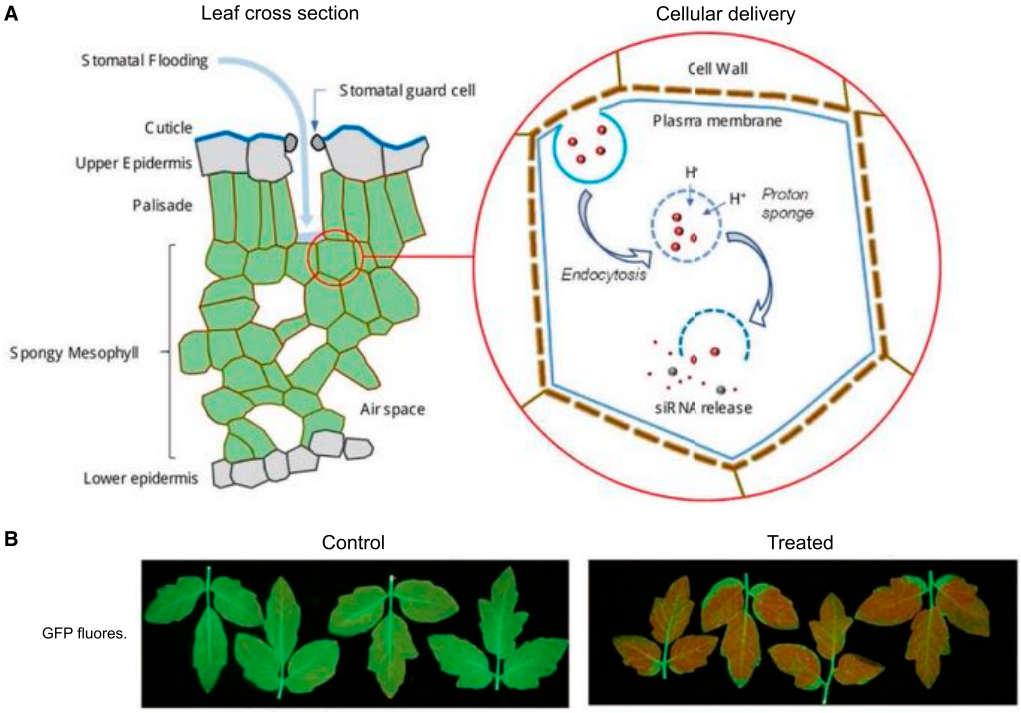

Figure 1. Carbon dot-delivered siRNA-mediated gene silencing in plants. A, Schematic representation of carbon dot leaf entry and intracellular siRNA release. B, Spray application of carbon dot-delivered siRNAs. GFP fluorescence (GFP fluores.) in leaves of a tomato reporter line was imaged after treatment with a non-GFP-specific siRNA (Control) or a GFP-specific siRNA (Treatment). Images were taken 5 d after application. Adapted from Schwartz et al. (2020).

Cunningham et al., 2018). The cellular uptake of nanocomplexes is facilitated by endocytosis (Fig. 1), and intracellular release of the nanocomplex is caused by an osmotically driven endosome burst, called the proton-sponge effect (Behr, 1997). The utilization of nanoparticles that respond either to intracellular stimuli (pH, redox state, and enzymes) or external stimuli (light or ultrasound) facilitates controlled cargo release within the cell (Wang et al., 2016; Cunningham et al., 2018).

In this issue of *Plant Physiology*, Schwartz et al. (2020) establish the use of carbon dots for the delivery of siRNAs as a novel tool for gene silencing in plants. Simple spray application of carbon dots results in highly efficient reporter and endogenous gene silencing in model and crop species and holds great potential for field application. In their study, Schwartz et al. (2020) optimized the chemical synthesis and purification of carbon dots before application. The low-cost bottom-up synthesis of carbon dots is based on a one-pot reaction using citrate or Glc with branched polyethyleneimine for carbon dot surface functionalization. Size-exclusion chromatography of prepared carbon dots revealed that carbon dots with an average size of 3.8 nm in diameter, combined with 22mer siRNAs, are most efficient for in planta gene silencing.

Whereas previous nanoparticle approaches in plants rely on particle bombardment (Klein et al., 1987) or leaf infiltration (Demirer et al., 2019, 2020), carbon dots with siRNA cargo are efficient for gene silencing upon low-pressure spraying application (Schwartz et al., 2020). GFP transcript and protein abundance were more than 80% reduced in reporter lines of wild tobacco (*Nicotiana benthamiana*) and tomato (*Solanum lycopersicum*) 5 d after application (Fig. 1). Remarkably, systemic spreading of silencing was observed in emerging leaves 12 d after application due to intercellular and long-distance movement of siRNAs (Melnyk et al., 2011).

Reporter gene independent validation was achieved by targeting the endogenous H and I subunits of magnesium chelatase. Magnesium chelatase catalyzes the insertion of magnesium into protoporphyrin IX, an essential step in chlorophyll biosynthesis, and knockdown results in leaf bleaching. Comparable to GFP silencing, endogenous gene silencing also reached an 80% reduction in mRNA level.

Carbon dot-based siRNA delivery into plant cells expands the spectrum of carbon-based nanoparticles for molecule delivery into plant cells and is an exciting tool for fundamental and applied plant science. The simple spray application makes it well suited for large-scale agricultural use. Furthermore, prepared carbon dots are also persistent and retain overall efficacy for at least 1 week of storage before application. Nevertheless, a comparable high efficacy with less established plant species needs to be shown, and fine-tuning cellular entry and intracellular siRNA release can further optimize broad-spectrum application.

Marc-Sven Roell[1,2]
ORCID ID: 0000-0003-2714-8729
Institute of Plant Biochemistry,
Heinrich-Heine University, 40225 Duesseldorf,
Germany

LITERATURE CITED

Behr JP (1997) The proton sponge: A trick to enter cells the viruses did not exploit. Chimia (Aarau) **51:** 34–36

Cunningham FJ, Goh NS, Demirer GS, Matos JL, Landry MP (2018) Nanoparticle-mediated delivery towards advancing plant genetic engineering. Trends Biotechnol **36:** 882–897

Demirer GS, Zhang H, Goh NS, Pinals RL, Chang R, Landry MP (2020) Carbon nanocarriers deliver siRNA to intact plant cells for efficient gene knockdown. Sci Adv **6:** eaaz0495

Demirer GS, Zhang H, Matos JL, Goh NS, Cunningham FJ, Sung Y, Chang R, Aditham AJ, Chio L, Cho MJ, et al (2019) High aspect ratio nanomaterials enable delivery of functional genetic material without DNA integration in mature plants. Nat Nanotechnol **14:** 456–464

Klein TM, Wolf ED, Wu R, Sanford JC (1987) High-velocity microprojectiles for delivering nucleic acids into living cells. Nature **327:** 70–73

Kwak SY, Lew TTS, Sweeney CJ, Koman VB, Wong MH, Bohmert-Tatarev K, Snell KD, Seo JS, Chua NH, Strano MS (2019) Chloroplast-selective gene delivery and expression in planta using chitosan-complexed single-walled carbon nanotube carriers. Nat Nanotechnol **14:** 447–455

Landry MP, Mitter N (2019) How nanocarriers delivering cargos in plants can change the GMO landscape. Nat Nanotechnol **14:** 512–514

Melnyk CW, Molnar A, Baulcombe DC (2011) Intercellular and systemic movement of RNA silencing signals. EMBO J **30:** 3553–3563

Schwartz SH, Hendrix B, Hoffer PH, Sanders R, Zheng W (2020) Carbon dots for efficient siRNA delivery and gene silencing in plants. Plant Physiol **184:** 647–657

Wang P, Lombi E, Zhao FJ, Kopittke PM (2016) Nanotechnology: A new opportunity in plant sciences. Trends Plant Sci **21:** 699–712

[1]Author for contact: marc-sven.roell@hhu.de.
[2]Senior author.
www.plantphysiol.org/cgi/doi/10.1104/pp.20.01012